

Characterisation, Inhibition, and Structural Analysis of Mycobacterial DNA Gyrase

Sara Rachel Henderson

Department of Biological Chemistry

John Innes Centre

December 2018

This thesis is submitted in partial fulfilment of the requirements of the degree of Doctor of
Philosophy at the University of East Anglia

© This copy of the thesis has been supplied on condition that anyone who consults it is understood to recognise that its copyright rests with the author and that no quotation from the thesis, nor any information derived therefrom, may be published without the author's prior, written consent.

Statement

The work submitted in this thesis is my own work, except where due reference is made to other authors, and has not been submitted to this or any other University for any degree.

Abstract

Tuberculosis is primarily a pulmonary condition caused by *Mycobacterium tuberculosis*, which causes a serious threat to human health. In 2016 more than 1.3 million people died of tuberculosis, meanwhile there were 10.4 million new infections worldwide. Treatment for tuberculosis currently takes a minimum of 6 months with a combination of four different antibiotics, but there is increasing resistance to the first line antibiotics. The second line antibiotics include the fluoroquinolones (moxifloxacin, levofloxacin and gatifloxacin), which target DNA gyrase, the only Type IIA topoisomerase in *M. tuberculosis*, of which there is limited structural and biochemical information available within the literature.

To address these problems, we sought to increase our knowledge of mycobacterial DNA gyrase through biochemical mechanistic studies, inhibition studies of known and novel inhibitors of DNA gyrase alongside structural studies by X-ray crystallography. This led us to determine that a fusion of the GyrB and GyrA subunits was fully active and, in some cases, potentially more active than using the individual subunits. In particular, we determined that a detectable and greater rate of ATPase activity was present in Mtb DNA gyrase than previously suggested. We found this rate to be highly DNA-dependent requiring a topologically unconstrained DNA substrate (linear or nicked plasmid) for the highest rates. In addition, we cloned, expressed, purified and partially characterised DNA gyrase from the thermophilic *M. thermoresistibile* for use in structural studies.

In investigating the novel tricyclic group of compounds optimised by Redx AntiInfectives, we determined that they act in a similar mechanism of action to novobiocin through biochemical studies. They differ in their binding pocket, as determined by X-ray crystallography, and mechanism of resistance, as determined by bacterial mutagenesis.

Table of Contents

Statement	i
Abstract.....	ii
Table of Contents.....	iii
List of Figures.....	x
List of Tables	xvii
Acknowledgements.....	xx
1. Introduction.....	1
1.1 Tuberculosis.....	1
1.2 Current treatments.....	3
1.2.1 Treatment for co-infection with HIV/AIDS.....	3
1.2.2 Treatment of latent tuberculosis.....	4
1.3 Mycobacterial infections.....	4
1.3.1 Mycobacterial properties.....	5
1.3.2 Latent infections and granuloma formation	6
1.3.3 <i>Mycobacterium smegmatis</i> as a homologue.....	7
1.3.4 <i>Mycobacterium thermoresistibile</i> as a homologue.....	8
1.3.5 Mycobacterial biofilms	9
1.4 DNA topology.....	10
1.5 DNA topoisomerases	13
1.5.1 Type IA topoisomerases.....	13
1.5.2 Type IB topoisomerases.....	14
1.5.3 Type IC topoisomerases.....	15
1.5.4 Type IIA topoisomerases	16
1.5.5 Type IIB topoisomerases	20
1.5.6 Topoisomerases in mycobacteria	20
1.6 DNA gyrase	21
1.6.1 ATP hydrolysis and the GyrB N-terminal domain	21
1.6.2 DNA gyrase core: GyrB C-terminal domain and GyrA N-terminal domain	24

1.6.3	The GyrA C-terminal domain and DNA wrapping.....	24
1.6.4	DNA gyrase: a proposed mechanism of action.....	25
1.6.5	DNA gyrase from <i>M. tuberculosis</i>	27
1.6.6	Fusion proteins of DNA gyrase	27
1.7	Structural biology of DNA gyrase	29
1.8	Inhibition of DNA gyrase	32
1.8.1	Inhibition of DNA gyrase by (fluoro)quinolones.....	34
1.8.2	Inhibition of DNA gyrase by aminocoumarins.....	35
1.8.3	Inhibition of DNA gyrase by naphthoquinones	38
1.8.4	Inhibition of DNA gyrase by simocyclinones.....	41
1.8.5	Pyrrolopyrimidine and tricyclic GyrB/ParE (TriBE) inhibitors.....	41
1.9	Project aims.....	44
2.	Materials and Methods.....	46
2.1	Bacteriology.....	46
2.1.1	Bacterial strains.....	46
2.1.2	Media and antibiotics	46
2.1.3	Preparation of chemically competent <i>E. coli</i> cells	48
2.1.4	Heat shock transformation of chemically competent cells.....	48
2.2	Molecular biology methods	48
2.2.1	Oligodeoxynucleotides (primers).....	48
2.2.2	Agarose gel electrophoresis	54
2.2.3	PCR and cloning	55
2.2.4	Site-directed mutagenesis	56
2.2.5	DNA purification	56
2.2.6	DNA concentration determination	57
2.2.7	DNA sequencing.....	57
2.3	Protein methods	57
2.3.1	Buffers and solutions	57
2.3.2	Protein expression.....	58

2.3.3	Protein purification	58
2.3.4	Sodium dodecyl sulphate – polyacrylamide gel electrophoresis (SDS-PAGE) 59	
2.3.5	Dialysis	60
2.3.6	Protein concentration	60
2.3.7	Protein concentration determination	60
2.3.8	Surface plasmon resonance	61
2.4	Compounds and solvents	61
2.5	DNA topology assays	62
2.5.1	Assay of DNA supercoiling by DNA gyrase	62
2.5.2	Assay of DNA relaxation by DNA gyrase	62
2.5.3	Assay of DNA decatenation by DNA gyrase.....	63
2.5.4	Assay of DNA cleavage by DNA gyrase	63
2.5.5	Assay of ATP turnover by DNA gyrase	64
2.5.6	Assay of DNA relaxation by topo IV	65
2.5.7	Assay to determine cleavage profile by DNA gyrase	66
2.6	Whole cell compound testing.....	66
2.6.1	MIC determination.....	66
2.6.2	Agar MIC determination.....	66
2.6.3	Time of kill	67
2.6.4	Disruption of biofilm assay.....	67
2.7	Bacterial mutant generation	68
2.7.1	Frequency of mutation experiment	68
2.7.2	Serial passage.....	69
2.8	Protein crystallography: crystal methods	69
2.8.1	Screening of crystallisation condition.....	69
2.8.2	Optimisation of crystallisation conditions	70
2.8.3	Seeding of crystallisation conditions	70
2.8.4	SDS-PAGE of crystals	70

2.8.5	Crystal soaking.....	71
2.8.6	Harvesting of crystals.....	71
2.9	Protein crystallography: data collection and structure determination.....	71
2.9.1	X-ray data collection.....	71
2.9.2	DIMPLE analysis.....	71
2.9.3	Processing of diffraction data	72
3.	Mechanistic Studies of DNA Gyrase from <i>M. tuberculosis</i> and <i>M. thermoresistibile</i> ..	73
3.1	DNA gyrase from <i>M. tuberculosis</i>	73
3.1.1	Construct development of the GyrBA fusion protein	73
3.1.2	Protein expression and purification of the GyrBA fusion protein	74
3.1.3	The GyrBA fusion protein is active in supercoiling	77
3.1.4	The GyrBA fusion protein is active in relaxation	79
3.1.5	The GyrBA fusion protein is active in decatenation.....	81
3.1.6	The ATP turnover rate of <i>M. tuberculosis</i> DNA gyrase is appreciable	84
3.1.7	Preliminary cleavage profile of <i>M. tuberculosis</i> DNA gyrase.....	91
3.2	DNA gyrase from <i>M. thermoresistibile</i>	94
3.2.1	Construct design, cloning, expression and purification	94
3.2.2	Crystallography trials of <i>M. thermoresistibile</i> DNA gyrase	94
3.2.3	DNA gyrase from <i>M. thermoresistibile</i> supercoils DNA.....	95
3.2.4	DNA gyrase from <i>M. thermoresistibile</i> relaxes DNA.....	98
3.2.5	DNA gyrase from <i>M. thermoresistibile</i> can decatenate DNA	100
3.2.6	ATPase stimulation of DNA gyrase from <i>M. thermoresistibile</i> by DNA....	101
3.2.7	Inhibition of <i>M. thermoresistibile</i> DNA gyrase by known inhibitors	104
3.3	Discussion.....	108
3.3.1	The mycobacterial DNA gyrase fusion proteins are active.....	108
3.3.2	DNA Gyrase from <i>M. tuberculosis</i> can give an appreciable ATP turnover rate	109
3.3.3	Is DNA gyrase able to convert positive supercoils in to negative supercoils?	111

3.3.4	What are the optimal assay conditions for a thermophilic bacterium?	112
3.3.5	Decatenation happens in 100 mM and 250 mM potassium glutamate	113
4.	Inhibition of Mycobacterial DNA Gyrase.....	115
4.1	Fluoroquinolone Antibiotics	115
4.2	Aminocoumarin Antibiotics.....	117
4.3	Naphthoquinone Antibiotics	119
4.4	<u>Tri</u> cyclic GyrB Par <u>E</u> (TriBE) antibiotics from Redx AntiInfectives	124
4.4.1	Growth Inhibition by Redx03863 and Redx04739	124
4.4.2	Inhibition of Mycobacterial Biofilms by Redx03863 and Redx04739	125
4.4.3	Time of kill for Redx03863	127
4.4.4	Inhibition of DNA Gyrase by Redx03863 and Redx04739	129
4.4.5	Redx03863 and Redx04739 competitively inhibit the ATPase reaction of DNA gyrase	132
4.4.6	Surface plasmon resonance analysis of the binding kinetics of Redx03863 and Redx04739	136
4.4.7	Bacterial mutant generation by Redx03863 and Redx04739 by serial passage	142
4.4.8	Bacterial mutant generation by Redx03863 and Redx04739 by frequency of resistance	147
4.4.9	Testing of the naphthoquinone model against Redx03863 and Redx04739	156
4.5	Discussion.....	159
4.5.1	Impacts from further studies on known antibiotics.....	159
4.5.2	Instability of 7-methyljuglone and impacts on further studies.....	160
4.5.3	Whole cell activity of the TriBE antibiotics	161
4.5.4	Consequences of the bacterial mutagenesis results.....	162
4.5.5	Consequences of the mode of action studies and the search for the binding site	167
5.	Crystallography of Mycobacterial DNA Gyrase.....	168
5.1	Crystallisation trials of full-length <i>M. tuberculosis</i> DNA gyrase	168
5.2	Crystallisation of the <i>M. tuberculosis</i> ATPase domain.....	170

5.3	Crystallisation trials of <i>M. tuberculosis</i> GyrB24 ATPase subdomain	171
5.4	Crystallisation trials of <i>M. smegmatis</i> B24 ATPase subdomain	175
5.5	X-ray diffraction and structure resolution of <i>M. smegmatis</i> B24 ATPase subdomain 177	
5.6	Crystallisation trials of <i>M. thermoresistibile</i> B24 ATPase subdomain	184
5.7	X-ray diffraction and structure resolution of <i>M. thermoresistibile</i> B24 ATPase subdomain	188
5.8	Site-directed mutagenesis based on the structure of <i>M. thermoresistibile</i> B24 ATPase subdomain bound to Redx03863	195
5.9	Structural comparison of <i>M. thermoresistibile</i> B24 ATPase subdomain bound to Redx03863 with the human topo II α ATPase domain	199
5.10	Discussion	201
5.10.1	Previously known structures	201
5.10.2	A future structure of Redx04739?	202
5.10.3	Use of homologues and loop deletion constructs	203
5.10.4	Understanding the binding site of novobiocin through crystallographic analysis 204	
5.10.5	Understanding the binding site of Redx03863 through crystallographic analysis and mutagenesis of GyrB	207
5.10.6	Implications of the binding sites	208
6.	Discussion	209
6.1	Mechanistic studies of DNA gyrase from <i>M. tuberculosis</i>	209
6.2	DNA gyrase from <i>M. thermoresistibile</i>	210
6.3	Inhibition of mycobacterial DNA gyrase	211
6.3.1	Prospects for the naphthoquinone antibiotic class	211
6.3.2	The TriBE antibiotics optimised by Redx AntiInfectives	212
6.4	Structural studies on mycobacterial DNA gyrase	213
6.5	Are we closer to a new antimycobacterial drug?	214
	List of Abbreviations	xx
	Literature Cited	215

Appendix..... 232

List of Figures

Figure 1.1.1 World map of the estimated new tuberculosis cases recorded per 100,000 population in 2017.	1
Figure 1.1.2 Cartoon representation of a classical granuloma containing <i>M. tuberculosis</i> typically in the lungs.	2
Figure 1.3.1 Cartoon representation of the Mycobacterial cell membrane and wall.	6
Figure 1.3.2 Phylogenetic tree of DNA gyrase B based on sequence from <i>M. tuberculosis</i> H37Rv.	9
Figure 1.4.1 Topology diagram at the replication fork.	11
Figure 1.4.2 Topology diagram at the site of transcription.	12
Figure 1.5.1 Domain alignment of eukaryotic and prokaryotic type II topoisomerases.	17
Figure 1.5.2 The likely strand-passage mechanism of action of the type IIA topoisomerases.	18
Figure 1.6.1 Mechanism of negative supercoiling by DNA gyrase	26
Figure 1.7.1 Comparison of the structures of type IIA topoisomerases.	30
Figure 1.7.2 Coverage of current structures of DNA gyrase from <i>M. tuberculosis</i> solved by X-ray crystallography	32
Figure 1.8.1 Model of full-length DNA gyrase from <i>M. tuberculosis</i> based on homology modelling to other known structures.	33
Figure 1.8.2 Chemical structures of examples from each of the four generations of quinolone antibiotics.	34
Figure 1.8.3 Chemical structure of the aminocoumarin novobiocin.	36
Figure 1.8.4 Two views of the model of diospyrin docked into the 3ZM7 crystal structure of the Mtb ATPase domain.	40
Figure 1.8.5 Structure of Simocyclinone D8.	41
Figure 1.8.6 Image of the binding pocket of compound 4 in the <i>Enterococcus faecalis</i> V583 ATPase sub-domain (4KSG).	43
Figure 1.8.7 Chemical structures of Redx03863 and Redx04739	43
Figure 1.9.1 Overview of the three-pronged approach of this PhD thesis.	45
Figure 2.5.1 Cartoon representation of the PL/LDH linked ATPase assay system used.	64
Figure 3.1.1 Cartoon representation of the three Mtb DNA gyrase constructs obtained from other lab members.	74

Figure 3.1.2 Induction of the Mtb GyrBA fusion protein under optimal expression conditions.	75
Figure 3.1.3 Purification method of the Mtb GyrBA fusion protein.	76
Figure 3.1.4 SDS-PAGE gels showing “Pure” GyrBA for crystallography and ATPase assays, and “Dirty” GyrBA suitable for topoisomerase assays.	77
Figure 3.1.5 Supercoiling activity comparison between the Mtb gyrase subunits and fusion constructs.	78
Figure 3.1.6 Induction of supercoiling as a function of potassium glutamate concentration in both the Mtb GyrA ₂ B ₂ individual subunits and the GyrBA fusion construct.	79
Figure 3.1.7 ATP-independent relaxation activity comparison between the Mtb gyrase subunits and fusion constructs.	80
Figure 3.1.8 Induction of ATP-independent relaxation as a function of potassium glutamate concentration in both the Mtb GyrA ₂ B ₂ individual subunits and the GyrBA fusion construct.	81
Figure 3.1.9 Expected banding pattern of a decatenation assay carried out and imaged on a native 0.8-1% agarose in TAE gel stained with ethidium bromide.	82
Figure 3.1.10 Decatenation assay using the kinetoplast DNA substrate.	83
Figure 3.1.11 Raw absorbance data for the PK/LDH linked assay carried out with <i>E. coli</i> or <i>M. tuberculosis</i> DNA gyrase A ₂ B ₂ constructs with relaxed pBR322*.	85
Figure 3.1.12 Visualisation of the topological state of 1 ng pBR322* over time after addition of 2 mM ATP during an ATPase linked assay.	87-88
Figure 3.1.13 A) Plot of absorbance at 340 nm monitoring the loss of NADH in the PK/LDH-linked assay of a DNA titration with linear pBR322*. B, C) Novobiocin-dependent ATP turnover rate with nicked pBR322* or negatively supercoiled pBR322* substrate.	89-90
Figure 3.1.14 Plasmid map of pBR322 showing all the single cutting restriction enzymes.	91
Figure 3.1.15 Preliminary cleavage profile optimisations with Mtb GyrA ₂ B ₂ .	93
Figure 3.2.1 Supercoiling activity comparison between the Mth gyrase subunits and fusion constructs.	97
Figure 3.2.2 Induction of supercoiling as a function of potassium glutamate concentration in both the Mth GyrA ₂ B ₂ individual subunits and the GyrBA fusion construct.	98

Figure 3.2.3 Comparison of the two constructs of <i>M. thermoresistibile</i> DNA gyrase in ATP-independent relaxation.	99
Figure 3.2.4 ATP-independent relaxation as a function of potassium glutamate concentration with both the Mth GyrA ₂ B ₂ individual subunits and the GyrBA fusion construct.	100
Figure 3.2.5 Mth Decatenation assay using kinetoplast DNA.	101
Figure 3.2.6 A) Plot of absorbance at 340 nm monitoring the loss of NADH in the PK/LDH linked assay of DNA titration with linear pBR322*. B) DNA titration on increasing the concentration of linear pBR322*.	103-104
Figure 3.2.7 Inhibition of Mtb and Mth DNA gyrase subunits A ₂ B ₂ and BA fusion constructs supercoiling activity by novobiocin (10-0.1 μM)	105
Figure 3.2.8 Activity of Moxifloxacin on the two alternate constructs of A/C) Mth DNA gyrase at 0.25 μM and B/D) Mtb DNA gyrase at 0.74 μM. Induction of cleavage complex assay	107
Figure 3.3.1 Alternative decatenation assay in development by Inspiralis Limited.	113
Figure 4.1.1 Activity of Moxifloxacin on the two alternate constructs of Mtb DNA gyrase at 0.74 μM.	116
Figure 4.2.1 A) Inhibition of supercoiling assay against both Mtb subunits and fusion proteins at 10-0.1 μM novobiocin. B) Rate of ATP turnover per GyrBA subunit plotted against the base 10 logarithm in μM of the novobiocin concentration.	118
Figure 4.3.1 Solvents tested against the Mtb DNA gyrase fusion construct in a supercoiling reaction.	120
Figure 4.3.2 Three-day time course of the inhibition of Mtb DNA gyrase fusion protein supercoiling activity of 7-methyljuglone.	121
Figure 4.3.3 Two views of the model of diospyrin docked into the 3ZM7 crystal structure of the Mtb ATPase domain.	123
Figure 4.4.1 Chemical structure of Redx03863 which was optimised to give the lead compound of Redx04739.	124
Figure 4.4.2 Percentage of colony forming units of <i>E. coli</i> ATCC25922 remaining when treated with 4x broth MIC ₁₀₀ Redx03863 compared to untreated bacterium over 6 hours.	128
Figure 4.4.3 Percentage of colony forming units of <i>M. smegmatis</i> ATCC19420 remaining when treated with 4x or 16x broth MIC ₁₀₀ Redx03863 compared to untreated bacterium over 2 days.	128

Figure 4.4.4 Inhibition of supercoiling assay carried out with 74 nM of each gyrase subunit.	130
Figure 4.4.5 Inhibition of the <i>E. coli</i> Type II topoisomerases by Redx03863 and Redx04739.	131
Figure 4.4.6 Inhibition of ATP-independent relaxation assay carried out with 0.5 μ M of each gyrase subunit.	132
Figure 4.4.7 ATP competition assay with Redx03863 and Redx04739 vs Mtb DNA gyrase.	133
Figure 4.4.8 A) Plot of the absorbance at 340 nm over time in the presence of varying amount of Redx03863. B, C) Plots of the rate of the novobiocin sensitive ATP turnover per GyrB subunit plotted against the base 10 logarithm of the concentration in μ M to determine the IC ₅₀ value. B) Redx03863, C) Redx04739.	135-136
Figure 4.4.9 Single cycle kinetics SPR results from the CM5 chip bound to the ATPase sub-domain from <i>E. coli</i> .	138-139
Figure 4.4.10 Single cycle kinetics SPR results from the CM5 chip bound to the Mtb ATPase sub-domain.	140-141
Figure 4.4.11 Plot showing the MIC ₁₀₀ values for <i>E. coli</i> ATCC25922 and <i>M. smegmatis</i> ATCC1940 when raised against Redx03863.	143
Figure 4.4.12 Plot showing the MIC ₁₀₀ values for <i>E. coli</i> ATCC25922 and <i>M. smegmatis</i> ATCC1940 when raised against Redx04739.	144
Figure 4.4.13 Visualisation of the mutant locations of the mutants generated by serial passage on a model made from 3 structures of <i>M. tuberculosis</i> DNA gyrase	146
Figure 4.4.14 Locations of the key mutations located in the GyrB NTD raised by frequency of resistance mutagenesis.	150
Figure 4.4.15 Time course of GyrB ^{G83S} at enzyme concentration of 0.158 μ M, over 2 hours.	152
Figure 4.4.16 Supercoiling assay using GyrB wild type, K159R, T167A and K202R at a final enzyme concentration of 150 nM of each subunit against Novobiocin.	153
Figure 4.4.17 Supercoiling assay using GyrB wild type, K159R, T167A and K202R at a final enzyme concentration of 150 nM of each subunit against Redx03863	154

Figure 4.4.18 Supercoiling assay using GyrB wild type, K159R, T167A and K202R at a final enzyme concentration of 150 nM of each subunit against Redx014739.	155
Figure 4.4.19 Redx03863 tested against the GyrBA fusion protein wild type and naphthoquinone single point mutants.	157
Figure 4.4.20 Redx04739 tested against the GyrBA fusion protein wild type and naphthoquinone single point mutants.	158
Figure 4.5.1 Structures of the VRT aminobenzimidazole dual-targeting compounds from Vertex Pharmaceuticals Incorporated.	166
Figure 5.1.1 Structural model of <i>M. tuberculosis</i> DNA gyrase.	169
Figure 5.3.1 Sequence alignment of the sub-ATPase domain constructs with and without the two long loops.	172
Figure 5.3.2 Visible light (A) and UV (B) image of the single crystal hit obtained when screening the Mtb GyrB24 SLD construct.	173
Figure 5.4.1 Image of crystals of Msm GyrB24 DLD before harvesting from the well for X-ray diffraction (left), and in the loop for data collection at the Diamond synchrotron beamline i04 (right).	176
Figure 5.4.2 Example output from DIMPLE indicating that crystals grown in novobiocin but soaked with Redx04739 still likely contained novobiocin.	176
Figure 5.5.1 Comparison of the crystallographic subunit interfaces of the published 4B6C structure (gold) and the new structure of the Msm GyrB24 ATP sub-domain double loop deletion construct (blue).	179
Figure 5.5.2 Visualisation of the differences in the sodium ion sites in the A and B chains of from the structure of the Msm GyrB24 ATPase sub-domain.	179
Figure 5.5.3 Visualisation of the third and fourth sodium ion sites on the B chain.	180
Figure 5.5.4 An omit map of the Novobiocin within the structure of Msm GyrB24 crystallised in the presence of novobiocin	181
Figure 5.5.5 Bonding interaction involved in the interaction of novobiocin with GyrB, with hydrogen bonding interactions visualised.	182
Figure 5.5.6 Visualisation of all the novobiocin mutants isolated from bacterial strains including potential hydrogen bonds.	183
Figure 5.6.1 SDS-PAGE gel run with pure Mth GyrB24 DLD protein and crystals.	186

Figure 5.6.2 Image of crystals of Mth GyrB24 DLD co-crystallised with novobiocin before harvesting from the well for X-ray diffraction (left), and in the loop for crystal screening at the Diamond synchrotron beamline i03 (right).	187
Figure 5.6.3 Image of crystals of Mth GyrB24 DLD co-crystallised with Redx03863 before harvesting from the well for X-ray diffraction.	187
Figure 5.7.1 Overview of the Mth GyrB24 sub-ATPase domain structure bound in the crystallographic dimer bound to 4 zinc ions including two bound at the non-biological dimer interface, and novobiocin.	190
Figure 5.7.2 The dual conformation zinc binding site at Histidine 61 in the A chain of the novobiocin-bound Mth GyrB24 sub-ATPase domain structure.	190
Figure 5.7.3 An omit map of the ligands within the structures of Mth GyrB24 crystallised in the presence of A) novobiocin and B) Redx03863	191
Figure 5.7.4 The novobiocin-binding site in the Mth GyrB24 sub-ATPase domain structure.	192
Figure 5.7.5 Binding site of Redx03863 within the Mth structure.	194
Figure 5.7.6 Detailed interactions of A) N52, D79 and G83 in Redx03863 bound structure of Mth GyrB (sub-ATPase domain) and B) N48, D75 and G79 in the C4 bound structure of <i>E. faecalis</i> GyrB24 (4KSG).	194
Figure 5.8.1 Activity testing of five of the seven mutants made in the binding domain of Redx03863.	196
Figure 5.8.2 Time course of the activity of the GyrB ^{WT} , GyrB ^{R141A} and GyrB ^{R141Q} mutants assayed at 74 nM with equal amounts of GyrA.	196
Figure 5.8.3 Inhibition of ATP-dependent supercoiling activity of 78 nM GyrB ^{WT} , GyrB ^{R141Q} , and GyrB ^{R141A} with 78 nM GyrA by novobiocin at a concentration range of 0.1-10 µM.	197
Figure 5.8.4 Inhibition of ATP-dependent supercoiling activity of 78 nM GyrB ^{WT} , GyrB ^{R141Q} , and GyrB ^{R141A} with 78 nM GyrA by Redx03863 at a concentration range of 3-300 nM and Redx04739 at a concentration range of 10-1000 nM.	198
Figure 5.8.5 Structural alignment of the Mth structures containing novobiocin and Redx03863 and the published 3ZKB crystal structure of the Mtb GyrB ATPase domain containing AMP-PNP.	199
Figure 5.9.1 Structural alignment of the Mth sub-ATPase domain bound to Redx03863 with the first 267 amino acids of Human topo IIα (4R1F).	200

Figure 5.9.2 A structural comparison of the key binding interactions of Redx03863 in the Mth sub-ATPase domain aligned with the ATPase domain of Human topo II α (4R1F).

201

List of Tables

Table 1.2.1 Treatment groups of drugs against tuberculosis including those against MDR-TB.	4
Table 1.5.1 Classification of DNA topoisomerases	14
Table 1.8.1 Novobiocin resistant mutants in DNA gyrase GyrB and the amino acid positions in the <i>E. coli</i> , <i>S. aureus</i> , and <i>M. tuberculosis</i> enzymes.	37
Table 1.8.2 Reported IC ₅₀ values of selected naphthoquinones against the <i>M. tuberculosis</i> DNA gyrase supercoiling reaction and their chemical structures.	39
Table 2.1.1 Genotypes of <i>E. coli</i> cloning and expression strains used.	46
Table 2.1.2 Summary of bacterial strains used for genomic DNA isolation, and compound susceptibility testing.	47
Table 2.2.1 Primers used in the alteration of existing constructs and synthesis of new constructs	49-50
Table 2.2.2 Primers designed and used for inducing single point mutations in the GyrB subunit of the GyrB or GyrBA expression plasmids	51
Table 2.2.3 Primers used to amplify the topoisomerase genes from genomic DNA.	52
Table 2.2.4 Sequencing primers used to sequence plasmids and amplified genes.	53-54
Table 2.2.5 Typical reaction components for PCR reactions carried out with Phusion® DNA Polymerase (NEB).	55
Table 2.2.6 Typical thermocycling reaction for a PCR reaction carried out with Phusion® DNA Polymerase (NEB).	56
Table 2.2.7 Typical reaction components for PCR reactions carried out with 2x GoTaq® Green Master Mix (Promega).	56
Table 2.5.1 Typical assay and dilution buffers used in the respective <i>E. coli</i> and mycobacterial DNA gyrase supercoiling assays.	62
Table 2.5.2 1x Assay buffer used in the PK/LDH-linked ATPase assay of <i>E. coli</i> and mycobacterial gyrases.	64
Table 3.1.1 The novobiocin-sensitive ATP turnover rate with 550 nM of the individual GyrA and GyrB subunits.	84
Table 3.1.2 The novobiocin sensitive ATP turnover rate with 200 nM of the Mtb GyrBA fusion protein.	86
Table 3.2.1 Sparse matrix crystallisation conditions trialled with purified Mtb GyrBA protein..	95

Table 3.2.2 ATP turnover rate with 508 nM of Mth individual GyrB or GyrBA subunits and 2 ng of pBR322* plasmid.	102
Table 3.3.1 Table of the optimal assay conditions for the Mtb and Mth DNA gyrase proteins in both the subunits and the fusion proteins.	109
Table 4.4.1 MIC ₁₀₀ data for the two novel RedxAI antibiotics Redx03863 and Redx04739 against a primary screen of bacteria.	125
Table 4.4.2 Inhibition of Biofilm formation against both <i>E. coli</i> ATCC25922 and <i>M. smegmatis</i> ATCC19420.	126
Table 4.4.3 IC ₅₀ values for novobiocin, Redx03863 and Redx04739 against the novobiocin sensitive rate in the ATPase-linked assay.	134
Table 4.4.4 Cross-resistance MIC ₁₀₀ values for the <i>E. coli</i> mutant strains raised against Redx03863 and Redx04739 through use of the serial passage method.	145
Table 4.4.5 Single point mutants identified from sequencing of the DNA gyrase and topo IV genes from the <i>E. coli</i> serial passage mutants.	146
Table 4.4.6 Single point mutants identified from sequencing the DNA gyrase genes <i>gyrA</i> and <i>gyrB</i> isolated from the <i>M. smegmatis</i> serial passage mutant <i>M. smegmatis</i> 04739 SP(29).	147
Table 4.4.7 Agar MIC ₁₀₀ values recorded against <i>E. coli</i> ATCC25922 and <i>M. smegmatis</i> ATCC19420 for Redx03863, Redx04739 and novobiocin.	147
Table 4.4.8 Frequency of Resistance values.	148
Table 4.4.9 Cross-resistance MIC ₁₀₀ values for mutants raised via frequency of resistance experiments.	149
Table 4.4.10 Single point mutants identified from sequencing the DNA gyrase genes <i>gyrA</i> and <i>gyrB</i> isolated from the <i>M. smegmatis</i> frequency of resistance mutants raised against Redx03863.	151
Table 5.3.1 XtalPred-RF results for the Mtb GyrB sub-ATPase domain constructs.	174
Table 5.5.1 Data collection and refinement statistics of the Msm B24 sub-ATPase domain structure.	178
Table 5.6.1 Crystal screening conditions yielding suspected protein crystals from the second iterative round of screening of the Mth GyrB24 DLD construct at 22 mg/ml.	185
Table 5.7.1 Table of crystallographic statistics for the structures of Mth GyrB24 sub-ATPase domain bound to novobiocin and Redx03863.	189

Table 5.10.1 Summary of the key crystallographic interactions between novobiocin or Redx03863 in either of the new Mth or Msm structures presented.

205-206

List of Abbreviations

Abbreviation	Meaning
-ve	Negative control
+ve	Positive control
(HhH)2 fold	Double helix-hairpin-helix fold
2xSTEB	two times sucrose Tris EDTA buffer
7-MJ	7-methyljuglone
Å	Angstrom (10^{-10} m)
ACDP	The Advisory Committee on Dangerous Pathogens
ADP	Adenosine di-phosphate
ADPNP	5'-adenylyl- β,γ -imidodiphosphate
AMP-PCP	Adenylylmethylenediphosphonate
AMP-PNP	Adenylyl-imidodiphosphate
APS	Ammonium persulphate
ART	Anti-retroviral treatment
ATP	Adenosine tri-phosphate
BCG	Bacillus Calmette-Guérin vaccine
BLASTn	Basic local alignment search tool - nucleotide
bMIC	Biofilm minimum inhibition concentration (minimum concentration to prevent growth of a biofilm)
bp	Nucleotide Base pair
CC ₅₀	Half maximal cleavage complex concentration
Cl	Cleavage
CO	Codon Optimised
cryoEM	Cryo-electron microscopy
CTD	C-terminal domain
dATP	Deoxyadenosine triphosphate
Dc	Decatenation
DLD	double loop deletion
DMSO	Dimethyl sulfoxide
DNA	Deoxyribonucleic acid
dNTPs	deoxyribonucleotide triphosphates
DOTS	Directly observed treatment short course
DSMZ	Deutsche Sammlung von Mikroorganismen und Zellkulturen
DTT	Dithiothreitol
EDTA	Ethylenediaminetetraacetic acid+B70
EtOH	Ethanol
F	forwards primer
FoR	Frequency of resistance
G	Genomic
HPA	Health protection agency
IC ₅₀	Half maximal inhibitory concentration
ⁱ PrOH	Iso-propanol

Abbreviation	Meaning
IPTG	Isopropyl β -D-1-thiogalactopyranoside
K_d	Dissociation constant
kDa	Kilo Dalton
kDNA	Kinetoplast DNA
LB	Lysogeny broth
LBTI	Latent tuberculosis infection
MBEC	Minimum biofilm eradication concentration (minimum concentration to totally kill a biofilm)
MIC	Minimum Inhibition Concentration
MIC(100)	Minimum concentration at which 100% growth inhibition seen
Moxi	Moxifloxacin
mRNA	Messenger ribonucleic acid
Msm	<i>Mycobacterium smegmatis</i>
Mtb	<i>Mycobacterium tuberculosis</i>
Mth	<i>Mycobacterium thermoresistibile</i>
MWCO	Molecular weight cut off
NAD ⁺	Oxidised nicotinamide adenine dinucleotide
NADH	Reduced nicotinamide adenine dinucleotide
NCBI	National center for biotechnology information
Novo	Novobiocin
NTD	N-terminal domain
OADC	Oleic Albumin Dextrose Catalase
OC	Open Circle
OD600	Optical density at 600 nm
Oligo	Oligonucleotide
PBS	Phosphate buffered saline
PCR	Polymerase chain reaction
PDB	Protein Data Bank
PEG	Polyethylene glycol
PK	Proteinase K
PK/LDH	Pyruvate kinase / Lactate dehydrogenase
PSI	Pounds per square inch
QRDR	Quinolone resistance determining region
R	reverse primer
Rel	Relaxation
RNA	Ribonucleic acid
RNAP	Ribonucleic acid polymerase
RPM	Revolutions per minute
RU	Response unit
Sc	Supercoiling
SD8	Simocyclinone D8
SDS	sodium dodecyl sulphate

Abbreviation	Meaning
SDS-PAGE	Sodium dodecyl sulphate – polyacrylamide gel electrophoresis
SLD	Single loop deletion
SOC	Super optimal broth with catabolite repression
SP	Serial Passage
SPR	Surface plasmon resonance
TAE	Tris base, acetic acid and EDTA
TB	Tuberculosis
TEMED	Tetramethylethylenediamine
TEV	Tobacco Etch Virus
TriBE	Tricyclic GyrB ParE Inhibitors
UV	Ultraviolet
UVA	Ultraviolet A
VRT	Aminobenzimidazole compounds made by Vertex Pharmaceuticals
WHO	World Health Organisation
WT	Wild-type

Acknowledgements

There are many people who have contributed to the completion of this PhD thesis, none more so than my primary supervisor Prof. Tony Maxwell who has continually made me feel guilty for my love of athletics throughout this project. The BBSRC and RedxPharma who have provided the funding for this PhD. My supervisory committee of Dr Dave Lawson and Dr Stephan Bournemann at the John Innes Centre alongside my iCASE supervisors' Drs Cedric Charrier, Anne-Marie Salisbury and Mark Craighead who have all provided me a wealth of knowledge. Special thanks to Anne-Marie for guiding and teaching me the microbiology throughout my iCASE placement at Redx AntiInfectives, and to Dave for being ever patient in teaching me to solve my data sets.

Special mentions must go to Ms Lesley Mitchenall who has taught me all the biochemical techniques I needed, been a listening ear and assisted with crossword solving when required. Also, to Dr Clare Stevenson who has helped me with the practical crystallography elements, including harvesting my crystals with her every steady hand, and for collecting datasets with Dave and Julia at crazy hours in the night! To Mr Brandon Malone you were the most amazing and enthusiastic summer student. To the lab support team and administrators that have made our lives so much easier through their continued support. Thanks, must go to all the present and former Maxwell group members, the former employees of Redx AntiInfectives, and those countless friends I have made over lunch in the last 4 years who have shared a shoulder to moan on or whom I have laughed with over the silly mistakes.

I thank our collaborators Drs Stephanie Petrella and Claudine Mayer (Institut Pasteur, Paris), Dr Michael Austin (UEA, Pharmacy) and finally Sean Ekins (Collaborative Drug Discovery) for support and assistance.

Away from the JIC a special mention must go to Mrs Sam Loveday-Hope who has helped me stay happy, healthy and focused. To my amazing boyfriend Chris Marshall, my best friends Katy "Belize" Sealy, Abielle Hallas, Liam Hunt along with the rest of the UEA/City of Norwich AC "Bouncy Squad", and my athletics coaches Denis Costello, Lizzie Costello and Michael Brown - I could not have completed this project without the distractions (and pain) you gave me. Finally, I must give a special mention to my amazing parents who have always been there when I have needed them.

“Just because they say it’s impossible doesn’t mean you can’t do it”

Sir Roger Bannister CH CBE

1. Introduction

1.1 Tuberculosis

In 2017 tuberculosis was the 9th biggest killer worldwide, and the biggest killer via an infectious agent (WHO, 2018a). In 2016 there were an estimated 10.4 million new cases of tuberculosis causing approximately 1.3 million deaths in HIV-negative patients. Within these cases an estimated 558,000 new cases were classified as drug-resistant with approximately 82% of these being multidrug-resistant (resistant to 2 or more of the first line drugs). These were most prevalent in China, India and the Russian federation (WHO, 2018a) (Figure 1.1.1).

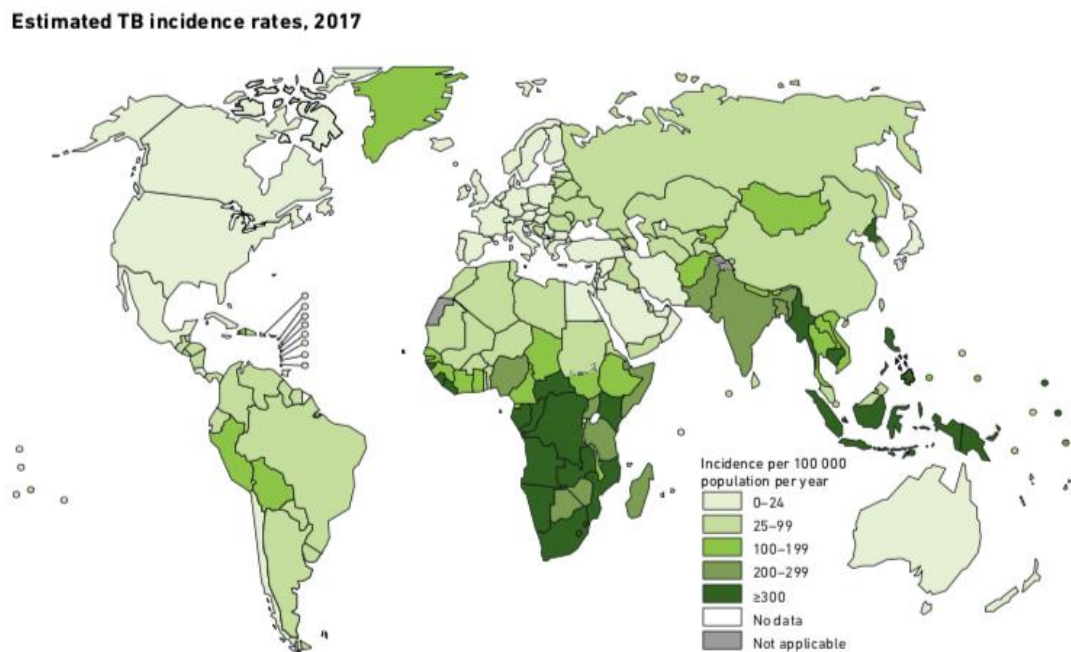


Figure 1.1.1: World map of the estimated new tuberculosis cases recorded per 100,000 population in 2017, indicating the worst affected areas to be south-east Asia and sub-Saharan Africa. Figure reproduced from Figure 3.4 (WHO, 2018a).

Tuberculosis is caused by the bacterium *Mycobacterium tuberculosis* (Mtb). Primarily it causes a pulmonary disease which spreads as an airborne pathogen. The difficulty with Mtb is that it commonly infects without resulting in an active infection (Styblo, 1980, Comstock, 1982). This non-active latent disease state is formed when the bacteria become encased in an immune response causing a granuloma to form in the lower respiratory tract. In this latent state of infection, the patient is unable to spread the disease, nor do they experience any symptoms. There are several different known pathologies of the granuloma but the classical caseous granuloma is the most widely studied. In this case the Mtb is surrounded by immune cells

including macrophages and dendritic cells, which are encased by both B and T cells. It is thought that fibroblasts encase the whole structure (Barry *et al.*, 2009) (Figure 1.1.2).

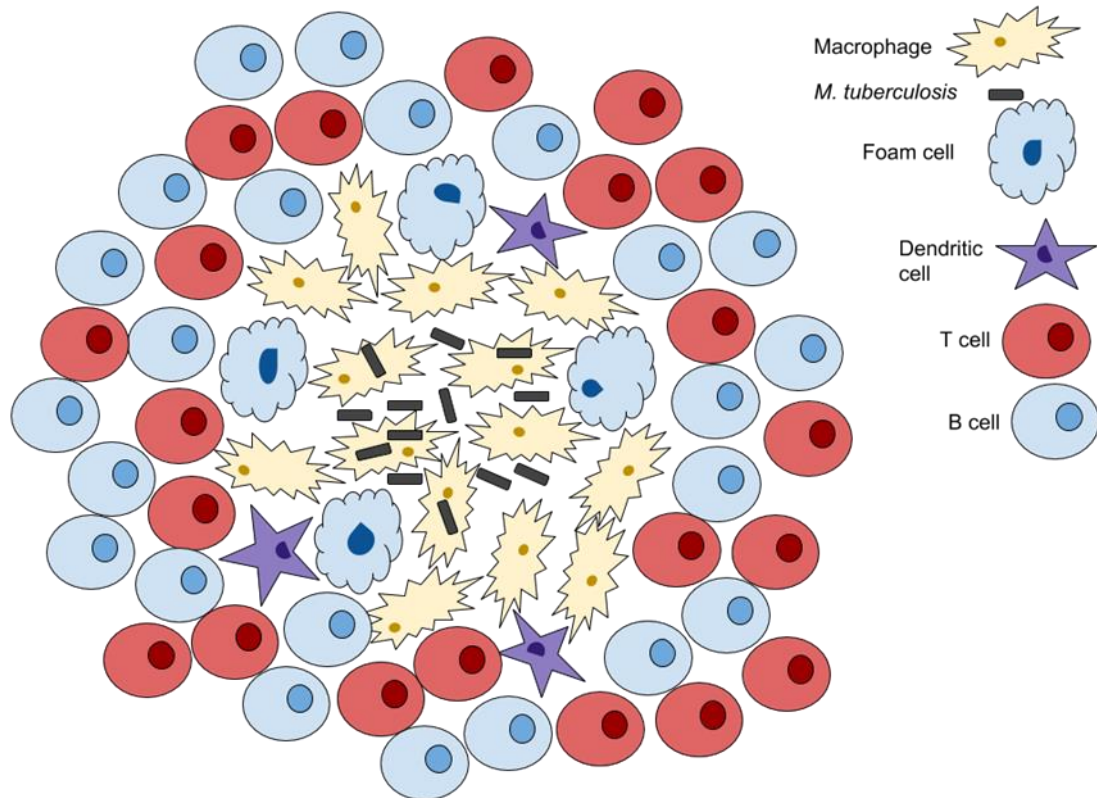


Figure 1.1.2: Cartoon representation of a representation of a classical granuloma containing *M. tuberculosis* typically found in the lungs. The *M. tuberculosis* cells are encased within or surrounded by macrophages which are surrounded by foam cells and dendritic cells. This layer of immune cells is then encapsulated by T and B cells. The *M. tuberculosis* inside the granuloma appear to enter a dormant state where they are not actively replicating, nor have they been killed. Adapted from (Ramakrishnan, 2012) and (Cadena *et al.*, 2017).

In many cases the patient will die from other causes unaware that they were infected with latent tuberculosis, however, in a percentage of cases the infection will progress into an active disease state causing tuberculosis (Saunders and Britton, 2007). It is more common for the infection to progress to an active disease state in patients that become immuno-compromised, and especially those who are co-infected with HIV/AIDS (Selwyn *et al.*, 1989). Currently, there is no clear evidence as to what causes the progression of the disease from a latent to an active disease state. For the most part even if a latent disease is discovered it is left untreated until an active infection is detected. This is largely because there is a major issue with

incomplete treatment of latent infections causing resistance, and complications treating any subsequent infections.

1.2 Current treatments

The current BCG vaccination programme was introduced in 1921, and is generally accepted to be only between 60-80% effective against the most severe forms of childhood meningitis tuberculosis infections, and less effective in pulmonary infections (Trunz *et al.*, 2006, Rodrigues *et al.*, 2011, Roy *et al.*, 2014). As the disease burden cannot be fully prevented even through complete vaccination, it is important to have effective treatments for those cases that are able to occur. At present there is only one approved standard course of treatment against tuberculosis – this is known as DOTS (directly observed treatment, short course) which consists of treatment via isoniazid and rifampicin for 6 months and additional treatment with pyrazinamide and ethambutol for the first 2 months (or longer as removal requires the pathogenic strain to be first identified as fully drug-sensitive) (WHO, 2010). Where a person is deemed to have drug-resistant TB they are treated using second line anti-tuberculosis treatments including a fluoroquinolone such as moxifloxacin or levofloxacin (WHO, 2010). It is recommended wherever possible to use different drugs from unique drug classes depending on the sensitivity of the infection (Table 1.2.1). Where the susceptibility of a drug is unknown it should be assumed that the strain is susceptible, but once resistance has been confirmed, drugs should not be used if there is a possibility of cross-resistance (WHO, 2010).

1.2.1 Treatment for co-infection with HIV/AIDS

With an estimated 374,000 tuberculosis deaths being in the patient group that were co-infected with HIV/AIDS in 2016, it is highly important to keep developing new strategies for treating these patients (WHO, 2017). However, there are additional challenges faced when treating patients who are co-infected with both tuberculosis and HIV/AIDS. This is primarily due to drug interactions between the anti-tuberculosis and anti-viral treatments leading to decreased efficiency of the drugs alongside increased toxicity (Zumla *et al.*, 2013). Currently, it is recommended that all patients begin a course of the DOTS tuberculosis treatments as above, alongside a treatment program of co-trimoxazole and anti-retroviral treatment to treat the HIV infection (WHO, 2010). This has led to a drive to create a novel treatment plan for those co-infected to treat susceptible strains in this patient group.

Table 1.2.1: Treatment groups of drugs against tuberculosis defined to be drug-resistant. Table adapted from Table 2 (WHO, 2018c).

Group	Drug
A: Include all three medicines	Levofloxacin OR Moxifloxacin Bedaquiline Linezolid
B: Add one or both medicines	Clofazimine Cycloserine OR Terizidone
C: Add to complete the regimen and when medicines from Groups A and B cannot be used	Ethambutol Delamanid Pyrazinamide Imienem-Cilastatin OR Meropenem Amikacin (OR Streptomycin) Ethionamide OR Prothionamide <i>p</i> -aminosalicyclic acid

1.2.2 Treatment of latent tuberculosis

Recent estimates predict that approximately 23% of the world population is currently infected with latent tuberculosis (LTBI) (Houben and Dodd, 2016). As discussed in section 1.1, LTBI is an asymptomatic state where the infective agent (*M. tuberculosis*) is encased and non-transmissible. In this state there is no immediate risk to the patient therefore treatment is not imperative. It is only recommended to treat a fraction of LTBI cases where there is a greater risk of developing the active disease, these include those with a HIV infection and those in low burden countries who are currently in prison, homeless or are illicit drug users (WHO, 2015). The currently used programme to treat LTBI is currently a 6-9 month course of isoniazid or a shorter 3-month course using a combination of rifampicin or rifapentine alongside isoniazid (Esmail *et al.*, 2012, Esmail *et al.*, 2014, WHO, 2015). The major issue with these treatment programmes is that because isoniazid mainly kills only replicated bacilli, it therefore may not kill the potentially non-replicating bacteria in the granuloma (Fox *et al.*, 1999).

1.3 Mycobacterial infections

Apart from tuberculosis there are several other infectious species within the *Mycobacteria* genus. These include infections such as bovine tuberculosis (*M. bovis*) and marine tuberculosis (*M. marinum*) alongside less infective environmental mycobacteria such as *M. smegmatis*. This gives the opportunity to study less infective bacteria in the laboratory in the place of *M. tuberculosis* as they contain several unusual properties as well as giving the option to look at homologues of proteins and enzymes.

1.3.1 Mycobacterial properties

Amongst the unusual properties of *Mycobacteria* is the distinctly slower growth rate than typical laboratory bacteria such as *Escherichia coli*. Typically, the doubling time for *Mycobacteria* is in the range of several hours to several days rather than around half an hour for *E. coli* (Cole *et al.*, 2001, Cox, 2003). This has been determined for *M. tuberculosis* to be about 72 times slower whilst in log-phase (Musuka *et al.*, 2013). Many of the *Mycobacterial* enzymes are significantly slower in their functions and reduced in redundancy than those found in faster growing species, however, the debate remains of whether this is result or cause of the slower growth rate (Harshey and Ramakrishnan, 1977, Hiriyanna and Ramakrishnan, 1986, Stephan *et al.*, 2005). Additionally, several traditionally essential genes, which cause lethal knockouts in other bacteria are found not to be present at all within the *Mycobacterial* genome (Bercovier *et al.*, 1986, Stephan *et al.*, 2005). One particularly noticeable example is in the topoisomerases where only two have been functionally annotated within the genome although a third was at one point postulated (Cole *et al.*, 1998, Jain and Nagaraja, 2005).

Secondly, *Mycobacteria* are defined as Gram-intermediate (Reynolds *et al.*, 2009) due to the presence of their unusual cell wall which is made of the very hydrophobic lipid – mycolic acid (Figure 1.3.1). This has an extensive synthesis mechanism which has been exploited as a drug target. The lipidic nature of the mycolic acid cell wall structure also makes mycobacterial cells very hydrophobic. This unique cell wall structure, like that of the outer membrane of Gram-negative bacteria, also provides a useful function to the cell in modulating entry of potentially lethal compounds to the cells (Nikaido, 2001). Although, some molecules will still make it across the membrane the numbers are greatly decreased, and with an effective efflux system it means that although some molecules may effectively kill the function of an essential protein, they will not be active against whole cells unless they can actively cross the membrane. Limiting the range of effectiveness of several compounds against TB and other mycobacterial infections (Nikaido, 2001). This also means that there is the possibility of making a mycobacterial specific inhibitor which can permeate the mycolic acid cell wall efficiently but possibly with a lower degree of specificity to penetrate through other bacterial membranes.

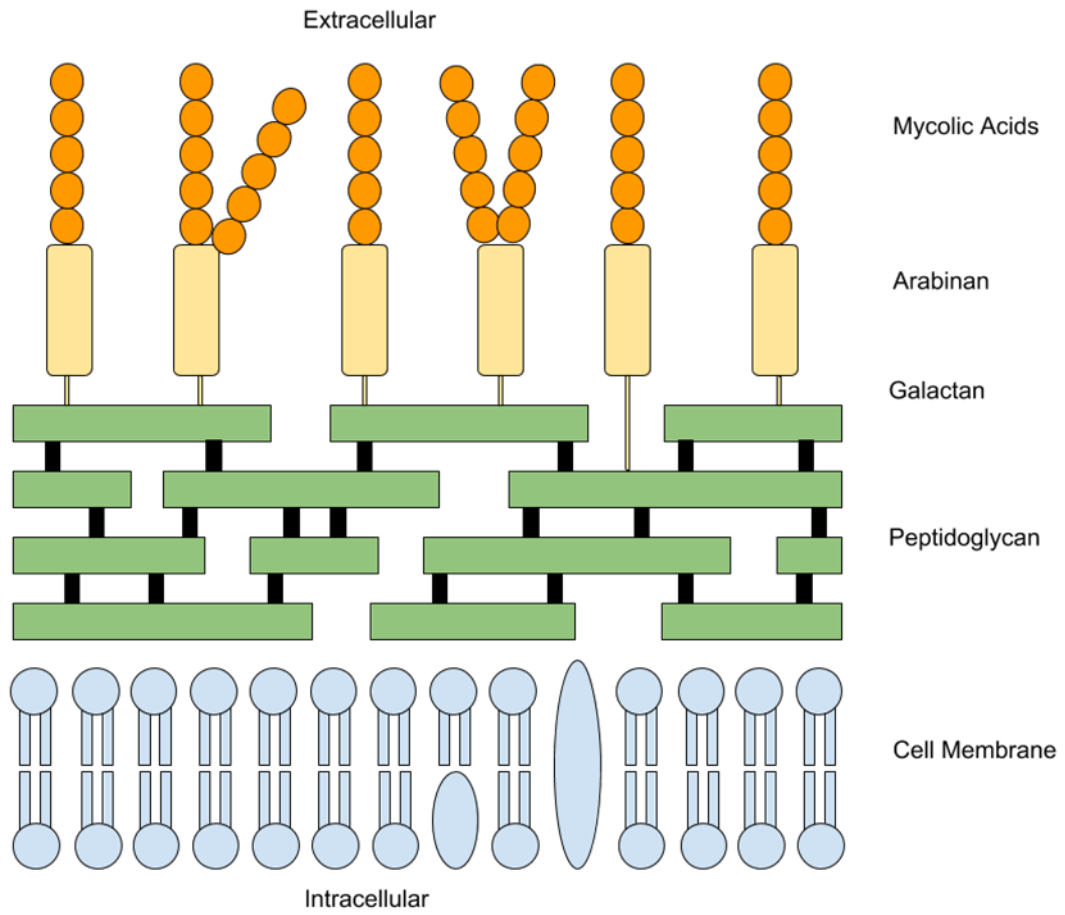


Figure 1.3.1: Cartoon representation of the Mycobacterial cell membrane and wall. The cytoplasmic or cell membrane is covered by a layer of peptidoglycan as with many other bacteria. The mycobacterial membrane then differs as this peptidoglycan membrane is further covered with a layer of arabinan and galactan which is additionally decorated with mycolic acids. This combination makes it very hydrophobic and difficult to penetrate.

1.3.2 Latent infections and granuloma formation

Granuloma is described by the Merriam-Webster medical dictionary (2018) as the “mass or nodule of chronically infected tissue with granulations that is usually associated with an infective process”. Although traditionally granuloma are primarily associated with tuberculosis infections, a wide range of bacterial and fungal species can cause them in both the human lungs and in other organs and species. However, they are a significant feature of mycobacterial infections forming in multiple different organs. For example, a *M. marinum* human infection commonly causes granuloma below the skin in what is known as “swimming pool granuloma”, but also causes these formations in their native fish hosts (Zumla and James, 1996). Typically, *M. tuberculosis* infections are initially isolated within granuloma most commonly within the lungs of infected patients long before any active infection may be discovered. This type of infection is difficult to identify in the lungs as a granuloma type

infection is commonly asymptomatic, with the current best method available for identifying the *M. tuberculosis* granuloma being the tuberculin skin test where a hypersensitivity response is observed in those with a latent infection (Esmail *et al.*, 2012, Lardizabal and Reichman, 2017).

Over recent years there have been developments into increasing our understanding classification of the granuloma and disease progression, although this is still not fully understood. However, the major importance of the granuloma is to provide an immune state in which the bacteria are surrounded by immune cells to contain the infection, but not eradicate the infection meaning that the infection can be induced at a later time, for example if a patient becomes immunocompromised in later life (Flynn and Chan, 2001). Furthermore, while the bacteria are contained within a granuloma it is thought that they have a significantly lower metabolic rate, which significantly decreases the effect of many antibiotics on them (Norton and Holland, 2012). Currently the preferred treatment for LBTI is a monotherapy course of isoniazid for 6 months, although shorter 3 months treatment courses of rifampicin or rifapentine with isoniazid in high TB incidence countries may be considered. These additional options along with a 3-4 months course of rifampicin monotherapy may be considered in low TB incidence countries (WHO, 2018b).

1.3.3 *Mycobacterium smegmatis* as a homologue

M. smegmatis was first identified in 1884, it is a common environmental mycobacterium which is rarely found to be a human pathogen (Tsukamura, 1976). On the few occasions when it has been identified as a human pathogen, it has mostly been described as forming skin lesions around wound sites (Newton *et al.*, 1993, Shimizu, 2012, Saffo and Ognjan, 2016). In only one case it was described to be like a typical *M. tuberculosis* lung infection (Vonmoos *et al.*, 1986) and once described as a systemic infection leading to death of an immune-deficient child (Pierre-Audigier *et al.*, 1997). Interestingly, there has also been a canine case described within the literature (Grooters *et al.*, 1995), although it is not normally a human or animal pathogen.

In addition to its potential to cause tuberculosis like infections, *M. smegmatis* has significant advantages as a laboratory bacterium as a surrogate. The major difference is that *M. smegmatis* is classed as a fast-growing *Mycobacterium*, which means that it has a doubling time in the order of hours not days (Cox, 2003), whilst maintaining a similar cell wall structure and having

a high degree of sequence homology within essential genes. This is underlined in the fact that *M. smegmatis* is classified within group 4 of the Runyon classification of mycobacteria with the other rapid growers (Runyon, 1959). The combination of the decreased pathogenicity, pathogenicity control and increased growth rate, makes *M. smegmatis* an ideal laboratory bacterium to use to study the effect of compounds on growing mycobacteria.

1.3.4 *Mycobacterium thermoresistibile* as a homologue

M. thermoresistibile is a thermophilic opportunistic pathogenic bacterium first described in 1966 (Tsukamura, 1966). Although the infection is relatively unheard of, 6 human and 2 feline infection reports have been described in the literature. The first human infection was described in 1981, within a female patient suffering from a tuberculosis-like infection with Langhans type granulomas which were successfully treated with rifampicin, ethambutol, and streptomycin (Weitzman *et al.*, 1981). As in many of the cases that have been described, the bacterial growth appears like that of *M. tuberculosis* except much faster with growth able to occur at 45°C, with viable growth recorded up to 52°C (Tsukamura, 1971, Weitzman *et al.*, 1981). Although, the initial case seemed to occur in a healthy individual several of the other case reports have occurred in individuals with significant health issues including diabetes mellitus. Furthermore, by no means is this disease limited to the lungs, as only two cases in humans and one in cats have been isolated as a pulmonary disease (Weitzman *et al.*, 1981, Liu *et al.*, 1984, Foster *et al.*, 1999). The second feline case was described primarily as having granuloma dermatitis, with skin lesions containing the bacterium (Willemse *et al.*, 1985). A similar case to this was found 3 months post-heart transplant near to the surgical scar, and importantly in this case the bacterium was found to be isoniazid-resistant (Neeley and Denning, 1989). The final three recorded cases were all associated with external implants with lesions or granuloma-type structures forming around the implant sites with the implants all being removed retrospectively. These were a mammoplasty implant (Wolfe and Moore, 1992), knee replacement (LaBombardi *et al.*, 2005) and surgical pin post tibia fracture (Suy *et al.*, 2013). All of these infections were successfully identified and treated using long term combination therapies.

Recently, the advantage of using thermophilic homologues to generate more stable enzymes has been routinely employed to gain improved structural and biochemical data. The use of *M. thermoresistibile* as a source of mycobacterial thermophilic homologues was first described in 2012 (Edwards *et al.*, 2012). Their reason for suggesting it as a homologue was due to its increased thermal stability due to its ability to grow at a higher temperature range than *M.*

tuberculosis while exhibiting similar infection symptoms as described above. At present, there are 35 entries in the protein data bank of structures of proteins from *M. thermoresistibile* including the structures of alpha-1,4-glucan:maltose-1-phosphate maltosyltransferase (GlgE) (Mendes *et al.*, 2015) and nitrilotriacetate monooxygenase component B (Zhang *et al.*, 2011).

Like *M. smegmatis* there is a high degree of conservation within the cell wall structure and good sequence homology in the essential genes with those from *M. tuberculosis*. Likewise, there is a high sequence homology between the gyrase genes with 91% identity in the GyrA and 88% in the GyrB protein sequences, as compared to 43% identity GyrA and 48% identity GyrB to the *P. aeruginosa* enzymes (Figure 1.3.2). This makes the *M. thermoresistibile* DNA gyrase homologues interesting candidates for both structural and mechanistic studies.

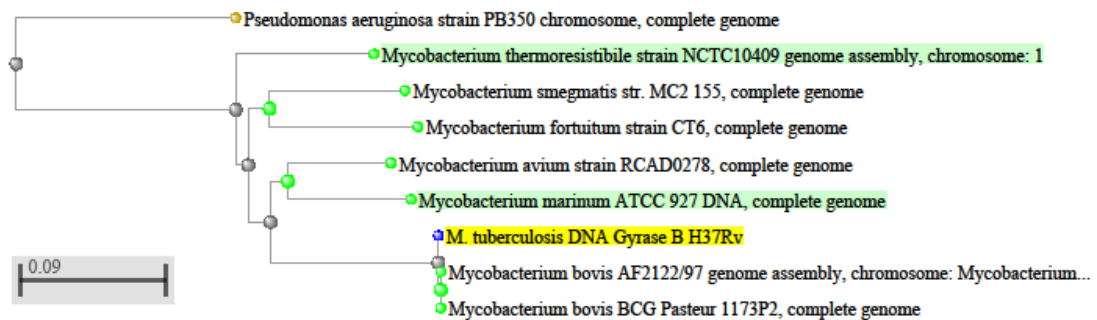


Figure 1.3.2: Phylogenetic tree of DNA gyrase B based on sequence from *M. tuberculosis* H37Rv. Alignment and sequence comparison made using BLASTn function of NCBI webserver, with distances being estimated via the same server. Alignment shows very little divergence in the DNA gyrase B gene within the *Mycobacterium* genus. Gram-negative *Pseudomonas aeruginosa* is included as a reference point.

1.3.5 Mycobacterial biofilms

Although our modern understanding of biofilms was formed as recently as 1978 (Costerton *et al.*, 1978), mycobacteria have been described for much longer as forming “aggregates” in solution, which are similar in nature to what we now think of as a biofilm (Löwenstein, 1920, Calmette, 1936). Furthermore, it has been known for a number of years that environmental mycobacteria are able to form biofilms, for example *M. avium* biofilms have been observed within the water pipes of large cities (Falkinham *et al.*, 2001, Norton *et al.*, 2004). Unusually, these mycobacterial biofilms form on both on surfaces as well as at the air-media boundary. This is in part due to the unique highly lipophilic mycolic acid cell wall that is present in all mycobacteria and allows mycobacteria to adhere to each other and surfaces (Ojha *et al.*, 2008,

Richards and Ojha, 2014). These biofilms formed by mycobacteria must have different characteristics to biofilms produced by other bacterial species as they lack several of the key components that promote biofilms in other species. These include the pili and fimbriae, as well as exopolysaccharide components of the extracellular matrix (Menozzi *et al.*, 1996, Zamora *et al.*, 2007).

The first known report of *M. tuberculosis* biofilms created within a laboratory system came in 2008 (Ojha *et al.*, 2008). There have also been historical cases presented in the literature where *M. tuberculosis* has been attributed as the cause for biofilm-like structures on implants (Spinner *et al.*, 1996, Sendi and Brent, 2016). However, only recently it has been demonstrated that within an *in vitro* granuloma model, that *M. tuberculosis* is capable of forming biofilms with a requirement for the presence of MmpL (mycobacterial membrane protein large). Although this has not been demonstrated *in vivo*, it suggests that mycobacterial biofilms may be important in the granuloma state. Indeed, there have been reports of non-tuberculosis mycobacterial species colonising the lungs sites of scarring caused by previous infections in a biofilm type infection (Wolinsky, 1979). These infections first form a biofilm then can colonise the host causing repeated infections. These repeat infections are likely to be because of increased resistance of the biofilm phenotype to antibiotics, which has been reported to be up to >100,000-fold increase in the MBEC (minimum biofilm eradication concentration) value compared to the MIC₁₀₀ value in four rapidly growing mycobacterial species (Munoz-Egea *et al.*, 2015). Overall, this makes the phenomena of mycobacterial biofilms a highly interesting and clinically relevant target to study to find new antimycobacterial agents that can effectively kill biofilms in addition to whole cells.

1.4 DNA topology

DNA topology is the three-dimensional geometry of DNA, typically this is thought of on the level of supercoiling within the cells – the ability of DNA to over or under-wind to produce more compact structures. However, the topic also covers knotting and catenation – how different pieces of DNA are intertwined. These topics are highly relevant when considering replication, transcription, and recombination of DNA, where the three-dimensional shape of the DNA is highly relevant in the initiation and propagation of all three processes.

In the absence of topoisomerases, the process of DNA replication would not be able to occur as positive supercoils would build up ahead of the replication fork. As replication approaches

the terminus there is a decreased amount of space for the positive supercoils to form, and hence a build-up of precatenanes occurs after the replication fork (Figure 1.4.1) (Postow *et al.*, 2001). Both of these features are highly dangerous for the cell if not resolved. In bacteria the relaxation of positive supercoils is processed mainly by DNA gyrase, which subsequently introduces negative supercoils into the DNA (Baker *et al.*, 1986), although topo IV is also able to remove positive supercoils (Khodursky *et al.*, 2000). In the absence of topo IV, DNA gyrase is solely responsible for this process in mycobacteria (Figure 1.4.1) (Manjunatha *et al.*, 2002, Aubry *et al.*, 2006a). On the other hand the precatenanes that are formed after the replication fork are commonly resolved by the type I topoisomerase topo III if there are nicks present in the DNA (Hiasa and Marians, 1994, Nurse *et al.*, 2003) or alternatively by topo IV (Zechiedrich and Cozzarelli, 1995), but, as neither of these enzymes are present in mycobacteria, it is DNA gyrase and topo I that must instead work together to resolve these structures (Figure 1.4.1). The daughter chromosomes produced by bacterial transcription are often found to be catenated, and hence must be decatenated before completion of cell division can occur (Wasserman and Cozzarelli, 1986). These catenanes are thought to be most commonly decatenated by topo IV (Adams *et al.*, 1992, Zechiedrich and Cozzarelli, 1995), although there is evidence that DNA gyrase is also capable of doing this as well (Steck and Drlica, 1984).

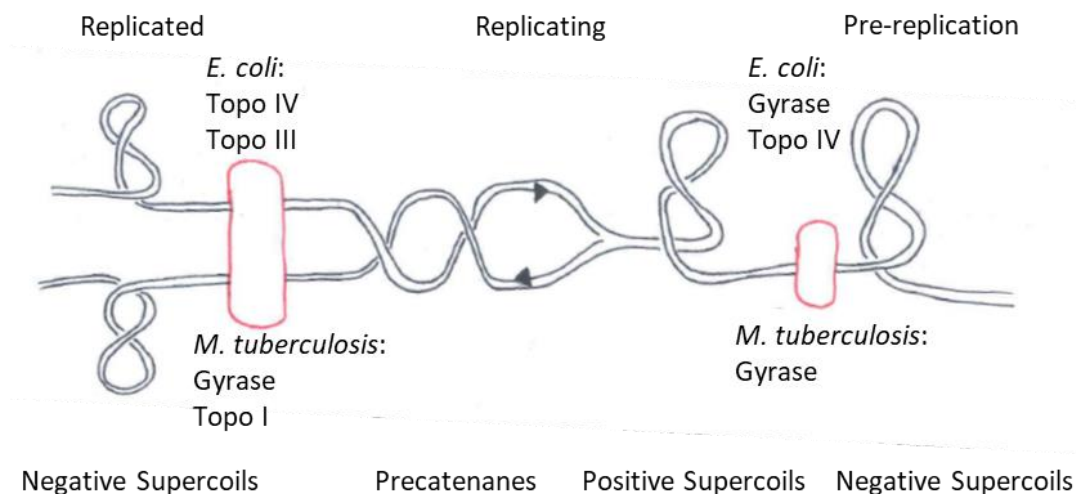


Figure 1.4.1: Topology diagram at the replication fork indicating the need for topoisomerases to remove the positive supercoils that accumulate before the replication fork and the precatenanes that associate after the replication fork. As *M. tuberculosis* does not have topo III or topo IV it relies on its remaining two topoisomerases, DNA gyrase and topo I, to remove the precatenanes and solely on DNA gyrase to remove the positive supercoils. Figure adapted from (Postow *et al.*, 2001) and (Higgins, 2007).

The second process where topoisomerases are crucial is in that of transcription. This is the process by which double-stranded DNA is opened to allow binding of RNA polymerase which allows mRNA to be transcribed for processing by the ribosome (Figure 1.4.2). When the DNA is opened it creates positive supercoils ahead of transcription and negative supercoils behind transcription as the RNA polymerase complex is unable to move around the DNA, hence the DNA moves around RNA polymerase; this process is known as creating “Twin Supercoiled Domains” (Liu and Wang, 1987, Wu *et al.*, 1988). The twinned supercoiled domains need to be resolved to ensure that the plasmid maintains an optimal negative supercoiled state. The positive supercoils ahead of transcription are relaxed by DNA gyrase and topo IV, meanwhile negative supercoils are introduced by DNA gyrase. The excess negative supercoils behind transcription are relaxed by topo I and topo IV (Zechiedrich *et al.*, 2000). In the absence of both topo III and topo IV in mycobacteria the positive supercoils are resolved by DNA gyrase and the excess negative supercoils by topo I and to a lesser degree DNA gyrase (Cole *et al.*, 1998).

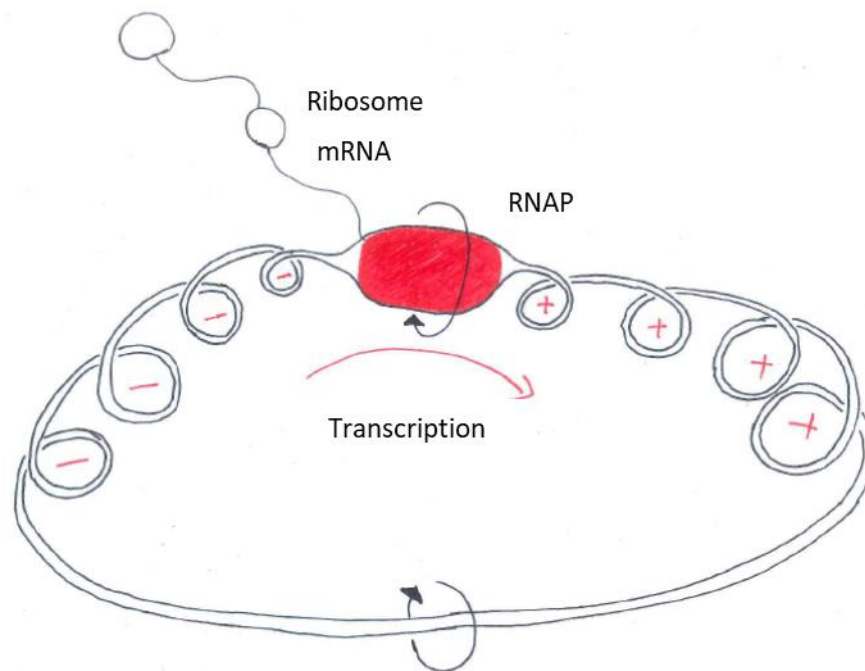


Figure 1.4.2: Topology diagram at the site of transcription where the DNA is separated to give access to RNAP to allow mRNA to be transcribed and proteins to be made by the ribosomes. Separation of the DNA strands results in negative supercoils to accumulate before the site of transcription and positive supercoils to be introduced after the site of transcription. Figure adapted and redrawn from (Wu *et al.*, 1988)

Finally, the process of recombination by which the chromosomes are rearranged to maintain genetic diversity by general and site-specific methods has important implications on topology, as these processes can result in catenated or knotted DNA products (Abremski *et al.*, 1983, Azaro and Landy, 2002). These interlinked and knotted products are resolved by the topoisomerase enzymes.

1.5 DNA topoisomerases

DNA topoisomerases are found in all domains of life and can be broadly split into two different classes which are known as type I and type II topoisomerases, depending on whether they cleave one or two stands of double stranded DNA in the process of altering DNA topology. These classes can be further split depending on structural and mechanistic features of the enzymes (Table 1.5.1).

1.5.1 Type IA topoisomerases

Type I topoisomerases cause transient single-stranded breaks in DNA. The type IA enzyme family have a 5' phosphate attachment to DNA during the process of single-strand breakage (Champoux, 2002). They do this with a preference for binding to a short single-stranded region of DNA within negatively supercoiled DNA (Wang, 2002). This group of topoisomerases share a common TOPRIM domain that is also found in type II topoisomerases and in the DnaG-type primases (Aravind *et al.*, 1998). This family of topoisomerases are only able to relax negatively-supercoiled and not positively-supercoiled DNA as they are only able to unpair the helix of negatively supercoiled DNA to produce a single-stranded region (Kirkegaard and Wang, 1985).

There are several enzymes classified into this group including bacterial topoisomerase I (topo I), and topoisomerase III (topo III) which is found in all three life kingdoms (Wang, 2002), as well as reverse gyrase which is exclusively found in thermophilic and hyperthermophilic eubacteria (Lulchev and Klostermeier, 2014). One point of note is that topo III, which traditionally is a relaxing and decatenation enzyme of DNA, has also been found to have the ability to cleave and relax RNA, making it one of the only known RNA topoisomerases (Wang *et al.*, 1996).

Table 1.5.1: Classification of DNA topoisomerases, with reference to reactions that each group is known to carry out, and where each of the topoisomerases are known to be present. Classification is mainly based on structural and mechanistic features.

Classification	Reactions	Enzymes	Species
Type IA	Relax negative supercoil	Topo I	Bacterial
	Decatenate ssDNA	Topo III	Eukaryotic, Prokaryotic, Archaeal
		Reverse gyrase	Thermophilic/ Hyperthermophilic archaea
Type IB	Relax negative and positive supercoils	Topo I	Eukaryotes, Virus
Type IC	Relax negative and positive supercoils	Topo V	Hyperthermophilic archaea
Type IIA	Relax negative and positive supercoils	Topo IV Topo II	Bacteria Eukaryotes, Bacteriophage
	Decatenate DNA		
	Relax negative and positive supercoils Decatenate DNA Negative supercoil	DNA gyrase	Bacteria, plants and possibly plasmodia
Type IIB	Relax positive and negative supercoils	Topo VI	Archaea, plants and possibly plasmodia
	Decatenate DNA	Topo VIII	Bacteria, Archaea

Bacterial topo I, including that from *M. tuberculosis*, has been described to be an efficient drug target, however, presently there are no clinically approved drugs against this target (Nagaraja *et al.*, 2017).

1.5.2 Type IB topoisomerases

The type IB topoisomerases have major differences to the type IA topoisomerases in their mechanism whereby the IB enzymes attach to the 3' phosphate as opposed to the 5' phosphate while causing single-stranded breaks allowing for alteration in the topology of DNA (Champoux, 2002). The IB enzymes, in contrast to the IA enzymes prefer binding to duplex

DNA after the cleavage of the single strand. This has led to the conclusion that the mechanism of action is through “controlled rotation”, by which the protein provides a controlled environment where a nicked piece of DNA can rotate to alter the supercoiling number in steps of 1 before religation of the nick (Redinbo *et al.*, 1998). Additionally, the structures of this group are unique from the IA enzymes (Redinbo *et al.*, 1998).

This group of enzymes is mainly confined to eukaryotic topo I – a relaxing enzyme which can relax both positive and negative supercoils in DNA (Wang, 2002). In addition to the eukaryotic topo I enzymes, this group also contains viral topoisomerase enzymes such as that from the vaccinia virus (Stivers *et al.*, 1997). This means that therapeutically the inhibition of this group of topoisomerases is limited to just anticancer and antiviral treatments. Presently Camptothecin is clinically used to inhibit human topo I for anticancer treatments (Ulukan and Swaan, 2002, Wethington *et al.*, 2008)

1.5.3 Type IC topoisomerases

To our current knowledge, the type IC topoisomerase group is unique to just topoisomerase V from the hyperthermophilic archaea *Methanopyrus kandleri* (Slesarev *et al.*, 1993, Taneja *et al.*, 2006, Rajan *et al.*, 2010). This topoisomerase is unusual due to its additional role in DNA repair, and high proportion of (HhH)₂ folds (Belova *et al.*, 2002, Forterre, 2006). Topoisomerase V is able to relax both positive and negatively supercoiled DNA through use of a rotational and swivel mechanism of action, utilising a single-nicked strand with a phosphotyrosine bond at the 3' end between the enzyme and the DNA (Slesarev *et al.*, 1993). It is known that the reaction of this enzyme is independent of ATP and magnesium ions like the type IA enzymes, and is also active in a wide range of salt conditions and temperatures above 65°C (Slesarev *et al.*, 1993). Although the mechanism of this type of topoisomerase is very similar to the type IB enzymes they have distinct structural features determining topoisomerase V to be classed as a type IC enzyme (Forterre, 2006).

Due to the limited species containing this class of topoisomerases, it has not investigated for medicinal use as; no known pathogenic species have currently been identified to encode a type IC topoisomerase.

1.5.4 Type IIA topoisomerases

The type IIA topoisomerases was the first discovered class of topoisomerases which alter the topology DNA by using double-stranded breaks (Liu *et al.*, 1980). Classified into the type IIA class is eukaryotic topoisomerase II (topo II), bacterial DNA gyrase and topoisomerase IV (topo IV) as well as bacteriophage topo II. Structurally, all three of these enzymes have a high degree of homology with all the enzymes in the classification containing the same domain arrangement, with several conserved featured including the TOPRIM (topoisomerase primase) domain, also found in type IA topoisomerases, and a catalytic tyrosine (Figure 1.5.1). The TOPRIM domain is structurally conserved consisting of around 100 amino acids found in some topoisomerases as well as DnaG-type primases and small primase-like proteins in bacteria and archaea (Aravind *et al.*, 1998). Although eukaryotic topo II forms dimers, whereas heterotetramers are formed by bacterial DNA gyrase and topo IV. Bacteriophage topo II has been reported to contain three subunits arranged into a heterohexameric arrangement (A₂B₂C₂) (Liu *et al.*, 1979, Seasholtz and Greenberg, 1983). There is significant evidence that all of these genes have a common ancestor, although from an evolutionary perspective they cluster into their respective groups of eukaryotic topo IIs including eukaryotic viral topoisomerases, T4 bacteriophage topo II, and the final group containing the bacterial type IIA topoisomerases sub-divided into topo IV and DNA gyrase (Forterre *et al.*, 2007).

The type IIA topoisomerases all form three major dimer interfaces, this results in the formation of two DNA gates, which is important in the conserved mechanisms of these enzymes (Berger *et al.*, 1996, Roca *et al.*, 1996). The mechanism of actions of all the enzymes causes a change in the linking number of DNA to change by 2 units per reaction cycle or to a knotting/unknotting reaction of DNA through the hydrolysis of two ATP molecules depending on the location of the two DNA segments (Brown and Cozzarelli, 1979, Bates *et al.*, 2011). The reaction mechanism is initiated by the formation of a dimeric or tetrameric enzyme in complex with DNA. ATP binding allows for cleavage of a gate segment of DNA and transport of the transport DNA segment through the gate segment. After passage of the transport segment of DNA religation of the gate segment occurs and release of the DNA through the C-gate with a change in the topology (Baird *et al.*, 1999). In addition, in the reaction cycle both ATP molecules are hydrolysed, although the exact timing of this is unknown (Figure 1.5.2). The directionality of the change in linking number (positive vs negative) may be determined by the wrap of the DNA around the CTDs (Kampranis and Maxwell, 1996). Eukaryotic topo II, bacterial topo IV and bacteriophage topo II are all relaxing enzymes of both positive and negative supercoils, and can decatenate DNA (Goto and Wang, 1982, Kreuzer and Jongeneel, 1983, Kato *et al.*, 1990). DNA gyrase is able to relax positive supercoils and introduce

negative supercoils in relaxed DNA (Higgins *et al.*, 1978, Mizuuchi *et al.*, 1978). Additionally, DNA gyrase can relax negative supercoils in DNA in an ATP-independent fashion (Gellert *et al.*, 1977, Sugino *et al.*, 1977). All of the type IIA topoisomerases hydrolyse ATP in a DNA-dependent fashion, and the free energy provided by this reaction enables these enzymes to relax and decatenate DNA past the distribution possible by ATP-independent enzymes in a process known as topology simplification (Rybenkov *et al.*, 1997, Stuchinskaya *et al.*, 2009).

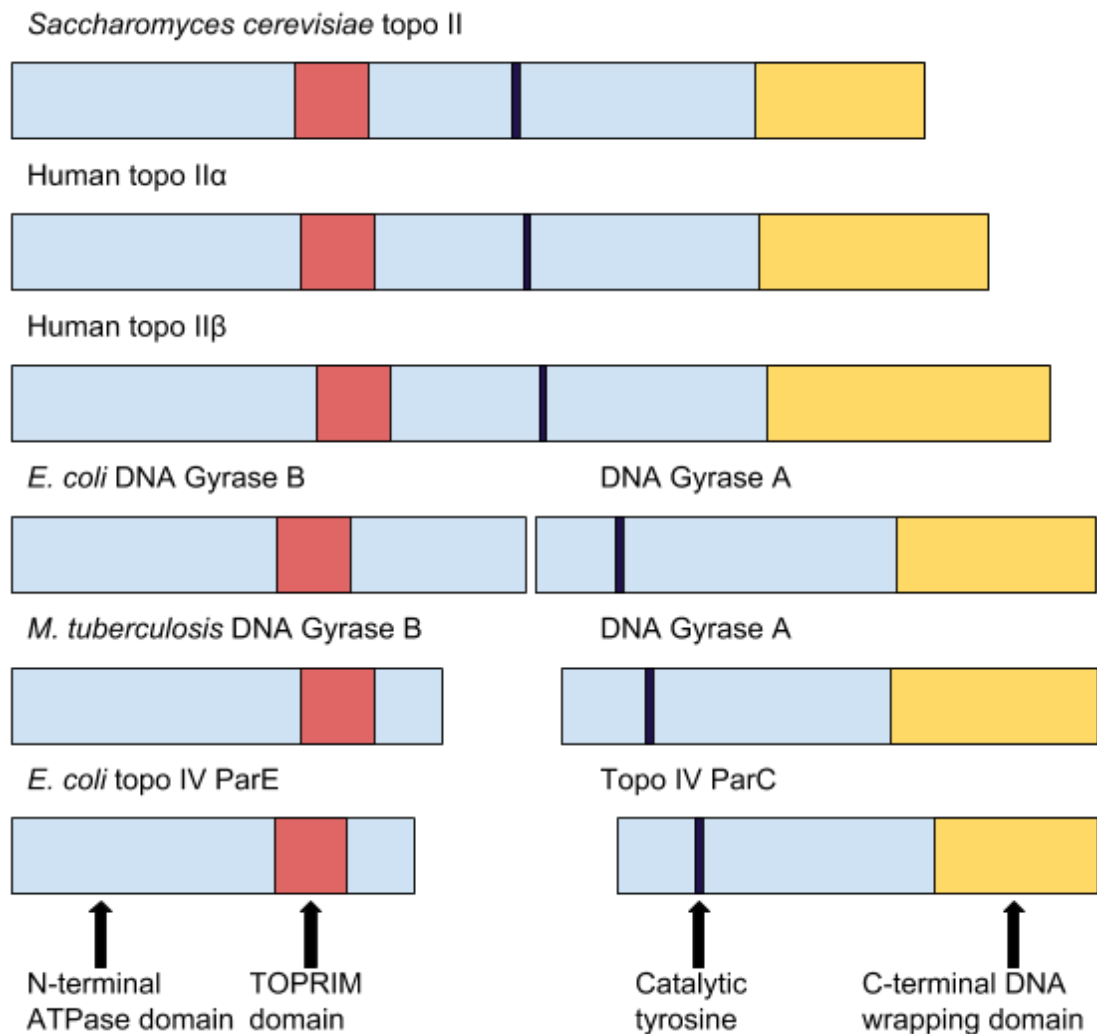


Figure 1.5.1: Domain alignment of eukaryotic and prokaryotic type II topoisomerases. The TOPRIM (topoisomerase-primase) domain is highlighted in pink, the catalytic tyrosine in purple and the C-terminal wrapping domain in yellow. The N-terminal ATPase domain is in the region between the protein N-termini and the TOPRIM domains of all of the proteins. All domains are to scale. The eukaryotic topo II proteins form active dimers, meanwhile the bacterial DNA gyrase and topo IV form active heterotetramers.

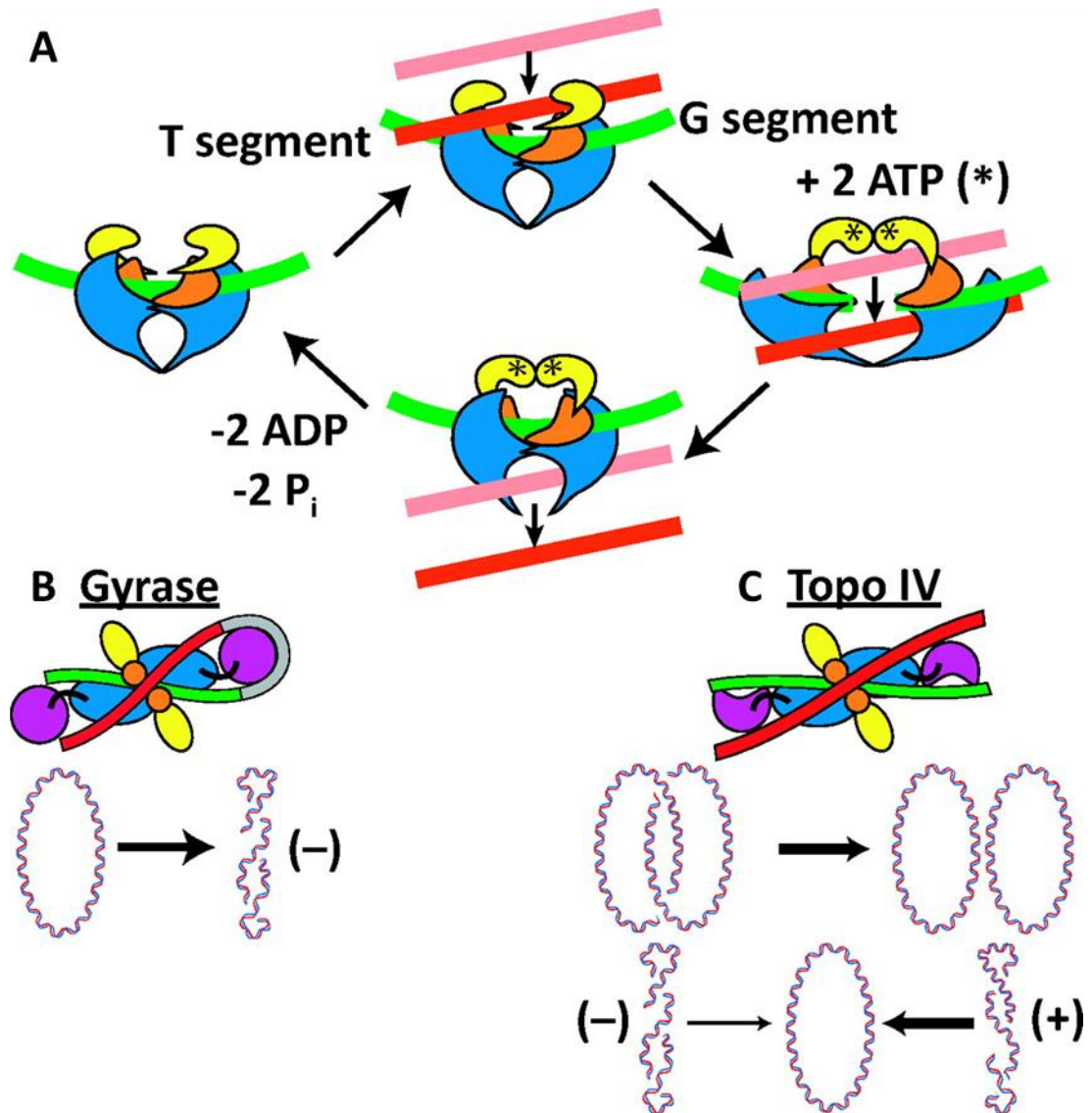


Figure 1.5.2: The likely strand-passage mechanism of action of the type IIA topoisomerases. A) The mechanism is initiated through the formation of a complex of two of each of the subunits with 2 ATP molecules in the N-terminal domains (yellow), and two segments of DNA known as the gate (G-segment) and transport (T-segments) segments. This is followed by cleavage of the G-segment of DNA (green) allowing passage of the T-segment of DNA (Pink/Red) through the G-segment. Subsequent hydrolysis of ATP allows for the complex to be reset ready for another reaction cycle. B) There is considerable evidence that DNA gyrase wraps a single piece of DNA around the CTDs in a positive supercoiled direction to allow for the introduction of negative supercoils. C) On the other hand, topo IV does not appear to wrap DNA around the CTDs, instead it preferentially decatenates and relaxes DNA. Figure adapted from (Neuman, 2010).

There is homology between the type IIA topoisomerase enzymes which is greatest at the N-terminals of the GyrA/ParC and GyrB/ParE subunits, including the ATPase domain (Hammonds and Maxwell, 1997). A substantial amount of work has been conducted on the

DNA gyrase ATPase domain from *E. coli* for the most part (see section 1.6.1). In addition, there has been a considerable effort to characterise this domain in yeast and human topo II(α) and a lesser effort in bacterial topo IV. Like DNA gyrase these enzymes all have significant stimulation of the ATPase activity by DNA, of between 4-fold for *S. pneumoniae* topo IV to 19-fold for yeast topo II (Lindsley and Wang, 1991, Hammonds and Maxwell, 1997, Laponogov *et al.*, 2018). This stimulation was found to be dependent on the presence of both ParC and DNA for topo IV. On the other hand, the eukaryotic topo II(α) could be stimulated by DNA in the absence of the C-terminal portion of the enzyme, although the length of DNA required was much shorter for the N-terminal domain on its own (Campbell and Maxwell, 2002). The kinetics of this mechanism appear to follow Michaelis-Menton kinetics in the absence of DNA, but instead have cooperative binding in the presence of DNA (Lindsley and Wang, 1991). In the case of *S. pneumoniae* the first structures of the ATPase domain bound to DNA has recently been shown confirming the predictions previously made for DNA gyrase (Wigley *et al.*, 1991, Laponogov *et al.*, 2018).

Although commonly bacteria have genes for both DNA gyrase and topo IV there are many occasions in nature when bacteria have been identified to only have DNA gyrase without topo IV. In single-cell eukaryotes such as *S. cerevisiae* only one copy of topo II is present whereas in higher eukaryotes such as *Homo sapiens* (humans) there are two copies identified labelled as topo II α and II β (Burden and Osheroff, 1998). Although DNA gyrase previously was thought to be predominantly a bacterial enzyme it has been recently found in plants including *Arabidopsis thaliana* and potentially some plasmodia species (Aravind *et al.*, 2003, Wall *et al.*, 2004).

This class of topoisomerases has been highly exploited in terms of medicinal use. This includes clinical use as an antibiotic target against both DNA gyrase and topoisomerase IV through the fluoroquinolones (Gellert *et al.*, 1977, Khodursky *et al.*, 1995) and as a target for anticancer treatments through inhibition of the human topo II enzymes by for example etoposide reviewed by Nitiss (2009). Recently, there have also been investigations into plant DNA gyrase in relation to generating novel herbicidal compounds (Wallace *et al.*, 2018), as well as the identification of DNA gyrase and topo VI plasmodium parasites having the potential for being a future target for anti-malarial compounds (Aravind *et al.*, 2003).

1.5.5 Type IIB topoisomerases

The type IIB topoisomerases, like the type IIA topoisomerases, also alter the topology of DNA through the use of double-stranded DNA breaks. These enzymes can both decatenate and relax negatively supercoiled DNA in an ATP-dependent reaction (Bergerat *et al.*, 1997). The main enzyme characterised within this class is that of the archaeal topoisomerase VI (topo VI) enzyme which is primarily found in archaea such as *Methanosarcina mazei* (Bergerat *et al.*, 1997), however more recently it has been discovered within the genomes of plants such as *A. thaliana* (Hartung and Puchta, 2000) and the *Plasmodium* parasites (Aravind *et al.*, 2003). Like the type IIA enzymes, structurally topo VI forms heterotetramers (A₂B₂), however, uniquely it only has two dimer interfaces, forming a single DNA gate (Bush *et al.*, 2015). A second topoisomerase VIII (topo VIII) has recently been added to this class of topoisomerases. It is the smallest known type IIB topoisomerase, and like human topo II it has the subunits fused to form a single subunit which dimerises. Presently topo VIII has only been identified in a small number of bacterial genomes and on plasmids from both bacteria and archaea (Gadelle *et al.*, 2014).

Currently, these enzymes are not used as drug targets although there have been recent attempts to utilise the plasmodium and plant topo VI enzymes as targets for antimalarial and herbicidal compounds (Bush *et al.*, 2018).

1.5.6 Topoisomerases in mycobacteria

It has been the wonder of the topoisomerase community since the genome of *M. tuberculosis* was published in 1998 (Cole *et al.*, 1998) that there were only two apparent topoisomerases identified – these being DNA gyrase and topoisomerase I, which is unusual but not unheard of in other species such as *Aquifex aeolicus* (Tretter *et al.*, 2010) which contains just one type IIA topoisomerase. Hence, there has been some suspicion that the mycobacterial DNA gyrase may have enhanced catalytic activities in the reactions that are traditionally thought of as topo IV reactions; these being enhanced relaxation and decatenation. The decatenation activity of DNA gyrase in *M. tuberculosis* has been reported as being up to 10-times more efficient than *E. coli* DNA gyrase, but still 25-times less efficient than the activity of *S. pneumoniae* topo IV (Aubry *et al.*, 2006a). This is somewhat like the results obtained by Manjunatha *et al.* (2002) who found that the *M. smegmatis* homologous gyrase has 7-times greater activity in decatenation than its *E. coli* homologue. In contrast the ATP-independent relaxation activities of both the *M. smegmatis* and *E. coli* gyrase enzymes were comparable needing a 10-fold increase in enzyme (Manjunatha *et al.*, 2002).

While the DNA gyrase found in *Mycobacteria* may appear to be slightly special in its ability to more effectively decatenate substrates than its Gram-negative homologues, there has also been a suspicion that there may possibly be further uncharacterised topoisomerases in the genome of these bacteria that are yet to be characterised. One potential novel topoisomerase was identified and somewhat characterised in *M. smegmatis* as a heterotetramer of two TopoN and two TopoM subunits (Jain and Nagaraja, 2005). Although there was little homology to other characterised topoisomerases, it appeared to relax negative supercoils in the presence of either ATP or dATP at a 10 nM concentration, as well as exhibiting decatenation activity on a similar level to that of *M. smegmatis* DNA gyrase. However, since the initial report of this putative type II topoisomerase it appears that there has been no further work carried out on this enzyme and it does not appear to have a homologue in *M. tuberculosis*.

1.6 DNA gyrase

DNA gyrase is a heterotetrameric enzyme first discovered in 1976 for its ability to introduce negative supercoils into DNA in an ATP-dependent manner (Gellert *et al.*, 1976), and has been studied in depth since. Initial studies revealed it to have a heterotetrameric active form consisting of two proteins – GyrA (97 kDa) and GyrB (90 kDa) for the *E. coli* enzymes (Higgins *et al.*, 1978, Mizuuchi *et al.*, 1978). The GyrA protein is largely associated with DNA binding and wrapping (Reece and Maxwell, 1991a, Reece and Maxwell, 1991b), while the GyrB protein has a role in ATP hydrolysis (Wigley *et al.*, 1991). Although the full-length DNA gyrase complex has never been solved by X-ray diffraction there have been several lower resolution structural studies (Costenaro *et al.*, 2005, Costenaro *et al.*, 2007, Baker *et al.*, 2011) and a recent cryo-electron microscopy structure to around 17 Å (Papillon *et al.*, 2013). These have somewhat confirmed the theorised structural arrangement proposed many years earlier, with a GyrB dimer sitting on top of the GyrA dimer, with DNA wrapping around the two GyrA CTD domains.

1.6.1 ATP hydrolysis and the GyrB N-terminal domain

One of the earliest observations indicated that DNA gyrase required ATP to insert negative supercoils into DNA (Gellert *et al.*, 1976). Initially it was assumed to require ATP hydrolysis and hence studies were carried out to confirm this. In the presence of ADPNP (non-hydrolysable ATP), DNA gyrase is only able to carry out one reaction cycle and is not able to be processive as it is in the presence of ATP (Sugino *et al.*, 1978). This is thought to be a

consequence of not being able to hydrolyse and hence release ADP from the enzyme; ADPNP remains tightly bound (Tamura *et al.*, 1992). This means that the enzyme is trapped in a DNA-bound form, and only limited incomplete supercoiling of a relaxed DNA substrate can be observed.

The first structure of any part of DNA gyrase to be solved was a 2.5 Å structure of the *E. coli* N-terminal 43 kDa domain of GyrB (GyrB43) (Wigley *et al.*, 1991). This structure was of a domain already known to be an ATPase (Ali *et al.*, 1993) and confirmed that ATP binding causes dimerization of GyrB, resulting in a 20 Å cavity for DNA binding. Although a cavity has been observed for DNA binding, no evidence for interaction of GyrB43 with DNA was initially determined, nor did it appear to form any interactions with the GyrA subunit (Ali *et al.*, 1993). Regardless of this, there is considerable evidence that DNA binding is important in the stimulation of the ATPase activity of GyrB (Maxwell and Gellert, 1984). It is indicated that in the case of the *E. coli* DNA gyrase heterotetramers either a fragment of 85±15 bp of DNA or higher concentrations of shorter fragments are needed to stimulate the ATPase activity, and from the data suggesting a sigmoidal dependence of short DNA fragment binding, it was inferred that two cooperative DNA binding sites must be occupied to stimulate ATPase activity (Maxwell and Gellert, 1984). Although approximately 85 bp are required to bind ATP it should be noted that this may not indicate the full DNA binding footprint, instead only the section required to induce the ATP hydrolysis reaction. No sequence specificity for induction of ATPase activity has been observed (Maxwell and Gellert, 1984), rather a preference for a substrate that appears to be a relaxed, linear or nicked form of double stranded DNA as opposed to one that is negatively supercoiled (Mizuuchi *et al.*, 1978, Sugino and Cozzarelli, 1980). Likewise, it has been shown that DNA gyrase from *M. tuberculosis* has a higher affinity for positively supercoiled DNA than other topological forms (Ashley *et al.*, 2017), and although this has not been demonstrated to induce ATPase activity it can be inferred.

Additional structural studies focusing on the GyrB43 domain indicate probable conformational changes in hydrolysis of the ATPase reaction (Stanger *et al.*, 2014). From solving a series of different crystal structures in the presence of different nucleotides and counter ions, they observed a 12° rotation opening the domain interface on hydrolysis of ATP. This appears to be independent of the tertiary γ -phosphate in ATP but appeared to be dependent on the presence of P_i as an intermediate structure was obtained when BeF_3 replaced P_i as the counter ion with ADP (Stanger *et al.*, 2014). This is important as it appears to suggest that a passage is opened for DNA to move through the GyrB molecule, assisting with the

mechanical role of the enzyme. Furthermore, from the structural and biochemical studies it was interpreted that DNA strand passage occurs prior to ATP hydrolysis and hence ATP hydrolysis is likely to be coupled to DNA release (Wigley *et al.*, 1991). There is still however, considerable doubt about the timings of ATP hydrolysis and ADP release in the mechanism of DNA gyrase.

Due to the dimerization of GyrB it is likely that two ATP molecules bind to the heterotetramer cooperatively (Maxwell and Gellert, 1986). The mechanism has been studied and it is hypothesised that the mechanism of DNA gyrase uses sequential hydrolysis of two ATPs, with the rate limiting step being the slow hydrolysis of the second ATP, with the second ATP hydrolysis resulting in a conformational change that allows for gate opening to release the DNA from the enzyme (Hartmann *et al.*, 2017). This would agree with the proposed mechanism for yeast topo II (Baird *et al.*, 1999), meanwhile the structural data presented above (Stanger *et al.*, 2014) and data from the *B. subtilis* enzyme suggest that there is significant reason to believe that the hydrolysis of ATP is synchronous (Gottler and Klostermeier, 2007).

It is known that there are several highly conserved residues in the ATPase domain. These include the aspartic acid at residue 46 (*E. coli*) which is required to coordinate magnesium binding (Wigley *et al.*, 1991, Lewis *et al.*, 1996), E50 and R76 which form an important salt bridge (Gross *et al.*, 2003). A second aspartic acid forms a direct hydrogen bond with the adenosine amino group of ATP (Gross *et al.*, 2003) which is highly specific and can only be mutated to a glutamic acid to retain activity (Gross *et al.*, 2003). Two further amino acids P79 and K103 have been further described to couple the ATPase activity to the supercoiling function of the enzyme as mutation is permissive to ATPase activity but not to supercoiling (Gross *et al.*, 2003). The catalytic active site of the ATPase reaction has been determined to contain the likely catalytic residues of E42 and H38 (Jackson and Maxwell, 1993). Finally, T165 is highly conserved within all type II topoisomerases. Mutation of this residue to serine is permissible although an alanine is not (Gross *et al.*, 2003), this may be explained due to direct and indirect bonding (via an ordered water molecule) to ATP (Lewis *et al.*, 1996).

The *E. coli* model DNA gyrase system has been used for the most part to investigate the mechanism of action, and relationship between ATP hydrolysis and the change in topology. There is however a smaller amount of data on the mycobacterial DNA gyrase ATPase domain, including structures of the full domain (Agrawal *et al.*, 2013). The data presented in the

literature suggests that *M. tuberculosis* does not have an appreciable rate of ATP hydrolysis that can be reliably tested (Agrawal *et al.*, 2013, Karkare *et al.*, 2013b, Shirude *et al.*, 2013), meanwhile the initial data for the *M. smegmatis* DNA gyrase does not suggest it to be much better (Manjunatha *et al.*, 2002), although other groups have been able to generate a high throughput ATPase assay system for this protein (Shirude *et al.*, 2013). As with the *E. coli* enzyme there is significant stimulation of the ATPase activity when both GyrA and DNA were included in the reaction, and this activity is abolished on the addition of novobiocin indicating specificity to DNA gyrase (Manjunatha *et al.*, 2002, Agrawal *et al.*, 2013). Overall, it is suggested that the coupling of the ATPase activity to DNA supercoiling is greater in Mtb DNA gyrase than in other enzymes such as *E. coli*, where the ATPase activity can be uncoupled from strand passage (Sugino and Cozzarelli, 1980, Bates *et al.*, 1996, Fu *et al.*, 2009, Bates *et al.*, 2011).

1.6.2 DNA gyrase core: GyrB C-terminal domain and GyrA N-terminal domain

The GyrA NTD includes the essential catalytic tyrosine (Y122 *E. coli*) (Horowitz and Wang, 1987, Wilkinson and Wang, 1990), meanwhile the GyrB CTD contains the TOPRIM domain. Results of studies carried out to probe the role of the GyrA subunit have previously demonstrated that all the NTD of GyrA is required to support supercoiling and decatenation, however weak and non-processive supercoiling is possible in the presence of just the first 572 amino acids (*E. coli*) and subsequently suggesting a role of residues 523-572 in active strand passage (Reece and Maxwell, 1991b).

The GyrB CTD contains the TOPRIM domain which has been demonstrated to be conserved across a wide variety of DNA-binding proteins including bacterial DnaG-type primases, types IA and II topoisomerases as well as RecR/M bacterial repair proteins (Aravind *et al.*, 1998), in addition to the tail domain (Costenaro *et al.*, 2007). This 47 kDa domain has a predominant role in interactions with both the GyrA subunit and DNA (Brown *et al.*, 1979, Chatterji *et al.*, 2000, Noble and Maxwell, 2002, Schoeffler *et al.*, 2010).

1.6.3 The GyrA C-terminal domain and DNA wrapping

The CTDs of GyrA are implicated to be involved in stabilising the DNA-protein complex through a sequence-independent DNA binding and wrapping mechanism (Reece and Maxwell, 1991a), and are essential for the process of negative supercoiling (Kampranis and Maxwell, 1996), indeed in their absence the protein is converted into an ATP-dependent

relaxing enzyme. Although they have been shown to bind stretches of double stranded DNA greater than 35 bp long (Reece and Maxwell, 1991a), independently the CTD is catalytically inactive suggesting their role to be accessory (Reece and Maxwell, 1991b). It is implied that the CTD preferentially binds to positively supercoiled DNA over negatively-supercoiled DNA in the presence of nucleotide, suggesting a topological substrate preference (Kampranis *et al.*, 1999a). The structure of the CTD has been solved from several species including *E. coli*, *M. tuberculosis* and *Xanthomanas campestris* (Ruthenburg *et al.*, 2005, Hsieh *et al.*, 2010, Tretter and Berger, 2012) all showing a composition of 6 blades forming a beta-pinwheel structure, although other structures have been demonstrated to be possible (Corbett *et al.*, 2004).

1.6.4 DNA gyrase: a proposed mechanism of action

There is a consensus within the field that there is one recognised mechanism of action for DNA gyrase. This was initially postulated by Brown and Cozzarelli (1979) who suggested that the reaction mechanism involved using a double-strand break to decrease the linking number of DNA by two on each reaction cycle.

It is thought that dimeric GyrA assembles together with two GyrB subunits and wrapping a section of DNA of *ca.* 128 bp around the CTDs in a positive wrap (Orphanides and Maxwell, 1994). The reaction cycle is then initiated through the binding of two ATP molecules causing the closure of the two GyrB N-terminal domains to trap a T-segment of DNA (Wigley *et al.*, 1991, Stanger *et al.*, 2014). This also allows for ligation of the G-segment of DNA through stabilisation by the two active-site tyrosine residues (Tyr-122 in *E. coli* DNA gyrase) (Horowitz and Wang, 1987, Cabral *et al.*, 1997). The T-segment is then able to pass through the G-segment before it is ligated possibly with the hydrolysis of one ATP molecule. However, this is unclear as there is some evidence to suggest that both ATP molecules are hydrolysed synchronously (Gottler and Klostermeier, 2007). However, more recently it has been suggested that the rate-limiting step of DNA supercoiling is the hydrolysis of the second ATP molecule within the reaction, as the DNA is only able to be released from the exit gate of DNA gyrase (interaction of the two N-terminal domains of GyrA) once hydrolysis of both of the ATP molecules has occurred (Wigley *et al.*, 1991, Corbett *et al.*, 2004, Hartmann *et al.*, 2017). Although this is just theory, there is considerable evidence that the reaction of DNA gyrase can only alter the linking number of DNA by minus 2 (Brown and Cozzarelli, 1979) giving considerable evidence for this mechanism (Figure 1.6.1).

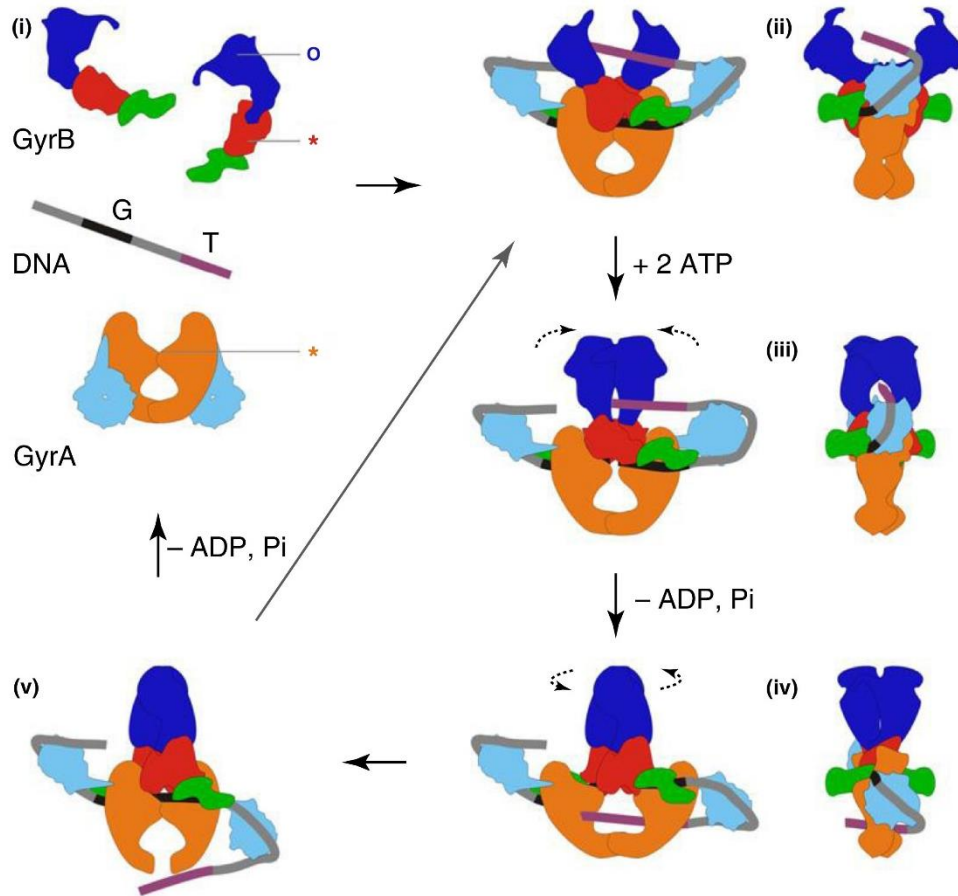


Figure 1.6.1: Mechanism of negative supercoiling by DNA gyrase. Domains coloured as follows: Dark blue GyrB-NTD, red GyrB-TOPPRIM, green GyrB-tail, orange GyrA-NTD, light blue GyrA-CTD. The transport (T) segment is coloured purple and the gate (G) segment black. From their free solution state (i) the active state combines to form a complex with the G segment bound between the GyrB-TOPPRIM and GyrA-NTD (ii) and with the addition of 2x ATP molecules the GyrB clamp can close capturing the T segment and allowing cleavage of the G segment (iii). Hydrolysis of the first ATP molecule allows for a conformation change allowing the T segment to be passed through the G segment (iv) this allows the G segment to be religated and the T segment to be released from the C-gate (v). Hydrolysis of the second ATP molecule then resets the enzyme allowing for subsequent cycles to proceed (i/ii). Reproduced from (Costenaro *et al.*, 2007).

However, although this is the generally accepted mechanism for DNA gyrase there has been some conflicting evidence against this mechanism as it has been observed that a DNA gyrase heterotetramer with one of its active-site tyrosine residues mutated to a phenylalanine is able to negatively supercoil DNA in steps of 2 (Gubaev *et al.*, 2016). As it is thought that both active site tyrosine residues are required to ligate the G-segment of DNA allowing for transport of the T-segment the authors proposed an alternative nicking and closing mechanism by which a single DNA strand is cleaved allowing for relaxation by rotation of the single strand

break. There are however, significant issues with these experiments. The first arises from the question of purification efficiency from the tandem affinity purification mechanism. Meanwhile, the second arises from the question of possible higher order multimers and potential subunit exchange not being fully accounted for.

1.6.5 DNA gyrase from *M. tuberculosis*

M. tuberculosis gyrase is encoded by the Rv006 and the Rv005 genes which are located next to each other in the genome (Cole *et al.*, 1998). It was first characterised as a recombinant enzyme purified with a His-tag by Aubry *et al.* (2006a). At this time, it was explained that it supercoils at a similar level of activity to other gyrases, but has enhanced activity in relaxation, cleavage and decatenation, although it is unable to decatenate to the same degree as a true topo IV enzyme. Of interest was that the cleavage specificity was compared across four more active quinolones (Aubry *et al.*, 2006a) alongside the DNA gyrase and topo IV from *S. pneumoniae*. This analysis demonstrated that the cleavage pattern shared the greatest similarity to that of other DNA gyrase enzymes as opposed to topo IV, and hence along with the information that the enzyme from Mtb can negatively supercoil DNA it has been classified as a DNA gyrase enzyme as opposed to a topo IV.

One of the most important problems scientists faced working on this enzyme early on was the confusion over the start codon. This came about because there were initially multiple possible start codons which were quickly reduced to two potential sites in the coding sequence leading to two different possibilities for GyrB, one starting with a valine start codon, the other with the more traditional methionine including an additional 40 amino acids (Madhusudan *et al.*, 1994, Karkare *et al.*, 2013a). *In vitro* it was found that no significance in activity or inhibition was seen regardless of the position of the start codon (Karkare *et al.*, 2013a). In addition, it was demonstrated that the promoter located upstream of the valine start codon gave a prominent level of promoter activity while the promoter upstream of the methionine start codon did not (Karkare *et al.*, 2013a). It is for these reasons that it was decided to work solely with the valine start codon for the work within this thesis.

1.6.6 Fusion proteins of DNA gyrase

Fusion proteins are created when two individual genes are fused together to give one open reading frame, resulting in the transcription of a single protein. These have been observed under certain conditions in nature. Equally, since the development of modern molecular

biology techniques it has been possible to make unnatural fusion proteins such as those with affinity and solubility tags for purification purposes, fluorescent tags for imaging, and most interestingly in this instance the combination of two proteins that dimerise for structural studies (Beckwith, 2000). Previously in the field of topoisomerases there have been initial studies on some fusion constructs of some topoisomerases (Lavasani and Hiasa, 2001, Trigueros and Roca, 2002, Papillon *et al.*, 2013). Additionally, many of the structural studies in the Klostermeier laboratory have been carried out using a fusion construct of *B. subtilis* DNA gyrase (Klostermeier, 2018).

The first recorded fusion in this field is that of the ParE-ParC fusion which was characterised as an active protein although it did appear to require more protein to produce the same results of the individual subunits (Lavasani and Hiasa, 2001). Importantly, it was demonstrated *in vivo* to complement a ParE or ParC knockout in a temperature-sensitive strain at a non-permissible temperature. Presently there has been much less work on GyrB-GyrA fusion proteins, but recently there have been several papers published utilising them (Gubaev and Klostermeier, 2011, Gubaev and Klostermeier, 2012, Lanz and Klostermeier, 2012, Gubaev and Klostermeier, 2014b, Gubaev and Klostermeier, 2014a, Lanz *et al.*, 2014, Gubaev *et al.*, 2016, Hartmann *et al.*, 2017, Stelljes *et al.*, 2018).

Structural studies often drive the development of fusion proteins and this is no different in terms of DNA gyrase. The core-fusion is a chimeric protein of the GyrA NTD and the GyrB CTD with DNA (see Figure 1.5.1 this section of DNA gyrase includes the TOPRIM domain and catalytic tyrosine but not the N-terminal ATPase domain or C-terminal domains of GyrA) (Schoeffler *et al.*, 2010, Srikannathasan *et al.*, 2015). This gave significant insight into the structure of this part of the enzyme. More recent advances have used a full-length gyrase fusion protein to obtain a low resolution cryoEM structure at 23 Å in the presence of a 155 bp DNA fragment (Papillon *et al.*, 2013). In this study it was determined that the *T. thermophilus* fusion protein that they worked with was as active in supercoiling as the native protein.

One of the most intriguing studies on a GyrBA fusion protein was carried out by Trigueros and Roca (2002) where they concluded that gyrase is unable to fully complement a yeast topo II knockout, but is able to remove positive supercoils in yeast cells. These results are not unsurprising considering the functional divergence between eukaryotic topo II and bacterial DNA gyrase.

A considerable amount of mechanistic studies on DNA gyrase have been carried out so far including several studies which for reasons of convenience have used fusion proteins. These appear to have been initiated by work carried out by (Gubaev and Klostermeier, 2011), where they utilised FRET labelling to help elucidate various parts of the DNA gyrase mechanism of action (Lanz and Klostermeier, 2012, Gubaev *et al.*, 2016). It has been demonstrated through the use of this work that a *B. subtilis* DNA gyrase fusion protein has equivalent activity to unfused subunits; therefore, it is interesting to determine if an equivalent fusion of the mycobacterial DNA gyrase will give the same results.

1.7 Structural biology of DNA gyrase

At present there are no full-length high-resolution structures of DNA gyrase or other type IIA topoisomerase from any species. There have however been many structural studies carried out of DNA gyrase, including a full length low-resolution cryoEM structure of *Thermus thermophilus* GyrBA fusion at around 17 Å. This structure has a 3-amino acid linker between the GyrB and GyrA subunits and was bound to ADPNP in the absence of DNA. However, within this structure the GyrA CTDs were not visible (Papillon *et al.*, 2013). Within the same paper there was a further structure obtained at 23 Å. This structure contained a DNA fragment and ciprofloxacin, and furthermore it was possible to observe the GyrA CTDs due to the stabilisation from the DNA wrapping (Figure 1.7.1A) (Papillon *et al.*, 2013).

The closest structure to the full-length DNA gyrase structure is the structure of the core fusion containing the GyrA NTD and GyrB CTD – there are several of these structures available in the PDB including that of the *S. aureus* (Srikannathan *et al.*, 2015) core fusion and more interestingly the *M. tuberculosis* fusion (Figure 1.7.1B) (Blower *et al.*, 2016). There is also a fusion structure of the homologous topo IV containing full length ParE fused to ParC55 from *S. pneumoniae* and additionally contains two DNA molecules bound at a resolution of 3.7 Å (Figure 1.7.1C) (Laponogov *et al.*, 2013). Finally, there is a structure of the first 1177 amino acids from *Saccharomyces cerevisiae* topo II which has been solved at a resolution of 4.41 Å in complex with nucleotide and DNA (Figure 1.7.1D) (Schmidt *et al.*, 2012). All together these structures give a good indication that DNA gyrase is arranged with the GyrB subunits sat on top of the GyrA dimer, with the G-segment of DNA being held between the GyrA and GyrB dimers. This indicates that the C-terminal domains of GyrA are likely to be flexible and external from the rest of the structure.

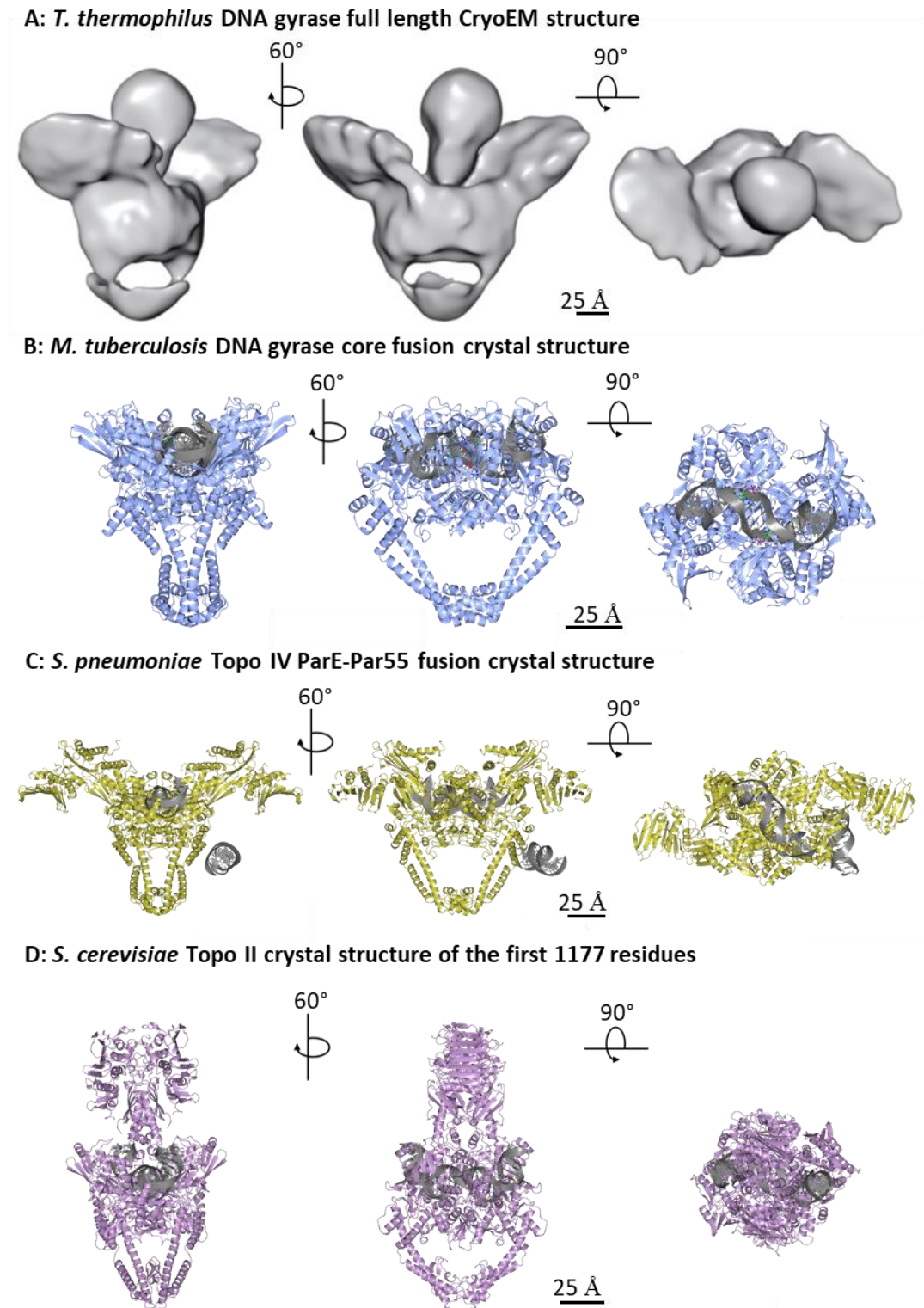


Figure 1.7.1: Comparison of the structures of type IIA topoisomerases demonstrating the most complete structural knowledge known to date with DNA highlighted in grey. A) Full-length fusion structure of *T. thermophilus* DNA gyrase solved by cryo-electron microscopy (23 Å) (Papillon *et al.*, 2013). B) Crystal structure of the *M. tuberculosis* DNA gyrase core fusion structure (5BS8) (2.4 Å) (Blower *et al.*, 2016). C) ParE-ParC55 crystal structure of topo IV from *S. pneumoniae* (4I3H) (3.7 Å) (Laponogov *et al.*, 2013). D) Crystal structure of the first 1177 residues from *S. cerevisiae* (yeast) topo II (4GFH) (4.41 Å) (Schmidt *et al.*, 2012). PDB accession codes are given in brackets.

There are more than 50 structures of the GyrB N-terminal ATPase domain or sub-domain within the PDB. Of particular note are three structures which contain novobiocin (1KIJ, 1AJ6, 4URO) (Holdgate *et al.*, 1997, Lamour *et al.*, 2002, Lu *et al.*, 2014), two structures of other aminocoumarins (1KZN, Chlorobiocin) (Lafitte *et al.*, 2002) and 4URM (Kbdelomycin) (Lu *et al.*, 2014), three structures of the full length *M. tuberculosis* ATPase domains 3ZKB, 3ZKD and 3ZM7 (Agrawal *et al.*, 2013), and finally two *M. smegmatis* GyrB24 drug-bound structures 4B6C (Shirude *et al.*, 2013) and 4BAE (Hameed *et al.*, 2014). The *M. tuberculosis* structures are of moderate resolution (2.9 Å) and are from two different similar constructs bound to non-hydrolysable ATP analogues. Again the *M. smegmatis* structures are solved at resolutions of 2.35 Å and 2.2 Å, both missing at least one flexible loop, but they do have inhibitors bound.

Overall, presently there is a considerable knowledge of the structural features of DNA gyrase from *M. tuberculosis*. This is represented by 18 structures being available within the PDB of sections from *M. tuberculosis* (Figure 1.7.2). There is a lot of redundancy within the region known as the core (C-terminal domain of GyrB and N-terminal domain of GyrA) as many of these structures are solved with marginally different compounds (Blower *et al.*, 2016).

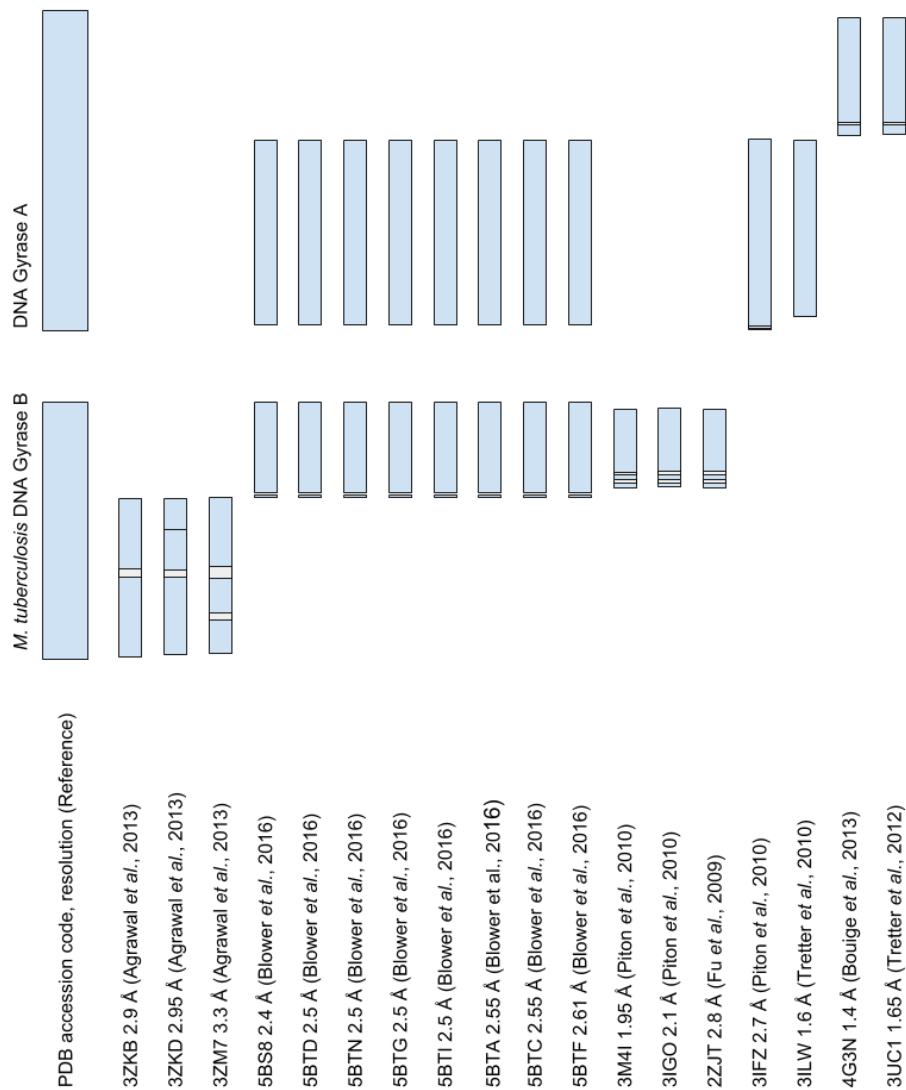


Figure 1.7.2: Coverage of current structures of DNA gyrase from *M. tuberculosis* solved by X-ray crystallography. Blue sections represent areas where structures have been solved, grey sections indicate where there is missing density and the structures have not been solved. The full-length protein arrangement and sizes are displayed at the top. For each structure, the PDB accession code, resolution and reference is shown.

1.8 Inhibition of DNA gyrase

As essential enzymes DNA topoisomerases, especially the type IIA enzymes, have been well-utilised as drug targets, including human topoisomerase II as an anti-cancer chemotherapy target (Liu, 1989), and DNA gyrase / topo IV from bacteria as antibiotic targets. Importantly the properties of human topo II cannot be replaced by DNA gyrase, indicating that there is a significant difference between the catalytic activity and inhibition profile of the two different enzymes (Trigueros and Roca, 2002). Clinically, currently only the quinolone type drugs are licenced antibacterial, although other inhibitors of both DNA gyrase and topoisomerase IV

also exist. The quinolones moxifloxacin, gatifloxacin and levofloxacin are all current second line anti-mycobacterial agents (WHO, 2010).

Other major classes of DNA gyrase inhibitors include the aminocoumarins (Maxwell and Lawson, 2003), the (flouro)quinolones (Van Bambeke *et al.*, 2005), naphthoquinones (Karkare *et al.*, 2013b), and the simocyclinones (Flatman *et al.*, 2005) (Figure 1.8.1). In addition to the major classes of inhibitors there are additional natural products that are known to inhibit DNA gyrase including albicidins (Hashimi *et al.*, 2007) and microcin B17 (Heddle *et al.*, 2001). Recently there have been several reviews of the use of DNA gyrase as a target for antituberculosis chemotherapy including (Nagaraja *et al.*, 2017, Kashyap *et al.*, 2018).

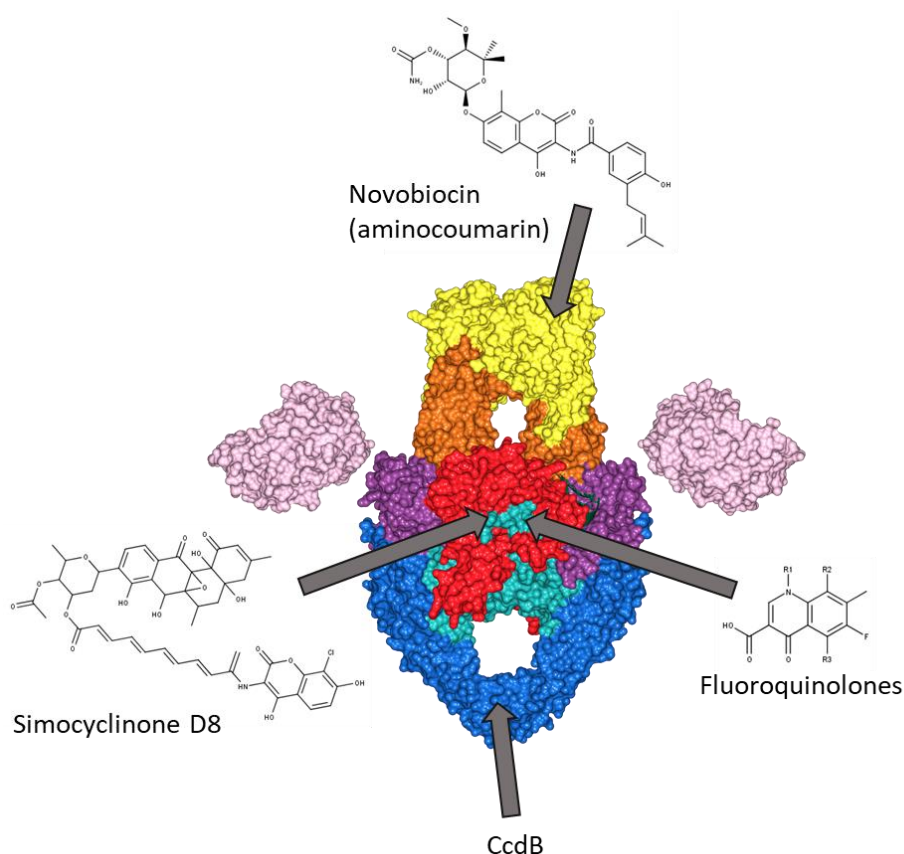


Figure 1.8.1: Model of full-length DNA gyrase from *M. tuberculosis* based on homology modelling to other known structures, indicating the binding sites of inhibitors. Each subdomain is indicated in different colours. Yellow: GyrB N-terminal B24 sub-domain including GHKL ATP-binding domain; orange transducer domain in the GyrB N-terminal domain; red GyrB C-terminal domain including TOPRIM domain, which binds the Mg²⁺ ion cofactor; teal is the winged helix domain (WHD) which is within the GyrA NTD and includes the catalytic tyrosine; purple is the tower domain (GyrA NTD); blue is the coiled-coil domain which forms the exit gate within the GyrA NTD; pink is the GyrA CTD which is thought to be responsible for DNA wrapping. Four groups of known DNA gyrase inhibitors and their known binding domains are indicated. Figure was reproduced from (Bush *et al.*, 2018).

1.8.1 Inhibition of DNA gyrase by (fluoro)quinolones

The quinolones are a class of inhibitors which act to stabilise the DNA cleavage complex inhibiting both the ATP-dependent negative supercoiling reaction and the ATP-independent relaxation reaction (Gellert *et al.*, 1977). To date there have been three generations of quinolone antibiotics all of which have been used clinically, these have included advancements in the chemical structure including the fluoro-group in generation 2 (Figure 1.8.2).

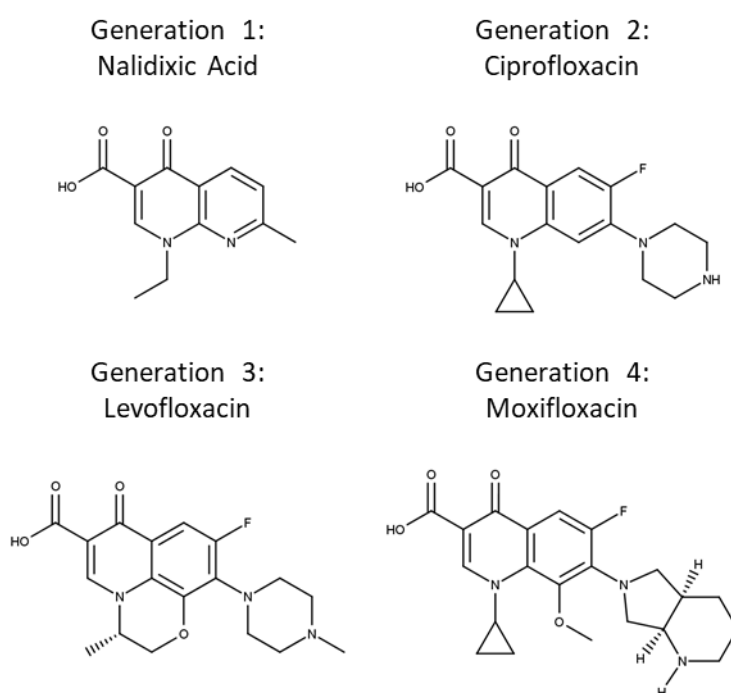


Figure 1.8.2: Chemical structures of examples from each of the four generations of (fluoro)quinolone antibiotics. Fluoroquinolones are characterised by the addition of the fluoro-group at position 8 of the scaffold.

Over the years there has been a considerable amount of work to determine the mechanism of action of quinolone, as well as optimisation to work to gain better clinical efficacy. To date there have been studies of the activity of multiple quinolones against TB gyrase (Onodera *et al.*, 2001, Aubry *et al.*, 2004), a crystal structure of the *M. tuberculosis* DNA gyrase core bound to DNA and moxifloxacin (Blower *et al.*, 2016), as well as multiple clinical studies of *M. tuberculosis* mutagenesis resulting in clinical resistance (Kocagoz *et al.*, 1996, Bozeman *et al.*, 2005, Aubry *et al.*, 2006b, Matrat *et al.*, 2006, Agrawal *et al.*, 2009, Avalos *et al.*, 2015, Rigouts *et al.*, 2016).

Two quinolone molecules bind to the DNA gyrase complex to stabilise the enzyme preventing religation of the DNA (Critchlow and Maxwell, 1996, Heddle *et al.*, 2000). This causes damage as the DNA is locked in a cleavage complex causing the cells to utilise DNA repair mechanisms and induce cell death (Drlica and Zhao, 1997).

1.8.2 Inhibition of DNA gyrase by aminocoumarins

Aminocoumarins are a class of antibiotics with a contrasting mechanism that includes novobiocin, coumermycin A1 and clorobiocin (Figure 1.8.3). Instead of inhibiting at the DNA gate, instead they are competitive inhibitors of ATP and bind partially across the ATP-binding site. This means that they inhibit only the negative supercoiling reaction of the enzyme and leave the ATP-independent relaxation reaction unaffected (Sugino *et al.*, 1978). Although the general mechanism of action for the coumarin antibiotics was quickly deciphered, the exact binding site took longer to determine through bacterial mutant isolation, with mutants being isolated in *E. coli* (del Castillo *et al.*, 1991, Contreras and Maxwell, 1992) and in *S. aureus* (Stieger *et al.*, 1996) (Table 1.8.1) (Kampranis *et al.*, 1999b). A further systematic study of the effects of mutations surrounding the ATP- and novobiocin-binding sites has further confirmed the crystallographic binding site through use of the ATPase reaction (Gross *et al.*, 2003).

The aminocoumarins have whole cell activity against Gram-positive bacteria only and clinically only novobiocin of the coumarins has been used, but can no longer be used due to a combination of low solubility, toxicity and spontaneous resistance forcing it to be removed from clinical use (David and Burgner, 1956, Kirby *et al.*, 1956, Colville *et al.*, 1957, Food and Drug Administration, 2011). Regardless of the flaws of novobiocin, the coumarin group of antibiotics are interesting for continued studies.

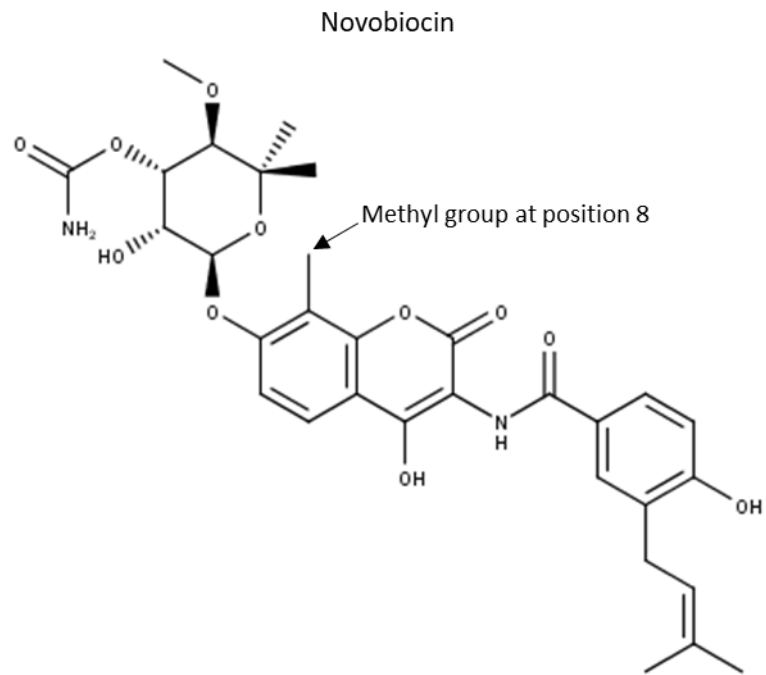


Figure 1.8.3: Chemical structure of the aminocoumarin novobiocin. Clorobiocin has an identical chemical structure, except the methyl group at position 8 of the coumarin ring is substituted for chlorine. Coumermycin A1 is a dimeric aminocoumarin with additional substitutions at the termini and in the linker region.

Table 1.8.1: Novobiocin-resistant mutants in DNA gyrase GyrB and the amino acid positions in the *E. coli*, *S. aureus*, and *M. tuberculosis* enzymes. The resulting mutations are indicated for the source organism or where not displayed in the *S. aureus* column. Bacterial mutants were raised as described and the enzymatic studies were carried out after analysis of the crystallographic structures.

	<i>E. coli</i>	<i>S. aureus</i>	<i>M. tuberculosis</i>	Reference
Bacterial Isolation <i>E. coli</i>	R136C/L/H G164V	R144 G172	R141 G168	(del Castillo <i>et al.</i> , 1991, Contreras and Maxwell, 1992)
Bacterial Isolation <i>S. aureus</i>	I48 G77 G81 I94 V120 R136 T165 M166	I56S G85S D89G I102S/V/T S128L R144I/S T173A/N I175T	V54 G83 A87 V99 V125 R141 S169 T170	(Stieger <i>et al.</i> , 1996, Fujimoto- Nakamura <i>et al.</i> , 2005)
Bacterial Isolation <i>S. pneumoniae</i>	V119	S128L	V125	(Munoz <i>et al.</i> , 1995)
Bacterial Studies Resistant Halophilic archaeobacterium	G81 S120 R136	D89G S129T R144H	A87 S126 R141	(Holmes and Dyallsmith, 1991)
Enzymatic studies (SPR)	N46D/L D73N R136C	N54 D81 R144	N52 D79 R141	(Kampranis <i>et al.</i> , 1999b)
Enzymatic studies (Sc and ATPase)	V43A E50A D73E R76A G77A/S I78A/L/V P79A I94A A100S K103A R136A/H/L/S T165A/V	I50 E58 D81 R84 G85 I86 P87 I102 A108 K111 R144 T173	V49 E56 D79 R82 G83 I84 P85 V99 A105 K108 R141 S169	(Gross <i>et al.</i> , 2003)

1.8.3 Inhibition of DNA gyrase by naphthoquinones

The naphthoquinones are a class of natural compounds which have been shown to have activity against DNA gyrase from *M. tuberculosis*. One of the major sources that they have been reported to have been isolated from *Euclea natalensis*, or the toothbrush tree, which has been associated with traditional medicine (Tannock, 1973, Khan and Rwekika, 1992). These compounds have a currently unknown mechanism of action, which is thought to occur through interaction with the GyrB N-terminal domain, but away from the site of ATP binding (Karkare *et al.*, 2013b). Hence, as they act through a novel mechanism of action it makes them interesting to study from a mechanistic point of view. This is important because cross toxicity to mammalian cell including intercellular oxidative stress from menadione likely prevents their use in the clinic (Brown *et al.*, 1991). The IC₅₀ values of the naphthoquinones vary largely with the most active compounds against DNA gyrase reported to be diospyrin and 7-methyljuglone (Karkare *et al.*, 2013b) (Table 1.8.2).

Two computational models predicting the binding site of diospyrin in the NTD of GyrB have been made independently. Between the two models there is a large degree of agreement between the published model produced by Chetty and Soliman (2015) and the unpublished model created by Dr S. Ekins (2015) (Figure 1.8.4). The major difference is in the structural models that the computational models are based on; the Ekins model is based on the 3ZK7 crystal structure (Agrawal *et al.*, 2013), whereas the Chetty and Soliman (2015) model utilised three homology models at higher resolution to obtain their binding pocket. At present neither of the computational models has been tested against the enzyme targets.

Alongside the biological analysis that these compounds have been subjected to, there has also been a substantial amount of work on the chemical properties of these compounds. In this area, several of the naphthoquinones have been described as unstable with concentration-dependent breakdown of these compounds often occurring (van der Kooy, 2007). In the case of 7-methyljuglone, only 75% was found to remain in the sample at 30 mins when dissolved in DMSO; less than 5% remained after one week. Only the poor inhibitors of DNA gyrase such as menadione and plumbagin were found to pure after one week when dissolved in DMSO. These stability issues raise significant concerns when working with this class of compound; it has been reported that 7-methyljuglone is relatively stable in the mycobacterial growth media (Middlebrook 7H9 supplemented with 5% glycerol and 20% DMSO), albeit with decreased solubility. Under these conditions 92% purity was retained at 8 hours enabling inhibition assays to be undertaken (van der Kooy, 2007).

Table 1.8.2: Reported IC₅₀ values of selected naphthoquinones against the *M. tuberculosis* DNA gyrase supercoiling reaction and their chemical structures. IC₅₀ values as reported in Karkare *et al.* (2013b)

	Reported IC ₅₀ vs <i>M. tuberculosis</i> DNA gyrase (supercoiling)/ μM	Chemical Structure
Diospyrin	15	
7-Methyljuglone	30	
Neodiospyrin	50	
Isodiospyrin	100	
Menadione	>200	

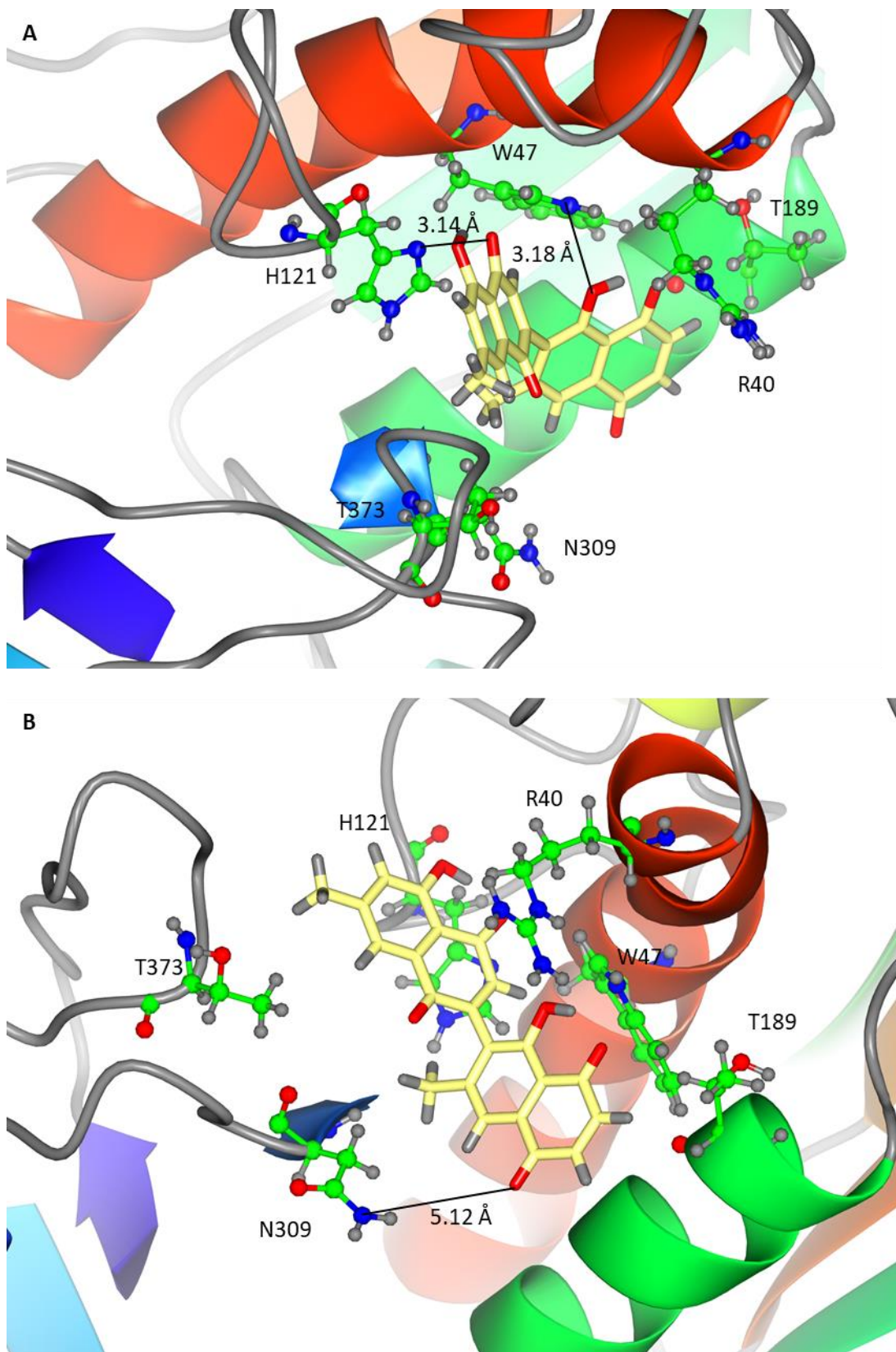


Figure 1.8.4: Two views of the model of diospyrin docked into the 3ZM7 crystal structure of the Mtb ATPase domain (Agrawal *et al.*, 2013) by Dr S. Ekins. Six amino acids of interest are shown with in specific interaction distances labelled. A) and B) show different orientations of the same structure.

1.8.4 Inhibition of DNA gyrase by simocyclinones

Simocyclinone D8 is a *Streptomyces* natural product that was originally isolated from *Streptomyces antibioticus* Tü 6040 (Schimana *et al.*, 2000, Theobald *et al.*, 2000, Galm *et al.*, 2002, Trefzer *et al.*, 2002). It is known to target DNA gyrase but unusually for a DNA gyrase inhibitor it does not have activity against bacterial topo IV in either *E. coli* or *S. aureus* (Oppegard *et al.*, 2009). SD8 has an unusual structure combining an aminocoumarin domain linked with a tetraene dicarboxylic acid and D-olivose linker to the Angucyclic polyketide head (Figure 1.8.5). Despite the presence of the aminocoumarin domain the target of SD8 is not GyrB, instead it inhibits DNA binding by GyrA (Flatman *et al.*, 2005). This has been proved using mutagenesis and X-ray crystallographic studies, which demonstrate that the binding site of SD8 is adjacent but not overlapping with that of the quinolones (Edwards *et al.*, 2009, Hearnshaw *et al.*, 2014). One major issue preventing the use of SD8 in the clinic is that there is considerable cross resistance to QRDR (quinolone resistance determining region) mutants, and as there is an increasing trend of recording cases of these in the clinic it makes it an impractical lead to follow further (Edwards *et al.*, 2009).

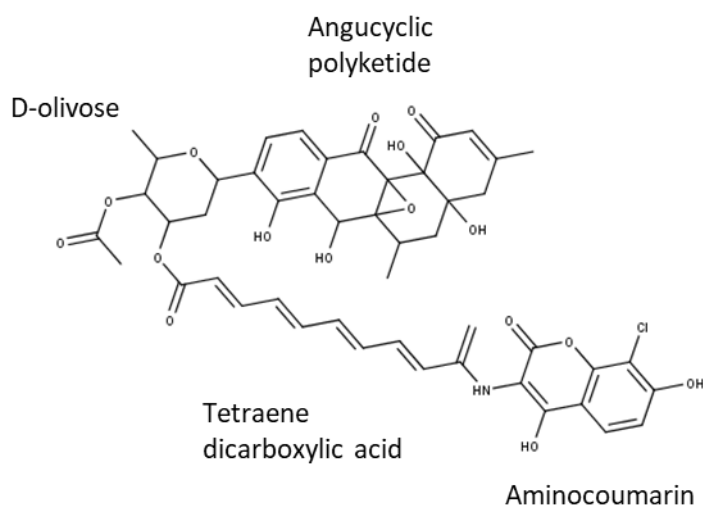


Figure 1.8.5: Structure of Simocyclinone D8 indicating the four different sections including the aminocoumarin and Angucyclic polyketide active heads. Image redrawn from (Edwards *et al.*, 2009) using Marvin sketch.

1.8.5 Pyrrolopyrimidine and tricyclic GyrB/ParE (TriBE) inhibitors

Pyrrolopyrimidine derivatives are a well investigated class of compounds, which have been developed in a variety of different contexts including as antibacterial agents (Dave and Shah, 2002, Hilmy *et al.*, 2010, Tari *et al.*, 2013b, Trzoss *et al.*, 2013), although other reported activities include being antidiabetic, herbicidal, diuretic and antineoplastic (Asif, 2016).

Several chemical optimisation studies have been carried out on these compounds showing them to have low level antibacterial activity mostly via the disk diffusion method, but without mode of action, toxicity or resistance studies being carried out. Hilmy *et al.* (2010) managed to produce compounds with MIC values better than those for ampicillin for *S. aureus*; these compounds also exhibited antifungal activity against *Candida albicans*. Subsequently, this class of compounds was further investigated by the company Trius therapeutics who described them to inhibit by a dual-targeting GyrB and ParE mechanism and crystallised the compounds in the likely binding pocket (Tari *et al.*, 2013b). These compounds appear to be stronger inhibitors of Gram-positive bacteria, with efflux pumps inhibiting their effectiveness against *E. coli* and other Gram-negative bacteria (Trzoss *et al.*, 2013). In addition to the published work on these compounds, the pyrrolopyrimidine compound class has been patented to be potentially useful for further clinical developments (Bensen *et al.*, 2012, Cooper *et al.*, 2016).

Further optimisations of the pyrrolopyrimidine compounds lead to the development of the novel TriBE class of inhibitors. These compounds have been significantly optimised to have significant efficacy against *S. aureus*, *S. pneumoniae* and *E. faecalis*, although in a mouse model they did not show activity as good as the clinical antibiotic levofloxacin. Equally against clinically-relevant bacteria they showed a range of activities, but importantly in antibiotic-resistant strains good activity was seen (Tari *et al.*, 2013a). Like the pyrrolopyrimidine compounds the active site of the compounds has been determined by crystallography in both DNA gyrase and topo IV (Figure 1.8.6). The gyrase binding pocket appears as determined by crystallography appears to have some possible overlap to both the ATPase binding site as well as the novobiocin binding site, however from the literature this binding pocket has not been confirmed with mutagenesis. The mechanism of action for these compounds has been determined to be through a dual targeting mechanism to both GyrB and ParE, which leads to very low frequency of resistance values, leading them to be an interesting series of compounds to explore further.

From the TriBE group of compounds Redx03863 has been further developed as an antimycobacterial agent by Redx AntiInfectives, from which they produced their lead compound of Redx04739 (Figure 1.8.7) (McGarry *et al.*, 2018).

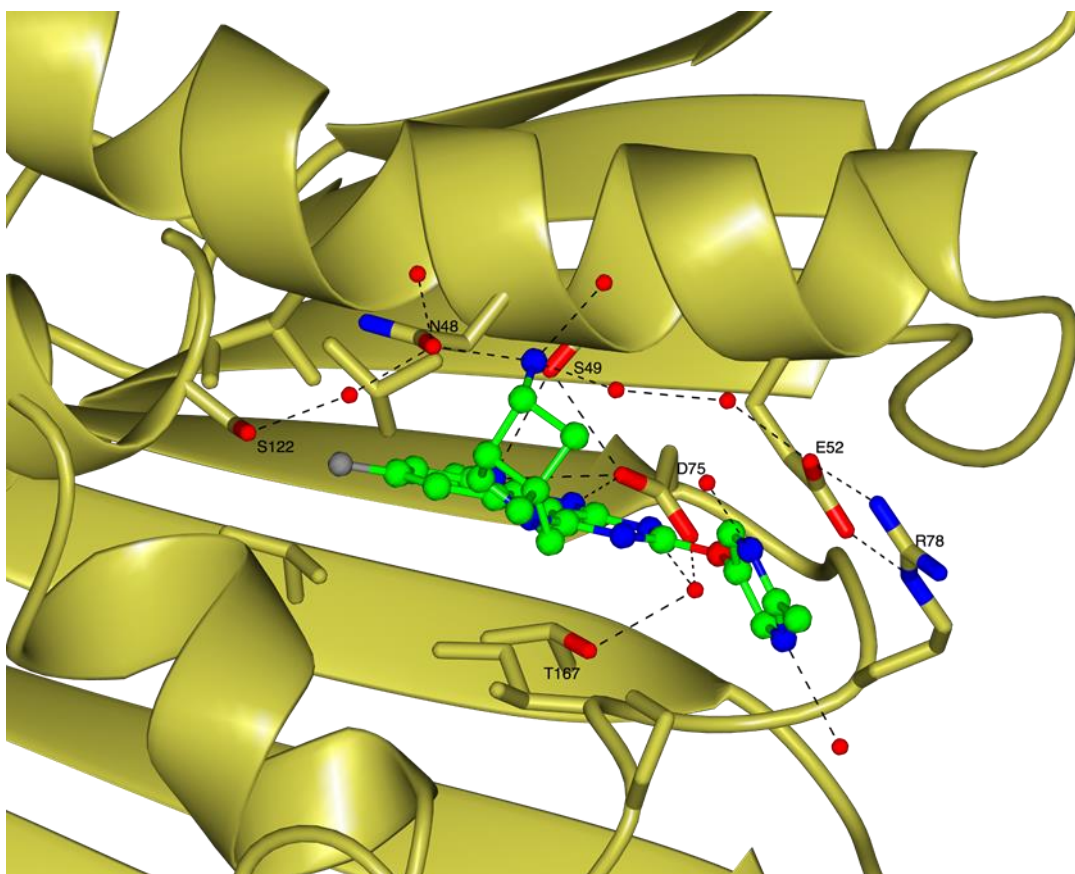
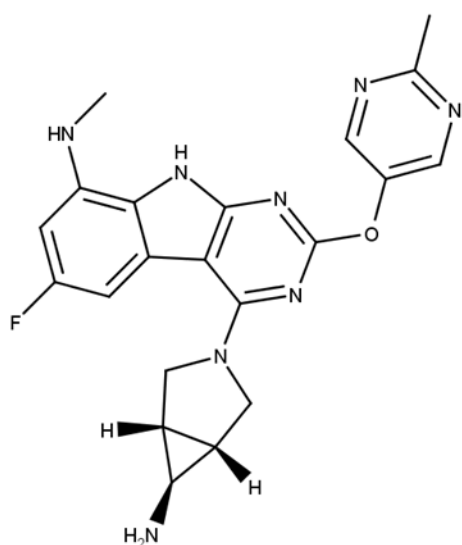


Figure 1.8.6: Image of the binding pocket of compound 4 in the *Enterococcus faecalis* V583 ATPase sub-domain (PDB entry: 4KSG). Key binding interactions and their residues shown. The residues correspond to the following residues in *M. tuberculosis* GyrB: N48 – N52; S49 – A53; E52 – E56; D75 – D79; R78 – R82; S122 – V125; T167 – S169 (Tari *et al.*, 2013a).

A: Redx03863



B: Redx04739

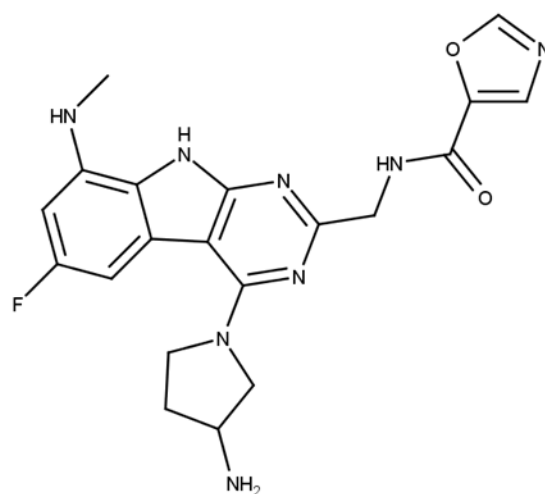


Figure 1.8.7: Chemical structure of Redx03863 which was optimised to give the lead compound of Redx04739

1.9 Project aims

The initial aim of the project was to crystallise and characterise the *M. tuberculosis* fusion protein (Mtb GyrBA) as, since the initial cloning of this fusion protein by Dr Fred Collin, there had been no comprehensive studies of its total activities, including the ATPase activity. Unsuccessful crystallisation trials led us to clone and perform initial characterisations on the DNA gyrase enzymes from *M. thermoresistibile* (Mth GyrA, GyrB, and GyrBA).

Our aim was always to further develop Mtb DNA gyrase as a drug target for novel antibiotics, and along our journey we were fortunate to work on two groups of compounds. The first was the problematic naphthoquinones, which were eventually dropped in favour of the modified TriBE compounds from Redx AntiInfectives. We investigated these compounds in collaboration with the company where we characterised them in terms of enzymatic and antibacterial properties. This also gave us the novel opportunity to gain additional crystallographic studies on the N-terminal domain of GyrB in the absence of crystals of the full-length enzyme. An overall summary of the project is shown in (Figure 1.9.1)

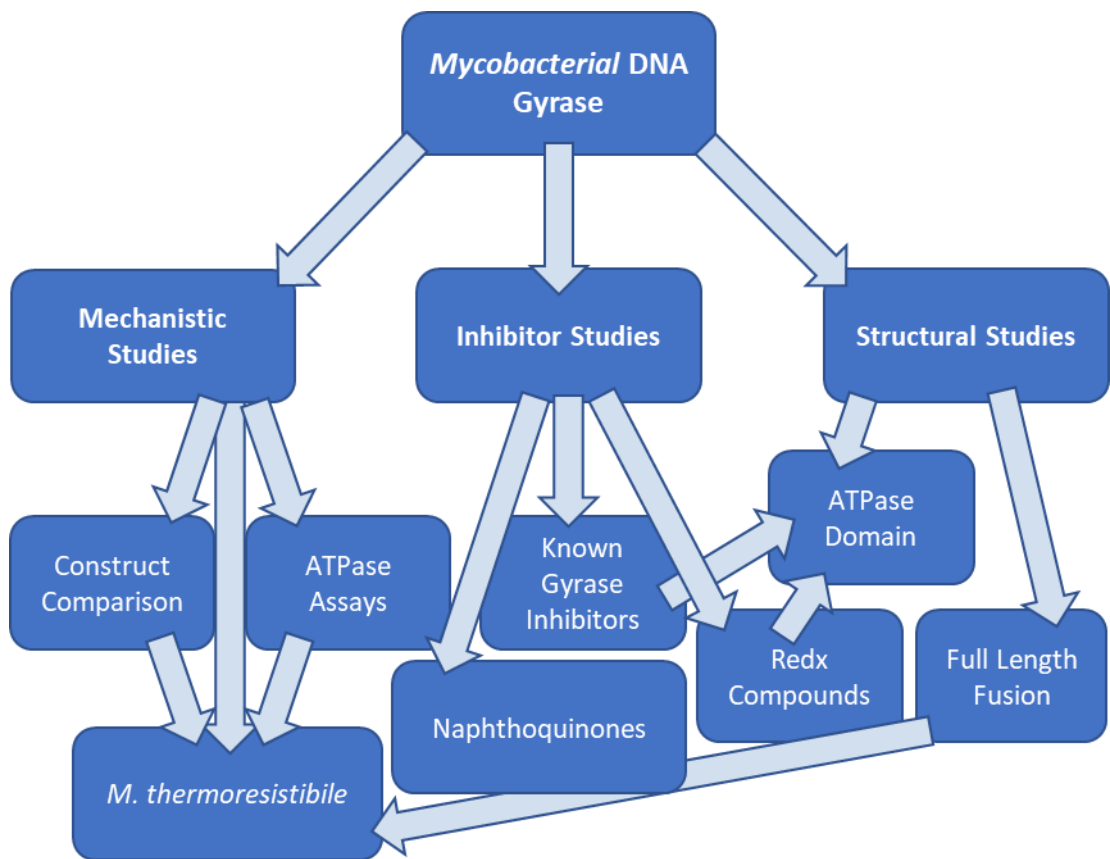


Figure 1.9.1: Overview of the three pronged approach of the PhD thesis presented to obtain mechanistic characterisation of the *M. tuberculosis* fusion protein; to characterise the various constructs presented against known inhibitors; as well as to characterise and perform structural studies on both the full length protein as well as the ATPase domain in complex with novel inhibitors.

2. Materials and Methods

2.1 Bacteriology

2.1.1 Bacterial strains

The *E. coli* cloning and expression strains used in this study are listed in Table 2.1.1

Table 2.1.1: Genotypes of *E. coli* cloning and expression strains used

Strain	Genotype
DH5 α (NEB)	F- ϕ 80lacZ Δ M15 Δ (lacZYA-argF) U169 deoR recA1 endA1 hsdR17 (rk -, mk +) phoA supE44 λ - thi-1 gyrA96 relA1
Stellar TM (Cloantech)	F-, endA1, supE44, thi-1, recA1, relA1, gyrA96, phoA, Φ 80d lacZ Δ M15, Δ (lacZYA - argF) U169, Δ (mrr - hsdRMS - mcrBC), Δ mcrA, λ -
BL21 (DE3) (NEB)	fhuA2 [lon] ompT gal (λ DE3) [dcm] Δ hsdS λ DE3 = λ sBamHIo Δ EcoRI-B int::(lacI::PlacUV5::T7 gene1) i21 Δ nin5
Rosetta TM 2 (pLysS) (Novagen)	F- <i>ompT hsdS_B</i> (r _B ⁻ m _B ⁻) gal dcm (DE3) pLysSRARE2 (Cam ^R)

Bacterial strains for genomic DNA isolation, compound and susceptibility testing are listed in Table 2.1.2. All bacteria are classified within group 2 of the ACDP hazard group to human health, which means that they have the potential to be a hazard to those working with them, but are unlikely to spread to the community, and effective treatment exists (HSE, 2013).

2.1.2 Media and antibiotics

For molecular biology applications the strains detailed in Table 2.1.1 were grown in LB-broth (Formedium: tryptone 10 g/l; yeast extract 5 g/l, sodium chloride 10 g/l) or on LB-agar (Formedium: tryptone 10 g/l; yeast extract 5 g/l, sodium chloride 10 g/l, agar 11 g/l) supplemented as appropriate with ampicillin (100 mg/l), kanamycin (30 mg/l), and chloramphenicol (34 mg/l). In transformation reactions, SOC medium (tryptone 20 g/l; yeast extract 5 g/l; sodium chloride 0.58 g/l; potassium chloride 0.186 g/l; magnesium chloride 2.03 g/l; magnesium sulphate 2.46 g/l; glucose 3.6 g/l) was utilised.

Table 2.1.2: Summary of bacterial strains used for genomic DNA isolation, and compound susceptibility testing.

Species name	Collection number	Obtained from	Source
<i>Acinetobacter baumannii</i>	NCTC13420	RedxPharma	Clinical Isolate
<i>Escherichia coli</i>	ATCC25922	RedxPharma/ HPA	Clinical Isolate
<i>Mycobacterium smegmatis</i>	ATCC19420	RedxPharma	Unknown source
<i>Mycobacterium thermoresistibile</i>	ATCC19527	DSMZ	Soil isolate
<i>Pseudomonas aeruginosa</i>	ATCC27853	RedxPharma	Clinical Isolate
<i>Staphylococcus aureus</i>	ATCC29213	RedxPharma	Clinical Isolate

All non-Mycobacterial strains in Table 2.1.2 were grown in Mueller-Hinton broth (Sigma: beef infusion solids 2 g/l; casein hydrolysate 17.5 g/l; starch 1.5 g/l) or on Mueller-Hinton agar (Sigma: beef infusion solids 2 g/l; casein hydrolysate 17.5 g/l; starch 1.5 g/l; agar 17 g/l). No antibiotics or supplements were added to Mueller-Hinton broth or agar.

All mycobacterial strains in Table 2.1.2 were grown in Middlebrook 7H9 broth (Sigma: ammonium sulphate 0.5 g/l; disodium phosphate 2.5 g/l; monopotassium phosphate 1 g/l; sodium citrate 0.1 g/l, magnesium sulphate 50 mg/l; calcium chloride 0.5 mg/l; zinc sulphate 1 mg/l; copper sulphate 1 mg/l; ferric ammonium citrate 40 mg/l; L-glutamic acid 0.5 g/l; biotin 0.5 mg/l) supplemented with Middlebrook OADC growth supplement (bovine albumin fraction V 5 g/l; dextrose 2 g/l; catalase 4 mg/l; oleic acid 50 mg/l; sodium chloride 0.85 g/l, 0.2% (v/v) glycerol and 0.05% (v/v) Tween-80 or on Middlebrook 7H11 agar (Sigma: casein enzymatic hydrolysate 1g/l; ammonium sulphate 0.5 g/l; monopotassium phosphate 1.5 g/l; disodium phosphate 1.5 g/l; sodium citrate 0.4 g/l; magnesium sulphate 50 mg/l; L-glutamic acid 0.5 g/l; ferric ammonium citrate 40 mg/l; pyridoxine 1 mg/l; biotin 0.5 mg/l; malachite green 1 mg/l; agar 15 g/l) supplemented with Middlebrook OADC growth supplement and 0.2% (v/v) glycerol.

2.1.3 Preparation of chemically competent *E. coli* cells

Fifty microliters of competent cells were grown overnight in 5 ml LB-broth (37°C, 200 rpm) with the appropriate antibiotics. One millilitre of the overnight culture was used to inoculate 100 ml LB-broth with the appropriate antibiotics grown at 37°C, 200 rpm until the optical density 600 nm (OD₆₀₀) reached a value of 0.3. The cultures were cooled on ice and pelleted at 4°C, 3000 rpm for 12 min. The supernatant was removed, and the pellets resuspended in total 12 ml ice cold 100 mM calcium chloride. The resuspended bacteria were pelleted at 4°C, 3000 rpm for 12 min. The supernatant was removed, and the pellets resuspended in 2.5 ml ice cold calcium chloride before supplementation with final concentration 25% (v/v) ice cold glycerol. 100 µl aliquots were flash-frozen in liquid nitrogen and stored at -80°C until use.

2.1.4 Heat shock transformation of chemically competent cells

Chemically competent cells (Table 2.1.1) were defrosted on ice, before supplementation with 0.5 µl purified plasmid, 5 µl of ligation reaction or 5 µl InFusion cloning reaction. The cells were mixed by flicking before being returned to ice for 10-20 min. The cells were transferred to a 42°C heat block for 45 s, briefly returned to ice (maximum 2 min) before addition of 250 µl SOC medium. Transformation reactions were placed in a 37°C shaking incubator (200 rpm) for 45-60 min before plating 50-100 µl of expression cells or the whole cloning reaction on to LB-agar with the appropriate antibiotics overnight at 37°C.

2.2 Molecular biology methods

2.2.1 Oligodeoxynucleotides (primers)

Multiple sets of primers were used in this thesis for various different purposes. The initial set of primers was used to generate new protein constructs (Table 2.2.1), the second were used to generate the three sets of single point mutants (Table 2.2.2). A third set of primers were used for the amplification of the type IIA topoisomerase from *E. coli* and *M. smegmatis* bacterial mutants (Table 2.2.3). Further primers were used for sequencing reactions (Table 2.2.4).

Table 2.2.1: Primers used in the alteration of existing constructs and synthesis of new constructs.

Protein	Forwards Primer	Reverse Primer	Annealing Temperature
GyrB plasmid modification	GTATTCGGCATA TG GCTGCC CAGAAAAAG	GGCCTCGTTTTT AACCCATA TG GTTATGTATAT	65°C
GyrBA plasmid exchange	TTGTATTTCCAGGGCGTGGCTGCC CAGAAAAAG	CAAGCTTCGTCA TCAATTGCCCGTCTGGTCTGCG	65°C
GyrB20	TTGTATTTCCAGGGCGGGCTGGAGGCCCGTC	CAAGCTTCGTCA TCACTCTCGTCGGTCAGG	62°C
GyrB24 (double his-tagged)	TTGTATTTCCAGGGCGGGCTGGAGGCCCGTC	CAAGCTTCGTCA TCAITTAACCCGGATAGTGAA	62°C
GyrB24	TTGTATTTCCAGGGCGGGCTGGAGGCCCGTC	AGGTGCG	62°C
GyrB24SLD	TTGTATTTCCAGGGCCCTCGAAGGGCTGGAGGC	CAAGCTTCGTCA TCA TTAACCCGGATAGTGAAAG	63°C
GyrB24DLD	TTGTATTTCCAGGGCCCTCGAAGGGCTGGAGGC	TGCG	63°C
Msm GyrB24 DLD	TTGTATTTCCAGGGC ATGCCGAAAAGAAATATGGT	CAAGCTTCGTCA TCTTAACCCGGATAGTGAAAG	60°C
Mth GyrB 24 DLD	TTGTATTTCCAGGGC ATGCTGGAAAGGTCTGGGA	GTGCG	60°C
Mth GyrB CO	TTGTATTTCCAGGGC ATGGCAGCC CAGAAAGAAA	CAAGCTTCGTCA TCA TTAACCCGGATAGTGAAAG	60°C
	AG	GGTACG	
	GCAG	AACACG	
	AG	GGTACG	
	TTGTATTTCCAGGGC ATGGCAGCC CAGAAAGAAA	CAAGCTTCGTCA TCA TTAACCCGGATAGTGAAAG	60°C
		CAC	

Protein	Forwards Primer	Reverse Primer	Annealing Temperature
Mth GyrA CO	TTGTATTTCCAGGGGCATGACCGATACCACCCCTG	CAAGCTTCGTCATCATTTAAACGCTATCCGGATC GG	60°C
Mth GyrB CO (GyrB)	TTGTATTTCCAGGGGCATGGCAGCCCAGAAAGAAA	GGTCATCAGCACATCCAGAAAACGCAC	60°C
Mth GyrB CO (GyrA)	GATGTGCTGATGACCCGATACCACCCCTG	CAAGCTTCGTCATCATTTAAACGCTATCCGGATC GG	60°C
Mth GyrB G	TTGTATTTCCAGGGCGTGGCTGCCCAGAAAGAA	CAAGCTTCGTCATCACTAAACGTCAGGAACCG A	60°C
Mth GyrA G	TTGTATTTCCAGGGCATGACTGACACCACGCTG	CAAGCTTCGTCATCATCAGACCCGAGTCGGGGT	60°C
Mth GyrB G (GyrB)	TTGTATTTCCAGGGCGTGGCTGCCCAGAAAGAA	AGTCATGAGAACGTCAGGAACCGA	60°C
Mth GyrB G (GyrA)	GACGTTCTCATGACTGACACCACGCTG	CAAGCTTCGTCATCATCAGACCCGAGTCGGGGT	60°C

Table 2.2.2: Primers designed and used for introducing single point mutations in the GyrB subunit of the GyrB or GyrBA expression plasmids based on the region predicted to be involved in the binding of Diospyrin, or residues predicted to be involved in binding of Redx03863 by site directed mutagenesis or from the crystal structure.

Mutant	Forwards Primer	Reverse Primer	Annealing Temperature
GyrBA-R40A	GACCGGTGAGGCAGGTTTACACCAT	ATGGTGTA AACCTGCCCTCACCCGGTC	55°C
GyrBA-R40Q	GACCGGTGAGCAAAGGTTTACACCAT	ATGGTGTA AACCTTGCTCACCCGGTC	56.5°C
GyrBA-W47F	ACCATCTCATTCGAGAGGTTGGTCGA	TCGACCACCTCTGCAATGAGATGGT	55°C
GyrBA-H121A	ATACTGGTGTCTGGCAGGCGTCCGG	CCGACGCCCTGCCAGACCACCAGATAT	56.5°C
GyrBA-T189A	AATACGACTTCGAAAGCAGTCGCCCGCC	GGCGGGCAGCTGCTTCGAAAGTCGTATT	58.2°C
GyrBA-N309A	CAACACCATCGCAACCCACGAGG	CCTCGTGGGTTGCCGATGGTGTGG	58.2°C
GyrBA-T373A	CCAGACCAAGGCAAAAGTTGGGCAACA	TGTTGCCCAACTTGGCTTGGTCTGG	56.5°C
GyrB-G83S	GGCCGCAGTATTCGGGTC	ACCGGAATGCTGCCGGCCGCTCGT	60°C
GyrB-K159R	GAACCCCTGGGCCCTCCGACAAG	GGCGCCCTTGTCGGAGG	60°C
GyrB-T167A	GACCAAGAAAGCGGGGTCAACCGGT	ACCGTTGACCCCGCCTTCTTGGTC	63°C
GyrB-K202R	TTCCTCAACCGGGGCTGACCAT	ATGGTCAAGCCCGCGGTTGAGGAA	63°C
GyrB-N52A	AGGTGGTCGACGCAGCGGTGACGA	TCGACCGCTGCGTCGACCACCTCCCAA	60°C
GyrB-E56A	AACGGGTCGACGCAGCGATGGCCGGTTAT	ATAACCGGCCATCGCTGCGTCGACC CGGTT	54°C
GyrB-D79T	TGTCGAGGTCGCCCTATGACGGCC	GGCCGTCATAGCGGACCTCGACA	60°C
GyrB-R82A	ACGACGGCCCGGCATTCCCGGT	ACCGGAATGCCGGCGCCGCTCGT	60°C
GyrB-R82Q	ACGACGGCCAAAGGCATTCCCGGT	ACCGGAATGCCCTTGGCCGCTCGT	60°C
GyrB-R141A	TCGAGATCAAGGCTGACGGGTACGA	TCGTACCCGTCAGCCCTTGATCTCGA	63°C
GyrB-R141Q	TCGAGATCAAGCAGGACGGGTACGA	TCGTACCCGTCCTTGCTTGATCTCGA	60°C

Table 2.2.3: Primers used to amplify the topoisomerase genes from genomic DNA extracted from *E. coli* ATCC25922 and *M. smegmatis* ATCC19420 and derived strains.

Mutant	Forwards Primer	Reverse Primer	Annealing Temperature
<i>E. coli gyrA</i>	AAACTGCGGGCTGTGTTAT	CAGCCAAACTTTACCGTGCC	70°C
<i>E. coli gyrB</i>	ACGAAAATTCGAAGATGTTTACCGT	TGAACGCCCTTATCCGGCCCTA	72°C
<i>E. coli parC</i>	GGAAAAGCGTATTGTTAAATCGCAAC	GCAAAGAGTTGTATATCAAGGCACA	68°C
<i>E. coli parE</i>	AAACGTATTACACCCTCTCCATCGC	TATTTCAACCCCGATCGTCGATTTTC	70°C
<i>M. smegmatis gyrA</i>	AAGGTCTCCGGTGAGATGGA	ACCTACAGCTCCTTAGCTCG	63°C
<i>M. smegmatis gyrB</i>	ATAGGTGGAACCGGGCTAC	GGCAGCGTCGTATCAGTCAT	66°C

Table 2.2.4: Sequencing primers used to sequence plasmids and amplified genes. Orientation indicated as (F) for forwards and (R) for reverse orientated primers.

Protein	Primers
<i>E. coli gyrA</i>	AAACTGCGCGGCTGTGTTAT (F) AATTCGGACGTCATGCCAA (F) CTACTCCCAGACCCAGTTGC (F) CGCGGAACTGTTGCGTATTC (F) TCTTCATGGCGACCGCTAAC (F) CAGCCAAACTTTACCGTGCC (R)
<i>E. coli gyrB</i>	ACGAAAATTCGAAGATGTTTACCGT (F) ATCCAGCGCGAGGGTAAAAT (F) TGGACAAAGAAGGCTACAGCA (F) AGGAAGTGGCGACGCTTATC (F) TGAACGCCTTATCCGGCCTA (R)
<i>E. coli parC</i>	GGAAAAGCGTATTGTTAATCGCAAC (F) TCGGAAGCATCTTCAATCACCA (F) CTGCCTGCAGTTCTTTCTTCA (F) ATATCCACGCGGTTGGAACG (F) GCAAAGAGTTGTATATCAAGGCACA (R)
<i>E. coli parE</i>	AAACGTATTACACCTCTTCCATCGC (F) GACCGTGTTTCACCAATGCG (F) CCCAGATATCTTCCGCCGAC (F) TATTTCAACCCGATCGTCGATTTTC (R)
<i>M. smegmatis gyrA</i>	AAGGGTCTCGGTGAGATGGA (F) TGGCGATGGAGATGTTGCGTG (F) CAGGTGCGCGACGGCAAG (F) CCTCGAGCGGCAGAAGATCG (F) AACCTCCTGGCCTTCCAGCC (F) ACCTACAGCTCCTTAGCTCG (R)
<i>M. smegmatis gyrB</i>	ATAGGTGGAAACGCGGCTAC (F) GCTGGAGGCCACGGTCCTG (F) TCGAGATCGCGATGCAGTGGA (F) CGACATCGGTGGGTTGCCG (F) GGCAGCGTCGTATCAGTCAT (R)

Protein	Primers
<i>M. tuberculosis gyrA</i>	TTGGCGATGGAGATGCTGAG (F) TCTGGGCGCTGGA (F) CCGGCATTTCACACATTGAGGACC (F) ACGTCAGCGACGAGGATTTG (F) CATGCGGTTCAATATCGACGAC (F)
<i>M. tuberculosis gyrB</i>	GGATGGCGGTGTCGAGGT (F) ACCTTTCACTATCCGGGTGGC (F) ATCCGCGCAAGTCCGAAGTGTATG (F) AAGGCCGGGAAGAAGATCAACAAG (F)
<i>M. thermoresistibile gyrA</i> (G)	AATCGACGAGGAGACAGTCG (F) CTGCGCATGGTCATCGAACT (F) GTGCGTGACGAGCTCAAG (F)
<i>M. thermoresistibile gyrA</i> (CO)	ATGCTGCGTGAAATTGATGA (F) ATCGTGTGGTCTGCGTATG (F) GCGTGGTATTGTTTCGTGATG (F) CAGAAGGTGATACTACTGGTTGC (F)
<i>M. thermoresistibile gyrB</i> (G)	TTGTATTTCCAGGGCGTGGCTGCCAGAAGAA (F) TATGACAAATCGGTCCCCG (F) CTTCCGGGCCGCGTTGAC (F) ATCATCAACGTCGAGAAGGC (F) ATGGGCGAGGACGTCGAG (F) CAAGCTTCGTCATCACTAAACGTCCAGGAACCGA (R)
<i>M. thermoresistibile gyrB</i> (CO)	TTGTATTTCCAGGGCATGGCAGCCCAGAAGAAA (F) TATGATAAAAGCGTTCCGGG (F) AGAAGGTTTTTCGCGCAGC (F) TTAATGTTGAAAAAGCGCGTA (F) GAAGATGTTGAAGCACGTCG (F) CAAGCTTCGTCATCATTACACATCCAGAAAACGCAC (R)
T7 Promoter	TAATACGACTCACTATAGGG (F)
T7 Terminator	CTAGTTATTGCTCAGCGGT (R)

2.2.2 Agarose gel electrophoresis

Agarose gel electrophoresis was prepared typically as 1% agarose (Melford) melted in 1xTAE buffer (Formedium) in a microwave oven (900 W) for 3 min at 70% maximum power with evaporated water added back in before casting. Gels to separate topological states were

typically run at 60 V for 200 mins. Gels to separate linear DNA fragments were typically run for 1 hour at 100 V. Gels were stained in ca. 2 µg/ml ethidium bromide before imaging in a SynGene Gel imaging system.

2.2.3 PCR and cloning

Primers were designed for the fragments of DNA to be cloned (Table 2.2.1; Table 2.2.3). Thirty cycles of PCR were typically carried out in 20 µl reactions with Phusion polymerase in the GC buffer as per manufacturer's instructions (Table 2.2.5; Table 2.2.6). Following successful amplification of the insert (confirmed by gel electrophoresis) the insert was purified by either gel purification or PCR clean up (see section 2.2.5). The vector was typically prepared by cleavage with restriction enzymes for at least 3 hours at 37°C before gel purification. The vector and insert were used in either a ligation reaction with T4 ligase (NEB) as per manufacturer's instructions or an In-Fusion cloning reaction (Takara Bio Inc.) as per manufacturer's instructions, followed by transformation into cloning cells with the appropriate antibiotics. Colony PCR with a primer in the vector and one in the insert (e.g. a cloning primer and a sequencing primer such as T7), with 2x GoTaq® Green Master Mix (Promega) to a total of 2.5-5 µl reactions were used to confirm positive results as per manufacturer's instructions (Table 2.2.7). The thermocycling procedure used was analogous to that of the Phusion® DNA polymerase protocol with an alteration to 6 mins in the initial denaturation step (Table 2.2.6). Positive results from colony PCR were amplified through overnight culture and performing a mini prep. Sequence analysis (section 2.2.7) was performed to confirm the correct sequence before purification.

Table 2.2.5: Typical reaction components for PCR reactions carried out with Phusion® DNA Polymerase (NEB).

Component	Final Concentration
MilliQ water	To final reaction volume
5X Phusion HF or GC buffer	1X
dNTPs	200 µM
Forwards Primer	0.5 µM
Reverse Primer	0.5 µM
Template DNA	5 pg/µl
DMSO	3% (v/v)
Phusion DNA Polymerase	1.0 units / 50 µl PCR reaction

Table 2.2.6: Typical thermocycling reaction for a PCR reaction carried out with Phusion® DNA Polymerase (NEB).

Step	Temp	Time
Initial Denaturation	95-98°C	2 min
30 Cycles	95-98°C	10-60 s
	Annealing Temperature	30-40 s
	72°C	2-4 min
Final Extension	72°C	10 min

Table 2.2.7: Typical reaction components for PCR reactions carried out with 2x GoTaq® Green Master Mix (Promega).

Component	Final Concentration
MilliQ water	To final reaction volume
2x GoTaq® Green Master Mix (Promega)	1X
Forwards Primer	0.5 µM
Reverse Primer	0.5 µM

2.2.4 Site-directed mutagenesis

Site-directed mutagenesis was performed through use of a PCR-based method by which primers were designed to be complementary to the base sequence around the mutants to change with the altered codon (Table 2.2.2). The PCR reaction was carried out using Phusion® DNA polymerase using the conditions previously described (Table 2.2.5; Table 2.2.6). Fifty picograms of the GyrB or GyrBA plasmids were used as the template DNA. After a successful PCR reaction, the template DNA was removed by digestion by DpnI (NEB) for 1 hour at 37°C in CutSmart buffer (NEB). The resulting plasmid DNA was heat-shock transformed into cloning cells (Table 2.1.1) with the appropriate antibiotics. Successful base change was confirmed by sequencing analysis of the coding sequence of the plasmid.

2.2.5 DNA purification

Linear DNA purification was either carried out by gel extraction and subsequent clean up kit (Qiagen Gel purification kit or NucleoSpin Gel and PCR clean up kit) or through use of a PCR clean-up kit (Qiagen PCR clean-up kit or NucleoSpin Gel and PCR clean up kit) following the manufacturer's instructions with the following alterations as described. Gels run for gel purification were typically made as 0.8% agarose in TAE, and gel slices were typically melted in the appropriate amount of buffer over an elongated time of 1-3 hour at temperatures ranging

between 37-50°C. The spin columns were eluted after a prolonged period of time (15-30 min) with the elution buffer at an elevated temperature of 30-40°C.

Plasmid DNA was purified by the Qiagen mini-prep kit following the manufacturer's instructions with the following alteration that the spin columns were eluted after a prolonged period (15-30 min) with the elution buffer at an elevated temperature of 30-40°C.

2.2.6 DNA concentration determination

DNA concentrations were estimated through use of a Nanodrop (ThermoFisher). Two microliter drops of DNA solution were compared to a buffer blank to obtain an absorbance reading at 260 nm which was converted by the machine with the Beer-Lambert into an estimate of the total DNA concentration.

2.2.7 DNA sequencing

DNA sequencing was performed by either SourceBioscience (Cambridge) or EuroFins Genomics.

2.3 Protein methods

2.3.1 Buffers and solutions

Buffer components were purchased from either Sigma Aldrich or Melford Chemicals.

The following buffers were routinely used in protein purification:

Lysis Buffer: 50 mM Tris-HCl pH 7.9, 400 mM NaCl, 20 mM imidazole

His-elution buffer: 50 mM Tris-HCl pH 7.9, 400 mM NaCl, 500 mM imidazole

TEV cleavage buffer: 50 mM Tris-HCl pH 7.9, 50 mM NaCl, 5 mM DTT

Gel filtration buffer: 50 mM Tris-HCl pH 7.9, 50 mM NaCl, 5 mM DTT

Mtb storage buffer: 50 mM Tris-HCl pH 7.9, 50 mM NaCl, 5 mM DTT, 20% (v/v) glycerol

2.3.2 Protein expression

Approximately 30-50 ng of plasmid DNA was transformed into the Rosetta™ 2 (pLysS) cell line via heat shock transformation (section 2.1.4). After overnight incubation on the correct antibiotics, single colonies were selected and grown in 100 ml LB in 250 ml conical flasks supplemented with the appropriate antibiotics and 0.5% (v/v) glycerol overnight (37°C, 200 rpm). 25-35 ml of the overnight culture was used to inoculate 1 L LB supplemented with the appropriate antibiotics in 2 L shaker flasks and grown at 37°C 200 rpm until OD₆₀₀ of *c.a.* 0.6 (0.4-0.8; 1.5-2.5 hours). Cultures were induced with typically 0.8 mM IPTG (Mtb) or 0.4 mM IPTG (Mth) and the temperature reduced to 28-30°C for 4.5 hours for the full-length subunits and fusion proteins. The Mtb ATPase domain and subdomain constructs were induced with 1 mM IPTG at 37°C for 4.5 hours, meanwhile the Msm and Mth loop deletion sub-ATPase domain constructs were induced at 30°C with 0.4 mM IPTG for 4.5 hours. The cultures were typically harvested at 5000 rpm for 8-10 mins (F8S-6x1000y or F9S 4x1000y rotor). Cells were resuspended in the lysis buffer except for the Mtb full ATPase domain construct (50 mM Tris-HCl pH 8, 400 mM sodium chloride, 20 mM imidazole) and the Msm and Mth loop deletion constructs (50 mM Tris-HCl pH 7.6, 400 mM sodium chloride, 20 mM imidazole). One EDTA-protease inhibitor tablet (Roche) was added per maximum 4 L of cells. Resuspended cells were stored at -80°C until purification.

2.3.3 Protein purification

Two to eight litres of resuspended cell pellets were defrosted from -80°C before lysis at 25,000 psi in a Constant Systems cell disruptor in one-shot mode or in an Avestin EmulsiFlex-B15 homogeniser at 40,000 psi. The lysate was centrifuged at a minimum of 17,500 rpm for 45 mins (SS34-rotor). The supernatant was removed and filtered at 0.45 µm before application to a 5 ml HisTrap HP or equivalent column. The column was washed in lysis buffer supplemented with 2-5% His-elution buffer before elution over a gradient from 5-100% His-elution buffer. Fractions were analysed on 8-12% SDS-PAGE gels depending on the size of the protein. Fractions deemed to contain the protein of interest were dialysed overnight against TEV cleavage buffer in the presence or absence of 1 mg TEV protease. If TEV cleavage was carried out, a second 5 ml HisTrap HP column was run collecting the flow-through followed by application to a MonoQ 10/100 column. The column was subsequently washed to a stable base line before eluting on a gradient 50 -1000 mM sodium chloride. If no TEV cleavage was carried out, the dialysed protein was directly run onto a MonoQ 10/100 column as described above. Fractions were analysed on 8-12% SDS-PAGE gels depending on the size of the protein. Fractions deemed to contain the protein of interest were pooled and concentrated to

less than 1 ml before application to a gel filtration column in gel filtration buffer (Superdex™ 75 10/300 for the GyrB24 constructs and HiPrep 16/60 Sephacryl S-400 HR for the GyrBA constructs). Fractions were analysed on 8-12% SDS-PAGE gels depending on the size of the protein. Fractions deemed to contain pure protein of interest were pooled and dialysed overnight against the Mtb storage buffer. Proteins were concentrated to the desired concentration before aliquoting and flash freezing in liquid nitrogen before storage at -80°C.

The Mtb GyrA and GyrB subunits (including mutants) were purified with a single column strategy using the initial HisTrap HP column before dialysis into Mtb storage buffer. The Mth GyrA and GyrB subunits were purified with a dual column strategy using the initial HisTrap HP column before TEV cleavage and a reverse HisTrap HP column and dialysis into the Mtb storage buffer.

The final preparations of the Msm and Mth GyrB sub-ATPase domains were performed at pH 7.6 and additionally supplemented with 1 mM EDTA for the MonoQ and Gel Filtration columns as well as in the final storage buffer.

2.3.4 Sodium dodecyl sulphate – polyacrylamide gel electrophoresis (SDS-PAGE)

Three different types of SDS-PAGE gels were used in this project. 8% polyacrylamide Tris-Glycine gels were used for the identification of the GyrBA fusion proteins (8% (v/v) acrylamide, 375 mM Tris-HCl pH 8.8, 0.1% (v/v) SDS, 0.1% (v/v) APS, 0.1% (v/v) TEMED) with a 4% stacking gel made as per the resolving gel with 125 mM Tris-HCl pH 6.8. Gels were typically run in a Tris-Glycine running buffer (25 mM Tris-base, 192 mM glycine, 0.1% (v/v) SDS) for 1 hour at 180 V.

12% acrylamide Bis-Tris gels were prepared and used for the identification of the GyrB sub-ATPase domain. The resolving gels were prepared to contain 0.35 M Bis-Tris-HCl pH 6.8, 12% (v/v) acrylamide, 0.1% (v/v) APS, 0.1% (v/v) TEMED, with a 0.5-1 cm of 5% (v/v) acrylamide stacking gel was set on top of the resolving gel to contain the wells. Gels were typically run in a 1x MOPS running buffer (50 mM MOPS, 50 mM Tris-HCl, 3.5 mM SDS, 1 mM EDTA, pH 7.3) for 1 hour at 180 V.

TruPage precast gels (10%) (Sigma Aldrich) were used for identification of the full-length subunits. Samples were prepared by boiling with 1x loading buffer (50 mM Tris-HCl pH 6.8, 2% (v/v) SDS, 100 mM DTT, 10 (v/v) glycerol and 0.05% (w/v) bromophenol blue). Gels were run in the TruPage running buffer for 1 hour at 180 V.

Samples for SDS-PAGE analysis were prepared by boiling in final 1x sample application buffer (50 mM Tris-HCl pH 6.8, 10% (w/v) SDS, 100 mM DTT, 10% (v/v) glycerol, 0.05% (w/v) bromophenol blue) prior to loading. All SDS-PAGE gels were stained with InstantBlue™ stain (Expedeon) and imaged in a SynGene gel imager.

2.3.5 Dialysis

Dialysis was conducted in SnakeSkin™ (Thermo Scientific) tubing (10 kDa MWCO) clipped with food clips attached to polystyrene flotation devices overnight at 8°C in 2 L buffer with a magnetic stirrer bead stirring at a low rate.

2.3.6 Protein concentration

Protein concentration was performed in Amicon Ultra centrifugal filters (Merck) with a maximum molecular weight cut off (MWCO) of half the monomeric molecular weight of the protein of interest. Concentration was typically carried out at between 3000-4500 rpm on a bench top centrifuge (Sorvell Legend RT) or at 14,000 xg in a bench top microcentrifuge at 4°C. Concentration analysis was carried out at regular intervals to determine the desired endpoint.

Pre-concentration of samples was additionally assisted by addition of 1-2.5% (w/v) PEG 35,000 to overnight dialysis solutions.

2.3.7 Protein concentration determination

Protein concentration was determined by taking multiple readings at 280 nm on a NanoDrop spectrophotometer system. Where the absorbance reading was above 1 unit, serial dilutions were made in the same buffer to calculate the concentration more accurately. Buffer blanks were carried out and subtracted from the protein readings. The protein concentration was then determined using the theoretical absorption co-efficient and molecular weight as calculated

by the ExPASy ProtParam tool (<https://web.expasy.org/protparam/>), via the Beer-Lambert Law:

$$A = \epsilon bc$$

Where A is the absorbance value (1 mm pathlength corrected to a 1 cm by the nanodrop software); ϵ is the absorbance co-efficient in units of $M^{-1} \text{ cm}^{-1}$ at the absorbance wavelength; b the path length (1 cm); and C the concentration of the protein (M). Therefore:

$$C = \frac{A}{\epsilon b}$$

To determine the concentration in units of mg/ml, the concentration in M was multiplied by the calculated molecular weight.

2.3.8 Surface plasmon resonance

Surface plasmon resonance was carried out in a Biacore T200 machine at 25°C with the assistance of Dr Rosaria Campilongo. The Mtb and *E. coli* GyrB sub-ATPase domains were bound at concentrations of 50 $\mu\text{g/ml}$ in 10 mM sodium acetate pH 4.5 to CM5 sensor chips after activation of the surface carboxyl groups through the injection of a mixture of N-hydroxysuccinimide (50 mM) and 1-ethyl-3-(3-diaminopropyl) carbodiimide (20 mM) from the Biacore amine coupling kit. Once the desired saturation was reached the active amines were deactivated through injection of ethanolamine.

The system was primed in the SPR running buffer (10 mM HEPES-NaOH pH 7.4, 150 mM sodium chloride, 3 mM EDTA, 0.05 % (v/v) Tween-20, 5% (v/v) DMSO). Two-fold compound dilutions of Redx04739 were prepared in the SPR running buffer from a maximum concentration 50 μM . These compound dilutions were injected across the chips in single-cycle kinetics, with the reference cell (chip no protein) being subtracted for analysis. Data was subsequently analysed in Microsoft Excel to generate K_d values.

2.4 Compounds and solvents

Novel compounds supplied by Redx AntiInfectives were made up as stocks to 12.8 mg/ml in 100% DMSO. Dilutions were made in broth for bacterial assays and in DMSO for enzymatic and crystallographic studies.

2.5 DNA topology assays

2.5.1 Assay of DNA supercoiling by DNA gyrase

Supercoiling assays were carried out in a 30 μ l reaction volume at varying concentrations of DNA gyrase always with 0.5 μ g relaxed pBR322* in 1x supercoiling assay buffer (Table 2.5.1). A 6 μ l reaction proportion was typically reserved for enzyme, dilution buffer (storage buffer of enzyme in the absence of enzyme (Table 2.5.1)), compounds and solvents. Reactions were typically incubated at 37°C in a waterbath for 30 mins unless otherwise stated. The reaction was stopped through addition of 30 μ l 24:1 chloroform: isoamylalcohol solution and 15 μ l 2x STEB buffer (40% sucrose, 100 mM Tris-HCl pH 8.0, 100 mM EDTA, 0.5 μ g/ml bromophenol blue), and vortexing before centrifugation (13,000 rpm 4 mins). The aqueous product was loaded onto native 1% (w/v) agarose in TAE gels. Gels were run as stated in section 2.2.2.

Table 2.5.1: Typical assay and dilution buffers used in the respective *E. coli* and mycobacterial DNA gyrase supercoiling assays

	<i>E. coli</i>	Mycobacteria
1x Assay buffer	35 mM Tris-HCl pH 7.5	50 mM HEPES-KOH pH 7.9
	24 mM potassium chloride	6 mM magnesium acetate
	4 mM magnesium chloride	4 mM dithiothreitol
	2 mM dithiothreitol	1 mM ATP
	1.8 mM spermidine	100 mM potassium glutamate
	1 mM ATP	2 mM spermidine
	6.5 % (w/v) glycerol	0.05 mg/ml bovine serum albumin
	0.1 mg/ml bovine serum albumin (acetylated)	(acetylated)
Dilution buffer	50 mM Tris-HCl pH 7.5	50 mM Tris-HCl pH 7.9
	100 mM potassium chloride	50 mM sodium chloride
	2 mM dithiothreitol	5 mM dithiothreitol
	1 mM EDTA	20% (v/v) glycerol
	50% (w/v) glycerol	

2.5.2 Assay of DNA relaxation by DNA gyrase

Relaxation assays were carried out in a 30 μ l reaction volume at varying concentrations of DNA gyrase always with 0.4 μ g supercoiled pBR322* in relaxation assay buffer (50 mM HEPES-KOH pH 7.9, 6 mM magnesium acetate, 4 mM dithiothreitol, 100 mM potassium

glutamate, 2 mM spermidine, 0.05 mg/ml bovine serum albumin (acetylated)). A 6-8 μ l reaction proportion was typically reserved for enzyme, dilution buffer (storage buffer of enzyme in the absence of enzyme), compounds and solvents. Reactions were typically incubated at 37°C in a waterbath for 1-2 hours as stated. 0.1 mg/ml proteinase K was added to the reaction and incubated at 37°C for 30 mins before addition of 30 μ l 24:1 chloroform: isoamylalcohol solution and 15 μ l 2x STEB buffer (40% sucrose, 100 mM Tris-HCl pH 8.0, 100 mM EDTA, 0.5 μ g/ml bromophenol blue), vortexing and centrifugation (13,000 rpm 4 mins). The aqueous product was loaded onto native 1% (w/v) agarose in TAE gels. Gels were run as stated in section 2.2.2.

2.5.3 Assay of DNA decatenation by DNA gyrase

Decatenation assays were carried out in a 30 μ l reaction volume at varying concentrations of DNA gyrase always with 200 ng kDNA in either decatenation buffer (40 mM Tris-HCl pH 7.5, 10 mM sodium chloride, 10 mM dithiothreitol, 1 mM ATP, 250 mM potassium glutamate, 6 mM magnesium acetate and 0.5 mg/ml bovine serum albumin (acetylated)) or supercoiling assay buffer (Table 2.5.1). A 6 μ l reaction proportion was typically reserved for the enzyme and dilution buffer (storage buffer of enzyme in the absence of enzyme (Table 2.5.1)). Reactions were typically incubated at 37°C in a waterbath for 30 mins. The reaction was stopped through addition of 30 μ l 24:1 chloroform: isoamylalcohol solution and 15 μ l 2x STEB buffer (40% sucrose, 100 mM Tris-HCl pH 8.0, 100 mM EDTA, 0.5 μ g/ml bromophenol blue), and vortexing before centrifugation (13,000 rpm 4 mins). The aqueous product was loaded onto native 0.8% (w/v) agarose in TAE gels. Gels were run as stated in section 2.2.2.

2.5.4 Assay of DNA cleavage by DNA gyrase

Cleavage assays were carried out in a 30 μ l reaction volume at 0.074 μ M *M. tuberculosis* or 0.25 μ M *M. thermoresistibile* DNA gyrase with 0.3 μ g supercoiled pBR322* in relaxation assay buffer. A 6 μ l reaction proportion was typically reserved for enzyme, dilution buffer (storage buffer of enzyme in the absence of enzyme (Table 2.5.1)), compounds and solvents. Reactions were typically incubated at 37°C in a waterbath for 30 mins. To trap the linear DNA, 0.1 mg/ml proteinase K and 0.2 (v/v) SDS were added to the reaction and further incubated at 37°C in a waterbath for 30 mins. The reaction was stopped through addition of 30 μ l 24:1 chloroform: isoamylalcohol solution and 15 μ l 2x STEB buffer (40% sucrose, 100 mM Tris-HCl pH 8.0, 100 mM EDTA, 0.5 μ g/ml bromophenol blue), and vortexing before centrifugation (13,000 rpm 4 mins). The aqueous product was loaded onto native 1% (w/v)

agarose in TAE gels. Gels were typically left for 15 mins before being run at 60 V for 200 mins. Gels were stained in 2 µg/ml ethidium bromide solution before imaging.

2.5.5 Assay of ATP turnover by DNA gyrase

The PK/LDH (pyruvate kinase/lactate dehydrogenase) assay (Figure 2.5.1) was carried out in 96-well flat bottomed micro-titre plates in 50 µl reaction volumes. A typical reaction contained 10 µl 5x ATPase assay buffer (Table 2.5.2), 1-2 ng pBR322*, 0.8 mM phosphoenolpyruvate, 0.75 µl PK/LDH solution (Sigma), 0.4 mM NADH, a 5 µl reaction volume was reserved for compounds, drugs and solvents, with reactions being carried out in 1% (v/v) DMSO.

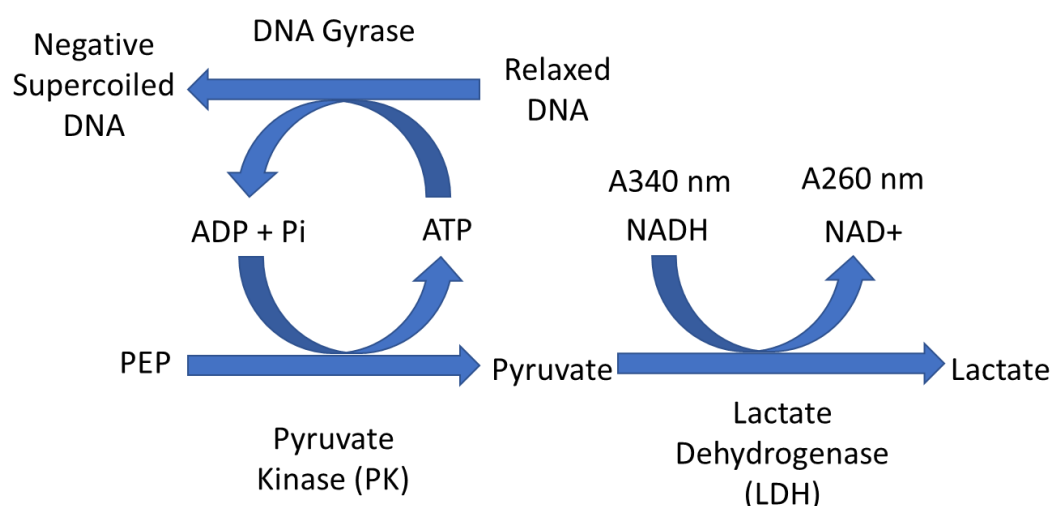


Figure 2.5.1: Cartoon representation of the PL/LDH linked ATPase assay system used. Three enzymes work co-operatively to convert PEP into Lactate while Relaxed DNA is negatively supercoiled, and ATP is continually regenerated, and NADH oxidised into NAD⁺ resulting in a decrease in absorbance at 340 nm which can be measured and using the Beer-Lambert law the number of ATP molecules hydrolysed by DNA gyrase can be calculated.

Table 2.5.2: 1x Assay buffer used in the PK/LDH-linked ATPase assay of *E. coli* and mycobacterial gyrases.

	<i>E. coli</i>	Mycobacteria
Assay buffer	50 mM Tris-HCl pH 7.5	50 mM HEPES-KOH 7.9
	1 mM EDTA	4 mM DTT
	5 mM magnesium chloride	6 mM magnesium acetate
	10% (w/v) glycerol	100 mM potassium glutamate

The rate of ATP turnover was calculated using the Beer-Lambert law ($\Delta A = \epsilon cl$). The extinction co-efficient (ϵ) of NADH at 340 nm of $6220 \text{ M}^{-1}\text{cm}^{-1}$, and a path length (l) of 1.37 mm were applied with the change of absorbance (ΔA) over a minimum time period of 30 mins directly after the addition of ATP being measured through use of the equation for linear regression ($y = mx + c$), using an x value of $1/60$ corresponding to 1 s. The resulting concentration decrease in NADH directly corresponds to the total number of ATP molecules turned over per second. To determine the number of ATP molecules turned over per individual GyrB or GyrBA subunit the final value was divided by the concentration of the protein in M. To account for the fraction of the ATP molecules turned over per second by contaminating enzymes, the novobiocin-independent rate when 100-200 μM novobiocin was included in the reaction was subtracted from the measured rate to give the novobiocin-dependent rate. All trial reactions were carried out in duplicate, and the errors calculated using the linear regression feature in GraphPad Prism. The final error value was calculated through the following equation: $\Delta Kd = \sqrt{(K^2 + Knov^2)}$.

IC_{50} values were obtained by performing non-linear regression [log(inhibitor) vs response – variable slope (four parameters)] on the novobiocin independent rates (Redx03863 and Redx04739) or absolute rates (novobiocin).

2.5.6 Assay of DNA relaxation by topo IV

Relaxation assays were carried out in a 30 μl reaction volume at varying concentrations of DNA gyrase always with 0.4 μg supercoiled pBR322* in relaxation assay buffer (50 mM HEPES-KOH pH 7.6, 100 mM potassium glutamate, 10 mM magnesium acetate, 10 mM dithiothreitol, 1 mM ATP, 0.05 mg/ml bovine serum albumin (acetylated)). A 6 μl reaction proportion was typically reserved for enzyme, dilution buffer (40 mM HEPES-KOH pH 7.6, 100 mM potassium glutamate, 1 mM dithiothreitol, 1 mM EDTA, 40% (v/v) glycerol), compounds and solvents. Reactions were typically incubated at 37°C in a waterbath for 1-2 hours as stated. 0.1 mg/ml proteinase K was added to the reaction and incubated at 37°C for 30 mins before addition of 30 μl 24:1 chloroform: isoamylalcohol solution and 15 μl 2x STEB buffer (40% sucrose, 100 mM Tris-HCl pH 8.0, 100 mM EDTA, 0.5 $\mu\text{g}/\text{ml}$ bromophenol blue), vortexing and centrifugation (13,000 rpm 4 mins). The aqueous product was loaded onto native 1% (w/v) agarose in TAE gels. Gels were run as stated in section 2.2.2.

2.5.7 Assay to determine cleavage profile by DNA gyrase

Three cleavage assays were carried out using either the mycobacterial supercoiling assay buffer containing ATP and 2 ng of relaxed pBR322* (120 µl final volume), or mycobacterial relaxation assay buffer (no ATP) with either 1.2 ng of negatively supercoiled pBR322* (120 µl final volume) or 1.2 ng of EcoRI-linearised pBR322* (50 µl final volume) in the presence of 3.3% (v/v) DMSO, with or without DNA gyrase subunits, and 50 µM moxifloxacin. The assay was incubated in a waterbath at 37°C for 30 min before addition of 0.1 mg/ml proteinase K and 0.2% (v/v) SDS, and further incubation in a waterbath at 37°C for 30 min. The assay was immediately subjected to the NucleoSpin Gel and PCR clean up kit following the manufacturer's instructions and being eluted in 40-50 µl of Buffer EB. A 20 µl digestion was performed on 10-16.5 µl of purified product with 10 units of BsaI-HF, EcoRI-HF and BsaI-HF in a waterbath at 37°C overnight. The products were analysed on native 1.2% (w/v) agarose in TAE gels run as stated in section 2.2.2.

2.6 Whole cell compound testing

2.6.1 MIC determination

A top concentration was selected to a maximum of 128 µg/ml and a two-fold dilution series was applied to the compound diluted in growth medium to a final concentration decrease of 2^{10} . A maximum final concentration of 1% (v/v) DMSO was used. Bacteria grown on agar were suspended in assay growth media to a dilution factor of 1/100 of the 0.5 McFarland constant (CLSI, 2012). An equal volume of the bacterial growth suspension and the compound dilution series were mixed, the positive growth control contained media without drug, the negative control contained 100 µl media in the absence of bacteria. The OD₆₀₀ was read and the bacteria were incubated for 20 hours for *E. coli* ATCC25922, *A. baumannii* NTCC13420, *Pseudomonas aeruginosa* ATCC 27853, and *Staphylococcus aureus* ATCC29213 at 37°C, or for 48 hours for *M. smegmatis* ATCC19420 at 35°C before taking visual and OD₆₀₀ readings. All data were confirmed as a minimum of n = 2 where both repeats were within a 2-fold difference.

2.6.2 Agar MIC determination

A top concentration was selected (maximum 64 µg/ml), and a 10X solution was made and a two-fold dilution series was applied to the compound diluted in broth to a final concentration decrease of 2^{10} . The maximum final concentration of 1% (v/v) DMSO was used. 100 µl of compound dilution or plain broth (positive and negative control wells) was mixed with 900 µl

of Muller-Hinton agar for *E. coli* or Middlebrook 7H11 agar for *M. smegmatis* both at 50°C and allowed to set in the wells of a 24-well plate. Two replicates were made at each drug dilution. The bacteria grown on agar were suspended in broth to a dilution factor of 1/100 of the 0.5 McFarland constant. 20 µl of bacterial suspension was used to inoculate each well. The plates were incubated for 20 hours for *E. coli* ATCC25922 or for 72 hours *M. smegmatis* ATCC19420. All data were confirmed as a minimum of n = 2 where both repeats were within a 2-fold difference. All experiments were performed at a minimum of two repeats.

2.6.3 Time of kill

A single 10 ml starter culture was inoculated with a single bacterial colony grown on agar incubated overnight for *E. coli* ATCC25922 or for 2.5 days *M. smegmatis* ATCC19420 at 37°C 200 rpm. 50 µl of the starter culture was subbed into 5 ml pre-heated medium and grown at 37°C 200 rpm until OD₆₀₀ 0.3. The inoculum was diluted to the 0.5 McFarland standard in broth and 250 µl was used to inoculate 50 ml prewarmed broth in 250 ml flasks. 100 µl was removed to form the T-5 plate dilutions made in sterile PBS. 200 µl of compound diluted in broth to form a 1000x or 4000x MIC stock was added to duplicate flasks. Duplicate flasks were kept aside as no drug controls. 100 µl was removed from each flask to form the T0 plate dilution series made in sterile PBS. All flasks were incubated at 37°C 200 rpm. Plate dilutions were taken at 30, 60, 120, 240, 360, 1440 min for *E. coli* ATCC25922 or 6, 12, 24, 48, 96, 144 hours for *M. smegmatis* ATCC19420 made in sterile PBS. Colonies were counted after 24-hour incubation at 37°C for *E. coli* ATCC25922 or after 3-day incubation for *M. smegmatis* ATCC19420 at 37°C. The percentage of colony forming units remaining was calculated as a percentage of the average number of colonies from the no drug control plates divided by those counted on each of the plates from the cultures treated with compound. The point at which no colony was counted on a plate emerging from a drug treated culture was defined as the time of kill.

2.6.4 Disruption of biofilm assay

Initially two 10 ml starter cultures were set up from solid medium of *E. coli* ATCC25922 and grown at 37°C. After 24 hours the culture was diluted to 1/10th of the 0.5 McFarland constant in broth. 200 µl was used to inoculate each well of a 96-well plate. A Calgary Biofilm device was attached, sealed and the plate was incubated at 37°C shaking at 400 rpm. After 24 hours the Calgary Biofilm device was washed twice in sterile 1x PBS for 5 min shaking at 400 rpm, before being incubated in a series of two-fold antibiotic and compound dilutions of 200 µl

starting at 1028 µg/ml for antibiotics and 64 µg/ml for compounds. The plate was incubated at 37°C 400 rpm. After 24 hours the bMIC was read and the Calgary Biofilm device was washed twice in sterile PBS for 5 min shaking at 400 rpm, before being incubated in 200 µl plain broth at 37°C shaking at 400 rpm. After 24 hours the MBEC was read to determine the lowest concentration that can effectively eradicate biofilms and inhibit shedding and growth in the wells.

The timings were altered to 48 hours for *M. smegmatis* with the exception that the drug incubation step was 72 hours.

2.7 Bacterial mutant generation

2.7.1 Frequency of mutation experiment

A 10 ml starter culture was inoculated with a single colony of *E. coli* ATCC25922 was grown for 24 hours or a single colony of *M. smegmatis* ATCC19420 was grown for 48 hours in broth. To generate inoculum 2 ml starter culture was concentrated to 1 ml by the pelleting of 1 ml of culture followed by resuspension of the pellet in a further 1 ml of culture. Fifty microlitres of each concentrated inoculum was used to inoculate each of four 10 ml half 90 mm Petri dishes, containing concentrations of the compound of interest at either 2x or 4x the agar MIC value. A further 50 µl of each concentrated inoculum at $10^0 - 10^{-7}$ were plated on 2 no-drug containing half 90 mm Petri dishes. Compound-free plates were incubated for 20 hours (*E. coli*) and 48 hours (*M. smegmatis*) at 37°C. Compound containing plates were incubated for 48 hours (*E. coli*) or 5 days (*M. smegmatis*).

Following successful isolation of mutants, a representative selection (maximum 8) was restreaked onto the base agar without antibiotics. After their growth period (24 hours *E. coli* or 48 hours *M. smegmatis*) the MIC of the parent strain was compared to the mutant strain to confirm mutagenesis. Two independent replicates were performed. After successful validation of resistance mutation, glycerol stocks of the strain were made by mixing colonies from the plate in a mix of 150 µl broth with 50 µl 80% (v/v) glycerol and frozen at -80°C. Mutants were characterised by cross-MIC testing against a panel of known antibiotics and other novel compounds of known mode of action. Additionally, 5 ml liquid culture was grown from each mutant and the genomic DNA extracted using the EdgeBio (85171) PurElute™ Bacterial Genomic kit as per manufacturer's instructions for *E. coli* strains. The manufacturer's protocol

was altered for *M. smegmatis* to break open the mycolic acid cell wall through the extension of incubation periods and by introducing the use of BeadBug™ prefilled tubed 0.1 mm/ 2 ml capacity (silica) for the vortexing steps to allow for mechanical breakage of the mycolic acid cell wall. PCR amplification of the DNA gyrase genes (*gyrA* and *gyrB*) and the topo IV genes (*parC* and *parE*) was performed using primers (Table 2.2.4), and purification of fragments was performed with the Qiagen PCR clean-up kit as per the manufacturer's instructions. The products were sent for sequencing (Eurofins) within the sequencing primers (Table 2.2.4).

2.7.2 Serial passage

Serial passage experiments were conducted by the same method as the broth MIC protocol (Section 2.6.1) with the following alterations. Technical duplicates were always performed. The plates were initially inoculated with a final dilution of 1/200 of a 10 ml starter culture of *E. coli* ATCC25922 incubated for 24 hours or *M. smegmatis* ATCC19420 incubated for 48-72 hours. All subsequent passages were performed with a final dilution of 1/100 from the ¼ MIC well every 24 hours (*E. coli*) or 48-72 hours (*M. smegmatis*). Glycerol stocks were made at least every 4 passages through addition of 33 µl 80% (v/v) glycerol to the ¼ MIC well and frozen at -80°C. The passage could be restarted from a 1/100 final dilution from the glycerol stock. Glycerol stocks were additionally prepared from the ¼ and ½ MIC wells when the MIC approached 64 µg/ml, with a top achievable MIC concentration of 128 µg/ml.

Upon an end being reached by either an MIC of greater than 64 µg/ml or a significant fold change in the MIC, a glycerol stock was made as described above, and an agar plate was streaked. Cross-resistance analysis and genomic extraction, PCR amplification of the type IIA topoisomerase genes with subsequent sequencing analysis was carried out as described in section 2.7.1.

2.8 Protein crystallography: crystal methods

2.8.1 Screening of crystallisation condition

Forty microlitre volumes of multiple 96-well commercial sparse matrix screens were aliquoted into the wells of Swissci 96-well 2-drop MRC sitting drop vapour diffusion crystallisation plates. An Oryx8 robot (Douglas instruments) was used to dispense 600 nl drops containing 300 nl of each protein and screen. Plates were sealed with Fortitude PCR seals and imaged at 20°C in a Minstrel™ HT UV robot (Rigaku).

The commercial sparse matrix screens (JCSG-*plus*TM, Morpheus®, The BCS screen, SG1TM screen, Structure screen 1 + 2, MIDAS*plus*TM, PACT *premier*TM, The PGA screenTM) were purchased in HT-96 format from Molecular Dimensions. The AmSO₄ suite and PEGs suite crystallisation screens were purchased from Quiagen. In addition, the inhouse KISS (keep it simple screen) screen was made and aliquoted by Molecular Dimensions. The KISS screen combines a buffer system (sodium acetate pH 4; sodium citrate pH 5; MES pH 6, HEPES pH 7, Tris-HCl pH 8, CHES pH 9) with PEG3350 (5-40% (w/v)) and ammonium sulphate 0.2-3.2 M.

2.8.2 Optimisation of crystallisation conditions

Crystal hits were optimised if they showed likelihood of containing protein (including those which did not show UVA-fluorescence). Conditions of interest were optimised in terms of pH, precipitant concentration and ionic strength, and pipetted in 40 µl well volumes by an Orxy8 robot (Douglas instruments). The wells were pipetted, sealed and the plates were imaged as per the method used for screening.

2.8.3 Seeding of crystallisation conditions

After semi-successful optimisation, seed stocks were made by harvesting wells of crystals in 40-100 µl mother liquor and vortexing for 4 mins with between one and three 1 mm glass beads (Sigma Aldrich). Seed stocks were stored at 4°C for short term storage or -20°C for long-term storage. When applying seed stocks to crystallisation optimisations the drop ratio was altered to contain 300 nl protein solution, 200 nl well solution and 100 nl seed stock without dilution.

2.8.4 SDS-PAGE of crystals

A well of sub-optimal crystals was chosen, and 2 µl of the well solution was added to the drop, and the full well of crystals was removed to a 1.5 ml Eppendorf. The crystals were pelleted at 2000 xg for 1 min and the supernatant was removed. The crystals were washed in 10 µl well solution. A total of 4 wash steps were completed. The crystals were pelleted, and the supernatant removed, before addition of 10 µl 5x loading buffer (250 mM Tris-HCl pH 6.8, 10% (w/v) SDS, 0.5 M EDTA, 50% (v/v) glycerol, 0.25 (w/v) bromophenol blue). The samples were boiled and run on 12% SDS-PAGE with a positive control of pure protein.

2.8.5 Crystal soaking

Novobiocin crystal-containing wells were selected and mother liquor supplemented with between 1-4% (v/v) DMSO 0.25-1 mM Redx03863 or Redx04739 and 25% (v/v) ethylene glycol was applied to these wells (1-2 μ l per 600 nl drop). Crystal soaks of between 20 min and several days were tested. These wells were harvested without the need of additional cryoprotectants as per section 2.8.6.

2.8.6 Harvesting of crystals

Crystals were harvested in Litholoops (Molecular Dimensions) by Dr Clare Stevenson. Crystals were either harvested from the well before being washed in a cryoprotectant and flash frozen in liquid nitrogen or cryoprotectant was added to the well solution before harvesting the crystals which were directly flash frozen in liquid nitrogen. Cryoprotectants were typically made to contain the well solution supplemented with 25% ethylene glycol.

2.9 Protein crystallography: data collection and structure determination

2.9.1 X-ray data collection

X-ray data collection was carried out on beamlines i03 and i04 under cryogenic conditions at the Diamond Synchrotron, Oxford, UK. X-ray data were collected for 3600 x 0.05-0.1° images at a wavelength of 0.97 Å (1.2782 Å for data collected at the zinc edge) to maximum resolution 1.2-1.3 Å with a beam size of 80x20 or 54 x40 μ m. All data sets were collected with a Pilatus3 6M hybrid photon counting detector (Dectris). Auto processing was carried out on the Diamond computers to determine the best data sets to work with.

2.9.2 DIMPLE analysis

A partially refined structure of the Msm GyrB sub-ATPase domain without ligands was uploaded to the ISPyB database prior to data collection. This was used by the Difference Map Pipeline (DIMPLE (Winn *et al.*, 2011)) to identify unmodeled density that could contain ligands of interest.

2.9.3 Processing of diffraction data

The Xia2 DIALS (Winter, 2010) datasets from auto processing after integration and scaling were merged (without further scaling) by AIMLESS (Evans and Murshudov, 2013). Expert molecular replacement (PHASER (McCoy *et al.*, 2007)) was carried out with a monomer of the 4B6C published structure of the *M. smegmatis* sub-ATPase domain (Shirude *et al.*, 2013) for the *M. smegmatis* structure. The resultant *M. smegmatis* structure was used for the molecular replacement of the *M. thermoresistibile* structures by PHASER. The model was largely completed through use of BUCCANEER (Cowtan, 2006) before iterative rounds of refinement (REFMAC (Murshudov *et al.*, 1997)) and manual model building (COOT (Emsley *et al.*, 2010)) until the structure appeared complete and no further improvement in the R-factors and geometries were observed. Structures were validated through MOLPROBITY (Chen *et al.*, 2010), PDB-REDO (Joosten *et al.*, 2009) and the PDB-validation server (Berman *et al.*, 2003).

3. Mechanistic Studies of DNA Gyrase from *M. tuberculosis* and *M. thermoresistibile*

Presently there have been several mechanistic and structural studies carried out on DNA gyrase from both *M. tuberculosis* and *M. smegmatis*. However, in the past these studies have focused on just the A₂B₂ heterotetramer, here we investigate if there are any mechanistic differences through using a (BA)₂ construct where the subunits have been fused to form a protein that resembles eukaryotic topo II. We have also carried out preliminary analysis of both of these constructs from the thermophilic mycobacterium *M. thermoresistibile* with the idea that it may be a stronger candidate for structural studies.

3.1 DNA gyrase from *M. tuberculosis*

3.1.1 Construct development of the GyrBA fusion protein

Three Mtb DNA gyrase constructs (GyrA, GyrB and GyrBA) were passed on from previous lab members Dr Steven J. Hearnshaw (SJH) and Dr Frederic Collin (FC; Figure 3.1.1). The GyrBA fusion construct was an idea designed and cloned by FC, expression and purification were optimised by SJH. The construct was initially designed to be GyrB fused N-terminally to GyrA, with a single lysine linker inserted as a restriction enzyme site to create the construct; at the C-terminus a TEV site was followed by a His-tag before the stop codon in the pET-20b(+) vector (Figure 3.1.1). On the original construct the extra 40 amino acids that have been determined not to be biologically relevant were included (Karkare *et al.*, 2013a). Both the GyrB and GyrBA constructs were altered initially by deleting the N-terminal 40 amino acids. Following this the C-terminal TEV sequence and His-tag was removed from the GyrBA construct and the GyrBA coding sequencing was inserted using In-Fusion cloning (Takarabio) into the pET28-MHL vector at the BseRI site. This inserted an N-terminal His-tag followed by the TEV cleavage sequence before the GyrBA coding sequence (Figure 3.1.1). The natural valine start codon was altered to a methionine for expression in *E. coli*.

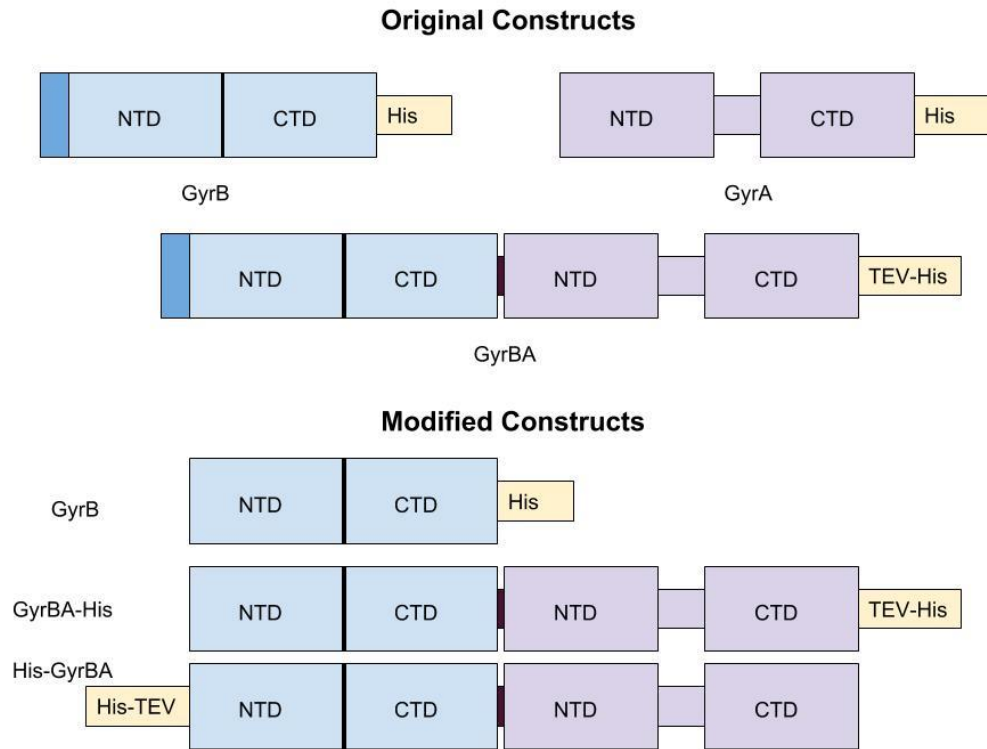


Figure 3.1.1: Cartoon representation of the three Mtb DNA gyrase constructs obtained from other lab members. The GyrB and GyrBA constructs contained the 40 amino acids at the N-terminus that have been defined as not being biologically relevant. The GyrBA construct was created with a single lysine linker between the GyrB and GyrA subunits. The original GyrB and GyrBA constructs were altered to remove the biologically irrelevant 40 amino acids. The C-terminal TEV-His-tag on the GyrBA construct was also moved to create a construct with a N-terminal His-TEV tag.

3.1.2 Protein expression and purification of the GyrBA fusion protein

Expression of the fusion protein had been partially optimised by SJH before the construct was altered. To determine if these conditions were still optimal, the expression conditions including cell lines, induction temperatures, media, and IPTG concentrations were trialled on a small scale to determine the preferred conditions. It was found that the cells expressed the 170 kDa protein in a variety of different conditions, but optimally in the Rosetta™ 2 (pLysS) cell line, by induction with 0.8 mM IPTG at 28-30°C, for a time greater than 4 hours (Figure 3.1.2a).

To determine if the expression conditions of the fusion protein produced active proteins the cell lysate assay was developed. This involved using cell lysate in a traditional supercoiling assay obtained on a small scale to see if activity was observed eliminating the need to purify

a protein before determining its activity. The method trialled included lysing 1 ml of cell pellet at OD₆₀₀ of 0.1 in 100 µl of lysis buffer via three rounds of freeze-thaw treatment followed by a 30 min spin to remove cell debris at 13,200 rpm bench top centrifuge (4°C). 3 µl of the clarified lysate showed significantly increased supercoiling activity compared to the uninduced sample under standard supercoiling assay conditions (Figure 3.1.2b).

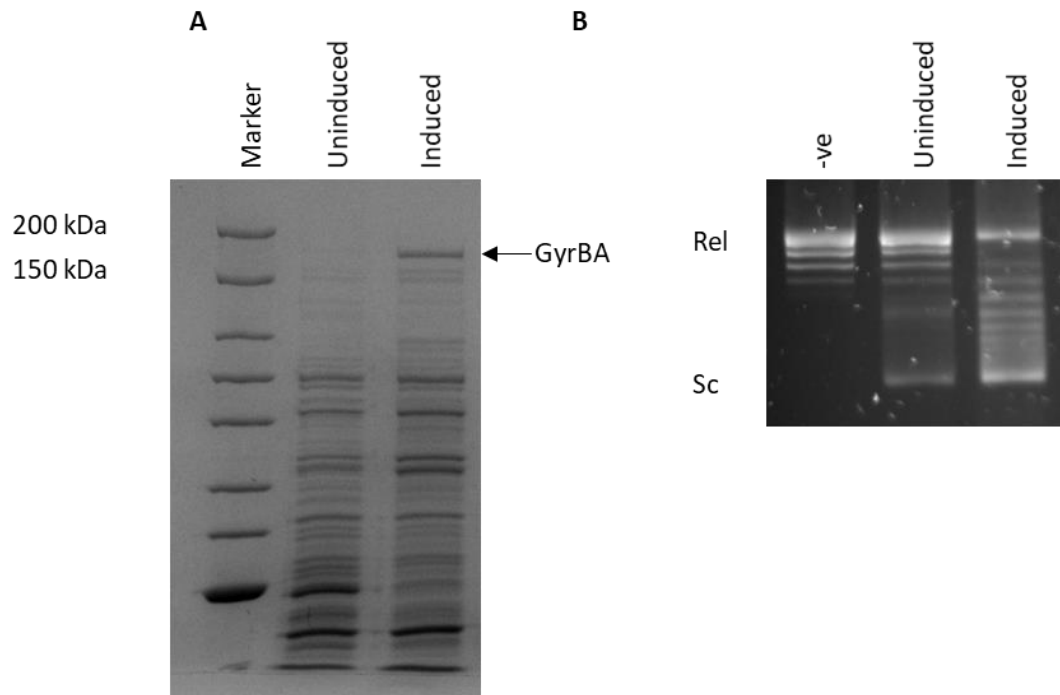


Figure 3.1.2: Induction of the 168 kDa Mtb GyrBA fusion protein under optimal expression conditions: *E. coli* Rosetta™ 2 (pLysS) cell line, before (uninduced) or after (induced) induction with 0.8 mM IPTG at 28°C for 4.5 hours. One millilitre of both samples was pelleted and resuspended in lysis buffer, so that a sample with an OD₆₀₀=0.6 was resuspended in 100 µl lysis buffer. The samples were lysed by 3 rounds of freeze-thaw treatment before centrifugation for 30 min at 13,200 rpm. A) 8% SDS-PAGE showing induction of a protein between 150-200 kDa likely to be the GyrBA fusion protein of 168 kDa. B) 1% agarose in TAE gel showing a lysate supercoiling assay carried out with 3 µl of clarified lysate suggesting that the GyrBA protein has increased activity in supercoiling compared to the uninduced sample.

After optimisation of expression on a small scale, the protein was expressed on a large scale (4-8 L). The lysing protocol was altered to use an Avestin EmulsiFlex-B15 homogeniser at 40,000 psi as a method of lysing the cells as use of repeated freeze-thaw cycles on a large scale was not found to be as efficient. After lysis and a centrifugation step (45 min, 17,500 rpm, SS-34 rotor), purification of the clarified lysate was trialled by a variety of methods

(Figure 3.1.3a), before the final purification protocol was reached (Figure 3.1.3b). The protocol was optimised to give the optimal balance of purity and yield and hence did not give consistently the highest purity protein which was obtained on a very small yield. Cleavage of the His-tag was not found to affect activity of the protein, therefore, the TEV protease cleavage step followed by a reverse HisTrap was not always performed.

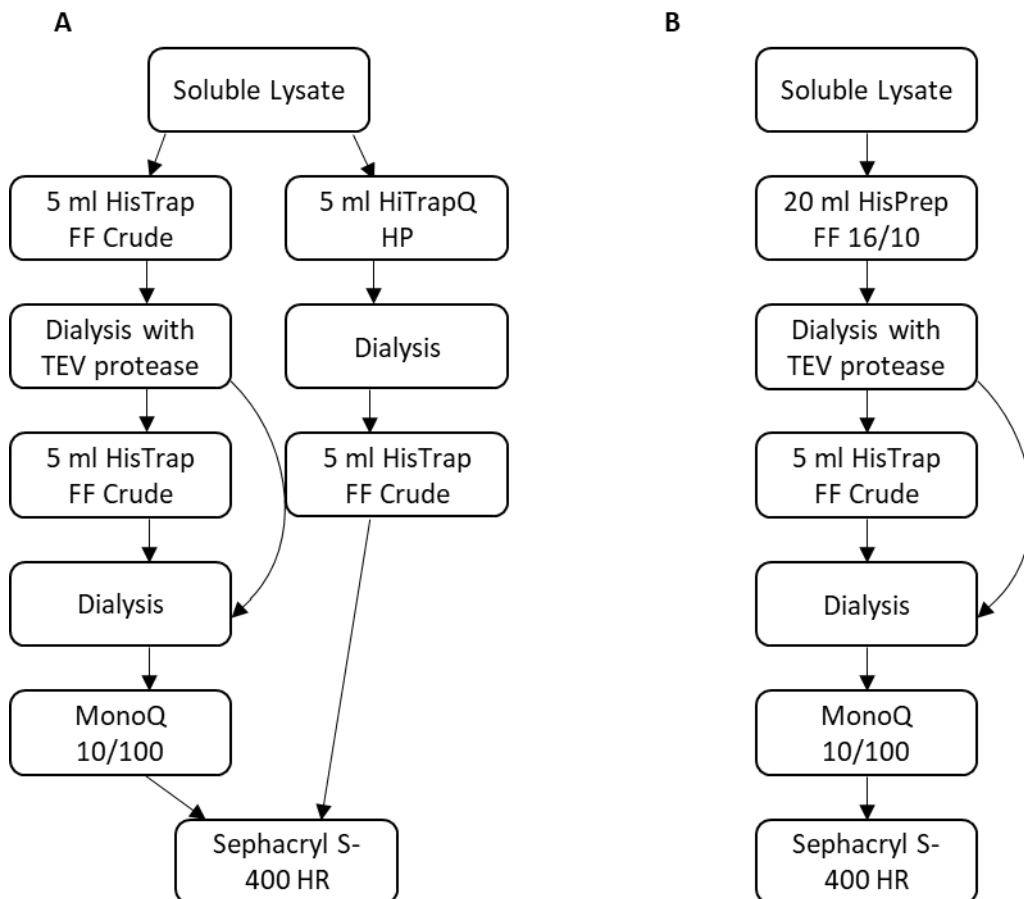


Figure 3.1.3: Purification method of the Mtb GyrBA fusion protein. A) Alternative purification methods trialled before B) obtaining optimal purification method. Cleavage of the His-tag and subsequent reverse His column was found to be optional in regards to activity, and the purity yield balance was not found to be significantly different with or without this step.

The protein obtained of the highest purity after size exclusion chromatography was judged to be suitable for crystallography trials and ATPase assays (Figure 3.1.4a) whereas for topoisomerase assays less pure fractions and including samples collected from a MonoQ column could be used (Figure 3.1.4b).

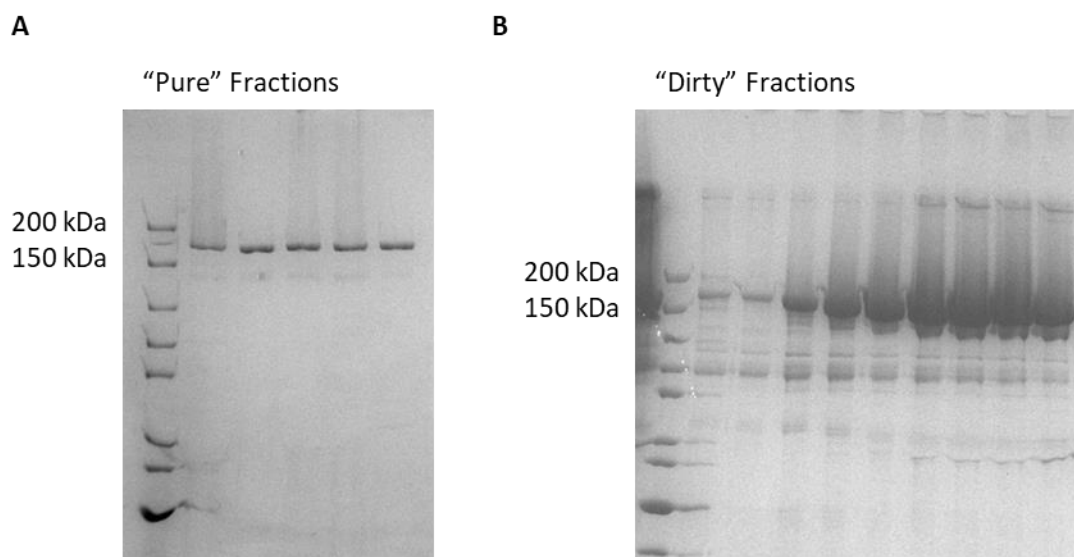


Figure 3.1.4: SDS-PAGE gels showing “Pure” GyrBA (168 kDa) for crystallography and ATPase assays, and “Dirty” GyrBA suitable for topoisomerase assays after S400 size exclusion chromatography.

3.1.3 The GyrBA fusion protein is active in supercoiling

As implied from the cell lysate assay, it was determined using purified proteins that the fusion construct is as active in supercoiling at the same concentration as the gyrase subunits (Figure 3.1.5a). After initial tests of activity under the previously published conditions (Aubry *et al.*, 2006a), it was determined that a concentration of 74 nM was appropriate to carry out further optimisations of the supercoiling reaction. To determine if there was any difference in the speed of supercoiling activity between the two different constructs, a time course was carried out. This determined that both constructs behaved very similarly with a satisfactory level of supercoiling being observed at 30 min (Figure 3.1.5b). Hence, for future experimentation it was determined that a 30 min incubation at 37°C with 74 nM of each gyrase or fusion subunit was sufficient. In terms of specific activity, this was found to be highly variable and preparation dependent, varying between 0.04×10^4 and 1.7×10^4 U/mg for the fusion construct, with values of around $0.2\text{-}0.4 \times 10^4$ U/mg for the individual subunits, where 1 U is the amount of enzyme required to fully supercoil 0.5 mg relaxed pBR322* in 30 minutes at 37°C.

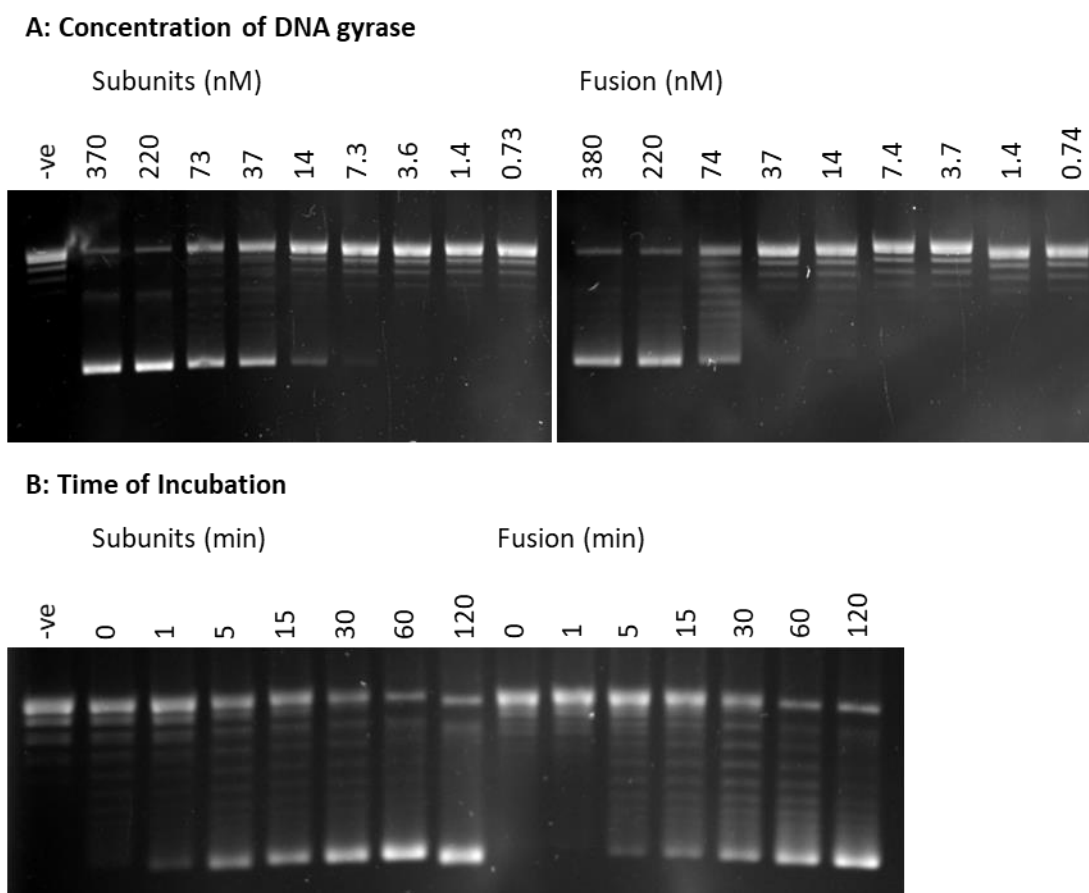


Figure 3.1.5: Supercoiling activity comparison between the Mtb DNA gyrase subunits and fusion constructs. A) Supercoiling as a function of decreasing concentration (370-0.73 nM) under fixed assay conditions (37°C, 30 min). B) Supercoiling as a function of increasing time (0-120 min) using 74 nM of each enzyme at a temperature of 37°C. -ve refers to reaction conditions lacking DNA gyrase at the final reaction time.

Potassium glutamate has been previously identified as a key factor in supercoiling activity of DNA gyrase, with the activity of Mtb gyrase being described as optimal in 100 mM potassium glutamate (Aubry *et al.*, 2006a). To ascertain if this was the same for the fusion protein, a titration of potassium glutamate (0-500 mM) was carried out with both constructs. It was determined that both an absence of potassium glutamate as well as high concentrations inhibited the activity of the enzyme. Our results were slightly different to the published result of 100 mM, under suboptimal assay conditions (40 nM enzyme, 18 min incubation) an optimal concentration was determined to be 200 mM for the individual subunits, whereas the fusion construct appeared to show good activity in concentrations ranging from 50-500 mM potassium glutamate (Figure 3.1.6).

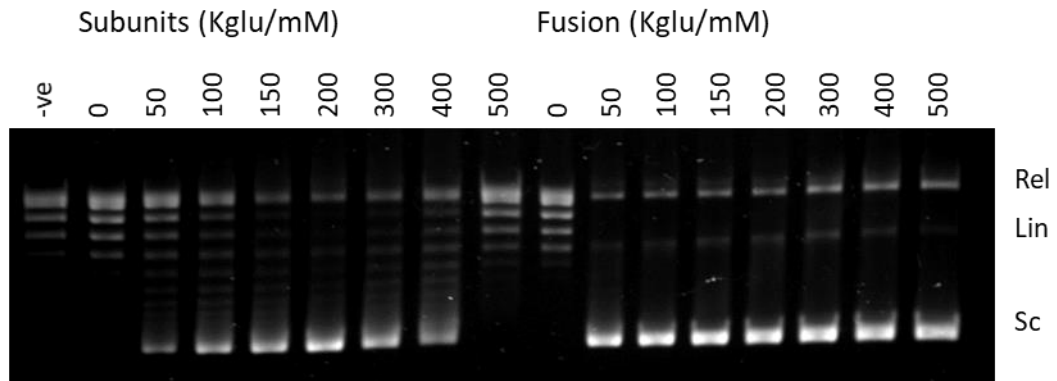


Figure 3.1.6: Induction of supercoiling as a function of potassium glutamate concentration in both the Mtb GyrA₂B₂ individual subunits and the GyrBA fusion construct. Forty nanomolar of each individual protein assayed for 18 min at 37°C with potassium glutamate concentrations ranging 0-500 mM. The expected positions of relaxed (Rel), linear (Lin) and negatively supercoiled (Sc) pBR322* is indicated. -ve control contains all assay components in the absence of DNA gyrase at the maximal potassium glutamate concentration.

3.1.4 The GyrBA fusion protein is active in relaxation

DNA gyrase can weakly relax negatively supercoiled DNA in the absence of ATP (Gellert *et al.*, 1977). It has been reported that this relaxation ability in the Mtb enzyme is better than gyrase from other species (e.g. those from *S. aureus* or *E. coli*) (Aubry *et al.*, 2006a). Hence, it was investigated if fusing the B and A subunits had any influence on this ability. It was determined that both constructs could perform relaxation, although the relaxation assay was tricky to work with owing to a high degree of cleavage observed making the visualisation of relaxation difficult to observe. However, at relatively high concentrations (>0.1 μ M) and long incubations (2 hours), relaxation is observed (Figure 3.1.7). The reaction appears to be slow, as even at 0.5 μ M, relaxation is not apparently observed until 30-60 min whereas at much lower concentrations of enzyme some supercoiling is already observed within the first 5 min (Figure 3.1.5). No significant differences between the behaviours of the two constructs under these conditions were observed.

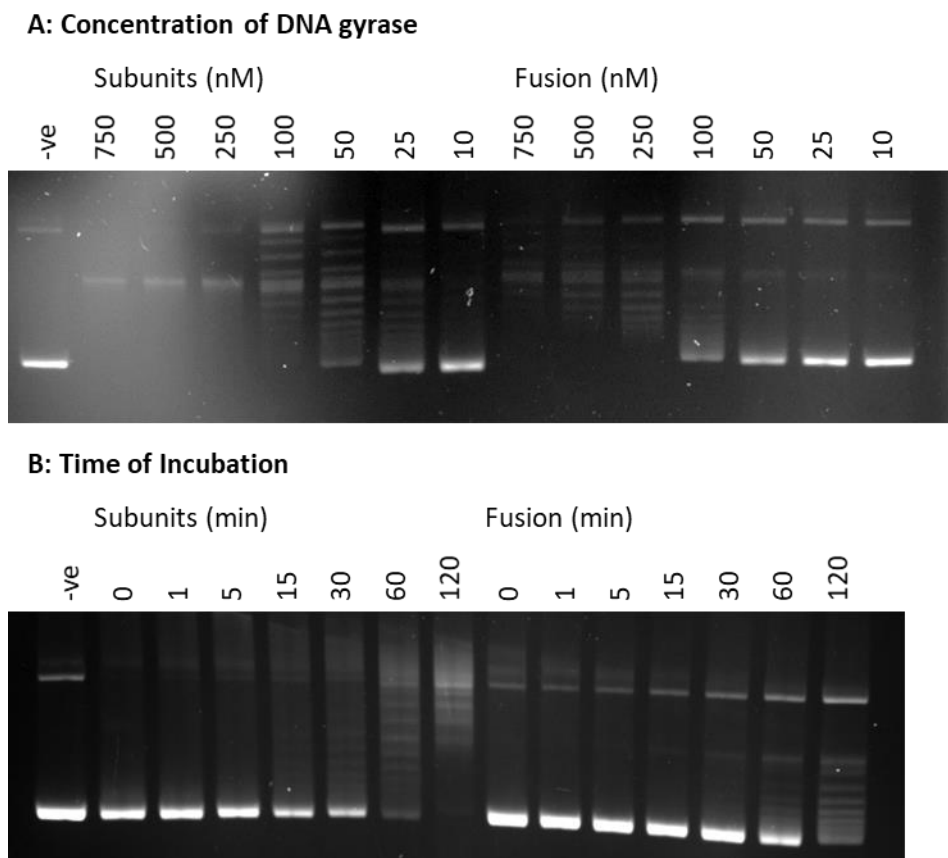


Figure 3.1.7: ATP-independent relaxation activity comparison between the Mtb gyrase subunits and fusion constructs. A) Relaxation as a function of decreasing concentration (0.75-0.1 μM) under fixed conditions (37°C, 2 hours). B) Relaxation as a function of increasing time (0-120 min) at 37°C and 0.5 μM enzyme concentration. -ve control contains all reaction components in the absence of DNA gyrase at the final incubation timepoint in the case of assay B. Linear bands observed are a consequence of the large amounts of enzyme and longer time required for this assay.

It has been reported in the literature that the relaxation activity is inhibited by the presence of potassium glutamate (Aubry *et al.*, 2006a). This was investigated to determine if the fusion protein behaves differently to the wild type. At a concentration of 0.5 mM enzyme with a 1 hour incubation period it was determined that like the ATP-dependent supercoiling reaction, high concentrations of potassium glutamate inhibited the relaxation reaction. The supercoiling reaction did not seem to occur in the absence of potassium glutamate (Figure 3.1.6), whereas there does appear to be weak relaxation activity under these conditions. Optimal concentration of potassium glutamate was determined to be between 100-200 mM for both constructs (Figure 3.1.8).

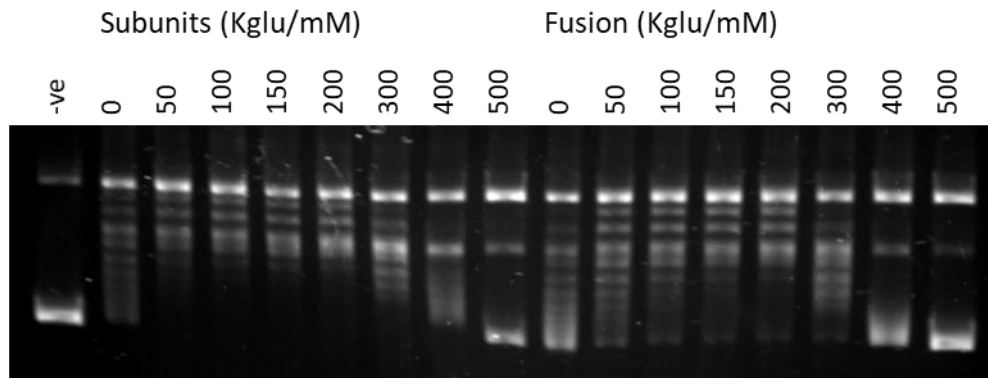


Figure 3.1.8: Optimisation of ATP-independent relaxation as a function of potassium glutamate concentration in both the Mtb GyrA₂B₂ individual subunits and the GyrBA fusion construct. 0.5 μ M of each monomeric protein was assayed for 1 hour at 37°C with potassium glutamate at concentrations 0-500 mM. -ve control contained all assay component in the absence of DNA gyrase at the highest potassium glutamate concentration. Linear bands observed are a consequence of the large amounts of enzyme and longer time required for this assay.

3.1.5 The GyrBA fusion protein is active in decatenation

Decatenation, the process of unlinking plasmids is typically carried out by topo IV in bacterial species (Zechiedrich *et al.*, 1997). In the absence of topo IV in mycobacteria there have been several reports that the decatenation activity of DNA gyrase is enhanced compared to DNA gyrase from other species that contain topo IV (Manjunatha *et al.*, 2002, Aubry *et al.*, 2006a). To determine if this was also true for the fusion protein, this was investigated using the commonly-used assay to visualise decatenation which utilises Kinetoplast DNA purified from *Crithidia fasciculata*. kDNA is a large network of entangled mini-circles which cannot enter an agarose gel so may be visible in the wells (Shapiro *et al.*, 1999) (Figure 3.1.9). In a positive assay result the mini-circles are released into their monomers and visualised within the gel either as a combination of nicked and supercoiled DNA in the case of DNA gyrase or as a combination of nicked and relaxed DNA in the case of topo IV. A linearising or nicking enzyme may also be able to release the mini-circles but will not form topoisomers (Figure 3.1.9).

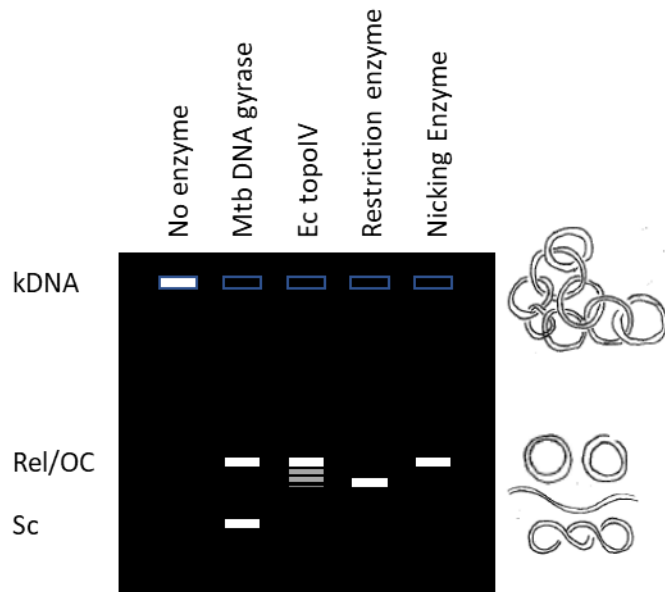
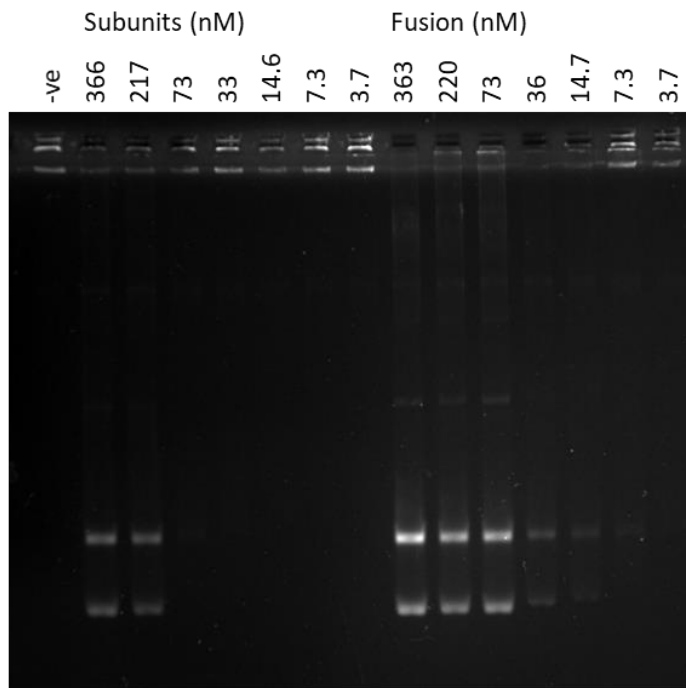


Figure 3.1.9: Expected banding pattern of a decatenation assay carried out and imaged on a native 0.8-1% agarose in TAE gel stained with ethidium bromide. No migration is observed in the absence of enzymes with the kDNA being stuck in the wells. *M. tuberculosis* DNA gyrase should result in a mix of open circular (nicked) and negatively supercoiled mini-circles entering the gel if the reaction is carried out. Topo IV decatenates the kDNA resulting in a mix of relaxed topoisomers and open circular DNA. A restriction enzyme would simply linearise the mini-circles and no other topoisomers would be visible. A nicking enzyme would result in open circular or nicked mini-circles.

It has been published that decatenation for this enzyme is preferential in assay conditions that are different to those of supercoiling and are characterised by a higher potassium glutamate concentration, the absence of spermidine, alongside a different buffer composition and pH (Aubry *et al.*, 2006a). To confirm this result for the fusion protein, the kDNA decatenation assay was carried out with both the supercoiling and decatenation assay buffers. Unambiguous evidence for some decatenation activity was demonstrated in both the constructs. This activity for the fusion protein was not seen to be different between the two buffer compositions. However, it does appear that the subunits show enhanced decatenation activity in the supercoiling assay buffer. The fusion protein showed enhanced decatenation activity in both buffers compared to the subunits (Figure 3.1.10).

A: Decatenation assay buffer



B: Supercoiling assay buffer

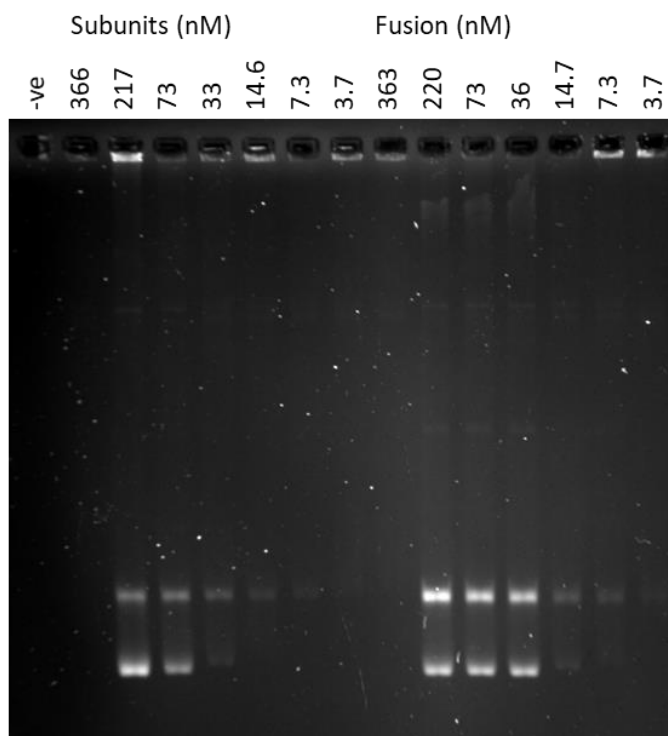


Figure 3.1.10: Decatenation assay using the kinetoplast DNA substrate. The kDNA is unable to enter the gel so may be seen in the wells of the gel, the product of a positive reaction shows a combination of open circular and negatively supercoiled mini-circles as seen by the two bands. A) was performed using the decatenation assay buffer, whereas B) was performed using the supercoiling assay buffer, with both reactions being performed at 37°C for 30 min. 0.8% (w/v) agarose in TAE gels were run at 60 V for 3 hours. -ve control contained all assay components in the absence of DNA gyrase in the appropriate assay buffer to confirm no decatenation is seen in the absence of DNA gyrase.

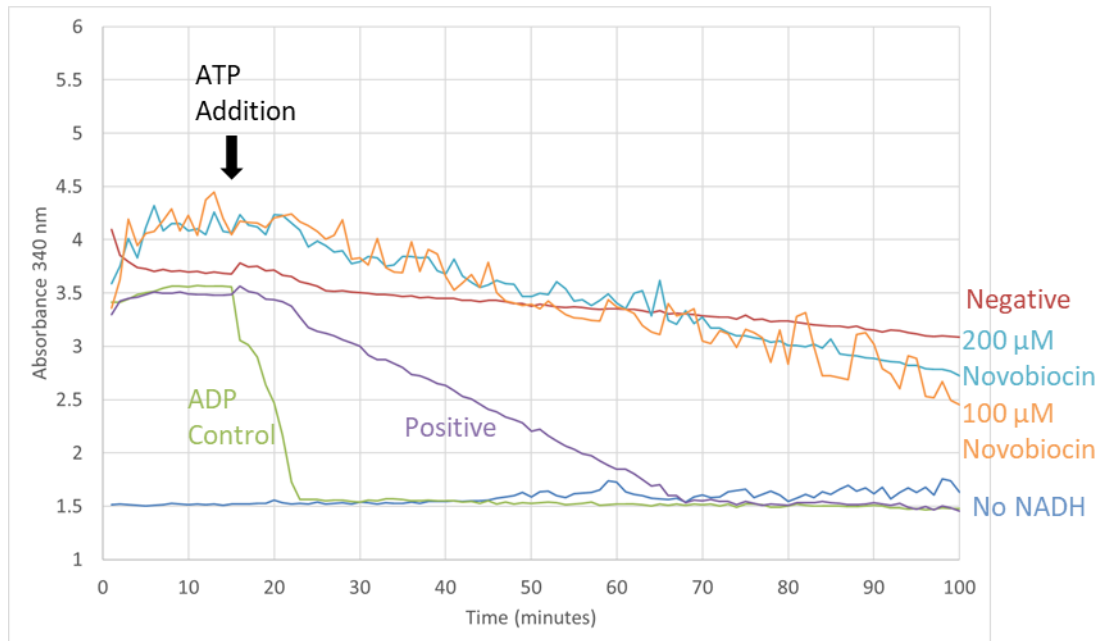
3.1.6 The ATP turnover rate of *M. tuberculosis* DNA gyrase is appreciable

In the literature it is reported that the ATP turnover rate of Mtb is too low to produce reproducible and reliable data for inhibitor studies (Karkare *et al.*, 2013b) (Shirude *et al.*, 2013). In this study this was investigated (see methods chapter 2.5.5), and it was found that an appreciable rate could be determined. Initial studies using relaxed pBR322* showed that the individual Mtb gyrase subunit complex (A₂B₂) at 550 nM showed a much shallower decrease in absorbance at 340 nm corresponding to a lower oxidation of NADH and therefore a lower ATP turnover rate compared to the same complex from *E. coli* at 222 nM (Figure 3.1.11). This corresponded to a rate of around 0.2 s⁻¹ per individual Mtb GyrB subunit compared to 1.4 s⁻¹ for *E. coli* gyrase when directly compared, suggesting that as previous data suggested the rate is indeed low compared to that of *E. coli* as stated in the literature (Agrawal *et al.*, 2013, Karkare *et al.*, 2013b, Shirude *et al.*, 2013). Interestingly, when the rate of ATP turnover was compared using linear, negatively supercoiled and relaxed pBR322* substrates on the *M. tuberculosis* A₂B₂ complex the rates were slightly higher but comparable (Table 3.1.1).

Table 3.1.1: The novobiocin-sensitive ATP turnover rate with 550 nM of the individual GyrA and GyrB subunits in the presence of 2 ng of pBR322* in three different topological forms measured over 48 min after addition of 2 mM ATP. Data is representative of minimum of two experiments with duplicate data for each assay.

pBR322* Topological Form	ATP Turnover per GyrB subunit / s ⁻¹
Relaxed	0.36±0.03
Negatively supercoiled	0.31±0.04
Linear	0.53±0.03

E. coli



M. tuberculosis

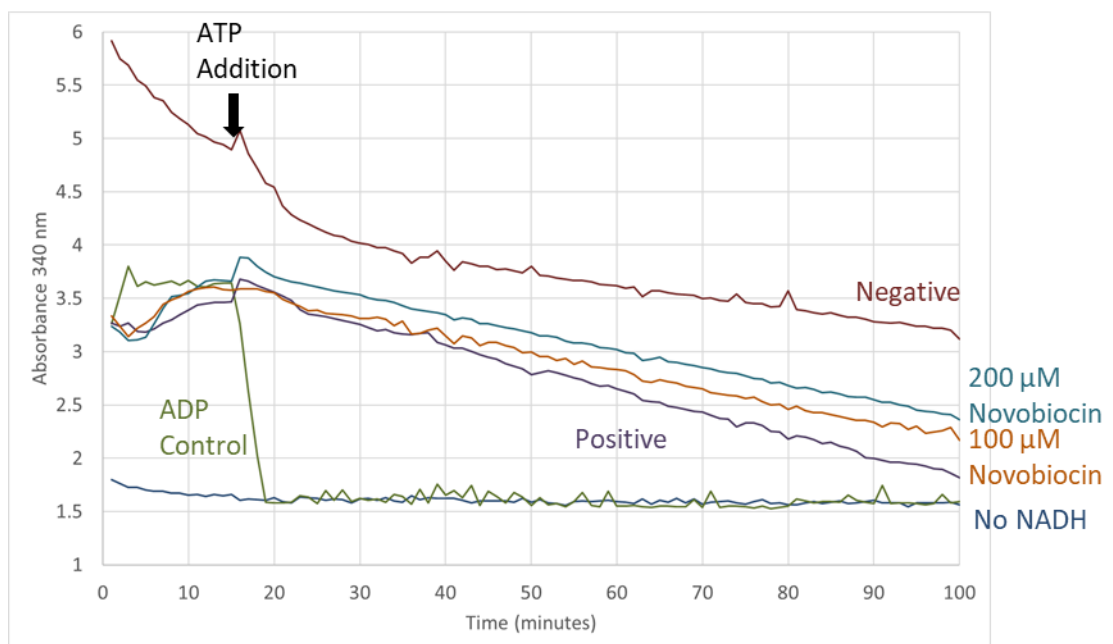


Figure 3.1.11: Raw absorbance data for the PK/LDH linked assay carried out with (Top) *E. coli* DNA gyrase (222 nM) with 1.5 ng relaxed pBR322* or (Bottom) *M. tuberculosis* DNA gyrase (550 nM) A₂B₂ constructs and 2 ng relaxed pBR322*. Despite a much larger amount of enzyme being used with the *M. tuberculosis* assay the results clearly demonstrate a greater rate of *E. coli* DNA gyrase. Negative, no NADH, and ADP controls contain DNA but no DNA gyrase, positive control contained DNA gyrase in the absence of novobiocin. ATP was substituted for ADP in ADP control, and no NADH was added to the no NADH control to obtain an absolute baseline.

We find that the rate of ATP turnover in the GyrBA fusion protein was very variable, likely depending on the purity of the protein. Initially it was found to be very comparable to that of the individual GyrB subunit. After swapping to a purer preparation of the fusion protein stock at a higher concentration, the rate was found to be consistently higher and more comparable to that of the *E. coli* protein in the presence of topologically unrestrained linear or nicked pBR322* substrates (Table 3.1.2). Surprisingly, it was found that if topologically-constrained relaxed or negatively supercoiled pBR322* substrates were used as the DNA substrate the ATP turnover rate was low (Table 3.1.2). Additionally, preliminary data indicates that there is a low ATP turnover rate in the presence of positively supercoiled DNA.

Table 3.1.2: The novobiocin-sensitive ATP turnover rate with 200 nM of the Mtb GyrBA fusion protein in the presence of 1 ng of pBR322* in four different topological forms measured over 45 min after the addition of 2 mM ATP. Data is representative of duplicate repeats.

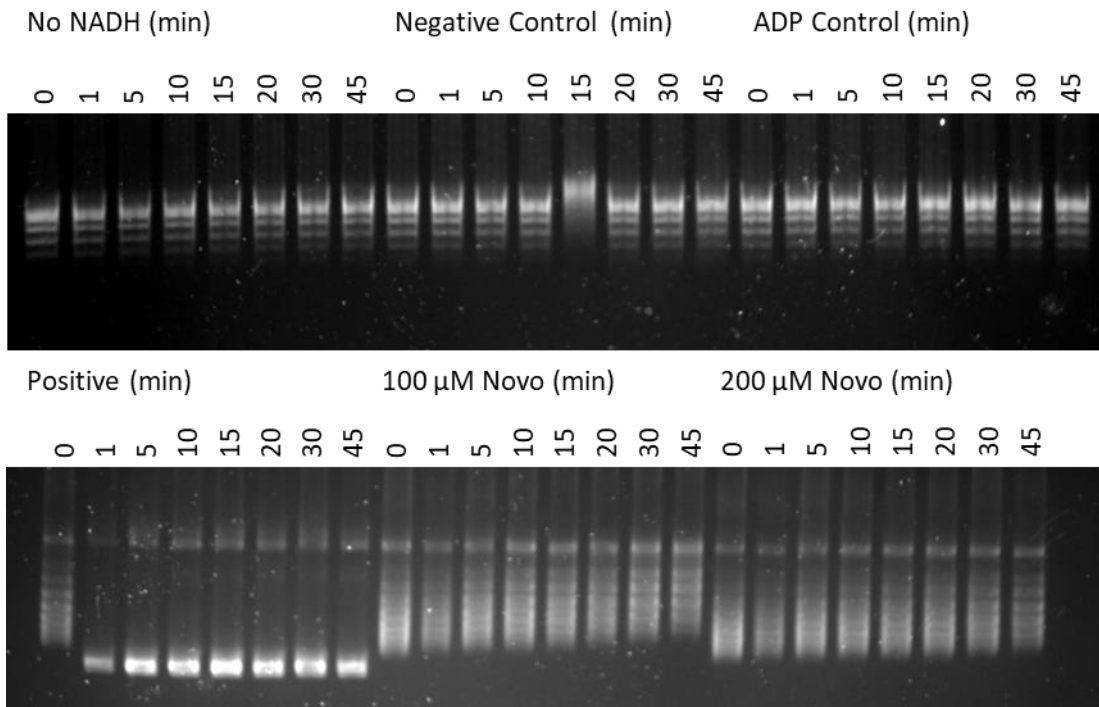
pBR322* Topological Form	ATP Turnover per GyrBA subunit / s ⁻¹
Relaxed	0.03±0.06
Negatively supercoiled	0.16±0.04
Nicked	1.27±0.20
Linear	1.00±0.10

To determine if the difference in the activity of Mtb DNA gyrase was due to a lack of stimulation from negatively supercoiled DNA, gel samples were taken at intervals over a 45 min time course after ATP addition, as well as following the absorbance at 340 nm to allow the topological state to be monitored alongside the ATP turnover rate. Unsurprisingly, at the high concentrations used in the topoisomerase reactions (200+ nM, compared to 74 nM in supercoiling reactions) it was found that the positively supercoiled and relaxed pBR322* substrates were rapidly converted into a plasmid that was negatively supercoiled (Figure 3.1.12). Although it is not possible to resolve positive and negative supercoils on a native agarose gel, it can be assumed that due to the lack of intermediate species at any timepoints that the positive supercoils were rapidly removed and negative supercoils inserted into the plasmid.

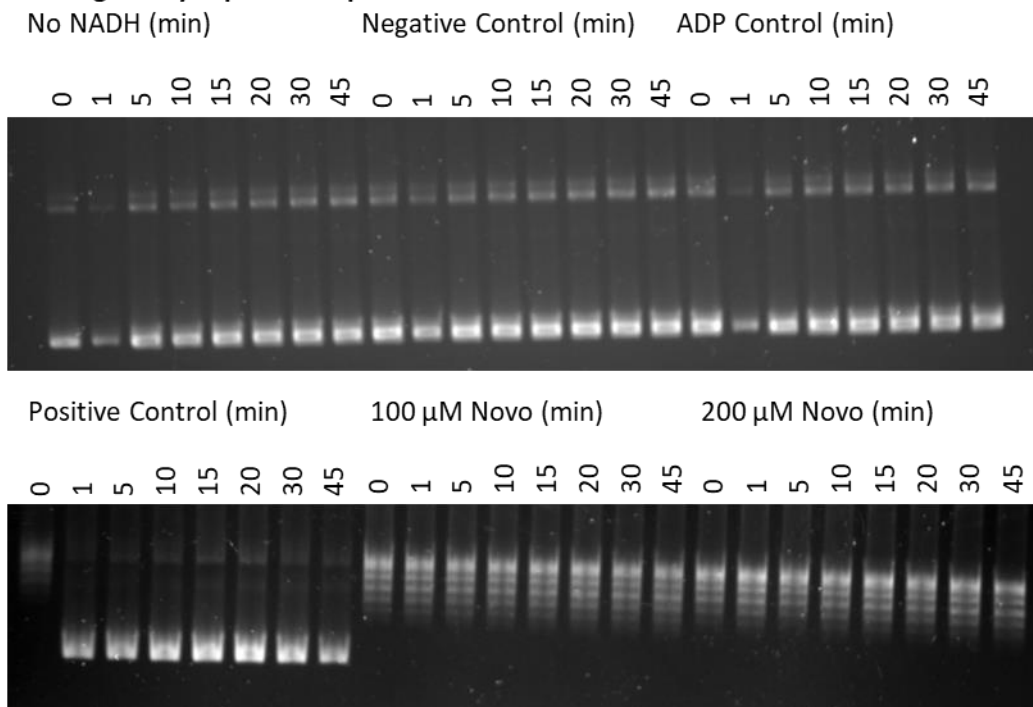
To investigate if the low rate was due to the DNA concentration being sub-optimal (i.e. not enough DNA was being used to stimulate the ATP reaction), DNA titrations were carried out. The concentration required to reach a maximal ATP turnover rate with the topologically restrained pBR322* substrates appears to be greater than for the topologically unrestrained

substrates. Despite this, it was also found that they were still unable to reach rates close to those reached by the unrestrained substrates (Figure 3.1.13).

A: Relaxed pBR322*



B: Negatively supercoiled pBR322*



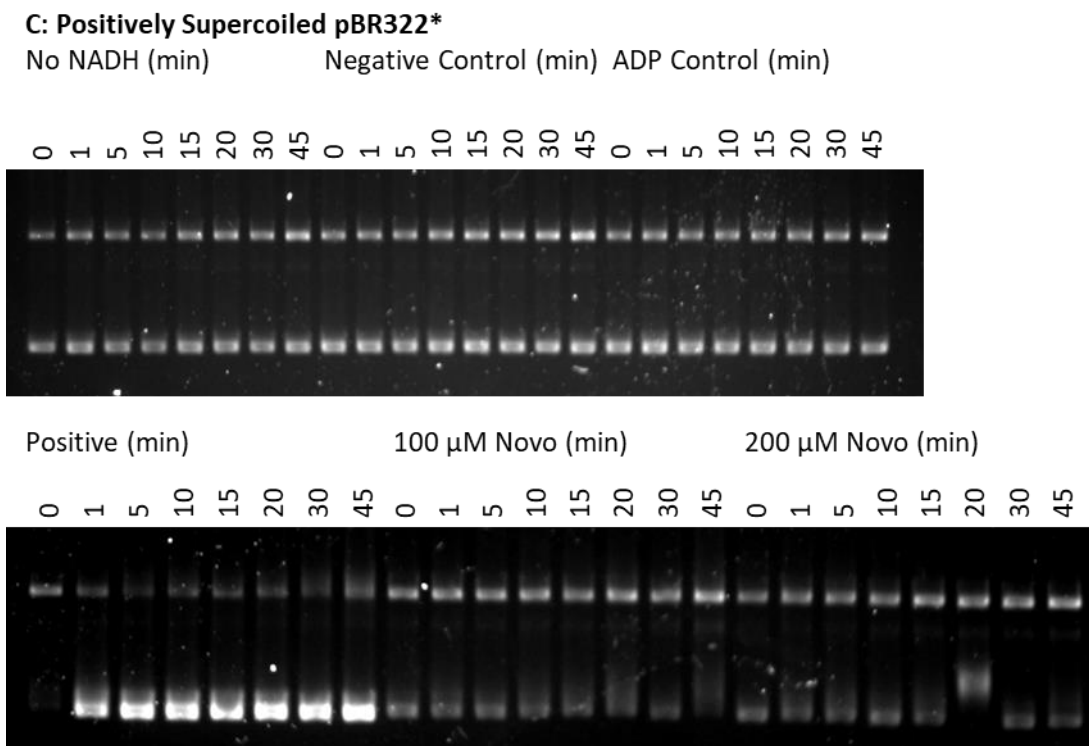
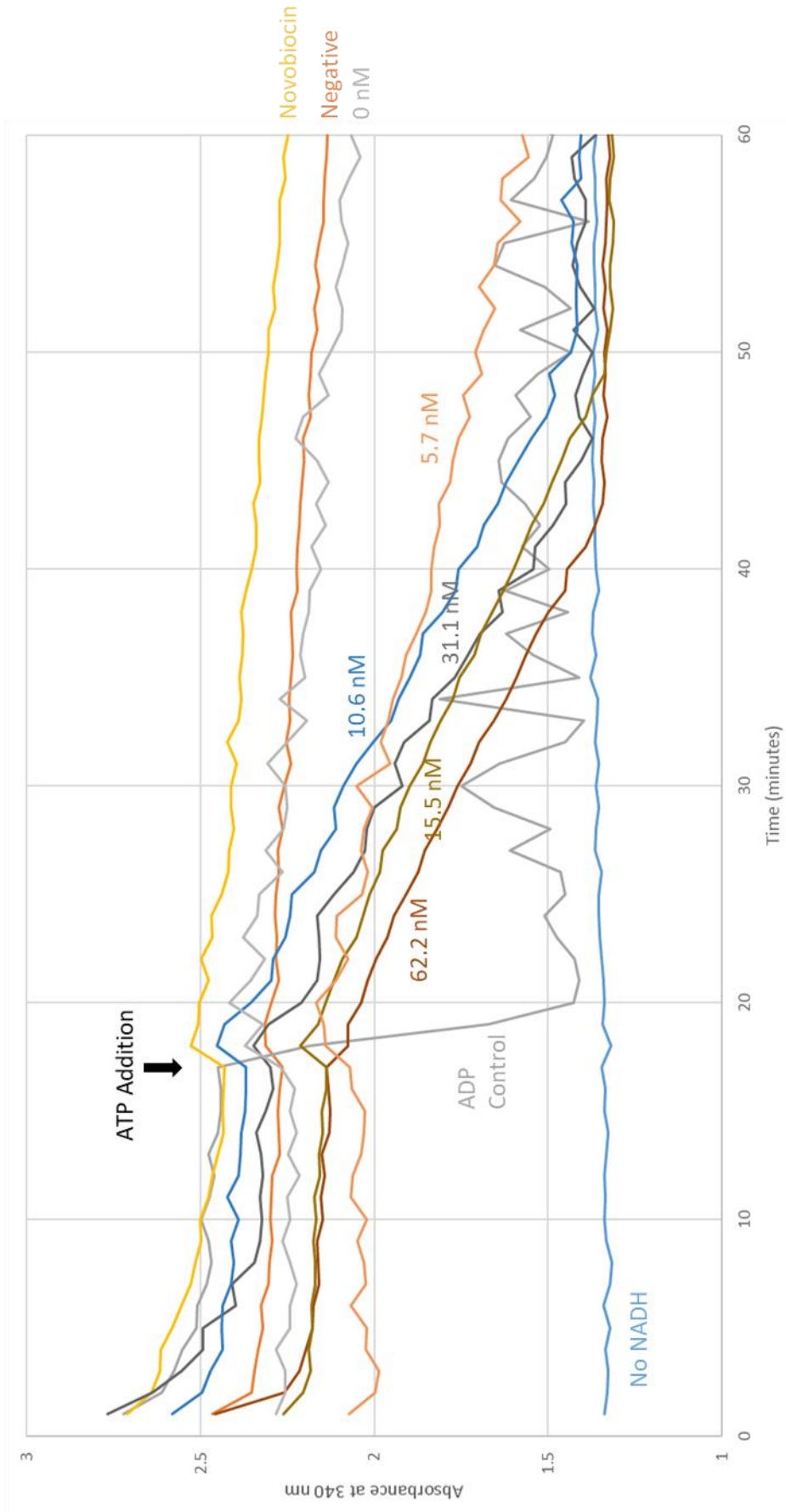


Figure 3.1.12: Visualisation of the topological state of 1 ng A) relaxed B) negatively supercoiled C) positively supercoiled pBR322* at 0, 1, 5, 10, 15, 20, 30, 45 min time points after addition of 2 mM ATP (ADP in ADP control) during an ATPase linked assay, visualised on a native 1% agarose in TAE gels. 200 nM enzyme assayed. The novobiocin controls block ATP activity allowing relaxation of negative supercoils as observed in B. The no NADH, negative and ADP controls do not contain DNA gyrase.

Unlike DNA gyrase from *E. coli* the rate of ATP hydrolysis in the absence of DNA was found to be negligible – the gradients obtained were very close to those of the negative and novobiocin controls (Figure 3.1.13a). This indicates that the ATP hydrolysis reaction is highly coupled to DNA binding. To confirm this the ATP hydrolysis rate for the ATPase domain alone in the absence of the rest of the DNA gyrase heterotetramers was analysed. The reported ATP turnovers of 0.02 s^{-1} for the *E. coli* GyrB43 fragment (Ali *et al.*, 1993) and 0.002 s^{-1} for the same Mtb fragment (Agrawal *et al.*, 2013) are equivalent to the average novobiocin-dependent DNA-independent rate of $0.05 \pm 0.08 \text{ s}^{-1}$ over a concentration range 2-64 μM . Due to this rate being extremely slow with the Mtb GyrB NTD it was determined to be almost undetectable even at the highest enzyme concentration used.

A



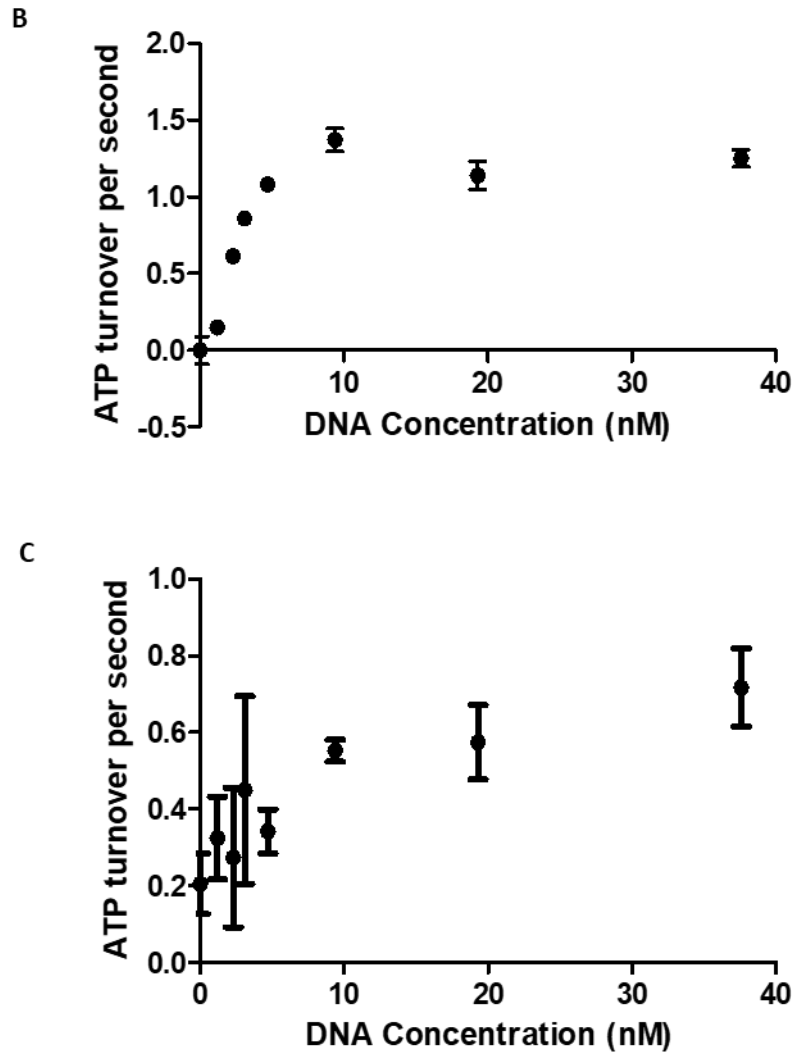


Figure 3.1.13: A) Plot of absorbance at 340 nm monitoring the loss of NADH in the PK/LDH-linked assay. Control samples (no NADH, negative without enzyme, positive with ADP not ATP) contained no DNA substrate or DNA gyrase. The novobiocin-independent rate was measured in the presence of 31.1 nM linear pBR322*. DNA titration with linear pBR322* with constant 250 nM GyrBA. B) Novobiocin-dependent ATP turnover rate with nicked pBR322* substrate measured using 150 nM GyrBA and nicked pBR322* concentration range of 0-37.6 nM. C) Novobiocin-dependent ATP turnover with negatively supercoiled pBR322* substrate measured using 150 nM GyrBA and negatively supercoiled pBR322* concentration range of 0-37.5 nM. All data is representative of multiple repeats and duplicate data points. Linear/Nicked represent the topologically unconstrained DNA class whereas negatively supercoiled DNA is representative of the topologically constrained DNA class. Error bars represent the range of data points collected for each data point, and all data were collected at a minimum of two duplicates.

3.1.7 Preliminary cleavage profile of *M. tuberculosis* DNA gyrase

In order to determine an optimal DNA fragment for structural studies of the full-length enzyme (X-ray crystallography and CryoEM) we investigated the cleavage specificity of Mtb DNA gyrase. Cleavage reactions on relaxed pBR322* in the presence of ATP and on negatively supercoiled and EcoRI-linearised pBR322* in the absence of ATP were carried out in the absence and presence of moxifloxacin. These were subsequently linearised with three restriction enzymes (BsaI, EcoR1 and SalI) to help identify where the cleavage was occurring (Figure 3.1.14).

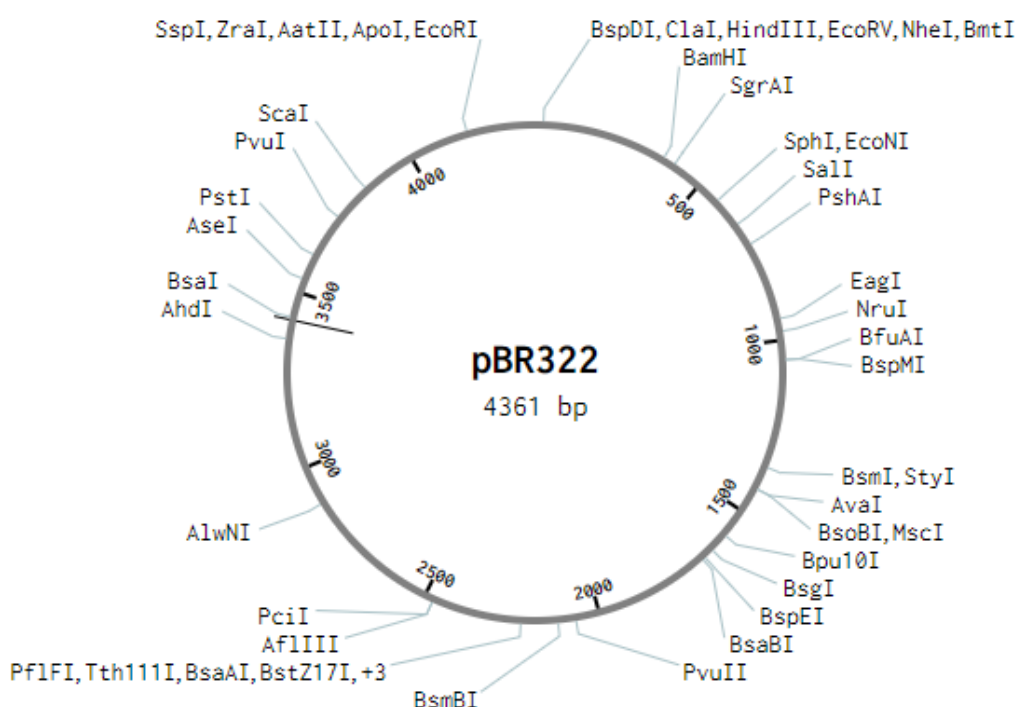


Figure 3.1.14: Plasmid map of pBR322 (benchling.com) showing all the single cutting restriction enzymes. SalI cuts at 652 bp, BsaI cuts at 3428 bp and EcoRI at 4360 bp. Cutting with these three restriction enzymes from intact pBR322* results in three fragments of 2776, 932 and 653 bp. Extra bands may be observed if there is additional cleavage by DNA gyrase.

The reaction with relaxed pBR322* was carried out in the presence of ATP. Confusingly an additional band of *ca.* 1600 bp was seen in the restricted substrate for the reaction with relaxed pBR322*. This can be explained as incomplete restriction by EcoRI, although it was not observed when DNA gyrase was added to the reaction mixture. The linearized product formed in the absence of moxifloxacin did not appear as prevalent as in the presence of moxifloxacin.

Under these reaction conditions no distinct banding pattern was observed in the presence or absence of moxifloxacin with or without the restriction enzymes. Instead in the presence of moxifloxacin a smear was seen suggesting that multiple linear cleavage was occurring but not at distinct positions around the plasmid (Figure 3.1.14a).

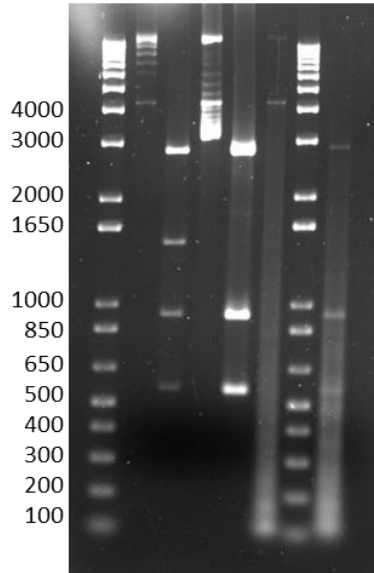
Like the cleavage with relaxed pBR322* and ATP, that of negatively supercoiled pBR322* in the absence of ATP was observed to be much greater in the presence of moxifloxacin than in its absence. Similarly, no distinct banding pattern was observed, with the results displaying a smear of DNA down the gel indicating a variety of differently sized DNA fragments being formed without a significant preference for any particular cleavage sites (Figure 3.1.14b).

In the absence of any enzyme in the linear substrate there is also a very faint contaminating band approximately 1500 bp shorter than pBR322* - this band did not appear to alter the cleavage profile of the substrate. In contrast to the relaxed and negatively supercoiled substrates, when using the linear substrate in the absence of ATP a distinct band pattern was observed, however no alteration to the pattern after restriction was observed, probably likely due to low proportions of each species being obtained (Figure 3.1.14c). Overall, further optimisation is needed for all the substrates in the reaction protocol to determine the cleavage profile in the presence of moxifloxacin.

This preliminary study demonstrates that in the presence of moxifloxacin linear DNA appears to give a discrete banding pattern suggesting preferential cleavage sites. This preliminary study clearly demonstrates that with further work an optimal DNA fragment should be able to be determined for use in structural studies.

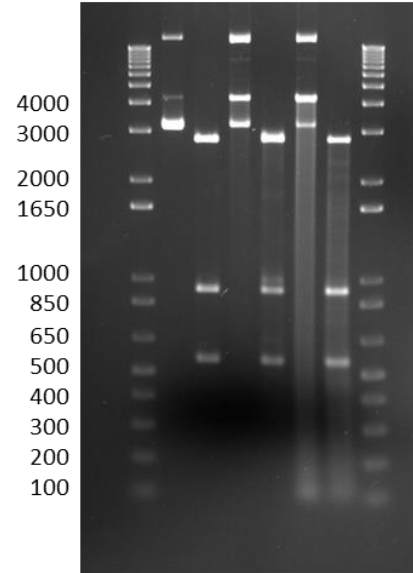
A: Relaxed pBR322*

Tb Gyrase	-	-	+	+	+	+
Moxi	-	-	-	-	+	+
Bsal			+	+		+
EcoRI			+	+		+
Sall			+	+		+



B: Negative supercoiled pBR322*

Tb Gyrase	-	-	+	+	+	+
Moxi	-	-	-	-	+	+
Bsal			+	+		+
EcoRI			+	+		+
Sall			+	+		+



C: EcoRI Linearised pBR322*

Tb Gyrase	-	-	+	+	+	+
Moxi	-	-	-	-	+	+
Bsal			+	+		+
EcoRI			+	+		+
Sall			+	+		+

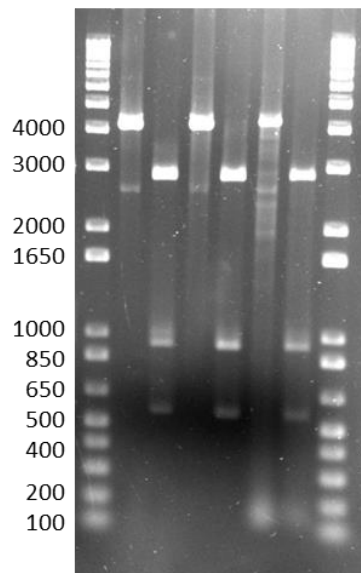


Figure 3.1.15: Preliminary cleavage profile optimisations with Mtb GyrA₂B₂ A) Relaxed pBR322* in the presence of ATP, B) Supercoiled pBR322* in the absence of ATP, C) Linear pBR322* in the absence of ATP. Control reactions were carried out in the absence of DNA gyrase and moxifloxacin. After cleavage with BsaI, EcoRI, and Sall expected cleavage bands of pBR322* are 2782, 926, 651 bp.

3.2 DNA gyrase from *M. thermoresistibile*

3.2.1 Construct design, cloning, expression and purification

The following sub-section of work was for the most part carried out by Mr Brandon Malone (BM; JIC Summer School Student, 2016) under the supervision of SRH. Constructs were designed based on the *M. thermoresistibile* ATCC19527 genomic sequence. These were additionally codon-optimised using the GeneArt service (Fisher Thermo Scientific). The constructs were cloned into the pET28-MHL expression vector with an N-terminal His-tag and TEV protease sequence via the InFusion cloning system (Takarabio). To make the GyrBA fusion construct a single amino acid linker (lysine) was added between the GyrB and GyrA. After the clones were confirmed as correct via sequencing (SourceBioscience) expression trials were carried out in a range of *E. coli* expression hosts and under a range of conditions. It was determined that the optimum conditions were the expression of the codon-optimised genes in the Rosetta™ 2 (pLysS) *E. coli* strain in LB with induction at OD₆₀₀ of 0.6, by addition of 0.4 mM IPTG at 28°C for 4-5 hours.

Large-scale expression using the optimised conditions followed. Harvested cells were resuspended in lysis buffer and stored at -80°C. Purification of the subunits was achieved through a two-column strategy: application to a 5 ml His Trap (GE) in lysis buffer with elution in lysis buffer + 500 mM imidazole on a gradient. The semi-purified fractions were dialysed overnight against TEV cleavage buffer, with 1 mg of TEV protease. The flow-through was collected from a second 5 ml His Trap column. In addition, a Sephacryl S400 size exclusion column was run on the GyrBA fusion protein in Gel Filtration buffer. Pure fractions analysed via 8% tris-glycine SDS-PAGE were collected, concentrated and dialysed against storage buffer before concentration, allotting and flash freezing to -80°C for storage.

3.2.2 Crystallography trials of *M. thermoresistibile* DNA gyrase

BM carried out multiple crystallisation screens on the GyrBA fusion protein. After running 6 sparse matrix screens (Table 3.2.1) and one optimisation based on conditions presenting with over nucleation being initially crystallised at 30°C, no crystal hits were obtained that were suitable for further optimisation or X-ray diffraction.

Table 3.2.1: Sparse matrix crystallisation conditions trialled with purified Mth GyrBA protein. No crystal hits suitable for optimisation or X-ray diffraction were observed at 4 weeks.

Enzyme Concentration (mg/ml)	Enzyme Conditions	Sparse matrix screens
2.8	Apo	JCSG- <i>plus</i> TM , PACT <i>premier</i> TM
2.4	0.118 mM 20-12p-8 doubly nicked oligo 10.1 mM MnCl ₂ 10.1 mM MgCl ₂ 2.9 mM Moxifloxacin 1.4% (v/v) DMSO	Structure screen 1+2, KISS
2.4	0.118 mM d20-447T doubly nicked oligo 10.1 mM MnCl ₂ 10.1 mM MgCl ₂ 2.9 mM Moxifloxacin 1.4% DMSO	Structure screen 1+2, KISS
2.3	5.6 mM AMP-PNP 0.111 mM 20-12p-8 doubly nicked oligo 9.7 mM MgCl ₂ 9.7 mM MnCl ₂	Morpheus®
2.3	5.6 mM AMP-PNP 0.111 mM d20-447T doubly nicked oligo 9.7 mM MgCl ₂ 9.7 mM MnCl ₂	Morpheus®
4.8	3 mM AMP-PNP 10.6 mM MgCl ₂ 10.6 mM MnCl ₂	JCSG- <i>plus</i> TM

3.2.3 DNA gyrase from *M. thermoresistibile* supercoils DNA

To our knowledge, we are the first people to work with DNA gyrase from *M. thermoresistibile*. From this point of view, it was important to determine its activity and possible function within the bacterium. Unsurprisingly, we found that the activity of the *M. thermoresistibile* enzymes

was very similar to that of the *M. tuberculosis* enzyme. The only significant difference observed was that the thermophilic enzyme bound significantly tighter to the DNA substrates tested and hence it was difficult to remove the protein at the end of assays. In relation to this, an additional incubation step with proteinase K was added prior to the addition of 24:1 chloroform : isoamyl alcohol and 2xSTEB.

Due to the high degree of homology between the Mtb and Mth enzyme sequences it was decided to initially assay the enzyme under the same conditions as the Mtb enzymes: 37°C for 30 min, to confirm activity before performing further optimisations. It was found that supercoiling occurred under the same conditions as the Mtb enzyme, although there was a requirement for a greater concentration of the Mth enzymes (Figure 3.2.1). At a concentration of 250 nM supercoiling was observed within 30 min, whereas the Mtb enzyme required about 15 min and a lower enzyme concentration to reach this level of supercoiling. Low levels of negative supercoiling were observed at lower concentrations or shorter times (Figure 3.2.1). It was confirmed that the fusion construct was also active to a similar level to the subunits, although there was a difference in the level of supercoiling that was achieved at 15 min, with both constructs achieving similar levels of supercoiling at 30 min. There appeared to be a visible amount of cleavage activity by the fusion construct when assayed at high concentration (750 nM) or for prolonged periods of time (>45 min), although this is likely to be due to impurities in the sample and did not appear to affect the interpretation of the results. In terms of specific activity this was determined to be similar for the subunits and fusion construct at 0.04×10^4 U/mg and 0.08×10^4 U/mg respectively. Although this is lower than those determined for the Mtb enzymes, we suggest that this was only one preparation and this value is likely to depend on a variety of factors that were not optimised within the scope of this experiment.

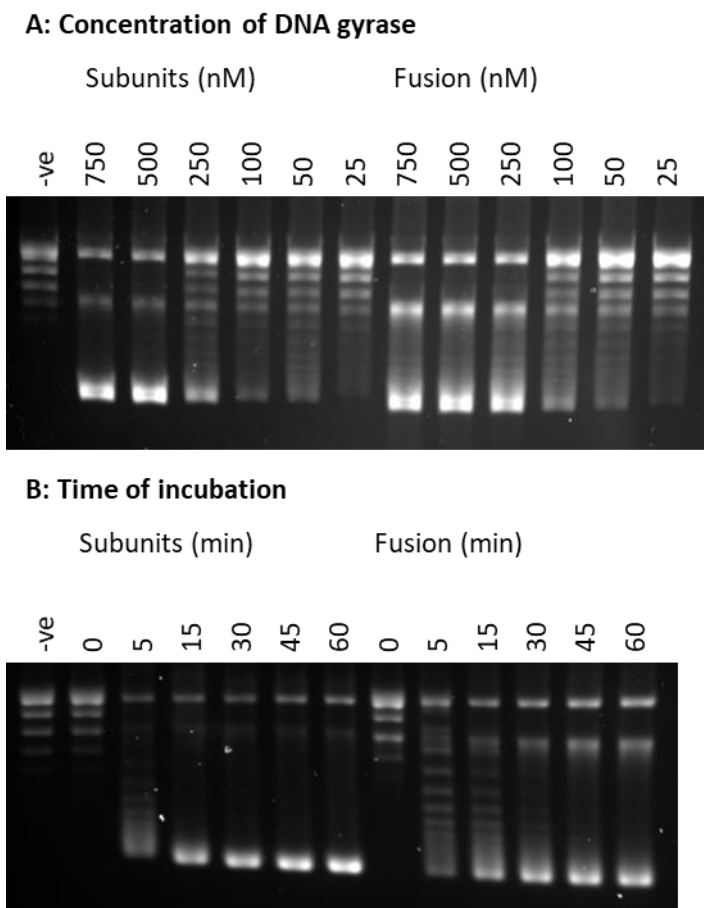


Figure 3.2.1: Negative supercoiling activity comparison between the Mth gyrase subunits and fusion constructs. A) Negative supercoiling as a function of decreasing concentration (750-25 nM) under fixed assay conditions (37°C, 30 min). B) Supercoiling as a function of increasing time (0-60 min) at constant 250 nM enzyme concentration and a temperature of 37°C. -ve controls contain DNA substrate in the absence of DNA gyrase. The linear bands observed are a consequence of the larger amounts of enzyme and longer incubation times.

As Mth DNA gyrase is a previously uncharacterised enzyme the optimal reaction conditions were investigated. Initially a range of potassium glutamate concentrations between 0-500 mM were assayed at a sub-optimal concentration (250 nM) and time (15 min) to determine if more optimal conditions could be obtained. It was determined that when assaying the individual subunits, they did not present any activity in the absence of potassium glutamate (Figure 3.2.2), increasing the concentration to 100-200 mM increased the activity of the enzyme to give maximal supercoiling activity. Raising the potassium glutamate concentration beyond 300 mM led to a decrease in the activity of the enzyme. Interestingly, when performing the same experiment with the fusion construct, the same pattern was not seen. Instead, from the very poor activity obtained in the absence of potassium glutamate an increase of activity appeared to be observed on increasing the concentration of potassium glutamate up to 150

mM where the activity level plateaued. Beyond this there did not appear to be a decrease in activity like the subunits (Figure 3.2.2)

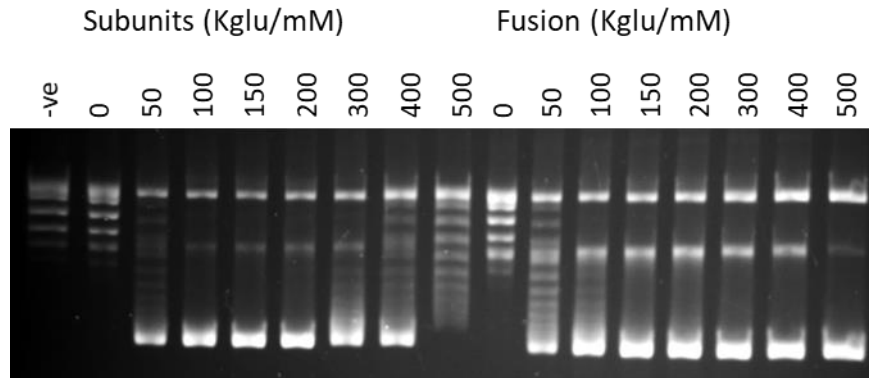


Figure 3.2.2: Induction of supercoiling as a function of potassium glutamate concentration in both the Mth GyrA₂B₂ individual subunits and the GyrBA fusion construct. 250 nM of each individual protein assayed for 15 min at 37°C with potassium glutamate concentrations ranging 0-500 mM. -ve control contains DNA substrate in the absence of DNA gyrase with 500 mM potassium glutamate. The linear bands observed are a consequence of the large amounts of enzyme and longer time required for this assay.

3.2.4 DNA gyrase from *M. thermoresistibile* relaxes DNA

In the absence of ATP, it was observed that Mth DNA gyrase was able to relax DNA. Like the supercoiling reaction it was determined that it was difficult to remove the protein from the DNA at the end of the reaction, potentially made more difficult by the increased protein concentration and time needed for this reaction to proceed. Hence, an incubation period with proteinase K was included to enhance the interpretability of the results. Additionally, there was a more prominent cleavage occurring which at points interfered with the interpretation of results (Figure 3.2.3). To better resolve the topoisomers from linear fragments in any future repeats should be additionally run on chloroquine gels.

ATP-independent relaxation was performed at 37°C with a small amount of relaxation being observed. Assaying the time of reaction, it was clear to see that leaving the biological (A₂B₂) enzyme longer assisted with relaxation activity, as it is much poorer at carrying out this reaction than the ATP dependent supercoiling reaction. High concentrations of the enzymes (1 μM) were also needed to observe relaxation (Figure 3.2.3).

It was very difficult to observe any relaxation with the fusion protein as the gels of the reactions showed a large amount of contaminating cleavage, and hence it was difficult to determine if the enzyme was relaxing the DNA or if the DNA was simply being linearized and cut to form a smear on the gel (Figure 3.2.3). It is possible that this cleavage activity was because of contaminations in the protein sample, or alternatively the enzyme may simply have a high intrinsic cleavage activity in the absence of ATP. It is suggested that this experiment needs to be repeated to confirm that this enzyme can relax DNA. Overall, the Mth enzymes appear to be weaker at the ATP-independent relaxation reaction than their Mtb counterparts.

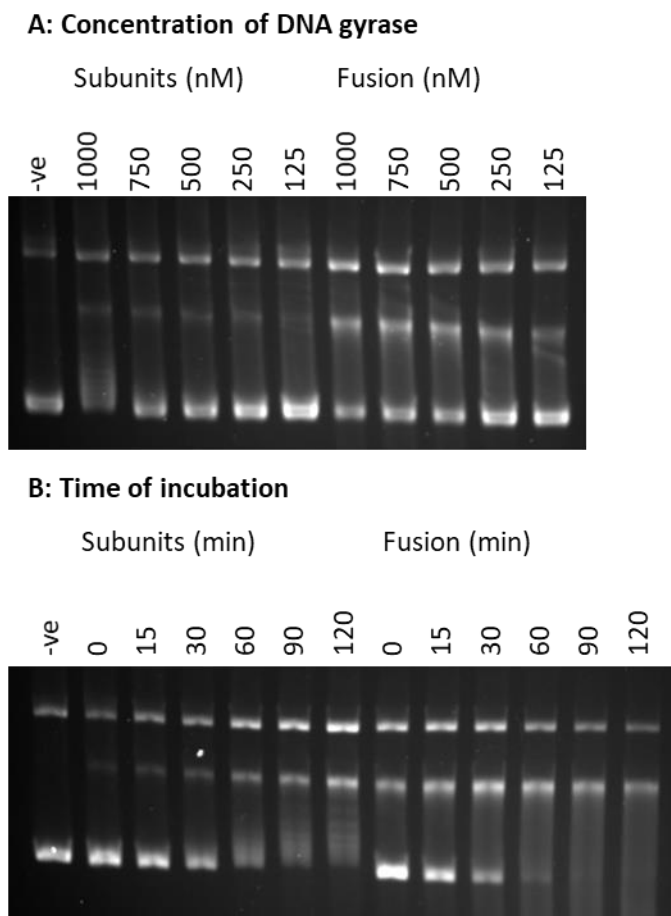


Figure 3.2.3: Comparison of the two constructs of *M. thermoresistibile* DNA gyrase in ATP-independent relaxation. A) Titration of the enzyme at monomeric concentration 125-1000 nM at fixed assay conditions (37°C for 1 hour). B) Time course 0-120 min at 37°C at a fixed enzyme concentration of 1 μ M and 150 mM Potassium glutamate concentration. -ve control was incubated under full assay conditions in the absence of DNA gyrase for the longest incubation time of the reaction. The linear bands observed are unavoidable and a consequence of the large amounts of enzyme and longer time required for this assay.

To optimise the relaxation reaction, the concentration of potassium glutamate in the reaction was altered under sub-optimal reaction conditions. Again, there was a significant cleavage band observed throughout, and some smearing from the fusion protein. Like the supercoiling reaction it was obvious that when assaying with the subunits both the absence of potassium glutamate and an excess of potassium glutamate inhibited this reaction (Figure 3.2.4). Optimal conditions when the subunits were assayed were found to be around 150 mM, with significant relaxation being observed between 100-150 mM (Figure 3.2.4). When the reaction was carried out with the fusion construct the reaction was uninterpretable due to contaminating cleavage (Figure 3.2.4).

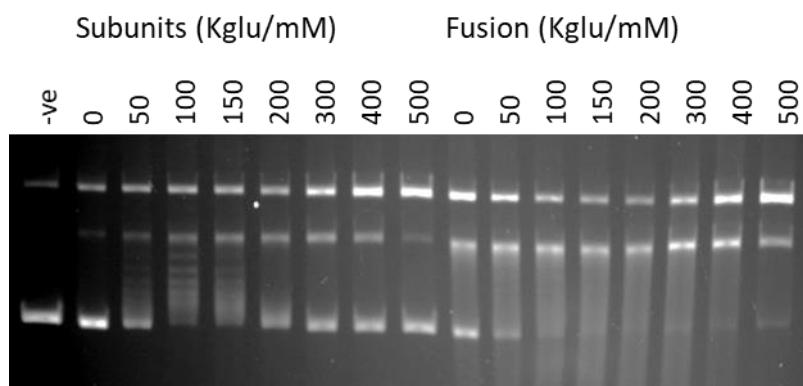


Figure 3.2.4: ATP-independent relaxation as a function of potassium glutamate concentration with both the Mth GyrA₂B₂ individual subunits and the GyrBA fusion construct. 1 μ M of each protein assayed for 1 hour at 37°C with potassium glutamate concentrations 0-500 mM. -ve control was incubated under full assay conditions in the absence of DNA gyrase with 500 mM potassium glutamate. The linear bands observed are unavoidable and a consequence of the large amounts of enzyme and longer time required for this assay.

3.2.5 DNA gyrase from *M. thermoresistibile* can decatenate DNA

Under ATP-dependent conditions it was found that Mth gyrase displayed weak decatenation activity. At this time ATP-independent conditions have not been trialled. The current decatenation assay utilising a kinetoplast DNA (kDNA) substrate can be difficult to interpret, as previously described, the kDNA substrate cannot enter a 1% agarose gel under native or intercalating conditions, with the product being observed further down the gel in supercoiled and nicked bands (Figure 3.1.9). The decatenation was studied under two different buffer conditions – the supercoiling assay conditions and a buffer recorded as a decatenation buffer (Aubry *et al.*, 2006a). The individual subunits appeared to prefer the supercoiling assay buffer when assayed for 30 min at 37°C (Figure 3.2.5). Very little decatenation was observed when the same conditions were assayed in the decatenation assay buffer (Figure 3.2.5). The activity

of the individual subunits in supercoiling assay buffer was comparable to the fusion protein which gave good levels of decatenation in both assay buffers (Figure 3.2.5).

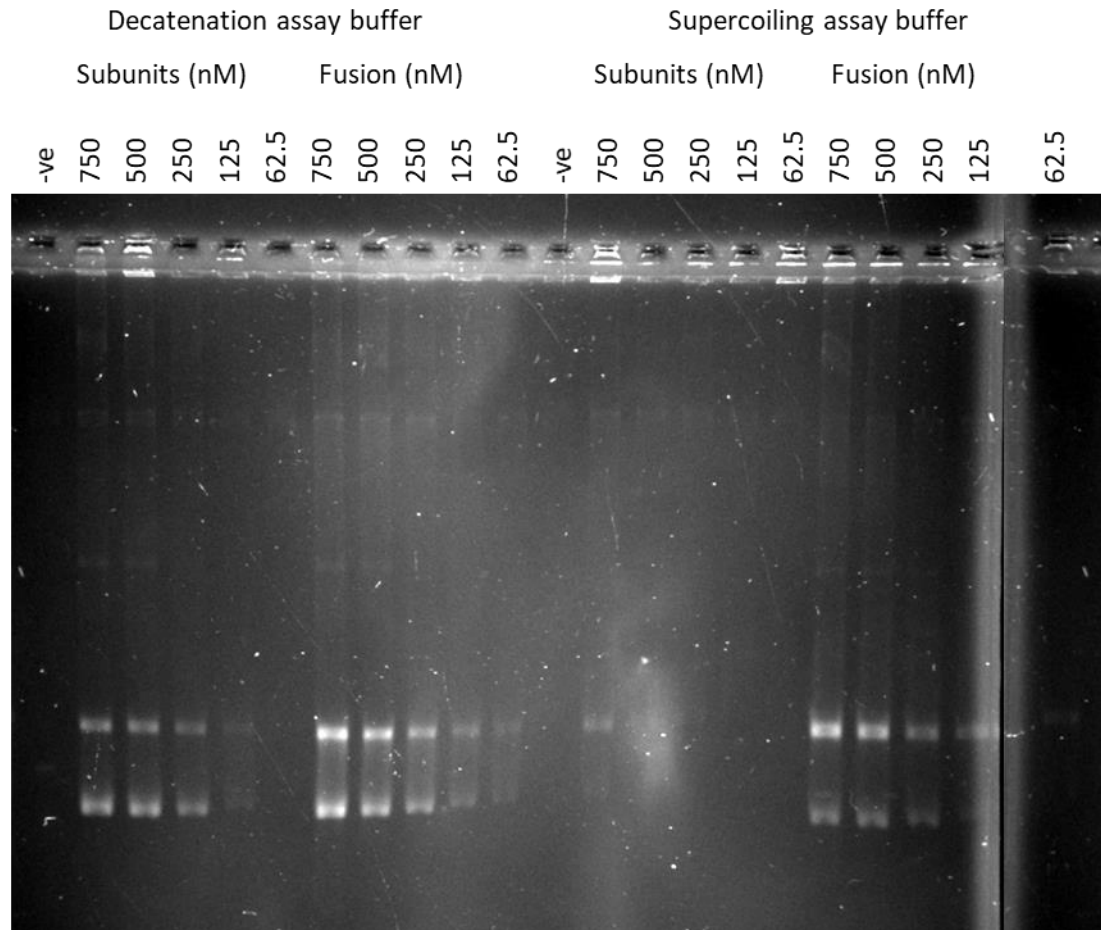


Figure 3.2.5: Decatenation assay using kinetoplast DNA. The kDNA is unable to enter the gel so may be seen in the wells of the gel, the product of a positive reaction shows a combination of open circular and negatively supercoiled mini-circles as seen by the two bands. Assay was performed using decreasing enzyme concentrations (750-62.5 nM) of each construct using both the decatenation assay buffer and the supercoiling assay buffer (see methods section 2.5.3). Reactions were performed at 37°C for 30 min.

3.2.6 ATPase stimulation of DNA gyrase from *M. thermoresistibile* by DNA

The ATPase-linked assay was initially carried out with both the individual subunits and the fusion protein to determine the ATP turnover rate of the enzyme. This was determined in duplicate assays by giving values much lower than those found for the Mtb fusion protein, but more comparable to those obtained for the Mtb subunits (Table 3.2.2). As the rates were much slower it produced larger comparable errors in the results, which made it particularly difficult to tell if there was indeed a greater stimulation of the ATPase activity with topologically

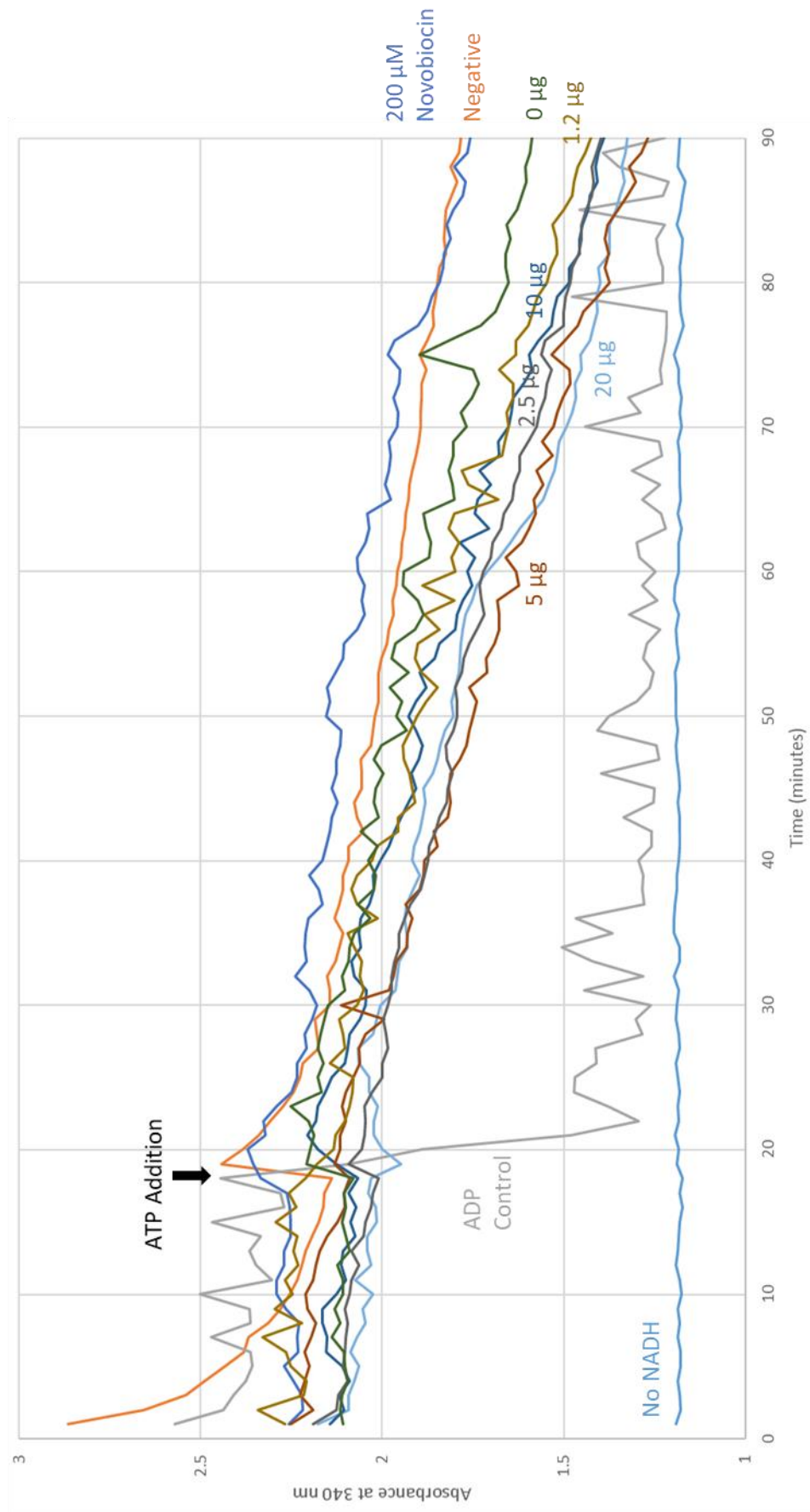
unconstrained DNA, compared to topologically constrained DNA. There may be a small difference between the results when topologically constrained and unconstrained DNA were used as substrates, suggesting a slight preference for unconstrained DNA.

Table 3.2.2: ATP turnover rate with 508 nM of Mth individual GyrB or GyrBA subunits and 2 ng of pBR322* plasmid of differing topologies measured over a 45 min period after the addition of 2 mM ATP. All rates displayed are the novobiocin sensitive rates. Data is the average of two repeats, and representative of multiple (more than 2) experiments.

pBR322* Topological Form	ATP Turnover / s ⁻¹	
	Subunits (GyrA ₂ GyrB ₂)	Fusion (GyrBA ₂)
Relaxed	0.16±0.14	0.13±0.06
Negatively supercoiled	0.12±0.02	0.28±0.02
Nicked	0.17±0.03	0.32±0.03
Linear	0.26±0.03	0.44±0.04

Using linear pBR322* and the individual subunits there was unambiguous evidence of a much lower ATP turnover in the absence of DNA. However, the rates obtained were inconsistent and low, with no obvious plateaux (Figure 3.2.6). This assay does appear to suggest that a DNA concentration of 2 ng, as was used with 504 nM of each of the subunits, does appear to be sufficient to stimulate ATPase activity, although it is unclear if this amount of DNA in the reaction may be sub-maximal (Figure 3.2.6). Due to the difficulties working with these enzymes in the ATPase linked assay, a DNA titration on any of the substrates was not performed with the fusion construct.

A



B

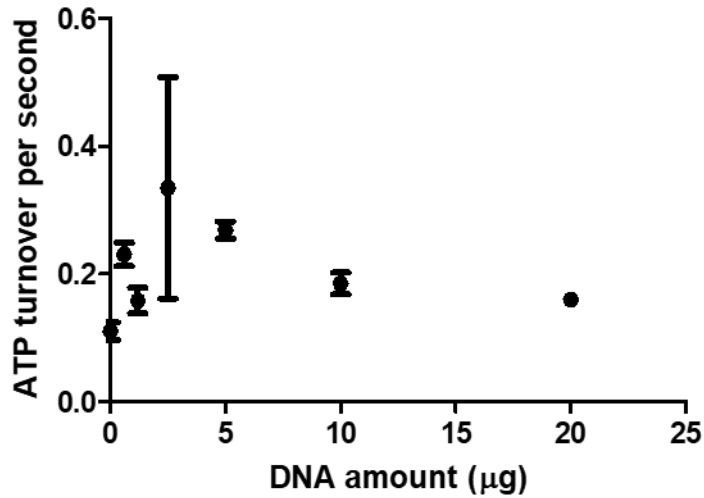
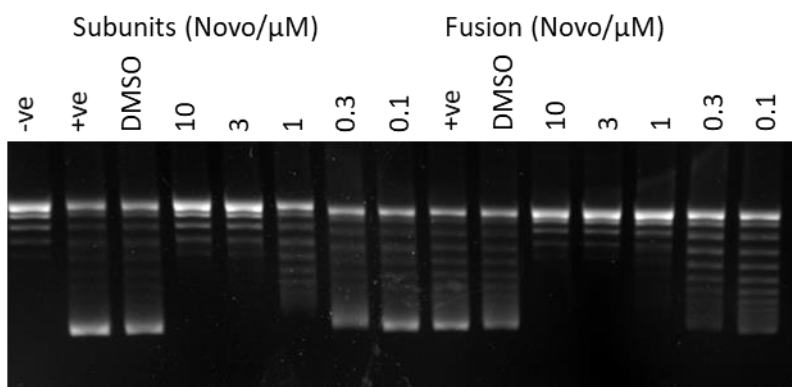


Figure 3.2.6: A) Plot of absorbance at 340 nm monitoring the loss of NADH in the PK/LDH linked assay, carried out with 508 nM of Mth GyrA and GyrB subunits. Control samples (no NADH, negative without enzyme, positive with ADP not ATP, novobiocin independent rate) contained no DNA substrate. DNA titration of 0-20 µg linear pBR322*. B) DNA titration on increasing the concentration of linear pBR322* from 0-20 µg when assayed with 508 nM of Mth GyrA and GyrB subunits.

3.2.7 Inhibition of *M. thermoresistibile* DNA gyrase by known inhibitors

To determine if Mth gyrase can be inhibited in the same way as Mtb gyrase, the inhibition profile of both the subunits and fusion constructs were compared to those of the Mtb subunits and fusion constructs. Inhibition of supercoiling was investigated by novobiocin – a competitive inhibitor of the ATPase reaction (Sugino *et al.*, 1978). Inhibition of the Mtb constructs was analysed at 74 nM enzyme at a concentration range of 10-0.1 µM novobiocin, giving an approximate IC_{50} value of *ca.* 1 µM for both constructs (Figure 3.2.7). This value is in approximate agreement with the literature value of 0.5 µM (Aubry *et al.*, 2006a). In comparison a concentration of 0.25 µM for the Mth gyrase enzymes was assayed with a concentration range of 10-0.1 µM, giving an approximate IC_{50} value of *ca.* 0.3 µM (Figure 3.2.7). Accounting for a 3x higher enzyme concentration in the Mth assay, it is possible that there could be an order of magnitude difference in the IC_{50} values of the two different gyrase enzymes from the different species. Interestingly, there does not appear to be any difference regardless of whether the GyrB subunit is fused to the GyrA subunit.

A: *M. tuberculosis*



B: *M. thermoresistibile*

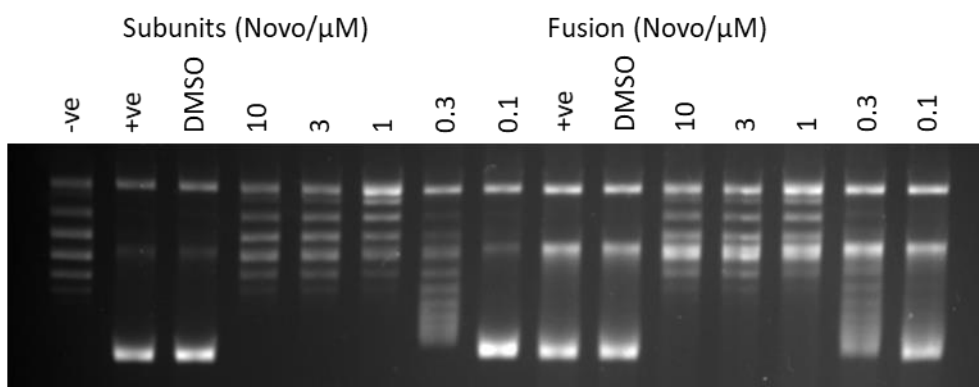


Figure 3.2.7: Inhibition of A) *M. tuberculosis* DNA gyrase subunits A₂B₂ and BA fusion constructs (74 nM) and B) *M. thermoresistibile* DNA gyrase subunits A₂B₂ and BA fusion constructs (250 nM) supercoiling activity by novobiocin (10-0.1 μM). All reactions except +ve control contained 1% DMSO. -ve control contained all reaction conditions except DNA gyrase, positive control contained DNA gyrase without DMSO, DMSO control contained all reaction conditions including 1% DMSO. The linear bands observed in the Mth assay are a consequence of the large amounts of enzyme required for this assay, and they do not affect the interpretation of this assay.

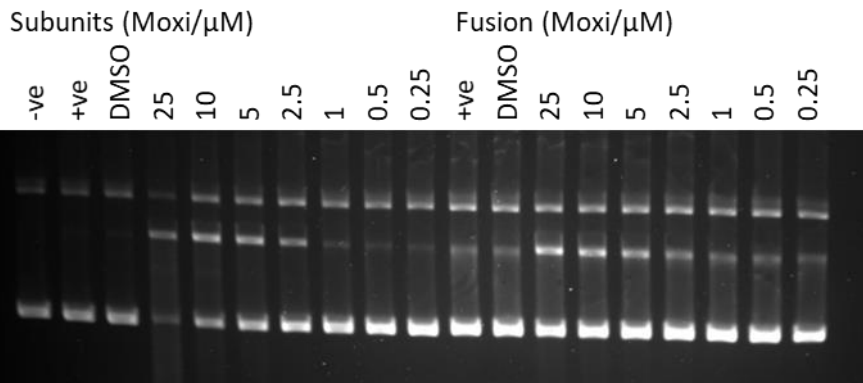
As novobiocin is a known competitive inhibitor of ATP in other gyrase enzymes (Sugino *et al.*, 1978), an ATPase titration was applied to determine the IC₅₀ value in the ATPase reaction. Unfortunately, after duplicate experimentation it was determined that the ATP turnover rate was too low to generate reliable data and hence this was not obtained. Likewise, as the specific ATPase assay was found to be very difficult when working with the fusion construct this experiment was not trialled (Table 3.2.2).

Inhibition of gyrase by a fluoroquinolone was also examined. Moxifloxacin was used as it has been reported to have a high degree of activity against Mtb gyrase (Blower *et al.*, 2016) and is routinely used as a second line antibiotic against TB (WHO, 2010). To determine the

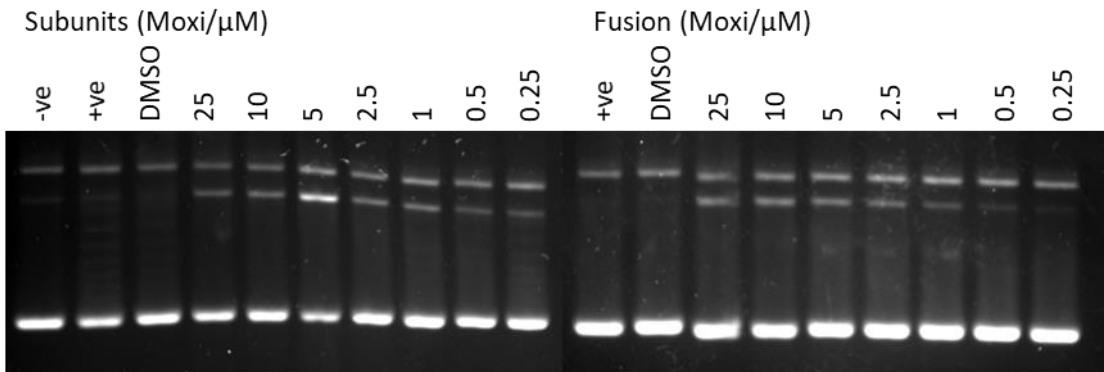
activity, inhibition of both supercoiling and induction of cleavage were analysed. Analysing the subunits, a CC_{50} value of *ca.* 2.5 μM was obtained when assaying using 0.25 μM of the Mth gyrase subunits. Difficulty was observed in obtaining an accurate CC_{50} value when using the fusion construct due to a prominent level of background cleavage in the no drug controls, however through gel analysis it was determined to be similar to that of the subunits (Figure 3.2.8). In contrast, a CC_{50} value for the individual gyrase subunits from the Mtb proteins has a CC_{50} value around 0.5-1 μM when assayed at 74 nM (Figure 3.2.8). The CC_{50} of the Mtb fusion protein appears to be similar to that of the subunits (Figure 3.2.8). Accounting for effects of protein concentration it suggests there is unlikely to be a significant difference in the cleavage response to moxifloxacin. Additionally, these values appear to be similar to those reported within the literature of 10 μM (Aubry *et al.*, 2004).

As the fluoroquinolones inhibit the relegation of DNA and stabilise the cleavage complex they also stop the propagation of the supercoiling reaction (Gellert *et al.*, 1977), hence the inhibition of supercoiling was compared between the four constructs. It was found that the supercoiling reaction was not inhibited as strongly by moxifloxacin as it was by novobiocin. Instead at 100 μM incomplete inhibition of supercoiling was observed at an enzyme concentration of 0.25 μM for both the Mth gyrase individual subunits and the fusion protein (Figure 3.2.8). Like the Mth enzyme, inhibition of Mtb gyrase was only possible at higher concentration of moxifloxacin at 74 nM of either construct. The IC_{50} values are in the order of approximately 25 μM for all of these constructs, which is somewhat similar to the value of 11.2 μM reported in the literature (Aubry *et al.*, 2004) (Figure 3.2.8). The differences in these values can likely be accounted for in the differences of the enzyme concentrations assayed for the two different source species of the proteins.

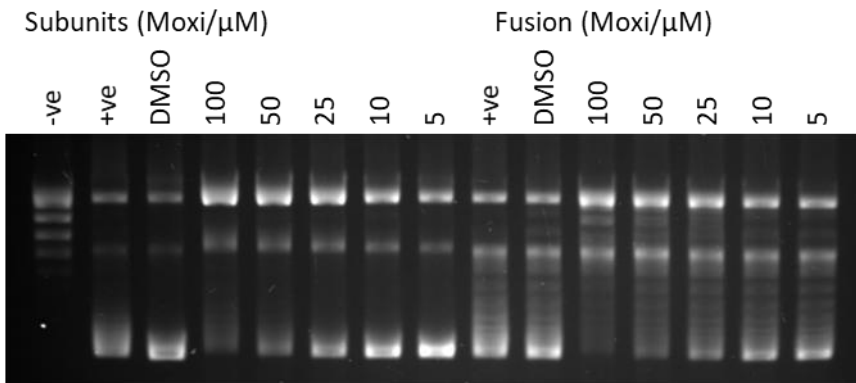
A: *M. thermoresistibile* Cleavage



B: *M. tuberculosis* Cleavage



C: *M. thermoresistibile* Supercoiling



D: *M. tuberculosis* Supercoiling

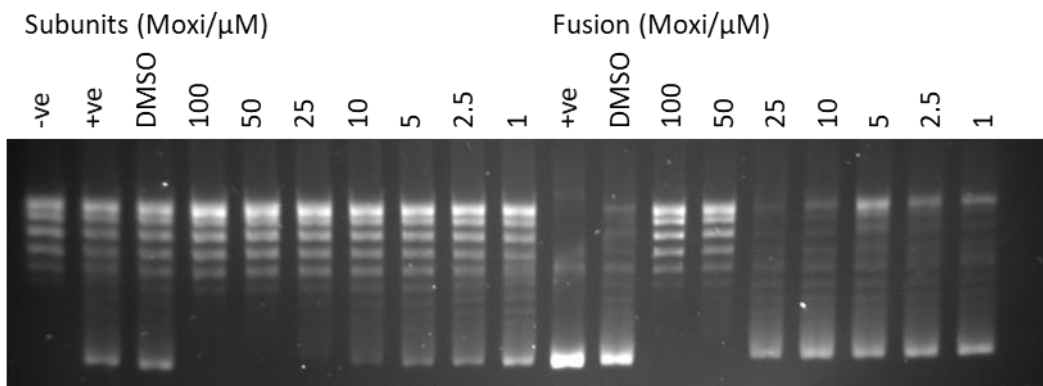


Figure 3.2.8: Activity of Moxifloxacin on the two alternate constructs of A/C) Mth DNA gyrase at 0.25 μM and B/D) Mtb DNA gyrase at 0.74 μM . Induction of cleavage complex assay using A) 25-0.25 μM B) 25-0.25 μM moxifloxacin. C) Inhibition of supercoiling assay using C) 100-5 μM D) 100-1 μM moxifloxacin. All assays except positive controls contained 3.3% (v/v) DMSO -ve control contained all assay components without DNA gyrase, +ve control contained all assay components in the absence of DMSO (or moxifloxacin), DMSO control contained all assay components and 3.3% (v/v) DMSO. The linear bands observed in the positive control/ DMSO control were controlled for in the calculation of the CC_{50} values. The linear bands observed in supercoiling are unavoidable and a consequence of the large amounts of enzyme and longer time required for this assay, and do not affect the result of this assay.

3.3 Discussion

3.3.1 The mycobacterial DNA gyrase fusion proteins are active

The results in this chapter clearly show that by fusing the C-terminus of GyrB to the N-terminus of GyrA you do not lose gyrase-specific activity in the fusion protein. This is somewhat surprising when you consider that no significant linker was inserted to separate the two subunits. However, when you put this result in context of other type IIA topoisomerases this is somewhat unsurprising as the eukaryotic topo II contains a similar domain arrangement to DNA gyrase and topo IV, but, unlike the bacterial proteins topo II contains one single protein subunit equivalent to that of a GyrBA subunit which also dimerises (Miller *et al.*, 1981).

Several studies, carried out in the Klostermeier laboratory, have used and described fusion proteins to be active (reviewed in (Klostermeier, 2018)). Additionally, the ParE-ParC fusion has been determined to have activity (Lavasani and Hiasa, 2001); the results here agree that the fusion proteins have activity in the absence of a linker between the proteins. These results are important in the context of structural studies which have been presented in the form of the core fusion protein structures (Srikannathan *et al.*, 2015, Blower *et al.*, 2016) and the full-length low resolution cryoEM structure (Papillon *et al.*, 2013) in demonstrating the potential biological relevance of these structures as it implies that these structures are likely to be biologically active. Additionally, it is hoped that these two new GyrBA proteins will be subjected to further structural studies to determine the full-length structure of DNA gyrase from a mycobacterial species.

In terms of the specific activity differences between the four proteins, no major differences were observed (Table 3.3.1), although there were some subtle differences. These included the Mth proteins being less active and hence requiring more enzyme for both supercoiling and decatenation to occur. It is however obvious that there is some difference between the subunits and fusion in terms of activity at high potassium glutamate concentrations. In the subunits a decline in the activity is clearly observable at high potassium glutamate concentrations whereas this is not visible when assaying the fusion construct (Figure 3.1.5; Figure 3.2.2) (Table 3.3.1). This discrepancy was not observed in the ATP-independent relaxation reaction. Furthermore, although both fusion proteins could decatenate effectively in both the decatenation and supercoiling assay buffer, the Mtb protein preferred the supercoiling buffer and the Mth proteins the decatenation buffer (Table 3.3.1).

Table 3.3.1: Table of the optimal assay conditions for the Mtb and Mth DNA gyrase proteins in both the subunits and the fusion proteins. Sc = supercoiling buffer; DC = decatenation buffer.

	<i>M. tuberculosis</i>		<i>M. thermoresistibile</i>	
	Subunits	Fusion	Subunits	Fusion
Supercoiling				
Concentration	73 nM	74 nM	250 nM	250 nM
Time	30 min	30 min	30 min	30 min
Potassium glutamate concentration	150-200 mM	50-500 mM	100-200 mM	150-500 mM
Relaxation				
Concentration	500 nM	500 nM	1000 nM	1000 nM
Time	2 hr	2 hr	1 hr	1 hr
Potassium glutamate concentration	100-200 mM	100-200 mM	100-150 mM	Undetermined
Decatenation				
Concentration	217 nM	73 nM	250 nM	250 nM
Preferred Buffer	Sc	Dc or Sc	Dc	Dc or Sc

3.3.2 DNA Gyrase from *M. tuberculosis* can give an appreciable ATP turnover rate

From the scope of this work it can be clearly observed that there is indeed an appreciable and detectable rate of ATP turnover. This rate is comparable to that of the published rate from the *M. smegmatis* enzyme of 0.39 s^{-1} (Manjunatha *et al.*, 2002), which appears to support the published literature that the protein was unsuitable to use for a high throughput assay system (Agrawal *et al.*, 2013, Karkare *et al.*, 2013b, Shirude *et al.*, 2013). It was however discovered that the GyrBA fusion protein appeared to give ATP turnover rates more comparable to those

from the *E. coli* enzyme (Table 3.1.2) (Maxwell and Gellert, 1984). It is unclear why this enzyme can give a much greater rate of ATP turnover; however, it is suggested that the purity of the enzyme stock used to obtain these rates was superior to the purity of the individual subunits. This could mean that the portion of the enzyme stock able to give a novobiocin-independent rate was significantly smaller than in the fusion protein hence preventing artificially lowered rates. The second explanation for this enhanced rate is that by fusing the proteins it has enhanced the ATPase activity of the proteins perhaps by reducing the time needed for a GyrB to bind to a GyrA subunit before the enzyme can process the reaction. A final consideration to make is that it has previously been observed that the ATPase rate of the human topo II α N-terminal domain is almost inactive when purified on a nickel column, but has much higher activity when purified on cobalt (Gardiner *et al.*, 1998). Typically, the fusion protein was subjected to further purification than the subunits which were generally purified only on nickel, hence, it would be interesting to purify these proteins without using a nickel column in the future to determine if this makes a difference.

It was found that like the *E. coli* enzyme it was difficult to obtain a rate of ATP turnover when the ATPase domain was used in isolation in the absence of DNA (Ali *et al.*, 1993). The rate presented here of $0.05 \pm 0.08 \text{ s}^{-1}$ was described to be in the same order as the published rate of 0.02 s^{-1} for the *E. coli* B43 subunit, and similar to the value for the equivalent Mtb fragment of 0.002 s^{-1} (Agrawal *et al.*, 2013). However, the quality of the results appeared to be questionable, and given that no rate could be detected for the *M. smegmatis* GyrB in the absence of GyrA and DNA it is questioned if this is simply an artefact of the experiment (Manjunatha *et al.*, 2002).

The full-length Mtb DNA gyrase fusion protein did not give an appreciable rate in the absence of DNA. This indicates a high degree of coupling between DNA binding and ATP hydrolysis. This phenomenon was also described for *E. coli* and *M. smegmatis* DNA gyrase, whereby a background rate of ATP hydrolysis by GyrB is unaffected by either addition of GyrA or double-stranded DNA, however the addition of both GyrA and double-stranded DNA led to an appreciable increase in the ATP hydrolysis (Maxwell and Gellert, 1984, Manjunatha *et al.*, 2002). A 1.5-2.5 fold increase in the ATPase activity of Mtb DNA gyrase in the presence of DNA has also been previously suggested by Agrawal *et al.* (2013). Previously the length of DNA fragment needed to stimulate ATP hydrolysis in *E. coli* DNA gyrase has been investigated (Maxwell and Gellert, 1984). This is only the second study where the effect of DNA topology has been compared, but the initial study was conducted with DNA plasmid

samples with relatively high estimated nicked contamination within the negatively supercoiled samples using *E. coli* DNA gyrase (Sugino and Cozzarelli, 1980). It was suggested in this paper that relaxed, linearised or nicked plasmids gave equivalent levels of ATP specificity and maximum velocity, although the authors do question the result of the relaxed plasmid pointing out that the substrates are rapidly converted into a negatively supercoiled plasmid. In the results presented here, we have demonstrated that there is unambiguous evidence for stimulation of ATPase activity in the presence of a linear or nicked plasmid as compared to one that is negatively supercoiled or relaxed when the fusion construct of Mtb DNA gyrase was used. This can be explained as we visualised samples from multiple timepoints in the ATPase reaction time course to determine the topological state of the DNA and found that there was rapid conversion of these substrates to a form which is negatively supercoiled. It is likely that the requirements for ATP hydrolysis of Mtb DNA gyrase require that DNA is bound in a right-handed orientation that negatively supercoiled DNA cannot readily adopt (Liu and Wang, 1978). This is not to say that there could be a significant difference between the enzymes from Mtb and *E. coli* allowing relaxed DNA to stimulate DNA gyrase and to allow it to remain stimulated for longer.

3.3.3 Is DNA gyrase able to convert positive supercoils in to negative supercoils?

In the scope of this work we briefly examined the rate of ATP hydrolysis in the presence of positively supercoiled pBR322*. To determine the topological state we ran a native agarose gel which showed all wells to be maximally supercoiled (Figure 3.1.12) with no apparent intermediate topoisomers. However, it is not possible to resolve the directionality of supercoils on a native agarose gel (Shure *et al.*, 1977), hence due to the lack of intermediate topoisomers it was assumed that the DNA substrate was rapidly converted into a negatively supercoiled plasmid. This would make sense in the context of the literature where it is known that Mtb DNA gyrase rapidly removed positive supercoils from DNA at a rate faster than it is able to negatively supercoil DNA (Ashley *et al.*, 2017). Three additional methods should be considered in the future to gain greater insight into point at which the plasmid is maximally negatively supercoiled. The first of these is to use a gel with added chloroquine, which increases the resolution of the topoisomers, and in combination with a native gel would indicate if a sample was positively or negatively supercoiled due to difference in the migration of the sample. The migration of DNA topoisomers is influenced by chloroquine as it intercalates to make DNA appear more positively supercoiled, which causes positive supercoiled and relaxed DNA to run faster, and negative supercoils to run slower than on gels performed in the absence of chloroquine (Shure *et al.*, 1977, Clark and Leblanc, 2009). Although it is possible to resolve positive and negatively supercoiled DNA on a 2D gel, this

method is impractical with large numbers of samples as run in this experiment (Wang *et al.*, 1982). The final method is a new non-gel based technique known as the Qiaxcel which is able to both resolve topoisomers better than in a native agarose gel and resolve positive and negative supercoils (Mitchenall *et al.*, 2018) (Unpublished data – Ms L.A. Mitchenall). It is proposed that this new method should be trialled in the future for resolving positive and negative supercoiling.

3.3.4 What are the optimal assay conditions for a thermophilic bacterium?

Preliminary assay conditions for the Mth proteins are described in Table 3.3.1 inferring that there are no significant differences between the proteins from Mth and the well-characterised Mtb homologues. This does not rule out alternative differences between the enzymes that have not yet been assayed, for example it has been reported that the *M. avium* DNA gyrase has been reported to have a low specific activity when compared with that from *M. smegmatis* and *E. coli* (Guillemin *et al.*, 1999). From these studies it implies that Mth DNA gyrase may have a lower specific activity like *M. avium*.

As a thermophilic bacterium one of the major considerations is the optimal operational temperature for proteins from this species may differ. It has been reported that growth is viable at temperatures up to 55°C which is significantly greater than that of *M. tuberculosis* (Edwards *et al.*, 2012). This suggests that the Mth DNA gyrase should have activity at temperatures greater than that of the Mtb DNA gyrase, therefore it would be interesting to see if the optimal growth temperature corresponds to the optimal assay temperature for Mth DNA gyrase in the future.

It was difficult to interpret the results of the relaxation and decatenation assays due to contaminating cleavage occurring. This was particularly observable when assaying the fusion protein in the ATP-independent relaxation assay (Figure 3.2.3; Figure 3.2.4). This is likely to be at least in part due to contamination in the protein purification which was not perfect. It is suggested that in the future the protein should be further purified to yield purer protein to determine if this is an intrinsic property of the protein or if it is because of a contamination. Additionally, it can be difficult to determine if decatenation is occurring through a cleavage mechanism whereby proteins are cleaved to release the mini-circles or if they are truly decatenated when using the current method. However, a newer alternative is currently being developed by Inspiralis Limited which uses a pair of intertwined plasmids of varied sizes

which can be unlinked in a decatenation reaction (Figure 3.3.1). If optimisation of this reaction can occur it is suggested that in the future this new assay should be attempted on this protein to determine with more certainty if decatenation is truly occurring (N. Waraich, Pers. Comm.).

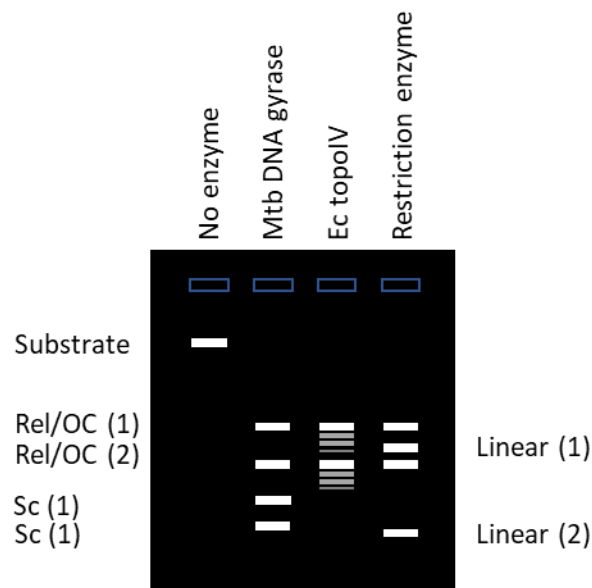


Figure 3.3.1: Demonstration of how an alternative decatenation assay in development by Inspiralis Limited using two interlinked plasmids of distinct sizes which can be resolved on a gel. Decatenation by DNA gyrase would result in two supercoiled bands alongside potentially two open circular nicked bands. Topo IV such as that from *E. coli* would result in two groups of relaxed topoisomers. Meanwhile a restriction enzyme would still be able to unlink the plasmids through a double stranded break but additional banding at decreased sizes should also be seen.

Overall, the data obtained alongside the evidence presented by Edwards *et al.* (2012) indicates that the Mth homologue of DNA gyrase and the fusion protein is a suitable candidate for structural studies of mycobacterial DNA gyrase. Although, the preliminary crystallisation studies were not successful, it is suggested that further trials should be carried out in the future with a purer protein stock alongside the use of cryoEM to attempt to resolve a high-resolution full-length structure of this highly interesting enzyme.

3.3.5 Decatenation happens in 100 mM and 250 mM potassium glutamate

It is suggested in the literature that Mtb DNA gyrase decatenates optimally in the decatenation assay buffer (Aubry *et al.*, 2006a). The results here clearly show that these conditions do not always result in the optimal decatenation conditions (Table 3.3.1). For some of the constructs this assay buffer does appear to be optimal, whereas others decatenate to a superior level in the assay buffer used for supercoiling. As described in section 3.3.4 it is possible that this

result is artificial hence it is suggested that when the substrate for the alternative decatenation assay substrate is commercially available the decatenation activities of these enzyme should be further optimised.

4. Inhibition of Mycobacterial DNA Gyrase

Presently there is increasing resistance being observed in the clinic against the current DOTS first line regime of antibiotics for the treatment of tuberculosis (WHO, 2017). Hence, there have been significant advances towards further drug discovery against *M. tuberculosis* to decrease the mortality rate and treatment times in recent year; some of which are reviewed within (Campanico *et al.*, 2018). We therefore investigated the inhibition of Mtb DNA gyrase with both previously known and unknown inhibitors, the results of which are within this chapter. The aim was to find a lead compound with a novel mode of action which could be further optimised into a compound that could be advanced to clinical use in the future. This was achieved initially by comparing the activity of the lesser known compound classes of the naphthoquinones and the tricyclic inhibitors (Redx AntiInfectives) including the novel Redx04739 to the known classes of DNA gyrase inhibitors of the fluoroquinolones and the aminocoumarins.

4.1 Fluoroquinolone Antibiotics

The quinolone antibiotics are clinically-used inhibitors targeting the bacterial type IIA topoisomerases DNA gyrase and topo IV through a dual-targeting mechanism in most bacteria. However, in the absence of topo IV only the single target of DNA gyrase is present in mycobacteria. Here we investigated the third-generation fluoroquinolone moxifloxacin, which is clinically used as a second-line antibiotic against *M. tuberculosis* against the two Mtb DNA gyrase constructs to determine if any difference in the inhibition was obtained by fusing the two subunits. The fluoroquinolones act through a known mechanism of action which includes inducing cleavage complexes via prevention of the religation reaction (Hedde *et al.*, 2000). Hence, we set out to determine both the IC₅₀ and the CC₅₀ of moxifloxacin against both the Mtb individual subunits and the fusion protein (see method sections 2.5.1; 2.5.4). The CC₅₀ of moxifloxacin was found to consistently be around 0.5-1 µM for both the fusion and subunit constructs (Figure 4.1.1A), on the other hand the IC₅₀ values were found to be much more modest of around 25 µM (Figure 4.1.1B). These values appear consistent between the two constructs analysed hence indicating that no difference in the inhibition of DNA gyrase occurs when using the fusion construct. The literature values for both the CC₅₀ and IC₅₀ values for moxifloxacin are around 10 µM (Aubry *et al.*, 2004).

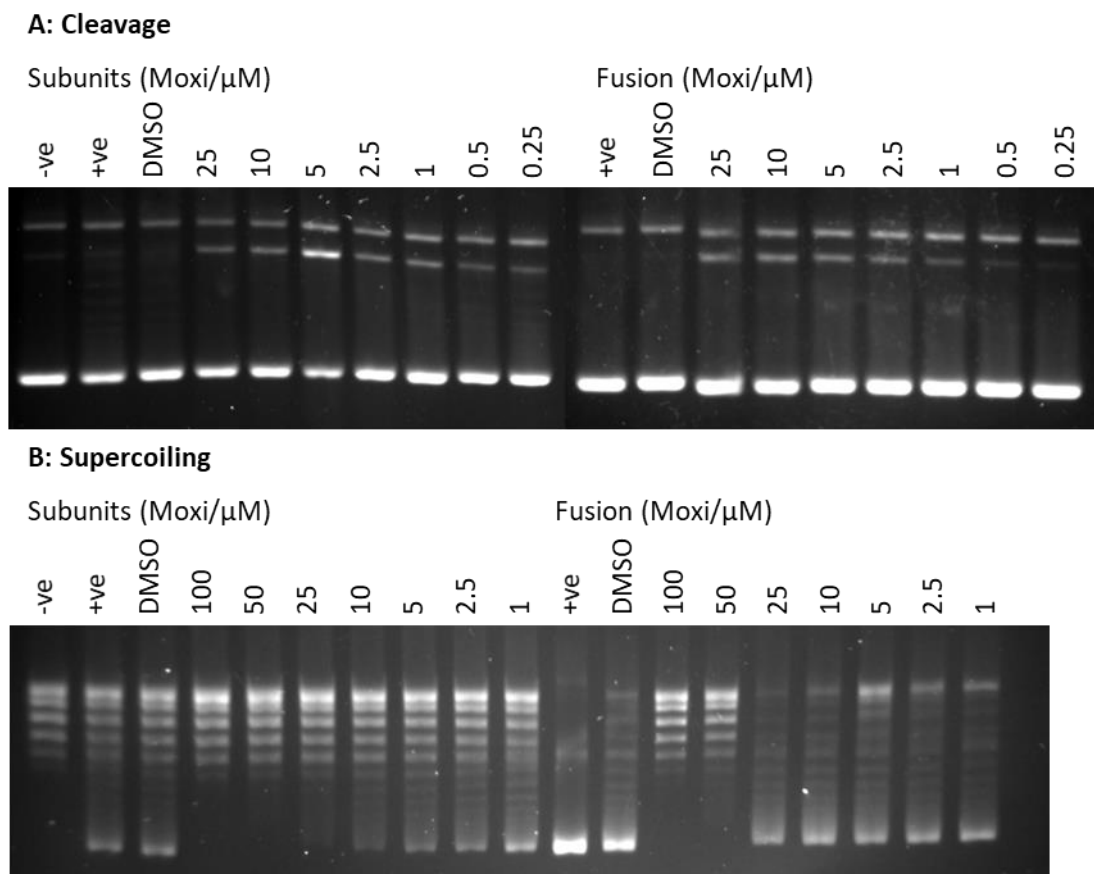


Figure 4.1.1: Activity of Moxifloxacin on the two alternate constructs of Mtb DNA gyrase at 0.74 μ M. A) Induction of cleavage complex assay using 25-0.25 μ M moxifloxacin. B) Inhibition of supercoiling assay using 100-1 μ M moxifloxacin. All assays except positive controls contained 3.3% (v/v) DMSO. -ve control contained all assay components in the absence of DNA gyrase, +ve and DMSO controls were carried out with all assay components in the absence of moxifloxacin. Enzyme concentration was chosen to be less than 100% supercoiling for better determination of the IC₅₀ values.

Overall, the data obtained here is in contrast to those in the literature as it indicates that the enzyme can function at higher concentrations of moxifloxacin than is required for transient induction of the cleavage complex. It is plausible, for instance, that the rate of supercoiling was simply decreased with the intermediate cleavage complex being stabilised as per the mechanism of action of microcin B17 (Pierrat and Maxwell, 2003). However, it is unusual that fluoroquinolones gives rise to such a significant difference in CC₅₀ and IC₅₀ values. It is instead suggested that as the CC₅₀ value was obtained in an ATP-independent reaction where a negatively supercoiled substrate was used in the absence of ATP, whereas, the supercoiling reaction was carried out in the presence of ATP and a relaxed substrate to generate an IC₅₀ value. It is possible that the presence of ATP or topology of the DNA substrate may influence these values, and hence, this should be investigated more thoroughly in the future. However, despite any differences in the values from those presented in the literature, this work clearly

demonstrates that there are no significant differences in our hands between the two inhibitions of the subunits or fusion constructs of Mtb DNA gyrase by moxifloxacin.

4.2 Aminocoumarin Antibiotics

The aminocoumarin family of non-clinical antibiotics, including novobiocin, inhibit DNA gyrase through competitive inhibition of the ATPase reaction (Mizuuchi *et al.*, 1978). To determine if the mechanism of action or the potency of these compounds was altered by fusing the DNA gyrase subunits together we investigated the IC₅₀ values for the inhibition of the supercoiling reaction against both the A₂B₂ heterotetramer and the GyrBA dimer (see methods section 2.5.1). It was initially determined that the IC₅₀ value of both constructs in the supercoiling reaction were determined to be approximately 1 µM when assaying against 74 nM enzyme monomer (Figure 4.2.1a). These values appear to be of a similar order of magnitude to the literature value of 0.5 µM (Aubry *et al.*, 2006a).

As the inhibition of supercoiling appeared to be equivalent between the two constructs of Mtb DNA gyrase and the ATP turnover of the GyrBA fusion construct has been determined suitable for inhibitor studies in the ATPase-linked assay, with experiments trialled to determine an IC₅₀ value for the ATPase reaction. An IC₅₀ value of the ATPase reaction was determined to be 0.21±0.04 µM (representative of duplicate repeats; Log(IC₅₀): -0.68±0.08) (Figure 4.2.1B). However, as the value obtained for the IC₅₀ is close to the enzyme concentration used within this reaction (200 nM), it is possible that a true IC₅₀ value was not obtained. This is because the limit of detection is defined by the enzyme concentration used in this reaction, therefore it is suggested from this result that the IC₅₀ value would be better represented as <0.21 µM. Although the ATPase reaction has been optimised for the Mtb GyrBA construct the reaction is still difficult to work with at low enzyme concentrations, and hence it was not possible to obtain data at lower enzyme concentrations to confirm the true value of this reaction.

Unusually the value of the IC₅₀ for the ATPase reaction appears to be somewhat smaller than the IC₅₀ value obtained in the supercoiling reaction. This is unexpected because novobiocin indirectly inhibits the ATP-dependent supercoiling reaction through competitively inhibiting the ATPase reaction that allows supercoiling to occur (Sugino *et al.*, 1978). Therefore, it is suggested that the true IC₅₀ for novobiocin is represented by the ATPase reaction, meaning that you would normally expect an equal or larger IC₅₀ value to be obtained for the ATPase

reaction. This can potentially be explained as there is a large degree of error in the values obtained, and if the inhibition of supercoiling experiment were to be repeated additional data pointed in the range used should be taken to increase the accuracy in the interpretation of the IC_{50} value. Likewise, although the value obtained is close to the limit of detection, it may be found to be accurate if it were possible to assay with lower enzyme concentrations in the future.

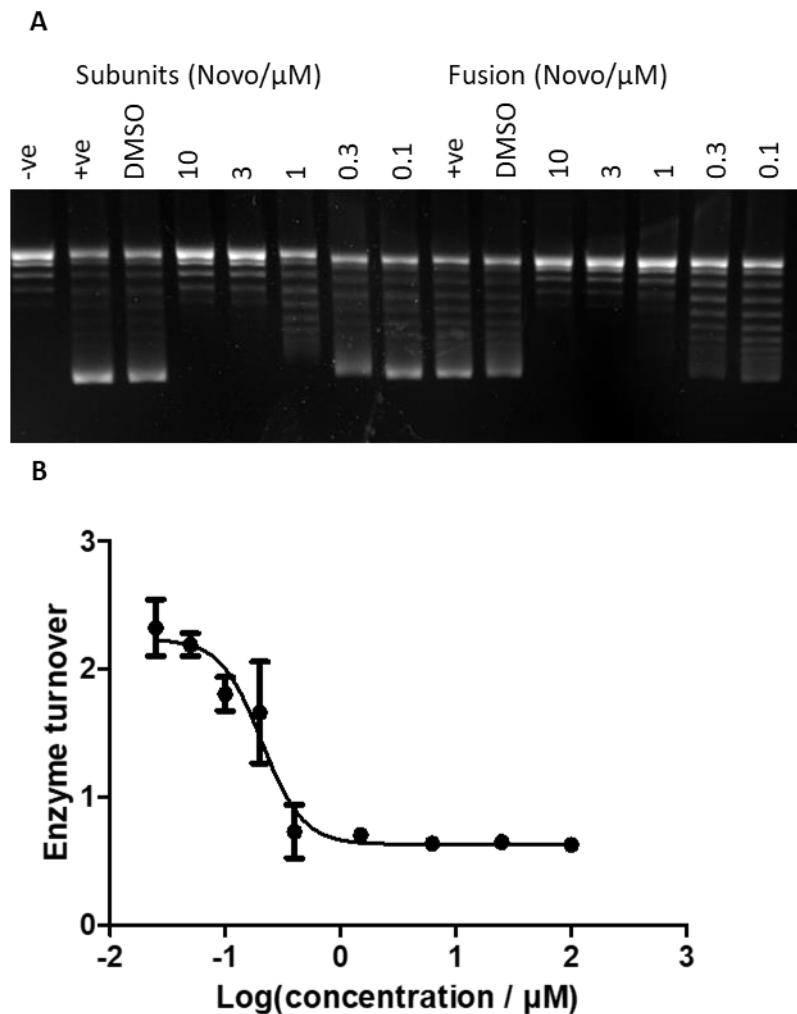


Figure 4.2.1: A) Inhibition of supercoiling assay against both the Mtb subunits and fusion proteins (protein concentration of 78 nM) by 10-0.1 μ M novobiocin in 1% (v/v) DMSO. -ve control contained all assay components in the absence of DNA gyrase. +ve control lacked DMSO, and the DMSO control contained all assay components in the absence of novobiocin. Enzyme concentration was chosen to be less than 100% supercoiling for better determination of the IC_{50} values. B) Analysis of an ATPase assay carried out with 200 nM GyrBA enzyme over a time period of 45 minutes with duplicate repeats. Plot shows the number of ATP molecules turnover per GyrBA subunit per second plotted against the base 10 logarithm of the novobiocin concentration in μ M. The IC_{50} value was determined to be 0.21 ± 0.04 μ M. Error bars represent the range of duplicate replicate points being plotted.

4.3 Naphthoquinone Antibiotics

Preliminary studies of the naphthoquinones were performed by Karkare *et al.* (2013b) who determined diospyrin to be inhibiting DNA gyrase at the N-terminal domain away from the ATPase site. Due to difficulties in the synthesis of diospyrin, we therefore sought to determine the mechanism of action of these compounds using 7-methyljuglone in collaboration with Dr MJ Austin (UEA, Pharmacy). The 7-methyljuglone was supplied in a powder form. When dissolving the powder in DMSO the solution formed was orange in colour. On leaving the compounds at room temperature or at -20°C, the solution turned progressively to a green colour, which appeared to have superior activity against Mtb DNA gyrase. MJA was able to determine that a reaction was occurring but was unable to identify the final reaction product obtained.

As it appeared that 7-methyljuglone dissolved in DMSO was chemically unstable resulting in a colour change in the solution, it was decided to investigate the stability of 7-methyljuglone in other solvents. Since some solvents are known to interfere with enzyme reactions a range of different solvents were trialled to determine which ones would be acceptable in the DNA gyrase supercoiling reaction (Figure 4.3.1). From this data it was determined that methanol would be the best alternate substitute for DMSO at concentrations less than 3.3% (v/v), but other possibilities included ethanol and isopropanol (at less than 1.7% (v/v)). Significant inhibition of the supercoiling reaction was observed when glycerol or PEG400 were added to the reaction (Figure 4.3.1). The unexpected result from glycerol (supercoiling was only visible at the 3.3% (v/v) but not 2.5 or 1.7% (v/v)) may be due to pipetting errors from the pipetting of viscous solutions, and as a consequence it was decided as a precaution to avoid the use of glycerol.

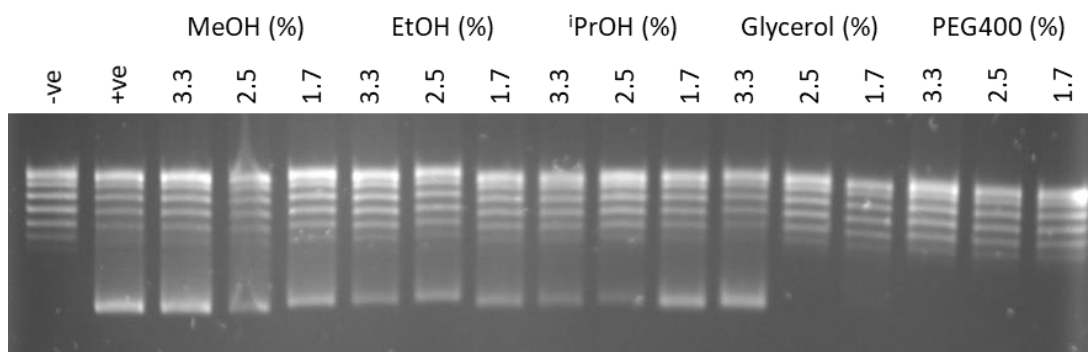


Figure 4.3.1: Supercoiling assay using 78 nM Mtb GyrBA to test which solvents inhibited the negative supercoiling reaction over a standard assay at 37°C for 30 minutes. All solvents were trialed at 3.3%, 2.5% and 1.7% (v/v) final reaction concentration. MeOH = methanol, EtOH = ethanol, ⁱPrOH = isopropanol. Data representative of multiple experiments. -ve control contained DNA substrate in the absence of DNA gyrase, +ve control contained no solvent. Enzyme concentration was chosen to be less than 100% supercoiling to better determine any enhancement or decrease in supercoiling within these reactions.

To confirm if 7-methyljuglone was chemically stable in methanol, a 3-day time course was performed. This experiment involved performing a supercoiling reaction with compound dilutions of freshly dissolved 7-methyljuglone in methanol which was repeated with the same stock of dissolved compound in methanol kept at room temperature after 24 and 48 hours to determine if a change in the inhibition of Mtb DNA gyrase was observed. From these results it was clear that pure 7-methyljuglone dissolved in methanol was a relatively poor inhibitor of DNA gyrase not resulting in full inhibition at 50 μ M (Figure 4.3.2a), as per the results found with the compound dissolved in DMSO. After one day, inhibition of supercoiling was observed at concentrations >30 μ M, indicating that a chemical alteration was already occurring (Figure 4.3.2b). The unknown product that formed after 2 days was determined to be a potent inhibitor of the Mtb DNA gyrase supercoiling reaction giving full inhibition of supercoiling at >5 μ M (Figure 4.3.2c).

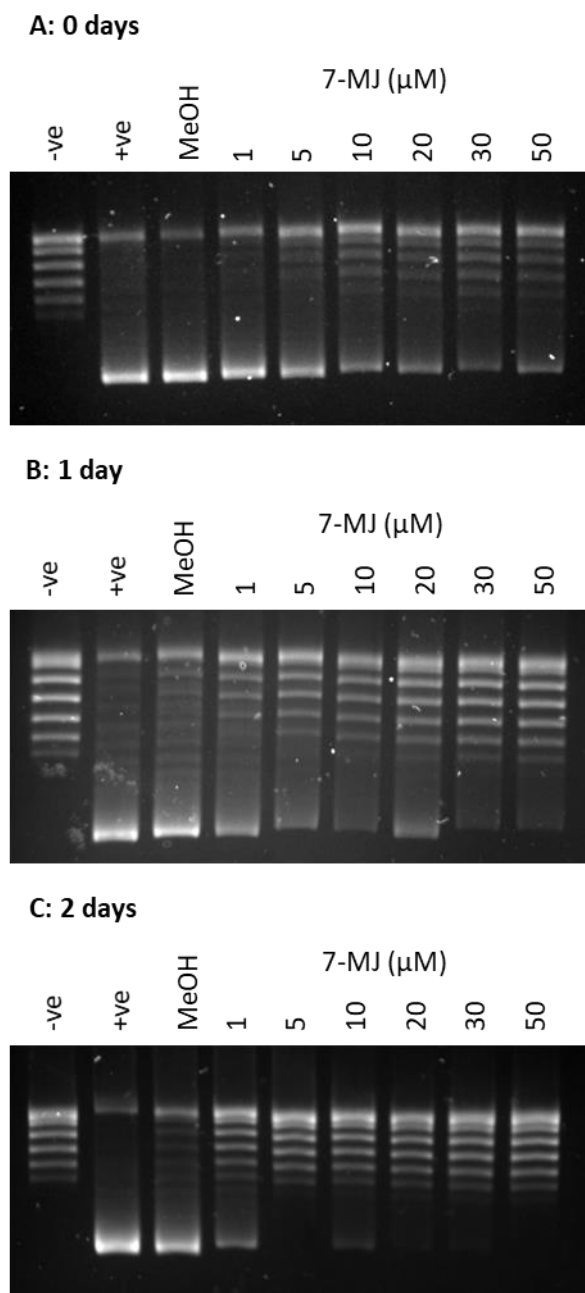


Figure 4.3.2: Three-day time course of the inhibition of Mtb DNA gyrase fusion protein supercoiling activity of 7-methyljuglone when dissolved in 100% methanol. A) freshly dissolved compound, B) compound after 1 day at room temperature, C) compound after 2 days at room temperature. Supercoiling assays were carried out with equivalent protein samples on three consecutive days at the same time of day. Enzyme concentration was chosen to be less than 100% supercoiling for better determination of the IC_{50} values.

Based on the literature it appeared that the naphthoquinones were promising inhibitors of DNA gyrase to explore further (Karkare *et al.*, 2013b). In this knowledge Dr S. Ekins (SE) of Collaborative Drug Discovery created a model of a proposed binding site of diospyrin to

determine the binding site and hence its mode of action. This model described a binding pocket in the GyrB NTD domain away from the ATPase site, as this domain was indicated previously to be involved in the mode of action of the diospyrin (Figure 4.3.3) (Karkare *et al.*, 2013b). From the model, multiple amino acid residues including R40, W47, H121, T189, N309, and T373 were hypothesised to be involved in the binding of diospyrin assuming the model created was correct. Based on these findings site-directed mutagenesis was performed on the modified pET20b(+) GyrBA plasmid to result in 7 new plasmids encoding mutants in the proposed binding region (R40A, R40Q, W47F, H121A, T189A, N309A, T373A). Expression and purification of 6 of these mutants was successful, yielding active fusion proteins. Unfortunately, the H121A mutant did not appear to express under the optimal fusion expression conditions, hence purification was not possible. However, it was decided not to actively test the model provided by SE as MJA was unable to synthesise diospyrin. Moreover, the 7-methyljuglone provided by MJA proved unstable and we were unable to identify an appropriate stable and active compound to test against the model. As we were unable to determine the true active compound at this time any compound tested could not be taken forwards as a clinical target and therefore further developments with these compounds have been stopped until a time when we can determine a stable and active compound. Although there are more stable naphthoquinones such as menadione these are reported to be only weak inhibitors of DNA gyrase and hence not ideal to test the model either (van der Kooy, 2007, Karkare *et al.*, 2013b).

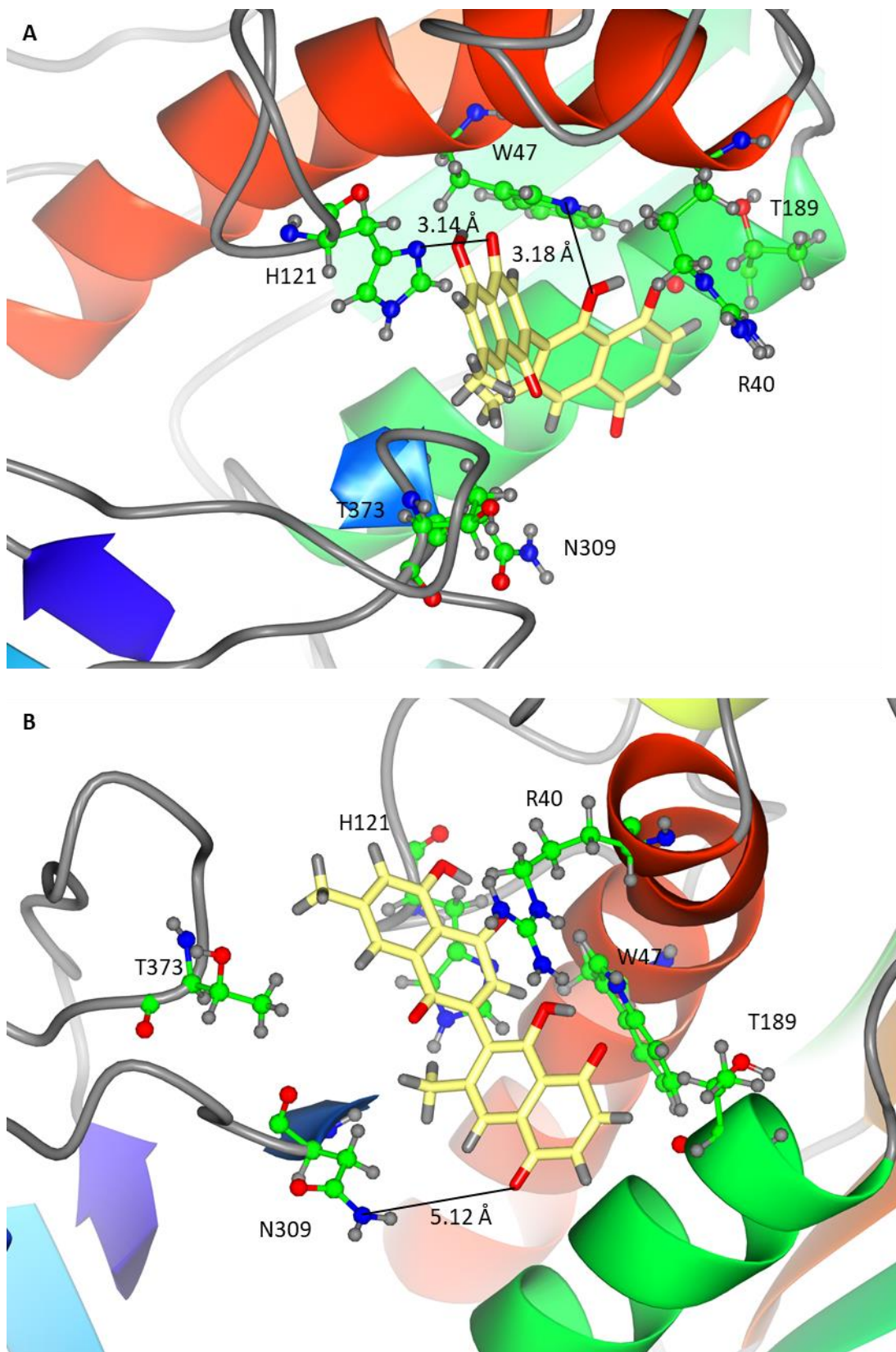
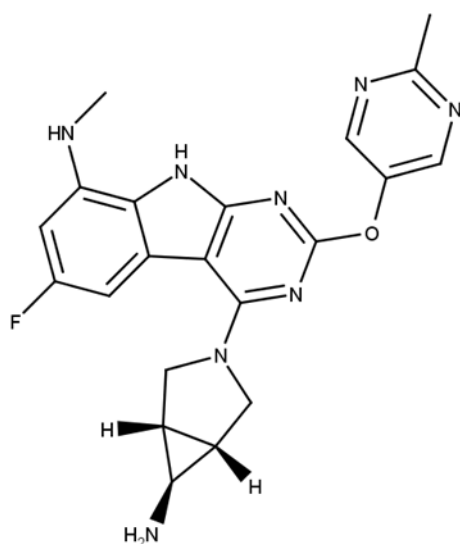


Figure 4.3.3: Two views of the model of diospyrin docked into the 3ZM7 crystal structure of the Mtb ATPase domain (Agrawal *et al.*, 2013) by Dr S. Ekins. Six amino acids of interest are shown with in specific interaction distances labelled. A) and B) show different orientations of the same structure.

4.4 Tricyclic GyrB ParE (TriBE) antibiotics from Redx AntiInfectives

The TriBE antibiotics are an optimisation of pyrroloprimidine antibiotics which were characterised as GyrB and ParE inhibitors in 2013 (Tari *et al.*, 2013a, Tari *et al.*, 2013b, Trzoss *et al.*, 2013). RedxAI followed up the initial work performed by Trius Therapeutic on these antibiotics through using a lead compound from the Trius series (Redx03863) (Bensen *et al.*, 2012), and performing further optimisations resulting in a new lead compound, Redx04739, for their mycobacterial compound series (Figure 4.1.1) (McGarry *et al.*, 2018). We determine here the bacterial growth inhibition, enzyme IC₅₀ values as well as determining the mechanism of action and searching for the binding pockets of both Redx03863 and Redx04739.

A: Redx03863



B: Redx04739

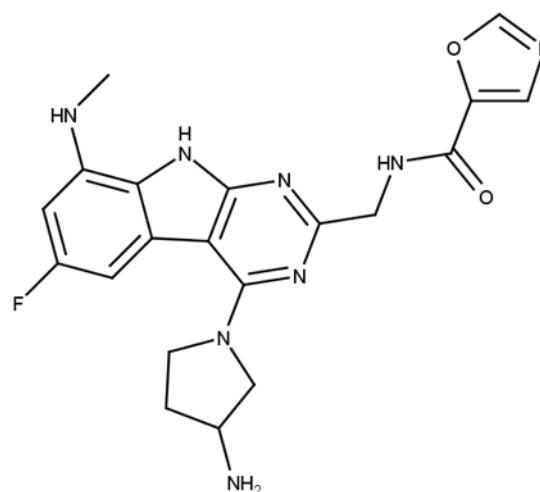


Figure 4.4.1: Chemical structure of Redx03863 which was optimised to give the lead compound of Redx04739

4.4.1 Growth Inhibition by Redx03863 and Redx04739

Initially we needed to confirm the effectiveness of these compounds against whole cells to compare their use as potential TB drugs, therefore broth MIC₁₀₀ testing was initially performed (see section 2.6.1). Additionally, it was important to determine if these compounds were broad spectrum or mycobacterial specific, hence these compounds were tested against a limited primary screen containing both Gram-positive and Gram-negative bacteria. The broth MIC₁₀₀ data demonstrated that the less potent lead antibiotic in the series (Redx04739) showed a high degree of selectivity towards the laboratory mycobacterial strain *M. smegmatis* ATCC19420 in comparison to the other bacteria tested (Table 4.4.1). In comparison the initial lead of Redx03863 showed broad spectrum activity against both the Gram-positive and Gram-

negative bacteria tested with superior activity compared to Redx04739 (Table 4.4.1). However, Redx04739 showed better selectivity against *M. smegmatis* ATCC19420 compared to Redx03863. Additional collaborative testing by the NIAID on behalf of RedxAI found that Redx04739 was highly potent against *M. tuberculosis* H37Ra and *M. tuberculosis* H37Rv under aerobic conditions (data not shown). This indicates that Redx04739 is an interesting compound to take forwards for further microbial and biochemical studies and to definitively determine the mode of action.

Table 4.4.1: MIC₁₀₀ data for the two novel RedxAI antibiotics Redx03863 and Redx04739 against a primary screen of bacteria containing both clinically-relevant Gram-negative and Gram-positive bacteria alongside the laboratory mycobacterium strain *M. smegmatis* ATCC19420. Data was taken at a minimum of 2 replicates with a maximum 2-fold difference between the two replicates.

Bacterial Strain	Redx03863 (µg/ml)	Redx04739 (µg/ml)
<i>Acinetobacter baumannii</i> NCTC13420	0.031	64
<i>Escherichia coli</i> ATCC25922	0.016	8
<i>Mycobacterium smegmatis</i> ATCC19420	0.016	0.25
<i>Pseudomonas aeruginosa</i> ATCC27853	4	32
<i>Staphylococcus aureus</i> ATCC29213	0.125	8

4.4.2 Inhibition of Mycobacterial Biofilms by Redx03863 and Redx04739

As it is possible for *M. tuberculosis* to form biofilms in clinically-relevant settings (Spinner *et al.*, 1996, Sendi and Brent, 2016) it was decided to investigate the effects of Redx03863 and Redx04739 against biofilms in a laboratory setting. The inhibition of biofilm growth assay was used to determine if compounds are effective in preventing growth, or killing bacteria within a biofilm grown reproducibly on Calgary biofilm pegs within the laboratory setting was initially carried out with the *E. coli* ATCC25922 strain (Harrison *et al.*, 2010) (see section 2.6.4). In this assay the compounds of interest were compared to the known biofilm inhibitor of moxifloxacin as well as novobiocin, a compound known to be inefficient against biofilms (Dr N Ooi, Pers. Comm.). It was found that in this assay both the compounds of interest had activity in preventing growth of a biofilm (bMIC – biofilm MIC) with Redx03863 as expected presenting with better activity than Redx04739. Unexpectedly Redx03863 performed as well, if not better than the positive control of moxifloxacin for this assay (Table 4.4.2). At the concentration range tested Redx04739 was unable to prevent the regrowth of a biofilm after

exposure to the compound (MBEC – minimum biofilm eradication concentration). On the other hand, Redx03863 was not only able to outperform Redx04739 in preventing regrowth of a biofilm, it also appeared to have improved activity compared to the moxifloxacin control used (Table 4.4.2).

Table 4.4.2: Inhibition of Biofilm formation against both *E. coli* ATCC25922 and *M. smegmatis* ATCC19420. Novobiocin is a known not to be an inhibitor of biofilms while moxifloxacin is a known positive biofilm inhibitor. Both Redx03863 and Redx04739 were trialled to determine their effectivity at both inhibiting biofilm growth (bMIC) and preventing regrowth (MBEC). Data was taken at a minimum of 2 replicates with a maximum 2-fold difference, where this was not possible the two alternative recorded values are shown and indicated with*.

	bMIC (µg/ml)		MBEC (µg/ml)	
	<i>E. coli</i>	<i>M. smegmatis</i>	<i>E. coli</i>	<i>M. smegmatis</i>
Redx03863	<0.125	>64	4	64/0.5*
Redx04739	16	>64	>64	16
Novobiocin (negative)	128	>1024	>1024	>1024
Moxifloxacin (positive)	<2	>1024	32	256/32*

Based on the growth rate of *M. smegmatis* it was necessary to increase the incubation times to allow a mature biofilm to grow. Consequently, the protocol for inhibition of biofilm growth and regrowth for *M. smegmatis* was optimised based on published data, to increase the biofilm growth and regrowth stages to 48 hours (from 24 hours) meanwhile the drug incubation stage before obtaining the bMIC was altered from 24 hours to 72 hours.

Unusually, the bMIC values found when using this protocol with *M. smegmatis* were high throughout testing even with moxifloxacin which is known to be an inhibitor of biofilm growth in *E. coli* ATCC25922 (Table 4.4.2). It was unclear if this was an artefact of the protocol being used (e.g. clumps of dead cells in the wells being observed) or if this was a true result. On the other hand, the MBEC value for regrowth after exposure to antibiotics showed clearly that Redx04739 had increased selectivity towards *M. smegmatis* ATCC19420 with an MBEC

value at least 4-fold lower than against *E. coli* ATCC25922 (Table 4.4.2). The value obtained for both moxifloxacin and Redx03863 is somewhat unclear as due to time constraints a third repeat was needed but could not be performed leaving an extensive range for the MBEC value (Table 4.4.2). Regardless, Redx03863 is likely to be similar if not better than moxifloxacin at effectively killing a biofilm from the preliminary data.

4.4.3 Time of kill for Redx03863

To determine if Redx03863 was causing cell death and the timeframe on which this was happening in the presence of Redx03863, a time of kill assay was employed to determine the difference in the growth kinetics of a culture in the presence and absence of Redx03863. This assay involved plating serial dilutions of duplicate cultures exposed to multiples of the MIC₁₀₀ of a compound and duplicate cultures not exposed to any treatment to compare the colony forming units and percentage of the surviving colonies at multiple timepoints to identify the time to kill the bacteria being tested. Unfortunately, due to the MIC₁₀₀ of Redx04739 against *E. coli* ATCC25922 being 8 µg/ml it was not possible to carry this experiment out with Redx04739 due to the concentration of DMSO within the growth media. Furthermore, because Redx04739 was not tested against *E. coli* ATCC25922 it was decided not to test it against *M. smegmatis* ATCC19420 as no direct comparison to *E. coli* was possible.

In the presence of Redx03863 it was determined that at 4x MIC₁₀₀ the percentage of colony forming units of *E. coli* was below 0.1% within 120 minutes of plating and 0.0001% (less than 30 colonies per culture compared to an excess of 10⁹ in the no drug control flasks) within 240 minutes. No colonies were found to be surviving after 24 hours (Figure 4.4.2). Overall, this suggests effective killing of *E. coli* ATCC25922 is occurring in the presence of Redx03863.

In contrast when the experiment was scaled for *M. smegmatis* no colonies were found to be surviving after 2 days in the presence of 16x MIC₁₀₀ Redx03863, with just two surviving colonies at 4x MIC₁₀₀. By 4 days no colonies were surviving in either culture. In general, the CFU count for both 4x and 16x MIC₁₀₀ had a similar percentage of the cultures containing no drugs, with there being less than 0.01% colonies surviving at 24 hours for both the 4x and 16x MIC₁₀₀ samples (Figure 4.4.3). Overall, this indicates that the drug is highly active against *M. smegmatis* grown in a laboratory setting, implying it would be suitable to take on to further studies, including animal models, depending on toxicity data not examined here.

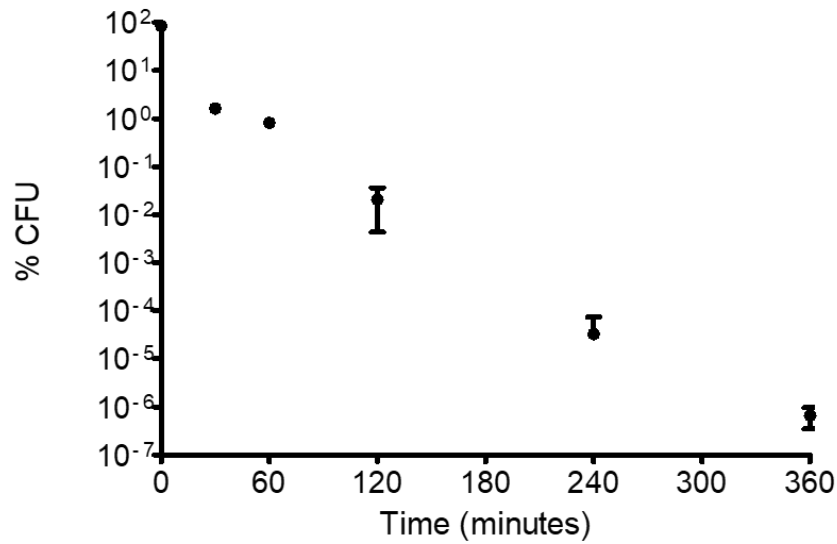


Figure 4.4.2: Percentage of colony forming units of *E. coli* ATCC25922 remaining when treated with 4x broth MIC₁₀₀ Redx03863 compared to untreated bacterium over 6 hours. Data recorded as two technical replicates, and representative of 2 experimental replicates. Error bar represent range of individual replicates.

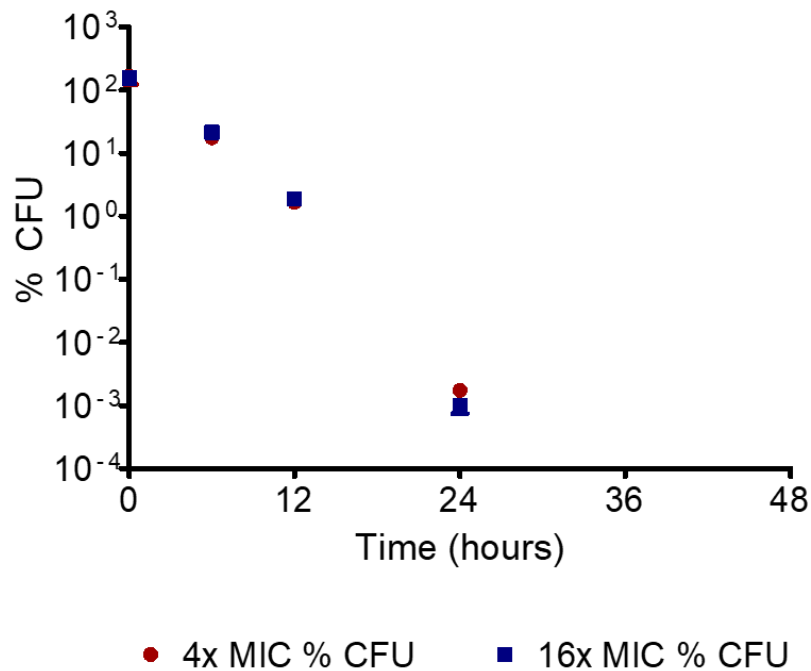


Figure 4.4.3: Percentage of colony forming units of *M. smegmatis* ATCC19420 remaining when treated with 4x or 16x broth MIC₁₀₀ Redx03863 compared to untreated bacterium over 2 days. No colonies were obtained at 2 days in the presence of 16x MIC₁₀₀ and from one of the 4x MIC₁₀₀ cultures and hence data could not be plotted. Data recorded as two technical replicates, and representative of duplicate experiments. Error bar represent range of individual replicates.

4.4.4 Inhibition of DNA Gyrase by Redx03863 and Redx04739

As the TriBE compound series was previously optimised from known DNA gyrase and topo IV inhibitors with some crystallographic data on other compounds in the same series, it was assumed that the molecular target would also be the type II topoisomerases for these two compounds (Bensen *et al.*, 2012, Tari *et al.*, 2013a). To confirm this, initially the compounds were tested against DNA gyrase from *M. tuberculosis* as they showed superior specificity for whole cell activity against mycobacterial species *M. smegmatis* (see section 2.5.1). It was observed that Redx03863 and Redx04739 inhibited the supercoiling reaction of Mtb DNA gyrase with nanomolar affinity (Figure 4.4.4) implying that, as suggested, the target of these novel drugs was DNA gyrase in *M. tuberculosis*. The compounds were additionally tested against the *E. coli* type II topoisomerase enzymes which they were found to inhibit, confirming a dual targeting mechanism within *E. coli*. Surprisingly the inhibition of *E. coli* DNA gyrase was found to be at least equal to that of Mtb DNA gyrase (Figure 4.4.5). The inhibition of topo IV was found to not be as potent but was still an inhibitor at a sub-micromolar level (Figure 4.4.5).

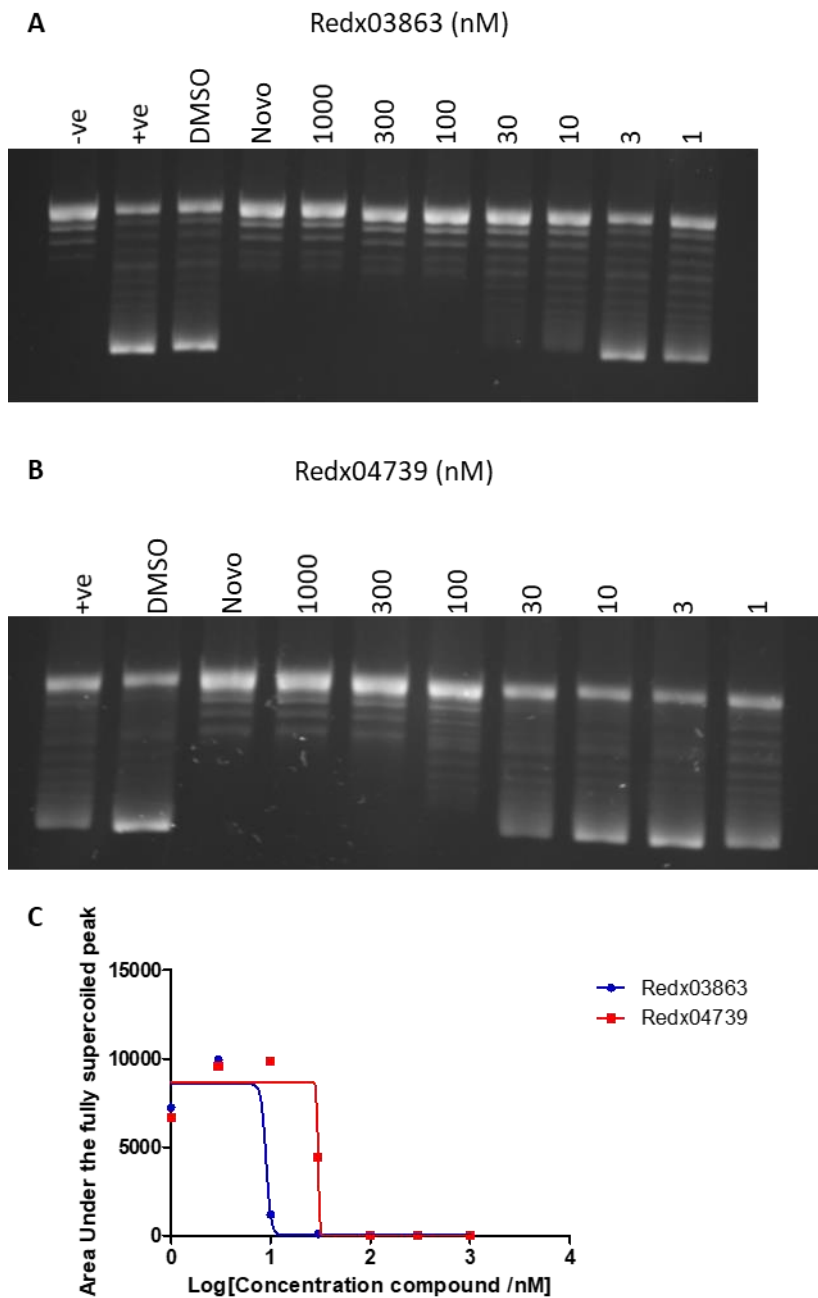
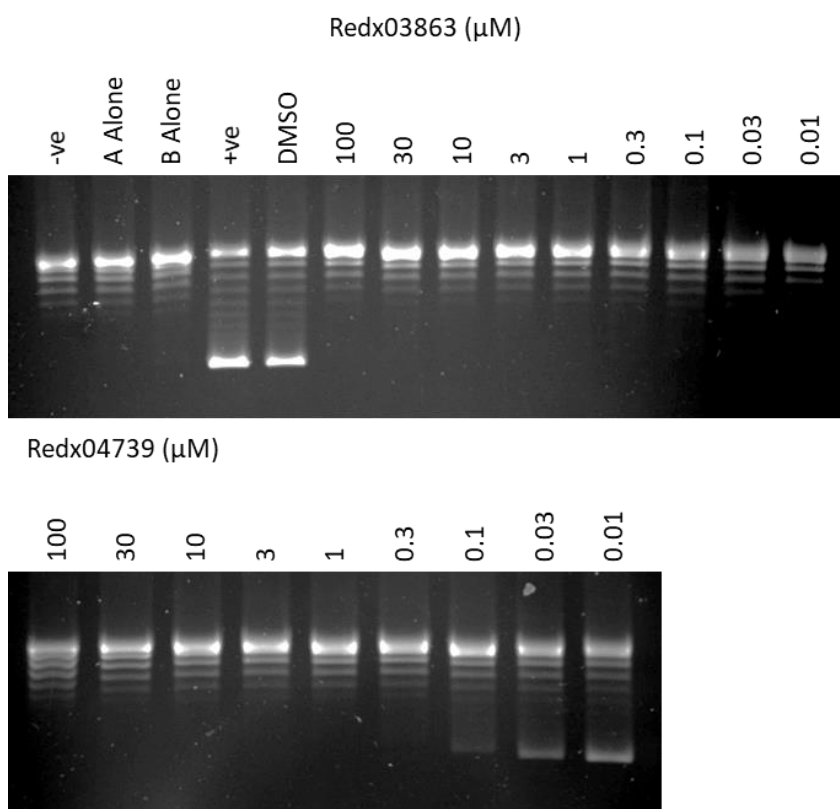


Figure 4.4.4: Inhibition of supercoiling assay carried out with 74 nM of each gyrase subunit against A) Redx03863 and B) Redx04739 (1000 nM – 1 nM in 1% DMSO). Controls included -ve (no enzyme), +ve (enzyme no compound), DMSO (enzyme in 1% DMSO), 10 μ M novobiocin in 1% DMSO. Apparent IC_{50} values of 10 nM for Redx03863 and 30 nM for Redx04739. Enzyme concentration was chosen to be less than 100% supercoiling for better determination of the IC_{50} values. C) A plot of the intensity of the supercoiled peak as determined with ImageJ plotted by GraphPadPrism to determine IC_{50} values - 9.025 nM Redx03863 and 30.01 nM Redx04739.

A: Inhibition of *E. coli* DNA gyrase



B: Inhibition of *E. coli* topoIV

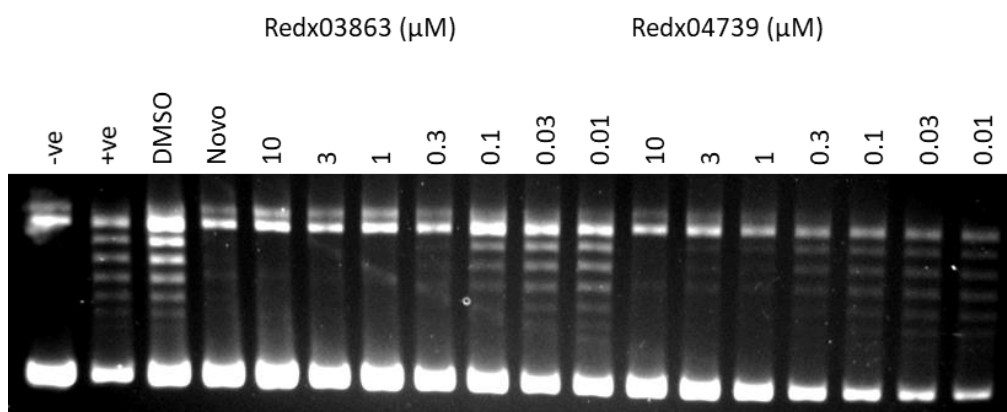


Figure 4.4.5: Inhibition of the *E. coli* Type II topoisomerases by Redx03863 and Redx04739. A) Inhibition of DNA gyrase supercoiling assay. Compound concentrations 100-0.01 μM . Assay run with 10 nM GyrA and 9 nM GyrB. IC_{50} of <10 nM Redx03863 and 10-30 nM Redx04739. A alone and B alone controls only contained one subunits in the absence of the other subunit. B) Inhibition of topoisomerase IV relaxation assay. Compound concentrations 10-0.01 μM . Assay run with 16 nM of ParC in an excess of ParE. IC_{50} 100-300 nM Redx03863 and 300-1000 nM Redx04739. -ve controls contained the DNA substrate in the absence of protein, positive controls contained both DNA substrate and protein in the absence of DMSO. DMSO controls contained the same solvent content as the reactions in the presence of DNA substrate and proteins. Enzyme concentration was chosen to be less than 100% supercoiling for better determination of the IC_{50} values.

4.4.5 Redx03863 and Redx04739 competitively inhibit the ATPase reaction of DNA gyrase

The binding pocket of the original TriBE compounds is within the ATPase domain (Tari *et al.*, 2013a), therefore experiments were carried out to determine if the mechanism of action involved inhibiting the ATPase reaction. Initially, the ATP-independent relaxation assay was conducted to determine if either of the compounds showed efficacy against this reaction. It was shown that there was little or no inhibition of the relaxation reaction at 300 nM (Figure 4.4.6), whereas full inhibition of supercoiling was observed at <100 nM for both compounds. It is found that at the high concentrations of DNA gyrase required to observe ATP-independent relaxation a cleavage band is also observed likely due to contamination in the enzyme purification as previously discussed in Chapter 3. Overall, because the compounds do not inhibit the ATP-independent relaxation assay it is suggested that their mode of action involves inhibition of the ATPase reaction.

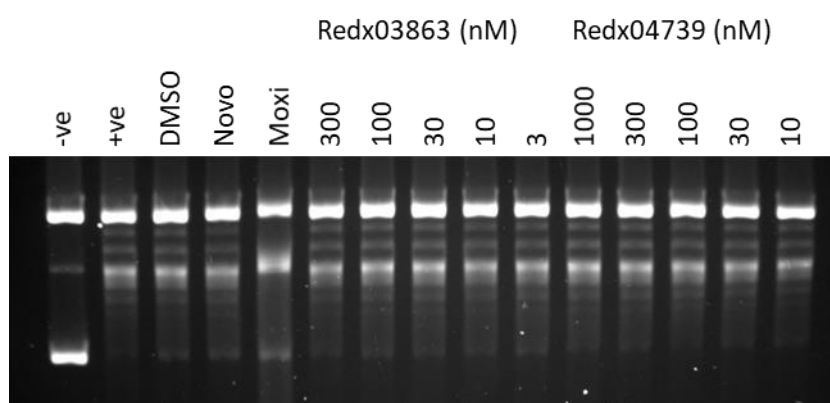


Figure 4.4.6: Inhibition of ATP-independent relaxation assay carried out with 0.5 μ M of each gyrase subunit. Controls included negative (no enzyme), positive (enzyme no compound), DMSO (enzyme in 1% DMSO), 10 μ M novobiocin in 1% DMSO and 50 μ M moxifloxacin in 1% DMSO. Concentration range of Redx03863 300 nM to 3 nM, Redx04739 1000 nM to 10 nM all in 1% DMSO. IC_{50} could not be determined in the concentration range tested. The linear cleavage band is because of the large amounts of enzyme and increased times required for this assay, and do not affect the results of the assay.

To further determine if the compounds were inhibiting the ATPase reaction competitively, two independent experiments were carried out. The first of these was an ATP-competition supercoiling reaction where ATP was titrated into the reaction under constant enzyme and compound concentrations. In this assay a control with the enzyme in 1% DMSO was used to demonstrate that no significant variation in the level of supercoiling occurred as the concentration of ATP was increased. Likewise, the negative drug control Simocyclinone D8

was used to demonstrate that inhibitors of DNA gyrase that are known to have a mode of action other than competitively inhibiting the ATPase reaction cannot be out competed by ATP (Flatman *et al.*, 2005). Novobiocin, a known competitive ATP inhibitor, showed a significant increase in supercoiling activity as the concentration of ATP was increased. Likewise, the level of supercoiling appears to increase with increased levels of ATP in the presence of either Redx03863 or Redx04739 (Figure 4.4.7). Overall, this suggests that the mechanism of action of these compounds is to competitively inhibit the ATPase reaction.

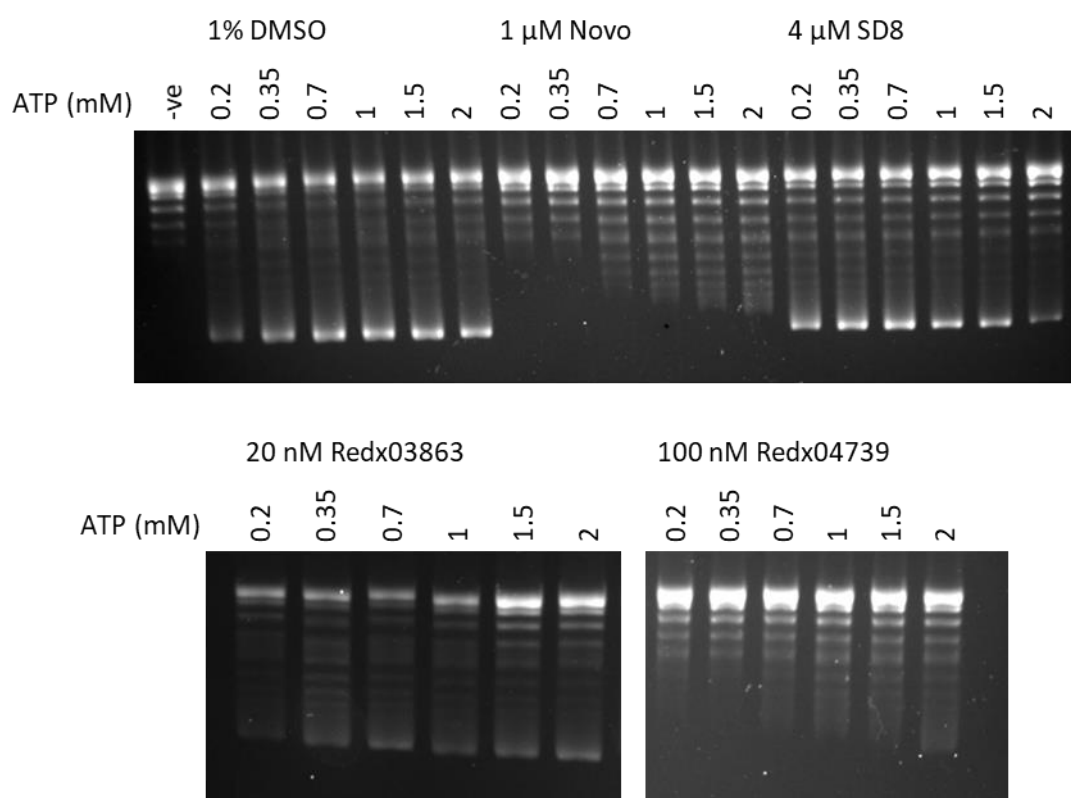


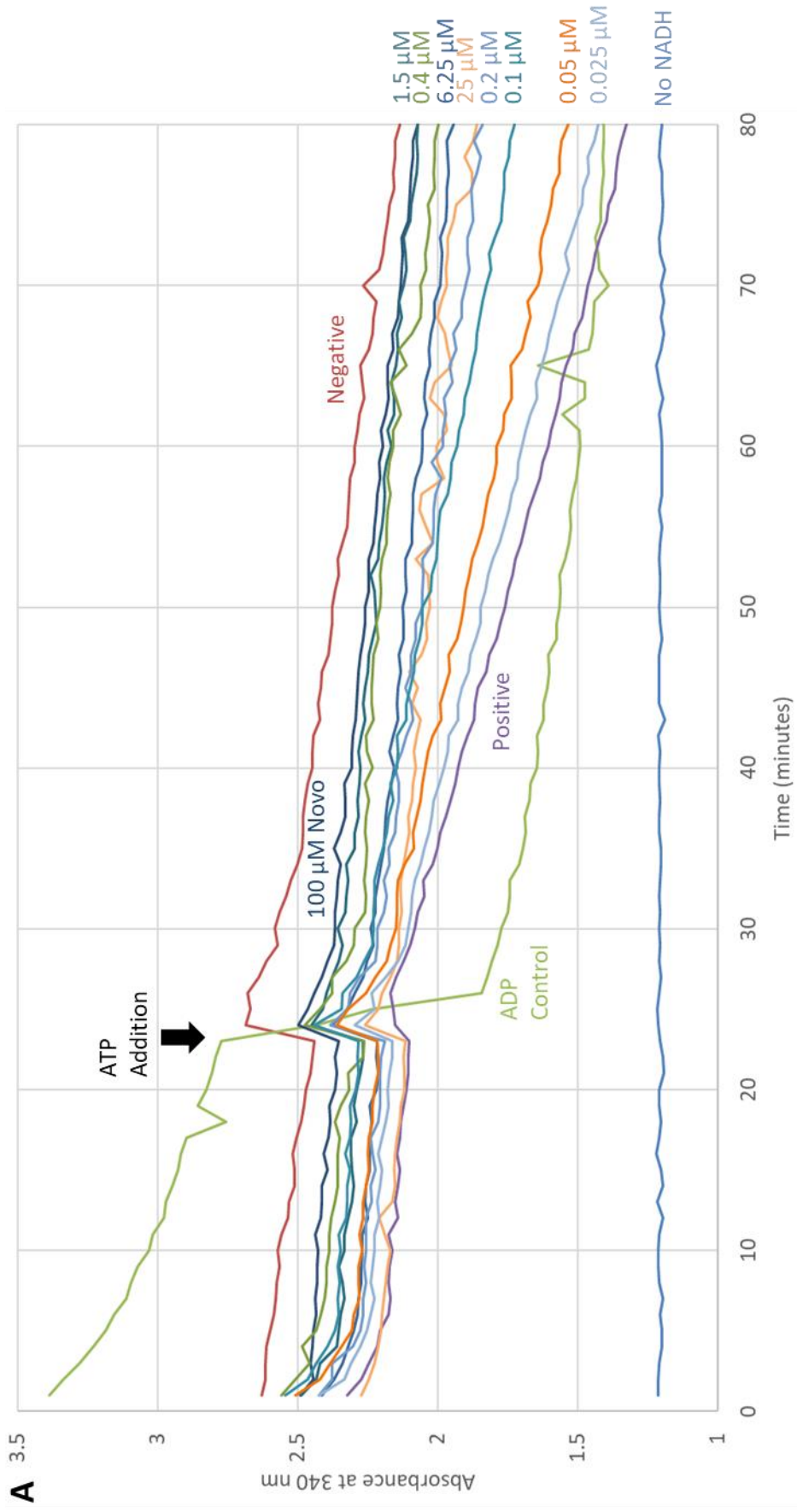
Figure 4.4.7: ATP competition assay. Assay run with 150 nM of *M. tuberculosis* DNA gyrase. All reactions were carried out in final DMSO concentration of 1% (v/v). The ATP concentration range of 0.2 mM to 2 mM was used. 1% DMSO, Novobiocin (Novo) at 1 μM, Simocyclinone D8 (SD8) at 4 μM, Redx03863 at 20 nM and Redx04739 at 100 nM were all assayed. -ve control contained all assay components in the absence of protein at 2 mM ATP.

The second experiment to confirm that the Redx compounds are competitive ATPase inhibitors was a titration of the compounds into the ATPase-linked assay with the Mtb fusion construct, which was determined to be optimal for use in this reaction (Chapter 3.1). As the limit of detection for the linked ATPase assay is determined by the concentration of the enzyme used in the assay, true values of the IC_{50} could not be determined as 200 nM enzyme

was assayed. It was possible however, to observe that these compounds are very tight binders resulting in apparent IC₅₀ values comparable to that of novobiocin (Table 4.4.3, Figure 4.4.8). The raw data shown for Redx03863 supports the calculated rates indicating that greater oxidation of NADH in the coupled reaction occurs in the assays with less than 0.2 μM Redx03863, whereas there is little to no difference in the assays carried out with between 0.4 – 62.5 μM Redx03863 or 100 μM novobiocin (Figure 4.4.8A). Similar raw data was observed when the assay was run with Redx04739 (data not shown). Overall, it can be clearly determined from these biochemical experiments that both Redx03863 and Redx04739 are competitive ATPase inhibitors like novobiocin.

Table 4.4.3: IC₅₀ values for novobiocin, Redx03863 and Redx04739 against the novobiocin sensitive rate in the ATPase-linked assay run with 200 nM GyrBA stimulated with 1 ng linear pBR322. IC₅₀ values generated by GraphPad Prism with non-linear regression (log(inhibitor) vs response – variable slope (four parameters)). Error given is the standard error in the IC₅₀ value as obtained from GraphPad Prism.

Compound	Apparent ATPase IC ₅₀ (nM)
Novobiocin	208±41
Redx03863	166±67
Redx04739	211±60



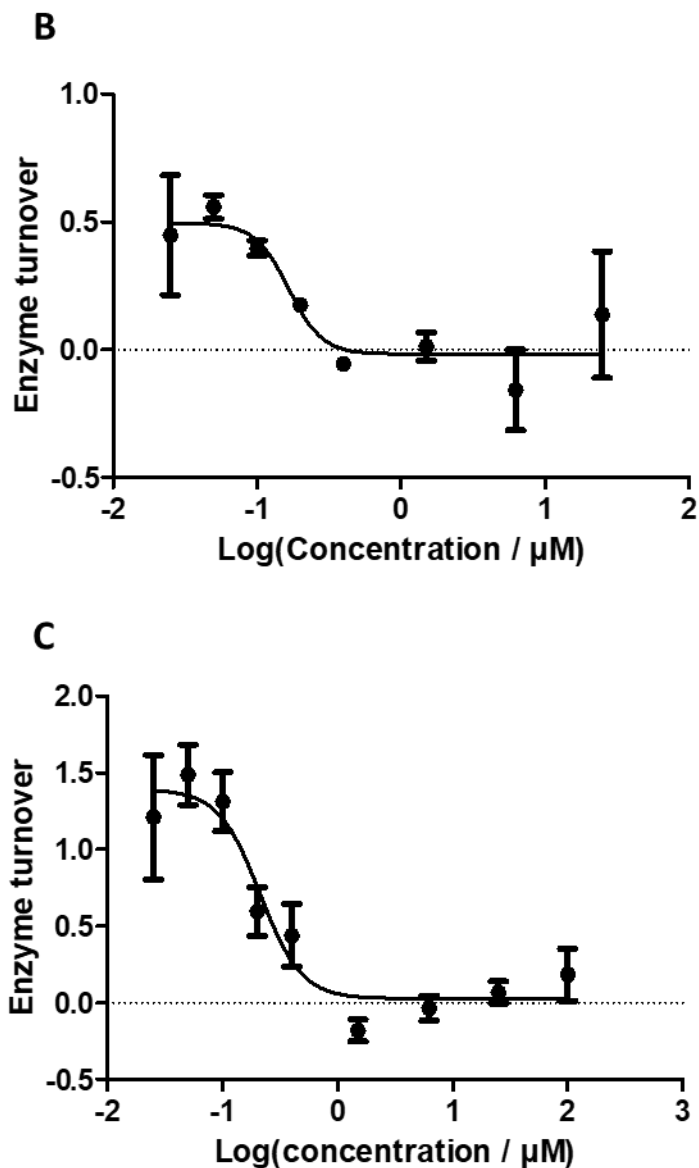


Figure 4.4.8: A) Plot of the absorbance at 340 nm over time in the presence of varying amounts of Redx03863 within an ATPase PK/LDH linked assay. B, C) Plots of the rate of the novobiocin-sensitive ATP turnover per GyrB subunit per second were plotted against the base 10 logarithm of the concentration in μM to determine the IC_{50} value. B) Redx03863, C) Redx04739. Graphs are representative of multiple replicates, with all data points being carried out in duplicate. GyrBA protein at concentration of 200 nM with a substrate of 1 ng of linear pBR322 was used to obtain all data sets. Non-linear regression (log(inhibitor) vs response – variable slope (four parameters)) was performed to obtain IC_{50} values of 166 ± 41 nM Redx03863 and 211 ± 60 nM Redx04739.

4.4.6 Surface plasmon resonance analysis of the binding kinetics of Redx03863 and Redx04739

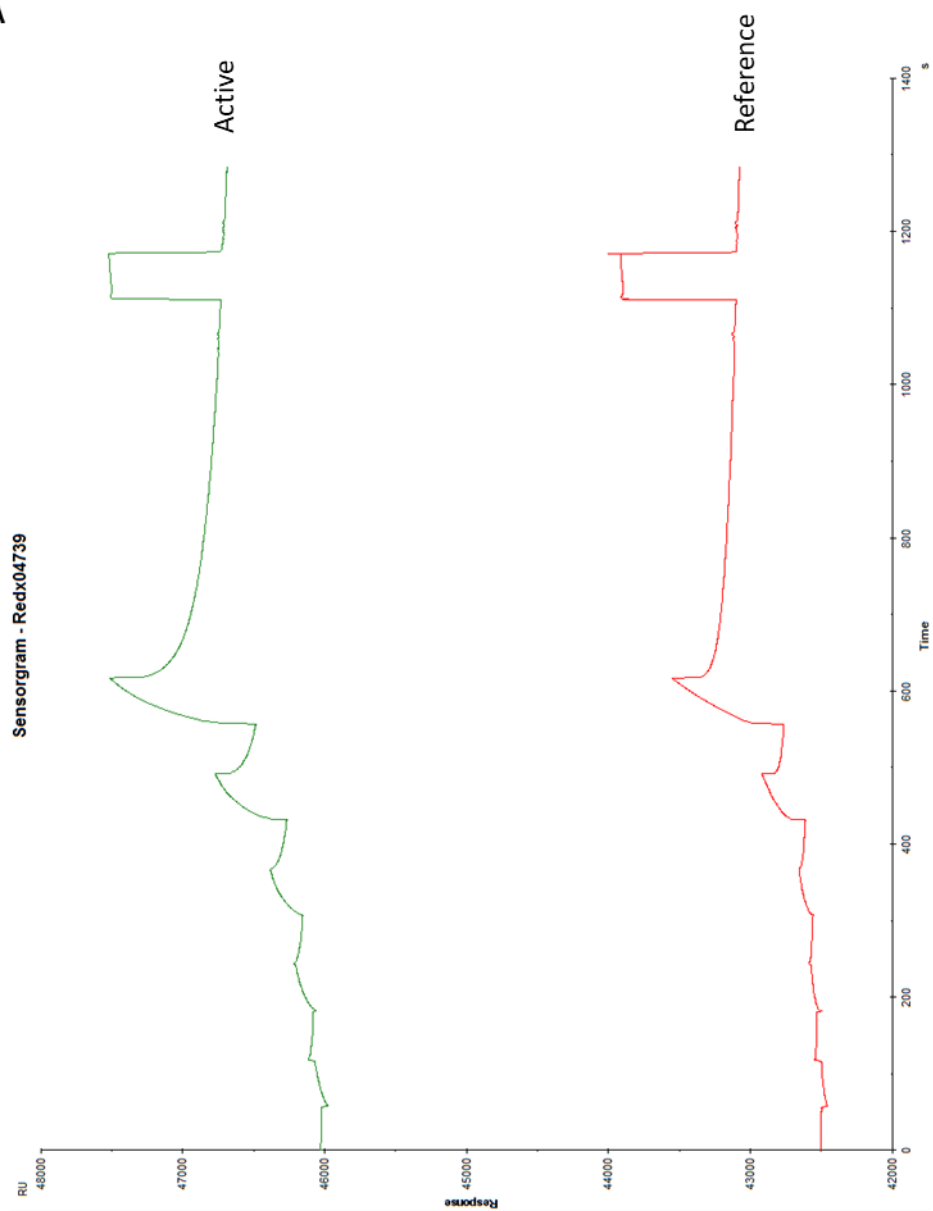
As we had determined that both Redx03863 and Redx04739 to be competitive inhibitors of the ATPase domain, hence it implied that both of these compounds bound at the ATP-binding

domain of GyrB. We hence sought to investigate the binding interactions between these compounds and the sub-ATPase domain of GyrB. For these studies we choose the technique of surface plasmon resonance (SPR), which can measure the interactions of immobilised proteins with a binding partner such as an inhibitor, cofactor or binding partner without the need for labels; as reviewed by Nguyen *et al.* (2015). Typically, SPR experiments work better with larger binding partners, however advancements in the technique have led to smaller molecules <300 Da being detected (Rich *et al.*, 2002). Therefore, with this knowledge and as previous groups had had good experiences with compounds of similar sizes on our Biocore T200 machine, we chose to trial our compounds which have molecular masses of 420 and 424. As we knew that both compounds were effective against Mtb and *E. coli* DNA gyrase we investigated the binding interactions of the ATPase sub-domains from both species. The proteins were successfully bound to CM5 sensor chips and subsequently single cycle kinetics were performed.

The protocol used for single cycle kinetics involved measuring the binding response in response to increasing concentrations of both compounds with intermediate intervals where the compounds were washed off the chips. It was however found that Redx03863 bound with very high affinity that saturated the chip and did not allow for washing and reusing of the chips and hence it was not possible to measure any kinetic data for Redx03863. This however, did strongly suggest that we were looking at the correct binding domain for Redx03863.

On the other hand, it was found that Redx04739 bound with lesser affinity to the chips and could be partially removed and hence some kinetic data could be obtained. However, there was significant background binding to the control chip meaning that the readings obtained were very low. Regardless, a K_d value of $12.11 \pm 0.92 \mu\text{M}$ was obtained for the *E. coli* sub-ATPase domain (Figure 4.4.9). Unfortunately, although it was clear that there was binding to the Mtb chip, it was not possible to generate a K_d value due to unusually high binding to the reference cell resulting in very high error values (Figure 4.4.10). Overall, although the data obtained for the SPR experiments were not ideal it did demonstrate that the GyrB sub-ATPase domain was likely to be the binding domain of both Redx03863 and Redx04739, suggesting this domain to be the correct domain to carry out any mutagenesis studies and crystallographic studies on.

A



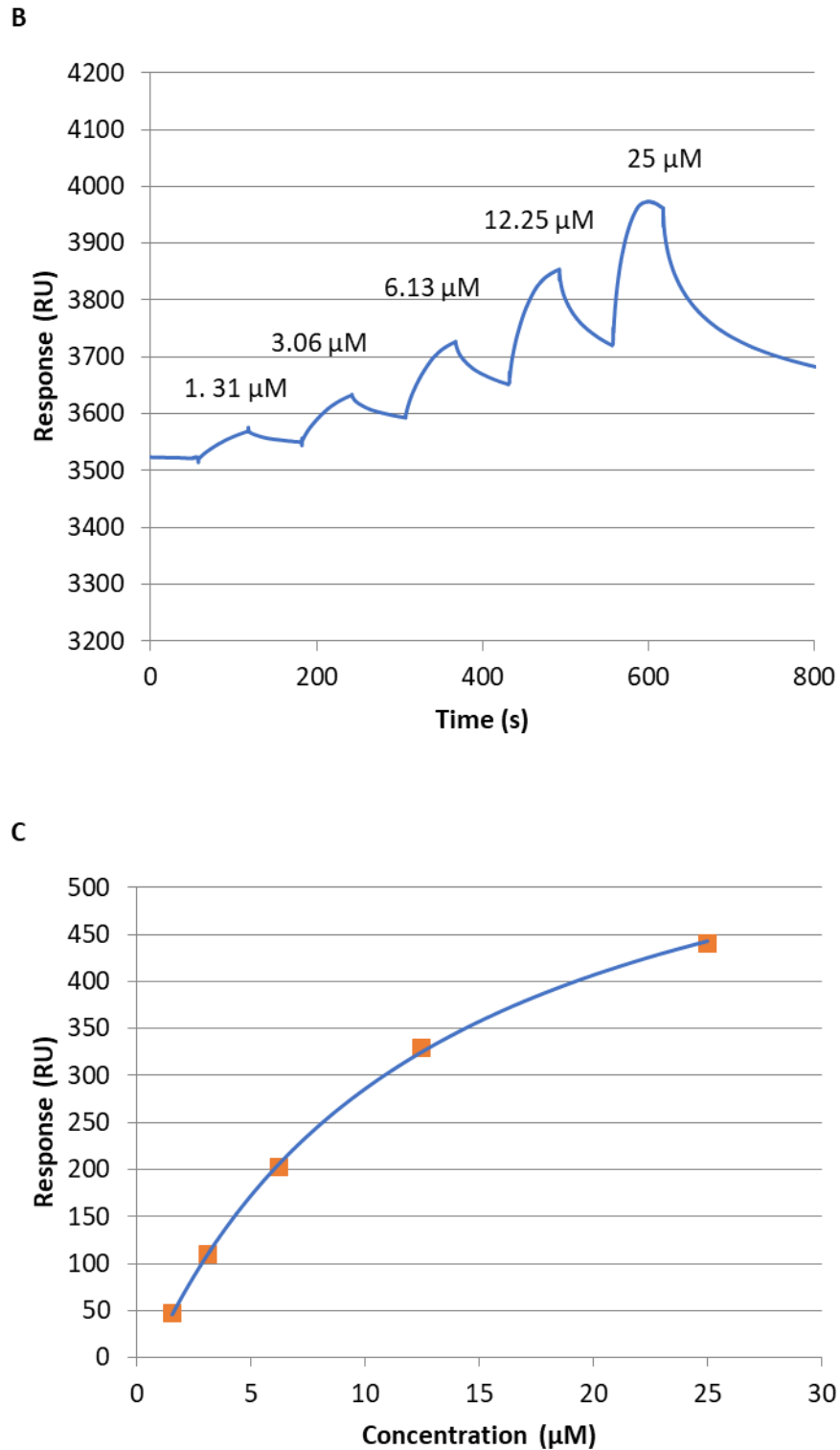
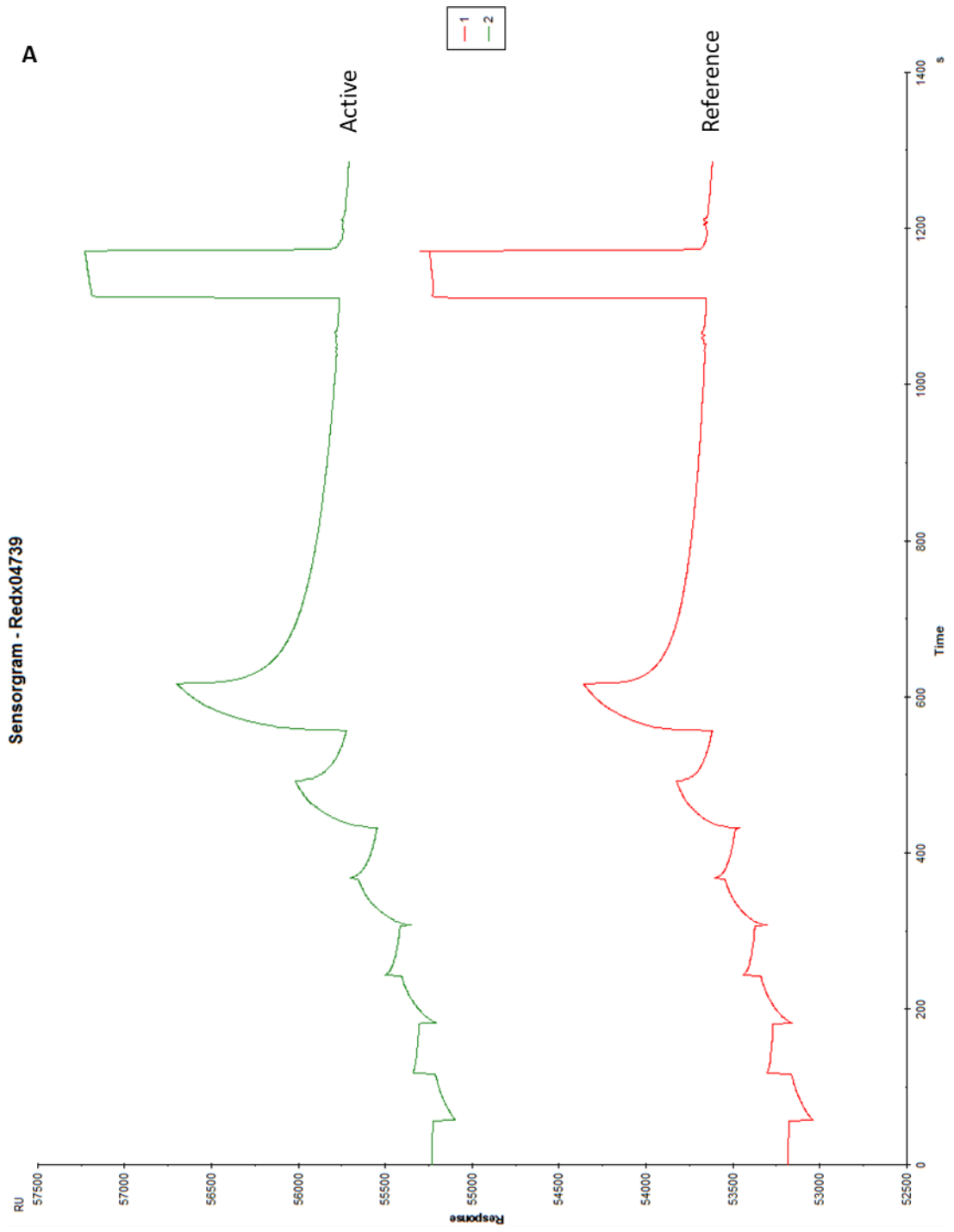


Figure 4.4.9: Single cycle kinetics SPR results from the CM5 chip bound to the ATPase sub-domain from *E. coli*. A) Sensorgram obtained from the Biocore shows that binding appears in a similar pattern to the reference (no protein bound chip) as to the active chip. B) Binding of Redx04739 is increased on increasing concentration of compound, but the baseline is not reached between concentrations. C) Plot of concentration of Redex04739 against the response. The blue line is a best fit curve to fit the data, indicating an estimated $K_d = 12.11 \pm 0.92 \mu\text{M}$.



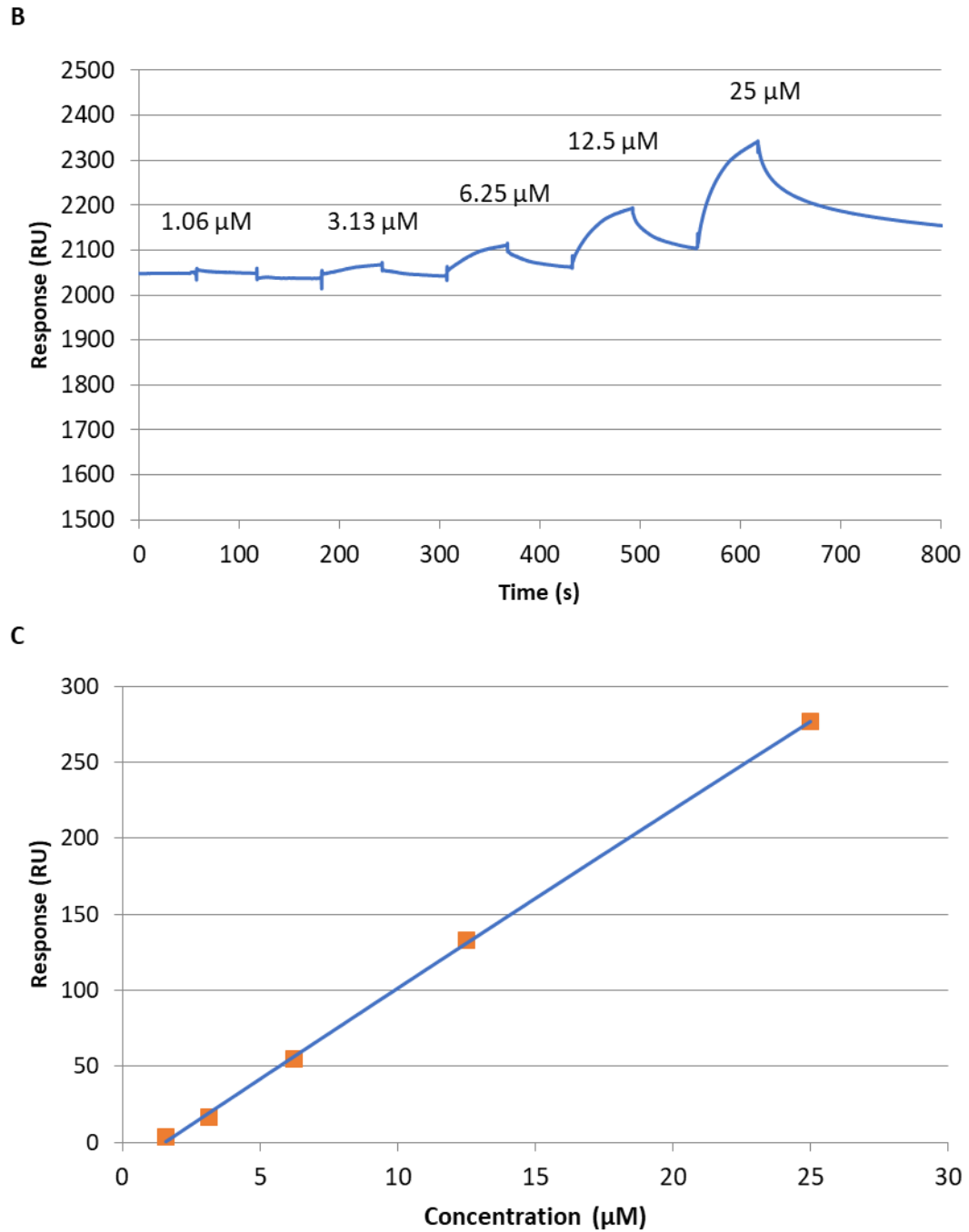


Figure 4.4.10: Single cycle kinetics SPR results from the CM5 chip bound to the Mtb ATPase sub-domain. A) Sensorgram obtained from the Biocore shows that binding appears in a similar pattern to the reference (no protein bound chip) as to the active chip. B) Binding of Redx04739 is increased on increasing concentration of compound, but the baseline is not reached between concentrations. C) Plot of concentration of Redex04739 against the response. The blue line is a best fit line of the data. No K_d value could be obtained.

4.4.7 Bacterial mutant generation by Redx03863 and Redx04739 by serial passage

To further identify the binding location of both Redx03863 and Redx04739, bacterial mutants were raised against Redx03863 and Redx04739 in *E. coli* ATCC25922 and *M. smegmatis* ATCC1940 by two independent methods. The first of these methods was the serial passage method whereby bacteria were passaged from cultures continually exposed to a quarter of the MIC₁₀₀ value until a resistant strain was isolated. This method is based on continual exposure to low levels of the compounds leading to accumulating mutations which confer partial resistance to the compound of interest and hence leading to increases in the MIC₁₀₀ values.

The established method used by RedxAI for serial passages with *E. coli* ATCC25922 was adapted for *M. smegmatis* ATCC19420 to increase the time between passages from 24 hours to between 2-3 days. In the assays carried out we attempted to obtain a strain with a MIC₁₀₀ value of ≥ 64 $\mu\text{g/ml}$. If this was not achieved in 50 passages but a significantly increased MIC₁₀₀ was obtained it was also considered to be successful and the resulting strain would be analysed for mutants.

It was found that the MIC₁₀₀ value of *E. coli* ATCC25922 increased steadily over the first 20 passages from an initial value of 0.016 $\mu\text{g/ml}$ to 1 $\mu\text{g/ml}$ (a 64-fold increase in MIC₁₀₀). The maximal MIC₁₀₀ value was found to be 4 $\mu\text{g/ml}$ at passage 49. The final strain *E. coli* 03863 SP(50) has a MIC₁₀₀ value of 2 $\mu\text{g/ml}$ resulting in an increase of 128-fold in the MIC₁₀₀ value from the initial starting value of 0.016 $\mu\text{g/ml}$. An additional intermediate strain *E. coli* 03863 SP(25) was taken after the 25th passage with an MIC₁₀₀ of 0.5 $\mu\text{g/ml}$, which was 32 times more resistant to Redx03863 than the wild type strain (Figure 4.4.11).

On the other hand, it was found that after 33 passages no meaningful change in the starting MIC₁₀₀ value was obtained in the *M. smegmatis* ATCC19420 starting strain, with many of the passages recording MIC₁₀₀ values below that of the starting culture (Figure 4.4.11). As no obvious increase was observed the technique was terminated with no further characterisation being performed.

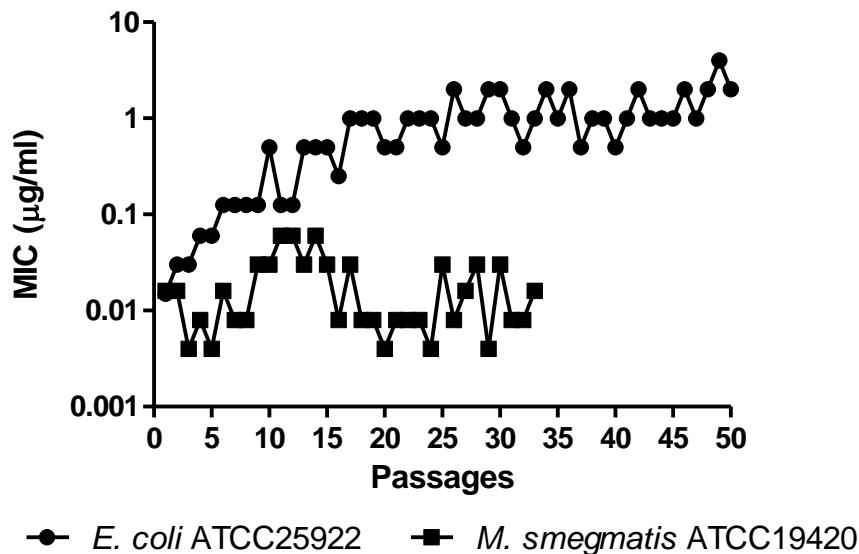


Figure 4.4.11: Plot showing the change in MIC₁₀₀ values (µg/ml) for *E. coli* ATCC25922 (closed circle) and *M. smegmatis* ATCC1940 (closed square) when raised against Redx03863. *E. coli* ATCC25922 was passaged every 24 hours, *M. smegmatis* ATCC19420 was passaged every 2-3 days. Passages were performed with a 1/100 dilution the ¼ MIC₁₀₀ well.

A strain of *E. coli* ATCC25922 with an MIC₁₀₀ value greater than 128 µg/ml could be raised in as little as 7 days against Redx04739. It was not possible to raise a strain that had resistance greater than 128 µg/ml due to the concentration of DMSO in the media being limiting. Regardless of this, the *E. coli* 04739 SP(7) strain had a 32-fold increase from the starting MIC₁₀₀ value (Figure 4.4.12).

Like *E. coli* ATCC25922 it was found that a resistant strain of *M. smegmatis* ATCC19420 raised against Redx04739 was generated at a much faster rate than Redx03863. After 29 passages an MIC₁₀₀ value of 128 µg/ml was achieved resulting in a 256-fold increase in the starting MIC₁₀₀ value. Like the other strains generated, the final strain *M. smegmatis* 04739 SP(29) was further analysed to determine differences to the wild-type strain (Figure 4.4.12). Interestingly, in terms of fold-change in the MIC₁₀₀ value for Redx04739 against *M. smegmatis* ATCC14920 and Redx03863 against *E. coli* ATCC25922 increased at very similar rates, with Redx04739 against *E. coli* ATCC25922 generated resistance marginally faster.

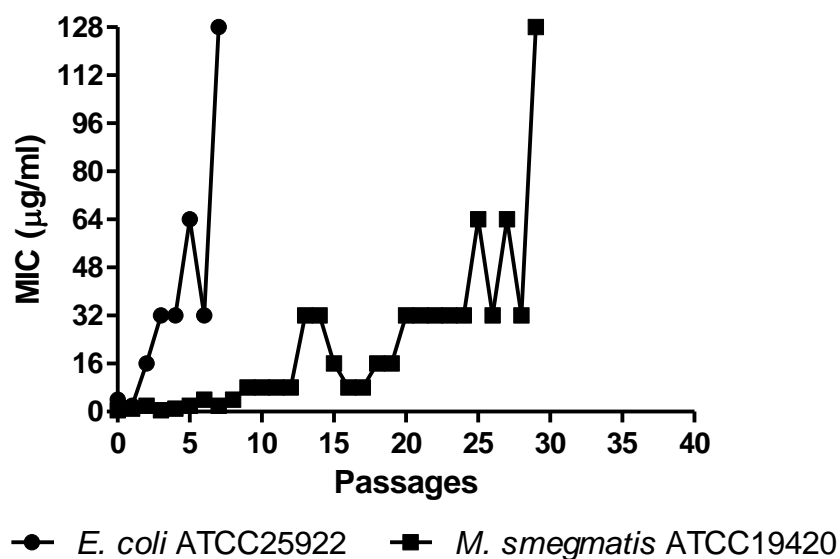


Figure 4.4.12: Plot showing the change in MIC₁₀₀ values (µg/ml) for *E. coli* ATCC25922 (closed circle) and *M. smegmatis* ATCC1940 (closed square) when raised against Redx04739. *E. coli* ATCC25922 was passaged every 24 hours, *M. smegmatis* ATCC19420 was passaged every 2-3 days. Passages were performed with a 1/100 dilution of the ¼ MIC₁₀₀ well. It was not possible to measure MIC₁₀₀ above 128 µg/ml.

Cross-resistance testing to other known DNA gyrase inhibitors was performed to determine if resistance mutants to the novel compounds induced resistance to known antibiotics. This information is important in determining if these compounds have common mechanisms of resistance which is important when considering their potential in the clinic. The *M. smegmatis* 04739 SP(29) strain was found to be a very sickly strain and after 4 days on a Middlebrook 7H11 plate supplemented with glycerol and OADC supplement only a single colony was found to have grown. Unfortunately, this precluded cross-resistance MIC₁₀₀ analysis from being carried out. It was however possible to gain this information about the three *E. coli* strains generated. Both of the strains raised against Redx03863 showed significant cross resistance to Redx04739, likewise the *E. coli* 04739 SP(7) showed 8-fold cross resistance to Redx03863 (Table 4.4.4). As the MIC₁₀₀ for novobiocin was found to be 64 µg/ml for novobiocin it was not possible to determine to what degree there was cross resistance to it for the *E. coli* 03863 SP(25) and *E. coli* 03863 SP(50) strains, but both of these strains gave rise to partially increased resistance to novobiocin (Table 4.4.4).

Table 4.4.4: Cross-resistance MIC₁₀₀ values for the *E. coli* mutant strains raised against Redx03863 and Redx04739 through use of the serial passage method. Compound dilutions above 64 µg/ml were not tested.

	Redx03863 (µg/ml)	Redx04739 (µg/ml)	Moxifloxacin (µg/ml)	Novobiocin (µg/ml)
<i>Escherichia coli</i> ATCC25922				
(WT)	0.016	8	0.016	64
<i>Escherichia coli</i> 03863 SP(25)	0.5	64	0.125	>64
<i>Escherichia coli</i> 03863 SP(50)	2	>64	0.5	>64
<i>Escherichia coli</i> 04739 SP(7)	0.125	>64	0.016	64

In addition to cross resistance MIC₁₀₀ testing, the mutants and wild type strains were further characterised through extraction of genomic DNA, PCR amplification and sequencing of the known type II topoisomerase genes to locate resistance mutants in the known targets. There were initial problems with obtaining the genomic DNA from the *M. smegmatis* strains due to problems with breaking open the mycolic acid cell wall. After including a mechanical step to break open the cell wall by vigorously vortexing the bacterial suspension with glass beads, high yields of genomic DNA suitable for PCR were obtained.

In the *E. coli* strains two mutations were seen within the GyrB gene (Table 4.4.5; Figure 4.4.13). The first of these was the F182Y mutation which corresponds to the Y185 position in the Mtb protein, meanwhile the second was that of T175N, which aligns with V179 in the Mtb protein, hence no further action was taken as the hydrophobic properties of valine are quite different to that of a threonine. As *E. coli* also contains topo IV and it has been confirmed that the compounds act via a dual targeting mechanism in *E. coli*, the topo IV genes were additionally sequenced. Two-point mutations were observed in the ATPase containing ParE subunit, however as both were found in a region that did not show good homology to the Mtb GyrB subunit no further action was taken. One single point mutation was found in each of the GyrA and ParC subunits although as the compounds are known to be competitive ATPase inhibitors no further action was taken at this time (Table 4.4.5).

Table 4.4.5: Single point mutants identified from sequencing of the DNA gyrase genes (*gyrA* and *gyrB*) and topo IV (*parC* and *parE*) genes from the *E. coli* serial passage mutants. Sequence alignment using Clustal Omega was performed to locate the comparable mutations in the wildtype Mtb gyrase proteins.

Strain	Protein	Mutation	Mutation in Mtb
<i>E. coli</i> 03863 SP(25)	GyrA	V501M	I478
	ParE	S338F	Non-conserved
<i>E. coli</i> 03863 SP(50)	GyrB	T175N	V179
		F182Y	Y185
	ParE	V84G	Non-conserved
<i>E. coli</i> 04739 SP(7)	ParC	W143L	F152
	ParE	S338F	Non-conserved

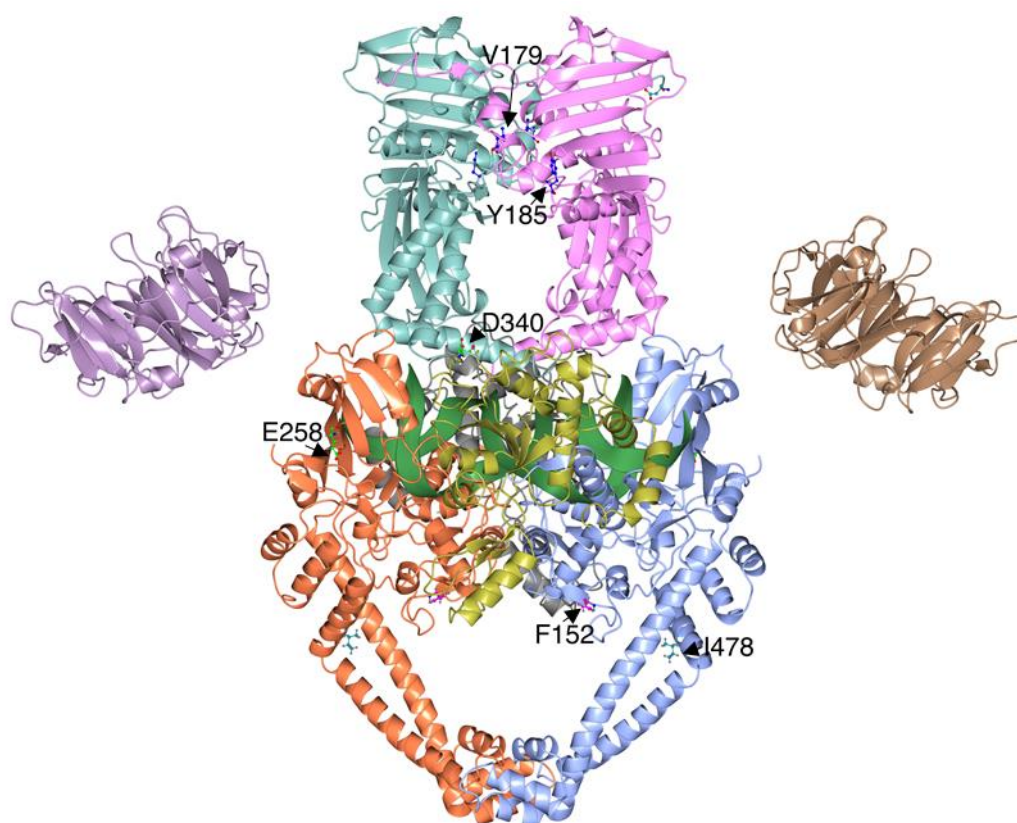


Figure 4.4.13: Visualisation of the mutant locations of the mutants generated by serial passage on a model made from 3 structures of *M. tuberculosis* DNA gyrase. The GyrB N-terminal domain is coloured pink and cyan; the GyrB CTD is coloured gold and grey; the GyrA NTD is coloured blue and coral; the GyrA CTD is coloured purple and brown. Mutants from the *E. coli* 03863 SP(25) strain are cyan (I478); from the *E. coli* 03863 SP(50) stain are blue (V179, Y185); from the *E. coli* 04739 SP(7) strain are pink (F152); from the *M. smegmatis* 04739 SP(29) strain are green (E258; D340). The mutants that did not demonstrate good conservation in the region on the Mtb DNA gyrase proteins are not shown. Model reproduced from with adaptation (Nagaraja *et al.*, 2017).

Two mutations were found in GyrA and one in GyrB of the *M. smegmatis* 04739 SP(29) strain. Like the *E. coli* strains none of these were found to be in the ATPase domain hence no further action was taken (Table 4.4.6; Figure 4.4.13).

Table 4.4.6: Single point mutants identified from sequencing the DNA gyrase genes *gyrA* and *gyrB* isolated from the *M. smegmatis* serial passage mutant *M. smegmatis* 04739 SP(29). Sequence alignment using Clustal Omega was performed to locate the comparable mutations in the wildtype Mtb proteins.

Protein	Mutation	Mutation in Mtb
GyrB	D340E	D340E
GyrA	E259K	E258K
	S839L	Non-conserved

4.4.8 Bacterial mutant generation by Redx03863 and Redx04739 by frequency of resistance

The second method by which bacterial mutants were obtained by was that of the frequency of resistance experiment - a plate-based method of mutant generation whereby wild type bacteria were exposed to concentrations of the compound of interest at multiples of their agar-MIC₁₀₀ values. As this method is agar-plate based we first conducted experimentation to generate the agar-MIC₁₀₀ values as these are often found to differ from their broth counterparts. An agar MIC₁₀₀ value of ≤ 16 $\mu\text{g/ml}$ is required to enable the frequency of resistance experiment to be viable at 4xMIC₁₀₀ due to the amount of compound the experiment required and the DMSO concentrations in the reaction. Unfortunately, this precluded Redx04739 being used in this experiment against *E. coli* ATCC25922 (Table 4.4.7).

Table 4.4.7: Agar MIC₁₀₀ values recorded against *E. coli* ATCC25922 and *M. smegmatis* ATCC19420 for Redx03863, Redx04739 and novobiocin. Values taken as a minimum of two data repeats with two technical replicates. The agar MIC₁₀₀ of novobiocin against *E. coli* ATCC25922 was not tested. It was not possible to test values above 64 $\mu\text{g/ml}$ in this method. Values marked with * indicates values previously made by an employee of Redx AntiInfectives.

Bacterial Strain	Redx03863	Redx04739	Novobiocin
<i>E. coli</i> ATCC25922	0.125*	>64	-
<i>M. smegmatis</i> ATCC19420	0.002	0.5	32*

It was found that no mutants were obtained when *E. coli* ATCC25922 was plated onto 4x MIC₁₀₀ Redx03863 leading to a very low frequency of resistance value despite increasing the

concentration of the inoculum used. The consequence of this was a decrease in the FoR value from $<2.25 \times 10^{-8}$ to $<2.94 \times 10^{-11}$ (Table 4.4.8). To try and obtain mutants the experiment was therefore repeated at 2x MIC₁₀₀, where a single mutant colony was obtained over two experimental repeats (Table 4.4.8). This mutant strain (*E. coli* 2x03863 FoR) was confirmed to be a true mutant through testing of the broth MIC₁₀₀ which was found to be 32 µg/ml, a 2096-fold increase in the MIC₁₀₀ value (Table 4.4.9). It was determined that *E. coli* 2x03863 FoR exhibited cross resistance with Redx04739 but interestingly increased sensitivity to novobiocin, indicating differences in the resistance mechanisms between these compounds (Table 4.4.9). When the type II topoisomerase genes were sequenced for this mutant strain only one mutation (S338F) was observed in the ParE gene which is not within the ATPase domain, hence at this time no further experimentation on this mutant was performed.

In contrast with the *E. coli* experiments, a high number of colony forming units were observed on 4x agar-MIC₁₀₀ plates when using this method with *M. smegmatis* ATCC19420 resulting in unusually high frequency of resistance values (Table 4.4.8). To confirm if this was an artefact of the assay when working with *M. smegmatis* ATCC19420, we carried out the assay with novobiocin which resulted in comparable results.

Table 4.4.8: Frequency of Resistance values. Measurements made at 2x and 4x agar MIC₁₀₀ of Redx03863 against *E. coli* ATCC25922 and at 4x agar MIC₁₀₀ of Redx03863, Redx04739 and Novobiocin against *M. smegmatis* ATCC19420. Control plates without compounds were measured at 1/3 days (*E. coli*/*M. smegmatis*), compound containing plates were counted at 2/5 days (*E. coli*/*M. smegmatis*). < indicates no resistant colonies were obtained.

	<i>E. coli</i> ATCC25922	<i>M. smegmatis</i> ATCC19420		
	Redx03863	Redx03863	Redx04739	Novobiocin
2x MIC ₁₀₀	$<1.65 \times 10^{-9}$ 8.20×10^{-10}			
4x MIC ₁₀₀	$<3.94 \times 10^{-11}$ $<2.25 \times 10^{-8}$	4.52×10^{-5} 5.31×10^{-5}	6.82×10^{-4} 5.81×10^{-4}	2.89×10^{-5} 2.95×10^{-5}

Table 4.4.9: Cross-resistance MIC₁₀₀ values for mutants raised via frequency of resistance experiments. *M. smegmatis* mutants raised against Redx03863 at 4x agar MIC₁₀₀ and *E. coli* mutants raised against Redx03863 at 2x agar MIC₁₀₀. A concentration range of drugs of 0.125-64 µg/ml was tested.

	Redx03863 (µg/ml)	Redx04739 (µg/ml)	Moxifloxacin (µg/ml)	Novobiocin (µg/ml)	Isoniazid (µg/ml)
<i>Mycobacterium smegmatis</i>					
ATCC19420 (WT)	0.016	0.5	0.125	2	32
<i>Mycobacterium smegmatis</i>					
4x03863 FoR 1a	0.25	4	<0.125	4	32
<i>Mycobacterium smegmatis</i>					
4x03863 FoR 1b	0.25	4	<0.125	64	32
<i>Mycobacterium smegmatis</i>					
4x03863 FoR 2a	0.125	4	<0.125	8	16
<i>Mycobacterium smegmatis</i>					
4x03863 FoR 2b	0.25	2	<0.125	4	32
<i>Escherichia coli</i>					
ATCC25922 (WT)	0.016	8	0.016	64	-
<i>Escherichia coli</i>					
2x03863 FoR	32	>64	0.016	0.5	-

When looking into a sub-selection of the mutants raised against Redx04739 it was not possible to confirm resistance using broth MIC₁₀₀ testing. On the other hand, the mutant strains raised against Redx03863 (*M. smegmatis* 4x03863 1a, 1b, 2a, 2b) all demonstrated at least 8-fold resistance in broth MIC₁₀₀ testing (Table 4.4.9). These four strains like the other mutants raised also exhibited cross resistance to Redx04739 with some indication for cross resistance to novobiocin, especially in *M. smegmatis* 4x03863 1b where a 32-fold increase was observed. The results observed indicate that there may be increased sensitivity to moxifloxacin as the MIC₁₀₀ value is decreased. However, the extent of this is unclear as testing was not carried out at a standard concentration range (64 – 0.125 µg/ml) preventing a true MIC₁₀₀ value of moxifloxacin from being obtained in this assay, and hence it is not possible to determine if a true decrease in the MIC₁₀₀ was observed in the *M. smegmatis* 4x03863 FoR strains (Table 4.4.9).

Interestingly, sequencing of the DNA gyrase genes from the *M. smegmatis* 4x03863 FoR 1a,1b,2a,2b strains revealed an unexpectedly high number of mutations – 5 in GyrA and 13 in GyrB (Table 4.4.10). The only one of these that was found in all four of the strains but not the wild type was the D340 mutant in GyrB and was also found in the *M. smegmatis* 04739 SP(29) strain. Most interestingly in three of these strains a point mutation of T167 to alanine was obtained which is located within the GyrB NTD. Furthermore, in the *M. smegmatis* 4x03863 FoR 2a strain there were K159R and K202R mutations and the *M. smegmatis* 4x03863 1b strain had a mutation at G83S, all of which are the GyrB NTD (Table 4.4.10; Figure 4.4.14). As there is a high degree of homology between the GyrB N terminal domains of the Mtb and Msm proteins it was decided to test these four positions to determine if they generated resistance to either of the compounds in the ATP-dependent supercoiling reaction of DNA gyrase.

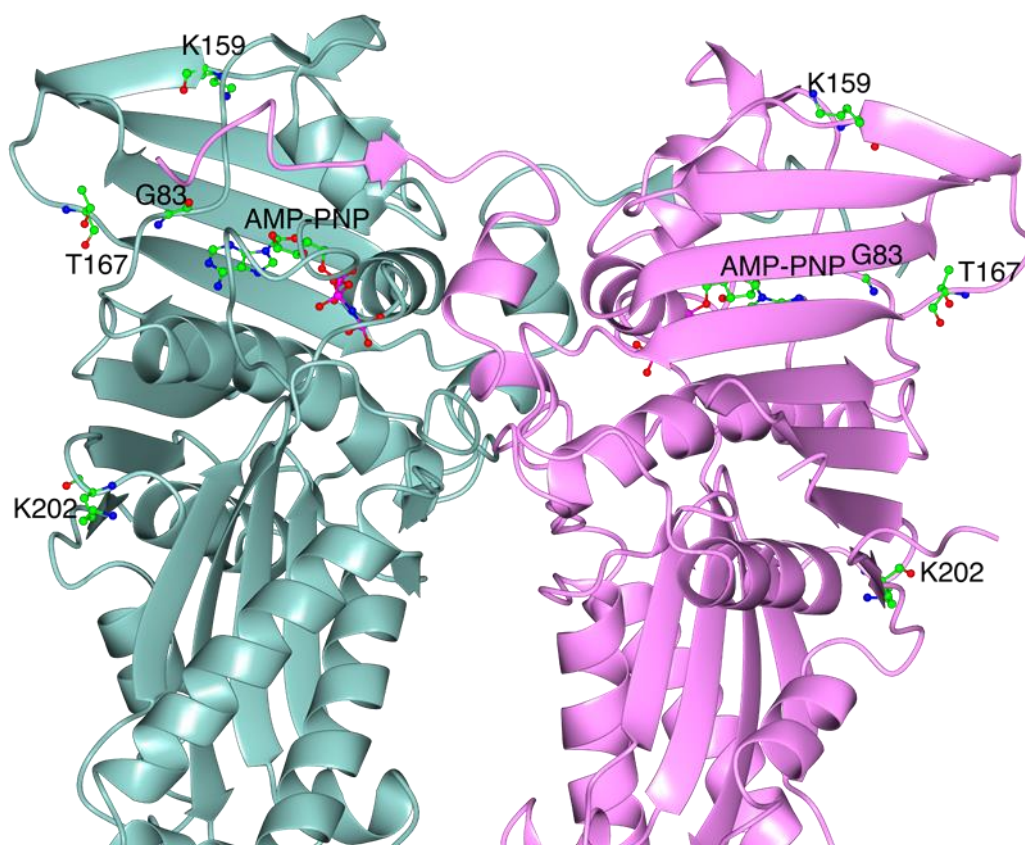


Figure 4.4.14: Locations of the mutations located in the GyrB NTD raised and identified by frequency of resistance mutagenesis. Residues shown on the known *M. tuberculosis* ATPase domain structure 3ZKB, indicating the AMP-PNP binding site as shown.

Table 4.4.10: Single point mutants identified from sequencing the DNA gyrase genes *gyrA* and *gyrB* isolated from the *M. smegmatis* frequency of resistance mutants raised against Redx03863. Sequence alignment using Clustal Omega was performed to locate the comparable mutations in the wildtype Mtb proteins

Strain	Protein	Mutation	Residue in Mtb
<i>M. smegmatis</i> 4x03863 FoR 1a	GyrB	T167A	T167
		D340E	D340
		E489K	E489
		D655N	D655
		D657K	D657
<i>M. smegmatis</i> 4x03863 FoR 1b	GyrA	F603D	F602
		L624P	L623
	GyrB	G83S	G83
		D340E	D340
<i>M. smegmatis</i> 4x03863 FoR 2a	GyrA	E259K	E258
		GyrB	K159R
	GyrB	T167A	T167
		K202R	K202
		D340E	D340
<i>M. smegmatis</i> 4x03863 FoR 2b	GyrA	A385D	A384
		L624P	L623
	GyrB	T167A	T167
		D340E	D340

These four mutants (G83S, K159R, T167A, K202R) were successfully obtained via SDM in Mtb GyrB and subsequent protein expression and purification was successful. Confusingly the G83S mutant did not appear to show any significant activity in supercoiling (Figure 4.4.15). This may be explained as although there is a very high homology between the Msm and Mtb proteins, it is possible that this position may be essential in the Mtb enzyme and not in the Msm protein. It is also plausible that the very low levels of supercoiling seen here is significant enough for survival of the bacteria.

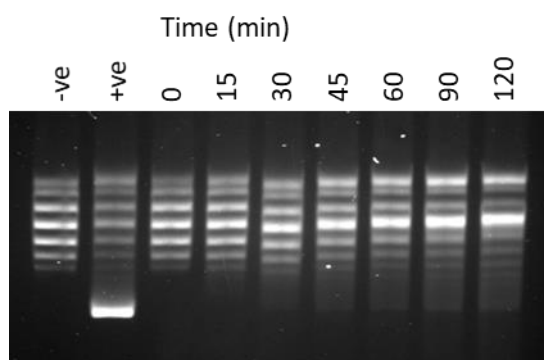


Figure 4.4.15: Time course of supercoiling of GyrB^{G83S} at an enzyme concentration of 0.158 μ M, at timepoints of 0,15,30,45,60,90,120 minutes. 0.147 μ M GyrA used throughout. WT +ve control at 0.147 μ M was made at 30 minutes and -ve no enzyme control at 120 minutes. The emergence of a linear cleavage band is as a result of longer incubation times and does not affect the results of this assay.

The other three mutants were active and did not appear to alter the supercoiling activity of the enzyme. The supercoiling activity of the K159R, T167A and K202R mutants was tested against novobiocin, Redx03863 and Redx04769 to determine if any of them were involved in the mechanism of action of the compounds. None of these mutants resulted in resistance to novobiocin which is unsurprising as the binding site is already known and none of these mutants have previously been implicated in the mechanism of resistance (Figure 4.4.16). Additionally, only the *M. smegmatis* 4x03863 FoR 1b strain had significantly increased resistance to novobiocin and none of these mutants were isolated from that strain (Table 4.4.10). Unfortunately, none of the mutants showed resistance to either Redx03863 (Figure 4.4.17) or Redx04739 (Figure 4.4.18) either. This may again be an artefact of the different species used, or because multiple mutants were required to work in synergy to get an effect. It is also possible that these compounds are mutagenic resulting in multiple single point mutations throughout the genome and the mutations are not involved in the mechanism of mutagenesis which is more likely to come from mutations in efflux pumps. This explanation seems somewhat likely as in particular K202 and K159 are unlikely to both be involved in the binding site due to the distance between the residues.

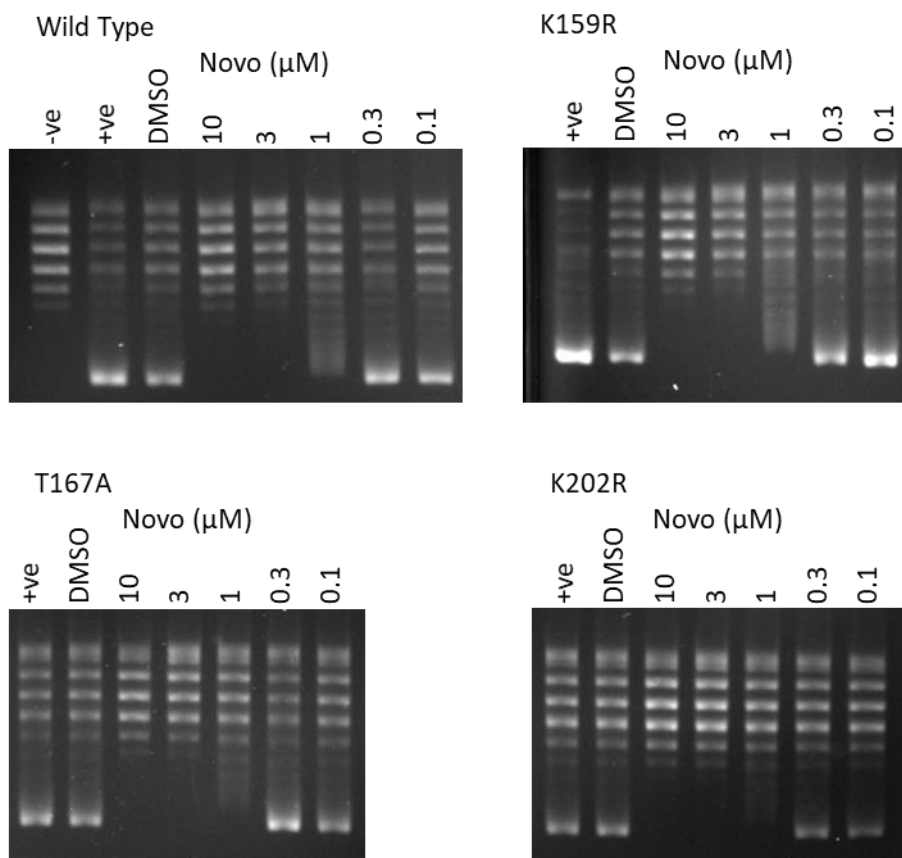


Figure 4.4.16: Supercoiling assay using GyrB wild type, K159R, T167A and K202R at a final enzyme concentration of 150 nM with 150 nM GyrA. -ve control contained DNA substrate in the absence of enzymes, DMSO control contained 1% DMSO in the absence of compounds; Novobiocin titration 10-0.1 μM assayed in 1% DMSO.

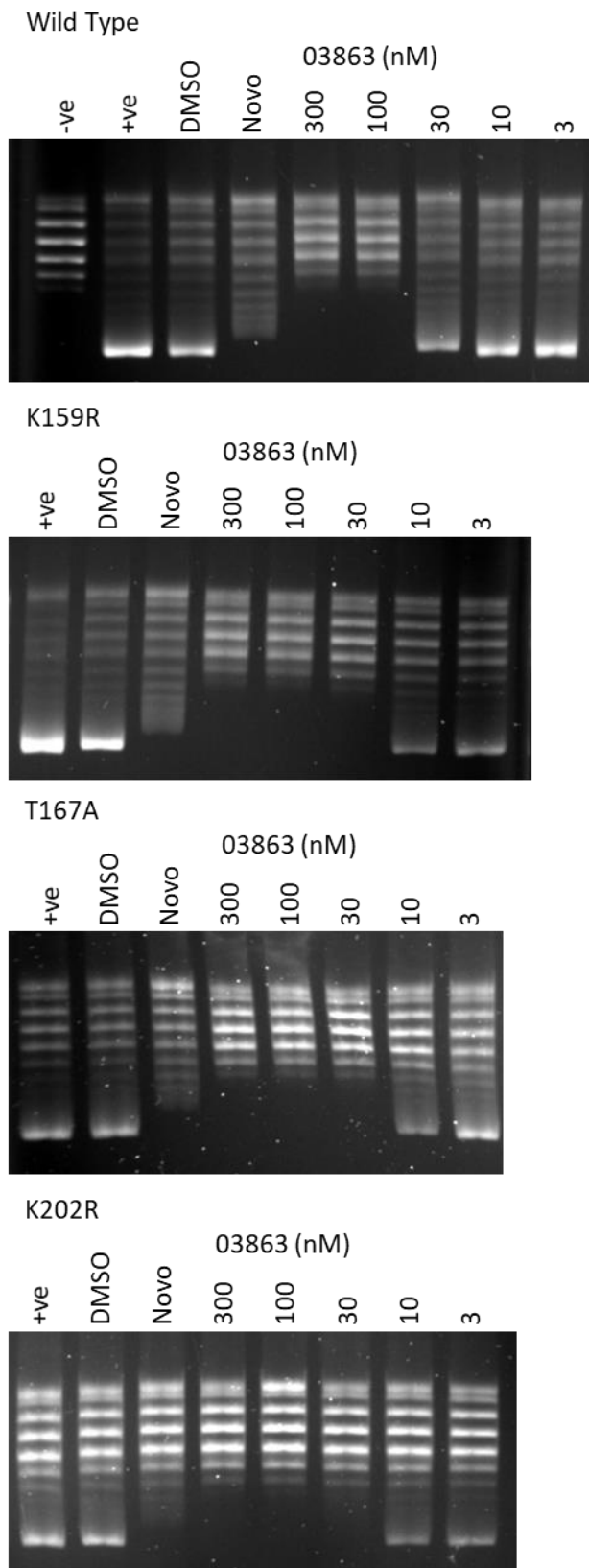


Figure 4.4.17: Supercoiling assay using GyrB wild type, K159R, T167A and K202R at a final enzyme concentration of 150 nM with 150 nM GyrA. -ve control contained DNA substrate in the absence of enzymes, DMSO control contained 1% DMSO in the absence of compounds; Novobiocin at 1 μ M; and compound dilutions 300-3 nM Redx03863.

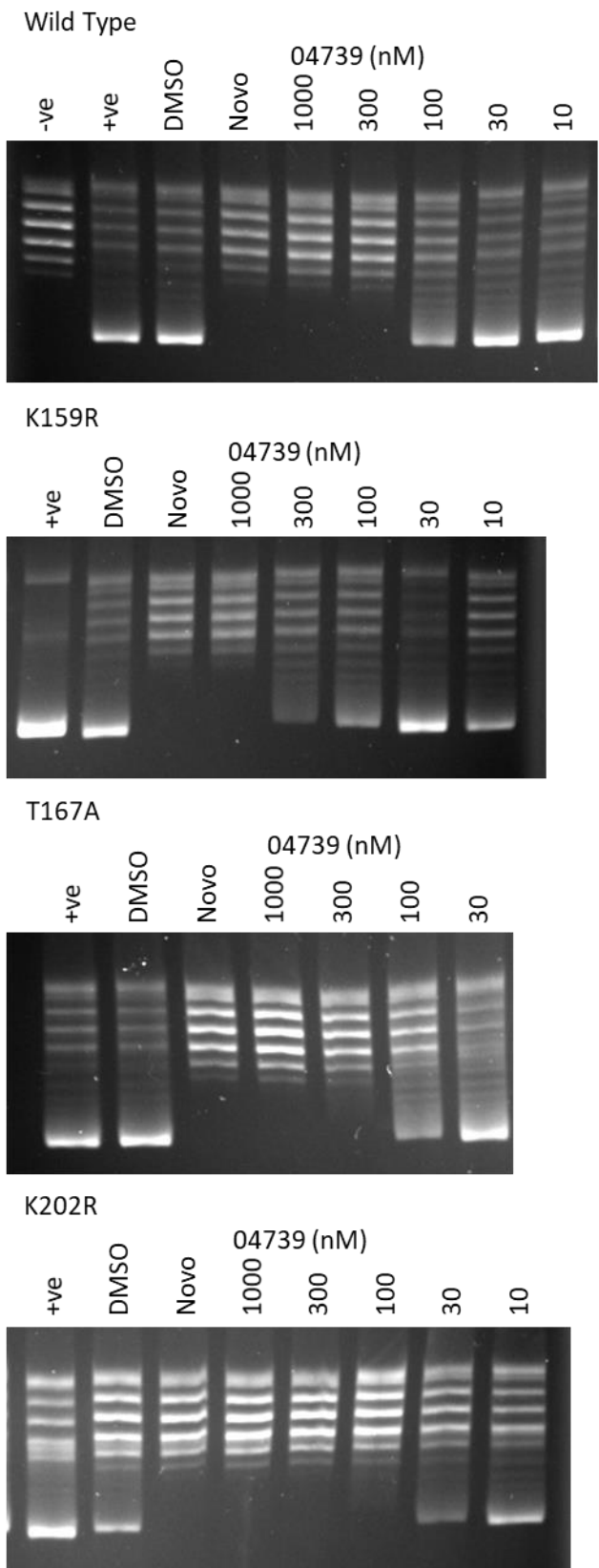


Figure 4.4.18: Supercoiling assay using GyrB wild type, K159R, T167A and K202R at a final enzyme concentration of 150 nM with 150 nM GyrA. -ve control contained DNA substrate in the absence of enzymes, DMSO control contained 1% DMSO in the absence of compounds; Novobiocin at 1 μ M; and compound dilutions 1000-10 nM Redx04739.

4.4.9 Testing of the naphthoquinone model against Redx03863 and Redx04739

A model of the 7-methyljuglone binding site was predicted computationally by SE within the GyrB NTD (as described in section 4.3) (Figure 4.3.3). Although this model was not tested against the naphthoquinones due to the instability of 7-methyljuglone, the site-directed mutagenesis and protein purification had already been carried out, and, as the binding site had not been determined by bacterial mutagenesis methods, it was decided to test this model against Redx03863 and Redx04739 to determine if these compounds interacted with this binding pocket.

All six mutants of the mutants made showed significant levels of supercoiling activity as compared to wild type DNA gyrase under standard supercoiling assay conditions. However, none of these mutants demonstrated any resistance to either Redx03863 (Figure 4.4.19) or Redx04739 (Figure 4.4.20) as compared to the wild type. Interestingly, several of the mutants (W47F, T189A, N309A, T373A) appear to show slightly increased sensitivity to Redx03863 and both W47F and N309A have increased sensitivity to Redx04739, however this is most likely to be due to the enzyme having decreased activity that was not optimised for this reaction. Of these the most marked difference was observed in the W47F where no supercoiling was observed within the concentration range tested, although it is unclear why this residue would increase the sensitivity to Redx03863 at this time. Overall, this was not an unexpected result, as from the biochemical data we know that these compounds are competitive ATPase inhibitors, and the predicted mode of action of diospyrin was to inhibit DNA gyrase within the GyrB N-terminal domain, but not at the ATP-binding site (Karkare *et al.*, 2013b).

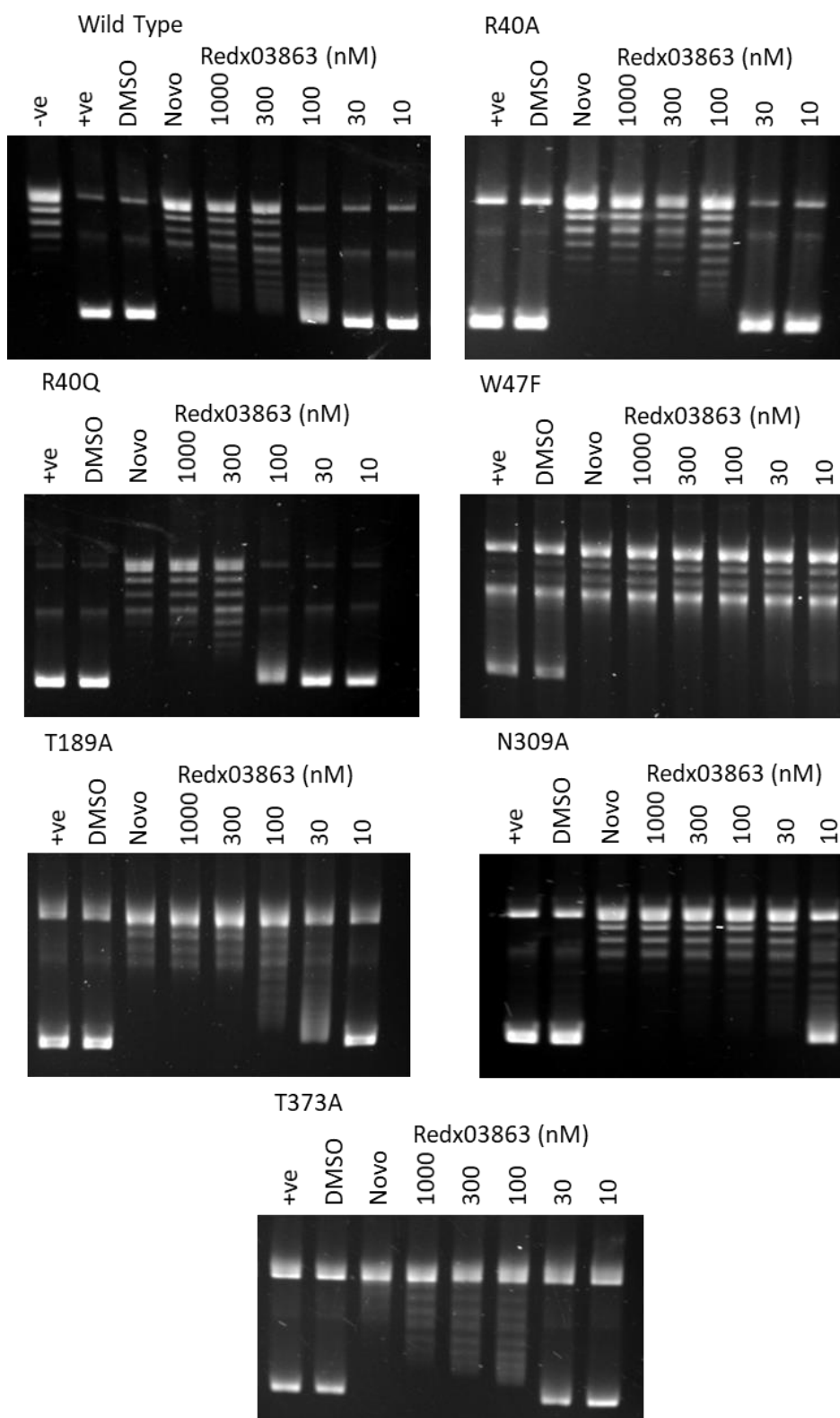


Figure 4.4.19: Redx03863 tested against the GyrBA fusion protein wild type and naphthoquinone single point mutants (R40A, R40Q, W47F, T189A, N309A, T373A) at a concentration of 74 nM. Controls used negative (no enzyme), positive, 1% (v/v) DMSO, and 10 μ M novobiocin in 1% (v/v) DMSO. Compound dilutions in 1000-10 nM Redx03863 in 1% (v/v) DMSO. The presence of a linear cleavage band in some of the reactions is as a result of impurities in the enzyme and does not affect the results of the assay.

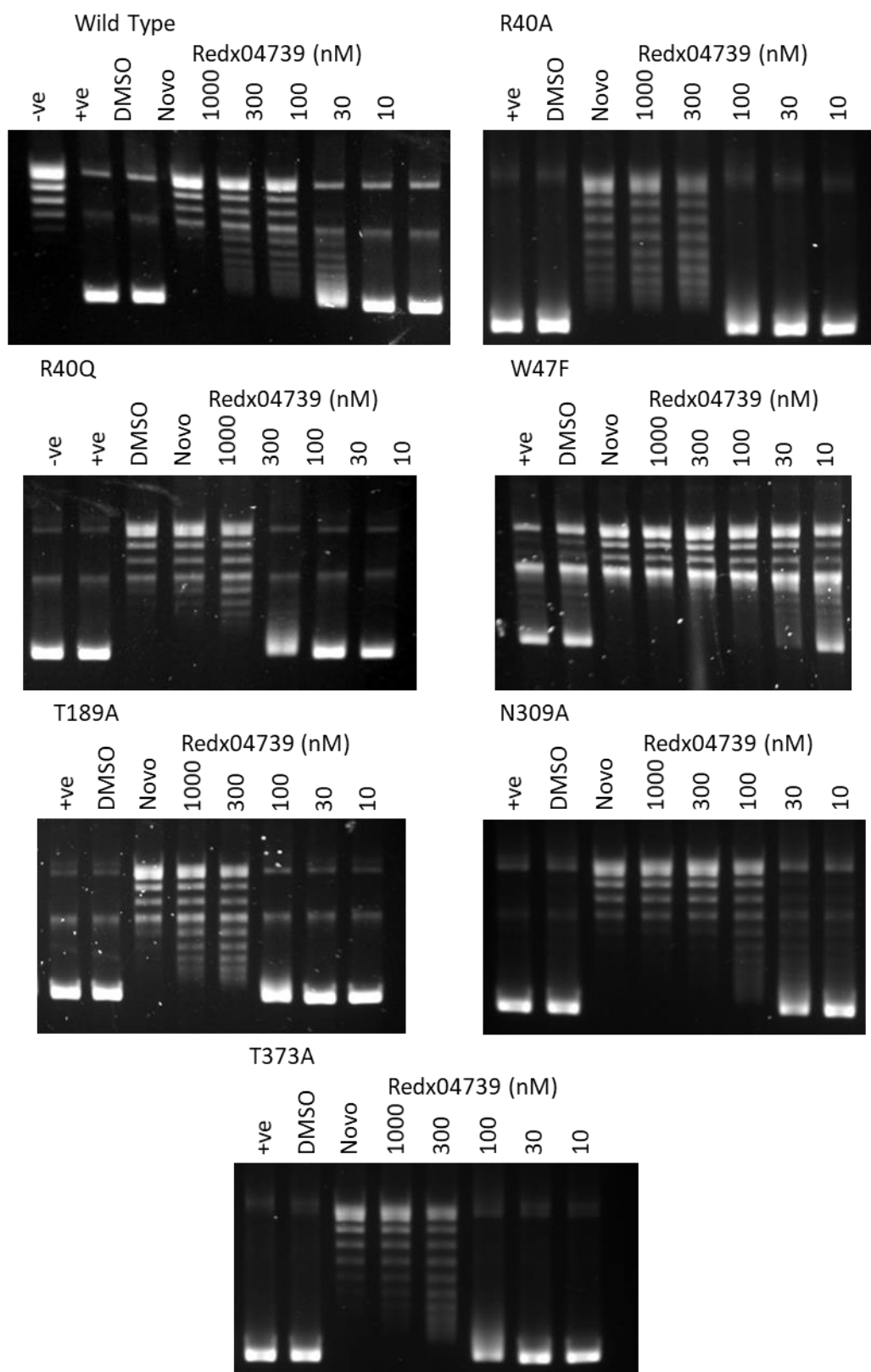


Figure 4.4.20: Redx04739 tested against the GyrBA fusion protein wild type and naphthoquinone single point mutants (R40A, R40Q, W47F, T189A, N309A, T373A). Controls used negative (no enzyme), positive, 1% (v/v) DMSO, and 10 μ M novobiocin in 1% (v/v) DMSO. Compound dilutions in 1000-10 nM Redx04739 in 1% (v/v) DMSO. The presence of a linear cleavage band in some of the reactions is as a result of impurities in the enzyme and does not affect the results of the assay.

4.5 Discussion

This chapter described work on four classes of Mtb DNA gyrase inhibitors. Potentially of the greatest interest in the context of developing new antibiotics for use in the clinic against active Tuberculosis is that of the TriBE class including Redx03863 and Redx04739, which have been investigated in detail here to confirm the mode of action. Despite this these compounds will probably never make it to the clinic as further optimisation is needed before they can be taken forwards. However, knowing the full mode of action should increase the chance of successful optimisation even if the full binding site was not confirmed from this work. The naphthoquinone 7-methyljuglone which was already known to have toxicity issues has been shown here to be unsuitable to be taken forwards as the pure compound is apparently not the active substance. Furthermore, as the active compound is unidentifiable the mode of action and binding site cannot be confirmed from this work.

4.5.1 Impacts from further studies on known antibiotics

The work studied here complements the current literature on the known DNA gyrase inhibitors moxifloxacin and novobiocin, demonstrating their inhibition of Mtb DNA gyrase fusion and subunit constructs to a similar extent to that previously described in the literature. The IC_{50} value presented here for novobiocin is very similar to the value presented by Aubry *et al.* (2006a), meanwhile the value we suggest for the IC_{50} of moxifloxacin is marginally larger while the CC_{50} value is marginally smaller than the literature values (Aubry *et al.*, 2004). However, we did find a larger than expected difference between the CC_{50} and IC_{50} values of moxifloxacin. Several proposed explanations have been presented including the idea that this is an effect that arises from the supercoiling assay being carried out in the presence of ATP and the cleavage reaction being carried out in the absence of ATP which may alter the efficacy of moxifloxacin.

We also suggest an apparent IC_{50} value for novobiocin of $0.21 \pm 0.04 \mu\text{M}$ for the ATPase assay here which to our knowledge is the first reported value of an IC_{50} value when using the Mtb enzymes in this assay, but also demonstrates the difficulties of this assay which requires large enzyme concentrations to get reproducible results. As the IC_{50} value obtained from this reaction is close to the enzyme concentration it prevented a true IC_{50} value from being determined due to reaching the limit of detection of the assay. Overall, the value presented is not dissimilar to the value presented for *E. coli* DNA gyrase of 90 nM (Contreras and Maxwell, 1992) supporting the idea that the limit of detection may have been reached within this assay. It is however quite surprising that the IC_{50} value for the supercoiling reaction was found to be

considerably larger than the IC_{50} of the ATPase reaction, as previously these values have been found to be similar in *E. coli* (Contreras and Maxwell, 1992). It is why unclear why this is not the case with *M. tuberculosis* DNA gyrase.

4.5.2 Instability of 7-methyljuglone and impacts on further studies

It is clear looking at the results obtained here alongside the prior results in the work of van der Kooy (2007) and Dr M.J. Austin (Pers. Comm.) that 7-methyljuglone is not itself active in inhibiting DNA gyrase. It is however plausible that a degradation or reaction product formed is instead likely to be the active agent causing the inhibition of supercoiling. At present the only information we have about the mode of action of the naphthoquinones is that diospyrin inhibits DNA gyrase likely within the N-terminal domain of GyrB but is not out competed by increasing concentrations of ATP in the Mtb DNA gyrase supercoiling reaction nor does it inhibit the ATPase reaction of *S. aureus* DNA gyrase (Karkare *et al.*, 2013b). Here we focussed our work on the less potent naphthoquinone 7-methyljuglone assuming the compound class to act through a common mechanism of action as 7-methyljuglone is half of a diospyrin molecule. As the reaction of the 7-methyljuglone does not appear to be straightforward (as no individual product could be identified) (Dr M.J. Austin Pers. Comm.), we could not test the compound reliably and comparatively against the computational model as the activity of the compound was evolving. This information may have also affected the parameters used to create the computational model (Figure 4.3.3) and hence a different binding pocket may have been identified if the work was repeated.

One of the initial questions arising from this work is should we continue to search for a more stable naphthoquinone which we would be able to reliably test the binding model on. The major issue arising is that the naphthoquinone menadione has been reported to have superior stability with >99% remaining after one week dissolved in DMSO (van der Kooy, 2007), but has also been reported to be very weak at inhibiting the supercoiling reaction of Mtb DNA gyrase with an IC_{50} value >200 μ M (Karkare *et al.*, 2013b). It is apparent that the less stable naphthoquinones appear to have greater activity against the enzymes, implying that there may be a link between the reactivity of the compounds and inhibition of DNA gyrase. Overall, it would be more productive to try and identify the reaction mixture generated from the less stable antibiotics to identify the active component and initiate a new series of studies and models based on these data.

4.5.3 Whole cell activity of the TriBE antibiotics

From the whole cell activity, Redx04739 shows greater activity against *M. smegmatis* than against the preliminary panel of Gram-negative bacterial species tested including *E. coli* as previously described by McGarry *et al.* (2018). The cell wall properties vary between the Gram staining of different bacterium, with Gram-negative bacterium having a lipopolysaccharide outer membrane beyond the peptidoglycan cell wall (Costerton *et al.*, 1974, Beveridge, 1999) whereas the Gram-positive bacteria are characterised as not having an outer membrane with their plasma membranes being simply covered with a layer of peptidoglycan (Shockman and Barrett, 1983). On the other hand, mycobacteria are somewhat unique in that they have a mycolic acid outer membrane in addition to their peptidoglycan layer (Brennan, 2003). This means there are permeability differences in the cell wall structures between Gram-negative bacteria and the mycobacteria that may be able to account for the differences in the activity on the whole cells which appear to have greater effects on mycobacteria despite the activity on the molecular targets being similar or better in the case of *E. coli* DNA gyrase.

It would have been predicted that the compounds should have been able to permeate the Gram-positive cell wall of *S. aureus* more easily, but the whole cell activity is comparable to that of the Gram-negative bacteria. Two of the potential explanations for this include differences in efflux pumps and differences in target enzyme resulting in less inhibition.

In addition to enhanced MIC₁₀₀ data of Redx03863 and Redx04739 against *M. smegmatis*, these compounds were also determined to have enhanced activity in killing *M. smegmatis* in a biofilm situation when compared to *E. coli* in a comparable experiment. The assay to compare the inhibition of biofilm growth was uninterpretable for *M. smegmatis* for an unknown reason, meaning no direct comparison can be made. The MBEC is however the superior measure as it determines the concentration of the compound or drug that is required to effectively kill the biofilm as opposed to the concentration required to stall the growth of a biofilm. The method developed and used for the *M. smegmatis* biofilm assay was not ideal as the drug incubation step used was 3 days meanwhile all the other steps were only two days. It is unclear if by lengthening the incubation with drugs the bMIC values were somewhat altered compared to the MBEC values.

The results obtained with regards to the biofilm inhibition demonstrate that these novel antibiotics have enhanced properties in accessing bacteria in enclosed environments such as the biofilm. Although typically *M. tuberculosis* is not thought of as a biofilm-forming infection in its active state, however, there are known cases of non-pulmonary *M. tuberculosis* infections, and in these cases there have been reports of biofilm-like structures forming over implants causing infections (Spinner *et al.*, 1996, Sendi and Brent, 2016). Additionally, although *M. tuberculosis* has not been reported to form an environmental biofilm, several environmental mycobacteria (e.g. *M. kansasii* and *M. xenopi*) are known to form biofilms in water systems, described as being found in hospital water reservoirs in the past (Carson *et al.*, 1988, Schulze-Robbecke *et al.*, 1992). All together this shows that although *M. tuberculosis* biofilms have rarely been detected in clinical settings they are important to consider as they have the potential to form biofilm-like infections.

Redx03863 appears to effectively and quickly kill both *E. coli* and *M. smegmatis* in liquid culture supplemented with at least four times the MIC₁₀₀ of the compound. The *E. coli* culture showed no surviving cultures at one day post-antibiotic addition whereas this stage was reached at just 2 days for the slower growing *M. smegmatis* cultures. Based on *M. smegmatis* having a doubling time in the region of several hours, it suggests that Redx03863 kills *M. smegmatis* more efficiently over fewer generations. The initial timepoints derived for the *M. smegmatis* assay were successfully derived from the timepoints used by Maurer *et al.* (2014), with later time points being evenly spread to obtain a protocol where no colonies should remain after 6 days. It is suggested that if the work was to be repeated in the future with *M. smegmatis*, that this would be a good method to follow again.

4.5.4 Consequences of the bacterial mutagenesis results

The TriBE group of antibacterial agents were originally developed to act in a dual-targeting mechanism (Bensen *et al.*, 2012, Tari *et al.*, 2013a). In the absence of topo IV it is likely that a single targeting mechanism occurs in *M. smegmatis* and hence is also inferred in *M. tuberculosis* (Cole *et al.*, 1998, Mohan *et al.*, 2015). The result of these compounds dual targeting both DNA gyrase and topo IV in *E. coli*, is to make the frequency of resistance rate very low as two spontaneous mutations in both targets are required to induce resistance as opposed to the single mutation in *M. smegmatis*. The difference in these values is possibly more surprising as the FoR value for *M. smegmatis* against Redx03863 is in the order of just 10⁻⁵ as opposed to the 10⁻¹¹ found in *E. coli*. The values were found to be of the same order when the FoR experiment was performed in the presence of 4x Redx04739 or novobiocin,

suggesting they are true results (Table 4.4.8). The high FoR results presented here are suggested to be an artefact of working with *M. smegmatis*, this is proposed because when working with the mutant set isolated on 4x Redx04739 plates it was not possible to conclusively confirm resistance to Redx04739, hence questioning the values obtained within this assay – for instance a “grow-through” effect may have occurred where the drug did not efficiently kill the bacteria before the efficacy of the compound was degraded, unfortunately it was decided not to carry out the time of kill experiment with Redx04739 and hence this theory was not tested. We do however know this is not likely to be the case for Redx03863 due to the results of the time of kill experimentation (Figure 4.4.3).

In contrast to the FoR results it was found that a resistant strain of *M. smegmatis* ATCC19420 could not be effectively raised against Redx03863 using the serial passage method whereas an *E. coli* ATCC25922 strain that had 128-fold increased resistance to Redx03863 was raised over a period of 50 days (Figure 4.4.11). This implies that continual exposure of a culture to a low compound concentration is less effective at producing resistant strains than the selection pressure of the high concentrations of compound on agar plates. Likewise, when considering this result in the context of the time of kill data, it suggests that the bacterium is effectively killed within 4 days and hence there should be no significant concerns over resistance generated in the time taken to treat an infection.

This same pattern was also obtained when the bacteria were passaged against Redx04739, although resistant strains were obtained over fewer passages (Figure 4.4.12). These results somewhat correlate to the FoR results were marginally higher FoR values against Redx04739 compared with those from Redx03863 were obtained (Table 4.4.8). It does however suggest that Redx04739 would not be less clinically effective against *E. coli* as it is able to generate resistance in a brief period of time (i.e. less than a typical course of antibiotics, i.e. 7 days). Conversely, it may be possible to use it clinically versus mycobacteria such as *M. smegmatis* as no significant increase in the MIC₁₀₀ value was obtained in the first 10 passages (>20 days), and although no time of kill data were obtained against Redx04739 it is suggested that whole cells should be killed effectively within this time. Furthermore, it is important to consider that a multiple drug regime is currently preferred for the treatment of tuberculosis, so future studies should be investigated in the presence of alternate antibiotics including synergy studies (WHO, 2010).

The cross-resistance profile of the resistance strains isolated was analysed and gave some interesting results. Firstly, it confirmed that the mechanism of action for both Redx03863 and Redx04739 is likely to be the same as cross-resistance was present in all strains raised against either compound (Table 4.4.4; Table 4.4.9). Secondly, despite moxifloxacin having a known mode of action that is different to the proposed mechanism of the novel compounds there appeared to be some cross-resistance of the *E. coli* 03863 SP(25/50) strains which increased over the passage number to final resistance of 32-fold to moxifloxacin (Table 4.4.4), although no mutations were observed in the QRDR (quinolone resistance determining region) within GyrA (Table 4.4.4). No cross resistance of this mechanism was observed for any of the FoR mutants analysed but presents an issue with the compounds if they are able to induce resistance to compounds with alternate modes of action.

Several of the mutants appear to have a degree of cross resistance or sensitivity to novobiocin. These for the most part are relatively small degrees of resistance (2-4 fold) although one strain (*M. smegmatis* 4x03863 1b) exhibited 32-fold resistance over the wild-type, meanwhile *E. coli* 2x03863 FoR appeared to generate 128-fold sensitivity to novobiocin (Table 4.4.4; Table 4.4.9). It has been previously presented within the literature that the G83S mutation (G85S *S. aureus*) is involved in the mechanism of resistance of novobiocin, and this point mutation is found in the *M. smegmatis* 4x03863 1b novobiocin resistant strain (Stieger *et al.*, 1996). We were unable to confirm if through the inhibition of supercoiling reaction if this point mutation was involved in binding of either of the Redx compounds due to the very low activity of this mutant. However, as the mechanisms of action are comparable, it is therefore plausible that the binding sites of these compounds overlap, and indeed the crystal structures of the TriBE compounds presented in (Tari *et al.*, 2013a) suggests overlap with the binding pocket of novobiocin (Holdgate *et al.*, 1997) and hence one single point mutation in this region (such as the G83S mutation) may affect the binding of both groups of compounds.

An interesting thing to consider in the future would be to examine the cross-resistance profiles of *M. smegmatis* ATCC19420 and *E. coli* ATCC25922 with the R141A and R136A GyrB mutants introduced. This is a primary residue involved in novobiocin resistance (del Castillo *et al.*, 1991, Holmes and Dyallsmith, 1991, Contreras and Maxwell, 1992, Stieger *et al.*, 1996, Kampranis *et al.*, 1999b, Gross *et al.*, 2003, Fujimoto-Nakamura *et al.*, 2005), and hence determining if in whole cell there is cross-resistance between novobiocin, Redx03863 and Redx04739 this residue would be important in confirming whether these compounds same binding site.

Sequencing of the type II topoisomerase genes from resistant strains was carried out, indicating a surprisingly large number of mutations within these genes, many of which did not appear to make sense in the context of the previously discussed mechanism of action. As the wild-type type II topoisomerase genes were additionally sequenced and only differences in the resistant strains reported here it was decided to continue with testing of only the mutants in the GyrB NTD. However, it is also considered possible that the mutants are an artefact of poor sequencing (the chromatograms (not shown) appeared normal), or that the compounds themselves induce increased mutagenesis. It appears unlikely that it results from an artefact of sequencing as there were several mutations that were observed in multiple resistant strains but not the wild type strain (e.g. GyrB T167A, GyrB D340E), as opposed to random mutations occurring suggesting that there may be a common resistance mechanism obtained from these mutations (Table 4.4.10).

One of the mutants that was sequenced contained a mutant of Gly83 to Ser which when purified appeared to lack supercoiling activity (Figure 4.4.15). This is surprising as it was expected that any mutants that were isolated from bacterial methods should support supercoiling in the cell and therefore it would be expected to support supercoiling *in vitro*. Furthermore, this mutant has been previously described to be involved in bacterial resistance mechanisms including against novobiocin in *S. aureus* (Stieger *et al.*, 1996) suggesting that that is not an essential amino acid *in vivo*. However, this mutation in *E. coli* has been previously reported to have only low level ATPase and supercoiling activity *in vitro* previously (Gross *et al.*, 2003). This theory is further enhanced through the evidence presented in this chapter that the mechanisms of actions of the aminocoumarins is remarkably like that of Redx03863 and Redx04739, although there does not appear to be consistent cross-resistance between these compounds and novobiocin.

The other three mutations that were introduced into Mtb DNA gyrase (K159R, T167A and K202R) did not show resistance to either compound or novobiocin suggesting that they are not involved in the resistance mechanism in *M. tuberculosis*. As discussed earlier, it does not preclude them from being involved in the resistance mechanism in *M. smegmatis* DNA gyrase (Figure 4.4.16; Figure 4.4.17; Figure 4.4.18). The most surprising of these negative results is that of the T167A mutations, which was independently identified in three of the four *M. smegmatis* 4x03863 FoR strains, implying it to be important in the resistance mechanism.

Additionally, there have been studies on two aminobenzimidazole compounds (VRT-125853 and VRT-752586) (Figure 4.5.1) demonstrating that resistance is generated against these compounds when T167 is mutated (Grossman *et al.*, 2007). Finally, T167V has been reported to be weakly involved in resistance to novobiocin (Stieger *et al.*, 1996). Overall, this suggests that the binding site of both Redx03863 and Redx04739 is likely to be close to the novobiocin-binding site as is the binding site of the VRT compounds (Holdgate *et al.*, 1997).

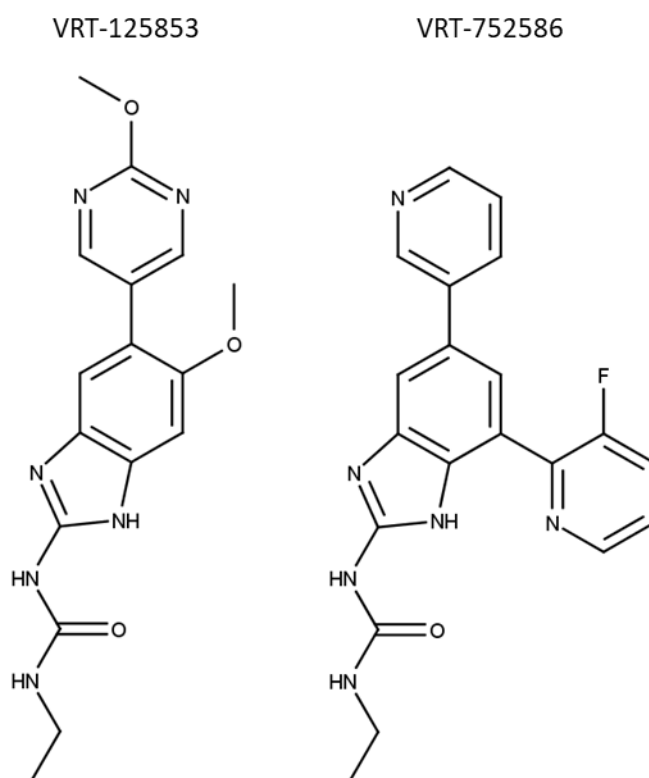


Figure 4.5.1: Structures of the VRT aminobenzimidazole dual-targeting compounds from Vertex Pharmaceuticals Incorporated (Grossman *et al.*, 2007).

Although there is a high degree of homology between the two different enzymes it is plausible that there may be some difference in how these compounds interact with the two different enzymes. Additionally, it may require multiple mutations to be made in parallel to enable resistance to be observed which was not carried out in this study and hence this theory cannot be discounted.

4.5.5 Consequences of the mode of action studies and the search for the binding site

From the enzymatic results shown in this section both Redx03863 and Redx04739 have a mode of action that involves competitively inhibiting the ATPase activity of GyrB. Importantly, it was demonstrated on the Mtb DNA gyrase through use of the ATPase linked assay, which, to our knowledge, is the first time this has been achieved for inhibition studies.

The binding domain of Redx04739 (and hence Redx03863) is suggested through the use of SPR to be within the ATPase sub-domain (Figure 4.4.9; Figure 4.4.10). The data obtained showed that very strong binding was occurring with the chip and that the compounds were difficult to remove after binding. A K_d value could however be obtained for Redx04739 for both the *E. coli* and *M. tuberculosis* ATP-subdomains, although the *M. tuberculosis* gave very large errors and hence is not quoted (Figure 4.4.9; Figure 4.4.10). Although, specific statistical values were not obtained it gave promise that the GyrB NTD was the correct place to be searching for the binding sites of Redx03863 and Redx04739, as predicted from the previous structural studies of compounds within this series (Tari *et al.*, 2013a). These results also confirmed that this was the correct domain to be using for subsequent crystallographic trials detailed in chapter 5.

Overall, Redx03863 and Redx04739 appear to be part of a useful class of inhibitors that could be further optimised to obtain a mycobacterial-specific inhibitor to be explored as a clinical option in the future. At present both compounds present with one major issue in their high frequency of mutation results in *M. smegmatis* with no direct DNA gyrase mutants involved in the mechanism of action being obtained. It is suggested that to overcome this in the future, a permeable *M. smegmatis* (or *E. coli*) strain could be exploited to generate resistance mutants. Finally, it was not possible within the work of this chapter to locate the specific binding site of these compounds, although we have determined that they bind within the sub-ATPase domain within the GyrB NTD and the mode of action has been confirmed as being a competitive inhibitor of the ATPase reaction. In the next chapter we will further discuss the binding site in the context of subsequent structural studies performed.

5. Crystallographic Studies of Mycobacterial DNA Gyrase

At present our structural understanding of DNA gyrase from *M. tuberculosis* is robust with the structure of each subunit of the enzyme having previously been solved (Tretter and Berger, 2012, Agrawal *et al.*, 2013, Blower *et al.*, 2016). From this structural information we can make an educated guess of the final arrangement of the subunits based on homology modelling and the low resolution cryoEM structure of *T. thermophilus* DNA gyrase (Figure 5.1.1) (Nagaraja *et al.*, 2017). Although we have some structural information, it is however important to keep expanding the structural information we have available to better rationalise both the activity and inhibition of mycobacterial DNA gyrase to assist with future drug discovery efforts. Hence, in this chapter we investigated the possibility of solving the full-length structure of DNA gyrase from *M. tuberculosis* in addition to further investigating the structures of mycobacterial ATPase domains bound to inhibitors to understand their mechanisms of action.

5.1 Crystallisation trials of full-length *M. tuberculosis* DNA gyrase

In the past there has been no high-resolution structure of full-length DNA gyrase from any species. To determine the full-length structure of DNA gyrase the fusion GyrBA protein was subjected to crystallisation trials to obtain protein crystals. The fusion protein was chosen as by fusing the two subunits it created a protein already complexed with lesser mobility and hence it was theorised that this may increase the chance of successful crystallisation. Indeed, there is an almost complete structure of the first 1177 residues of *S. cerevisiae* topo II available in the PDB (Figure 1.7.1) supporting the idea that the fusion protein may be a better target for crystallisation trials (Schmidt *et al.*, 2012).

It was discovered that at a concentration of 2.2 mg/ml with a CTD-His-tag removed there was little precipitation, but no crystals were observed in the KISS, Morpheus® and JCSG-*plus*TM screens. This implied that the protein concentration was too low and hence the protein was not able to enter the nucleation zone. When increasing this to a concentration of 7.5 mg/ml (with the CTD-His-tag present) in the same three screens no crystals were obtained although a better balance of precipitation and clear drops was observed.

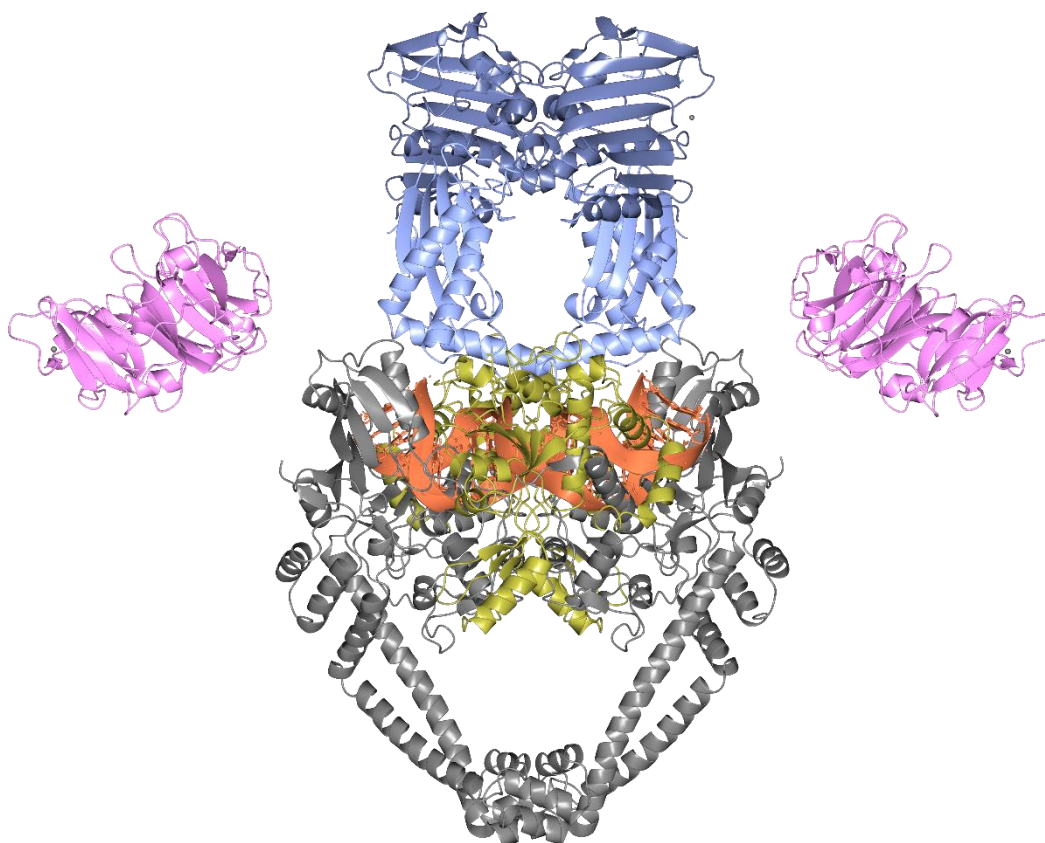


Figure 5.1.1: Structural model of *M. tuberculosis* DNA gyrase. The model was made by taking the existing crystal structures (5BS8, 3UC1, and 3ZKB) and using the program COOT to assemble a model of the A₂B₂ complex. Domains are coloured as follows: GyrB-NTDs, ice blue with B24 sub-domain highlighted in dark blue; GyrB-CTDs, gold; GyrA-NTDs, grey; GyrA-CTDs, pink. DNA is in a coral ribbon representation. Abbreviations: CTD, C-terminal domain; NTD, N-terminal domain. Figure edited from (Nagaraja *et al.*, 2017).

As the enzyme is relatively mobile in the absence of DNA, as demonstrated by the CryoEM structure where the CTDs were not visible in the absence of DNA, it was decided to introduce DNA fragments into the crystallisation conditions starting with two published 20 bp fragments that had been previously optimised to determine the structure of the *S. aureus* DNA gyrase core-fusion (GyrB CTD – GyrA NTD). However, when introducing the annealed 20-12-p-8 or 20-447T published DNA fragments (Srikannathasan *et al.*, 2015) in the presence of moxifloxacin with or without magnesium and manganese ions, no crystals were obtained. There was however, one confirmed salt crystal – well A5 of the Morpheus® screen in the presence of both ions, DNA and moxifloxacin. This is somewhat unsurprising as around 70 bp are required to wrap each of CTD's, requiring approximately 128 bp to wrap both CTD in the absence of a nucleotide and likely increases to around 142 bp on binding of ADPNP (Orphanides and Maxwell, 1994).

To additionally try to stabilise the enzyme further we looked to use a nucleotide as there is considerable evidence that the GyrB ATPase containing NTDs dimerise in the presence of a nucleotide (Ali *et al.*, 1993) increasing the stability of the complex. Therefore, we attempted crystallisation in the presence of both hydrolysable (ADP) and non-hydrolysable nucleotides (AMPPNP) to determine the optimal crystallisation conditions. However, at 7.5 mg/ml with or without a C-terminal His-tag there was no evidence of protein crystallisation in the JCSG-*plus*TM, Structure screen 1+2 or KISS screens in the presence of 1 mM ADP-Li salt and 5 mM magnesium chloride. Equally, after dialysing an untagged protein into the supercoiling assay buffer composition in the presence or absence of AMP-PNP (non-hydrolysable ATP) no crystals were obtained. Overall, sixteen 96 well screens of the full length fusion *M. tuberculosis* DNA gyrase construct were set up with only salt crystals being obtained.

5.2 Crystallisation of the *M. tuberculosis* ATPase domain

From the biochemistry presented in Chapter 4 it was determined that the TriBE compounds Redx03863 and Redx04739 bound to the N-terminal of GyrB as competitive inhibitors of the ATPase reaction. To locate the binding site of Redx03863 and Redx04739 within this domain and enhance our knowledge of the Mtb ATPase domain it was attempted to co-crystallise the full ATPase domain in the presence of both compounds. Previously, the ATPase domain of *M. tuberculosis* had been crystallised (Roue *et al.*, 2013), resulting in the crystal structures 3ZKB, 3ZKD and 3ZM7 (Agrawal *et al.*, 2013). The construct of this domain was a kind gift of Drs C. Mayer and S. Petrella (Institut Pasteur, Paris) and purification and crystallisation were performed as before (Agrawal *et al.*, 2013). The protein was crystallised at 10.6 mg/ml with 5.2 mM magnesium chloride and 5.2 mM AMP-PCP, in a hanging drop arrangement with 1 μ l drops with 1 μ l of well solution (15-30% (w/v) PEG1500, 0.8-1.3% (v/v) myoinositol, 100 mM MES pH 6.5, and 5 mM magnesium chloride, total well volume 400 μ l). Under these conditions the protein formed multiple thin plate-like crystals often clumped together. The protein did not crystallise in the absence of the AMP-PCP, and only produced small crystals in the presence of either Redx03863 or Redx04739 when crystallised with AMP-PCP.

With some minor optimisations it was found that we were able to get some crystals suitable for X-ray diffraction, however the crystals obtained did not diffract beyond 3.3 Å. It was not possible to resolve the structure of either of the data sets collected in the predicted space group

of C222₁, or the lower symmetry space groups of C2, P2, or P1. As this construct did not crystallise in the absence of AMP-PCP the decision was made not to continue with this structure as it is believed that the binding sites of AMP-PCP and the two Redx compounds should overlap (Tari *et al.*, 2013a), and hence efforts of co-crystallography with both AMP-PCP and either Redx03863 or Redx04739 would not be successful. Instead the decision was made to move to the GyrB24 ATPase sub-domain construct which in other species has been crystallised in the absence of an ATP analogue.

5.3 Crystallisation trials of *M. tuberculosis* GyrB24 ATPase subdomain

To overcome the problems with crystallisation that were faced with the full-length ATPase domain, it was decided to try and crystallise the smaller ATPase sub-domain containing the ATP and novobiocin binding sites. Furthermore, SPR experimentation in Chapter 4 gave a strong indication that Redx03863 and Redx04739 both bound with high affinity to this domain. Overall this suggested that the GyrB24 ATPase subdomain was a good target for crystallisation.

The ATPase subdomain was initially cloned without the last β -strand of the domain (see sections 2.2.3, 2.8.1). This was purified, and no crystals were obtained with this construct when bound to either Redx03863 or Redx04739 overnight at low protein concentration (<1 mg/ml) and subsequently concentrated to around 4 mg/ml for use in the JCSG-*plus*TM screen. After realising that the final β -sheet in the construct was missing the construct was not trialled further.

Subsequently, the construct was remade to include the correct C-terminus, however from five 96-well screens with both compounds only one crystal hit was obtained although, this was not followed up due to a lack of UV-fluorescence in the crystal. Following, this lack of success, it was decided to remove a pair of potentially long flexible loops which are not visible in the crystal structure of the full-length ATPase domain, to form two constructs from here on known as B24 SLD (single loop deletion) and B24 DLD (double loop deletion) (Figure 5.3.1).

The two loop deletion constructs were successfully expressed in Rosetta2TM pLysS cells, grown in LB media with induction with 0.4 mM IPTG at OD₆₀₀ 1.0, 37°C for 4.5 hours. The constructs were lysed using a homogeniser at 40,000 psi then the soluble cell lysate was

subsequently purified using a three-column strategy (5 ml HisTrap FF, MonoQ 10/10, S75 10/300) yielding 2.6 mg of pure B24 SLD protein. The DLD construct was easier to work with and purified to give approximately 26 mg of pure protein, at a concentration of 17.3 mg/ml.

```

GyrB24      GLEAVRKRPGMYIGSTGERGLHHLIWEVDNAVDEAMAGYATTVNVVLLLEDGGVEVADDG      60
GyrB24SLD  GLEAVRKRPGMYIGSTGERGLHHLIWEVDNAVDEAMAGYATTVNVVLLLEDGGVEVADDG      60
GyrB24DLD  GLEAVRKRPGMYIGSTGERGLHHLIWEVDNAVDEAMAGYATTVNVVLLLEDGGVEVADDG      60
*****

GyrB24      RGIPVATHASGIPTVDVMTQLHAGGKFDSDAYAISGGLHGVGVSVNVALSTRLEVEIKR      120
GyrB24SLD  RGIPVATHASGIPTVDVMTQLHAGGKFDSDAYAISGGLHGVGVSVNVALSTRLEVEIKR      120
GyrB24DLD  RGIPVATHASGIPTVDVMTQ-----VGVSVNVALSTRLEVEIKR      100
*****

GyrB24      DGYEWSQVYEKSEPLGLKQGAPT KKTGSTVRFWADPAVFETTEYDFETVARRLQEMAFLN      180
GyrB24SLD  DGYEWSQVYEKSEPLGLKQGAPT KKTGSTVRFWADPAVFETTEYDFETVARRLQEMAFLN      180
GyrB24DLD  DGYEWSQVYEKSEPLGLKQGAPT KKTGSTVRFWADPAVFETTEYDFETVARRLQEMAFLN      160
*****

GyrB24      KGLTINLTDERVTQDEVDVSDVAEAPKSASERAAESTAPHKVKSRTFHYPG      234
GyrB24SLD  KGLTINLTDERDG-----KSRTFHYPG      202
GyrB24DLD  KGLTINLTDERDG-----KSRTFHYPG      182
*****

```

Figure 5.3.1: Sequence alignment of the sub-ATPase domain constructs with and without the two long loops, created based on the published *M. smegmatis* structures. The second loop is replaced by the two amino acids found in the *E. coli* GyrB subunit (DG) in the absence of the flexible loop.

Due to the low aqueous solubility of Redx03863 and Redx04739, 19.2 µg of each compound was bound to 210 µl of B24 SLD at 5.4 mg/ml with 0.7% (v/v) DMSO for 1 hour, before concentrating up to *ca.* 10 mg/ml. Three sparse matrix screens were trialled (JCSG-*plus*TM, PEG suite, AmSO₄ suite screens). No crystal hits were obtained. The remaining protein was used in the Structure screen 1+2 at 7.9 mg/ml co-crystallised with 0.7 mM novobiocin. One potential hit was obtained with well conditions 2 M sodium chloride, 10% (w/v) PEG6000 (Figure 5.3.2). As no more protein of this batch was available, and because no UV fluorescence was observed it was chosen not to follow this lead at this time.

Due to the lack of successful crystallisation the His-tag was removed from the B24 DLD protein which was purified and concentrated to 26 mg/ml. Three sparse matrix screens (KISS, Morpheus®, and JCSG-*plus*TM) were all set up for crystallisation trials under apo conditions. In addition, the His-tagged B24 DLD protein was concentrated to 38 mg/ml and the PEG and JCSG-*plus*TM screens were trialled both in the presence and absence of 1.6 mM novobiocin. Regardless of all these efforts no further crystal hits were obtained for optimisation or harvesting.

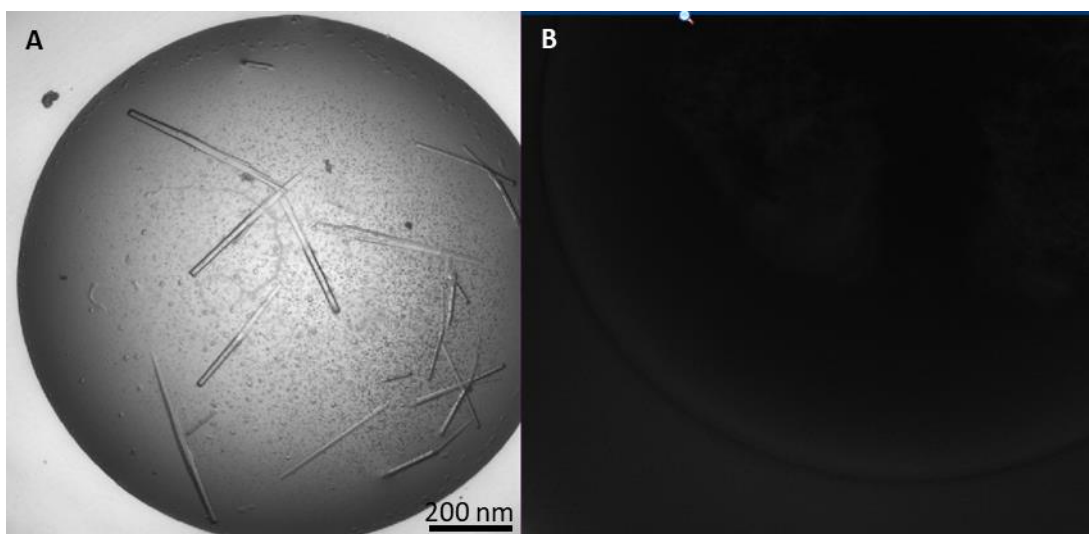


Figure 5.3.2: Visible light (A) and UV (B) image of the single crystal hit obtained when screening the Mtb GyrB24 SLD construct. Crystals obtained in the presence of 0.7 mM novobiocin at 7.9 mg/ml in 2 M sodium chloride and 10% (w/v) PEG6000. Image taken at 9 days.

Multiple screens were set up with the B24 DLD protein at 17.3 mg/ml in an apo form, or in the presence of 0.7 mM novobiocin, 0.25 mM Redx03863 or 0.25 mM Redx04739. Only two conditions were identified to optimise. The first of these conditions was that of the apo protein in 200 mM magnesium chloride, 100 mM Bis-Tris-HCl pH 5.5, 25% (w/v) PEG3350, with the second being novobiocin-bound protein in 100 mM Bis-Tris-HCl pH 6.5, 25% (w/v) PEG3350. However, after 2 rounds of optimisations no further hits were obtained, and the conditions were dropped as they were not reproducible and presumed to be salt.

Due to the lack of crystals being obtained from extensive screening it was decided to perform some basic bioinformatics on the constructs, hence, all the current constructs were put through the XtalPred-RF database to determine their likelihood of crystallising (Slabinski *et al.*, 2007). The results are summarised in (Table 5.3.1) indicating that the constructs being worked with were sub-optimal in terms of the Expert-Pool classification of 2, which only suggests them to have approximately a 50% chance of crystallisation. Furthermore, the results of the Random Forest classifier were in a wider range of classifications, indicating the best construct to be attempting crystallisation on was the one missing the last beta-strand, and that the HisGyrB24, GyrB24SLD and HisGyrB24DLD constructs were the next best alternatives (Jahandideh *et al.*, 2014).

Table 5.3.1: XtalPred-RF results for the Mtb GyrB sub-ATPase domain constructs. EP-class: Expert Pool classification; RF-Class: Random Forest Classification. None of the seven proteins are placed within the groups most likely to crystallise.

Construct	EP-Class	RF-Class	Length (AA)	Gravy Index	Instability Index (II)	Isoelectric point (pI)	Coiled coils	Longest disordered region	% Coiled structure
GyrB20	2	3	191	-0.18	26.68	4.93	0	14	34
HisGyrB24	2	4	252	-0.37	32.75	5.41	0	17	43
GyrB24	2	5	234	-0.27	30.70	4.96	0	15	38
HisGyrB24SLD	2	6	222	-0.37	31.38	5.60	0	18	39
GyrB24SLD	2	4	205	-0.26	29.41	5.05	0	15	37
HisGyrB24DLD	2	5	202	-0.40	30.09	5.54	0	16	38
GyrB24DLD	2	5	185	-0.28	27.80	4.95	0	14	35

5.4 Crystallisation trials of *M. smegmatis* B24 ATPase subdomain

As the 4 progressive iterations of the Mtb GyrB24 constructs did not yield protein crystals after screening 4896 conditions it was decided to move towards the use of a homologue. In the past, two structures of *M. smegmatis* GyrB24 have been published (Shirude *et al.*, 2013, Hameed *et al.*, 2014) in the absence of an Mtb structure. Both structures had at least one loop deleted, as per the loop deletion constructs designed for the Mtb protein. Based on the crystallisation conditions of these constructs and considering the solubility of the Redx compounds, it was decided to only clone the double-loop deletion construct, which was published to crystallise at a lower pH. The Msm GyrB24 gene was synthesised and codon-optimised by Invitrogen GeneArt (ThermoFisher Scientific) and subsequently the synthesised gene was sub-cloned into the pET28-MHL vector at the BseRI sites. The protein was successfully expressed in the transformed *E. coli* BL21 cell line in 6 L LB induced with 0.4 mM IPTG at 30°C for 4.5 hours. The protein was purified following the previously published procedure (Shirude *et al.*, 2013) to yield more than 160 mg of pure protein at a concentration of 17 mg/ml.

Crystallisation screening was carried out at 17 mg/ml in the presence or absence of 1 mM novobiocin, Redx03863 or Redx04739. Initially screening was carried out at a range of conditions around the published crystallisation conditions (0-30% (w/v) PEG8000, 100 mM sodium acetate pH 5.6, 200 mM calcium acetate). Initial crystal hits were obtained within 2 days in the presence of novobiocin. Crystals grown in 9% (w/v) PEG8000 were harvested in 50 µl mother liquor and crushed by vortexing for 4 min with 3 mm glass beads to form a seed stock. Crystals of Msm GyrB24 supplemented with 1 mM novobiocin were grown in 15% (w/v) PEG8000, 100 mM sodium acetate pH 5.6, 200 mM calcium acetate and were harvested after 5 days in a cryoprotectant of the mother liquor supplemented with 25% (v/v) ethylene glycol, 1 mM novobiocin by Dr Clare Stevenson (Figure 5.4.1).

Extensive co-crystallisation with Redx03863 and Redx04739 was carried out, including using the reconcentration method where the compound was added to the protein at a low protein concentration and subsequently reconcentrated, no co-crystals were obtained with or without the seed stock and subsequent dilutions as described above (Hameed *et al.*, 2014).

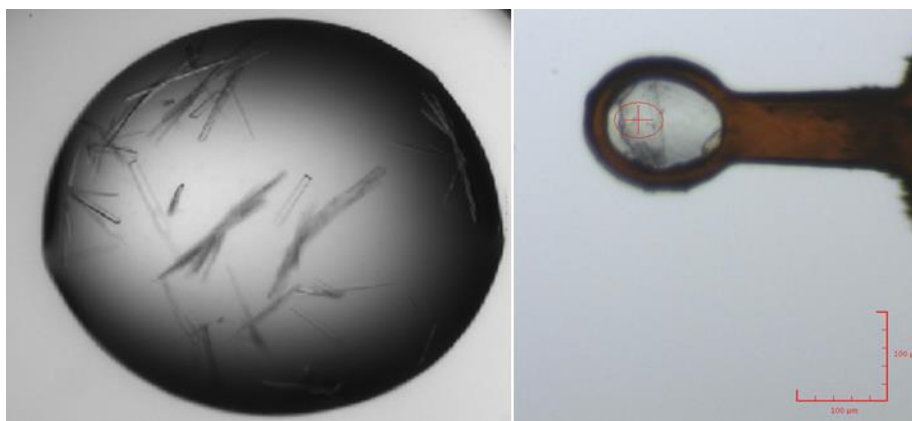


Figure 5.4.1: Image of crystals of Msm GyrB24 DLD before harvesting from the well for X-ray diffraction (left), and in the loop for data collection at the Diamond synchrotron beamline i04 (right). Crystals grown in 15% PEG (w/v) PEG8000, 100 mM sodium acetate pH 5.6, 200 mM calcium acetate at protein concentration 17 mg/ml supplemented with 1 mM novobiocin. No UV absorbance was observed from the crystals.

To try to obtain a crystal structure of the compound-bound structure in the absence of co-crystallised proteins the decision was made to trial crystal soaks with the compounds. However, as the crystals only grew in the presence and not the absence of novobiocin, soaking was carried out on novobiocin-bound crystals. Soaking was trialled over time periods greater than 6 hours at low compound concentration in DMSO concentrations less than 2% (v/v). However, it was found not to be successful as either the crystals dissolved, or the compounds did not out soak the novobiocin in the crystals leaving only novobiocin density visible in the structure when viewed with DIMPLE (automated refinement and ligand screening software) (Figure 5.4.2).

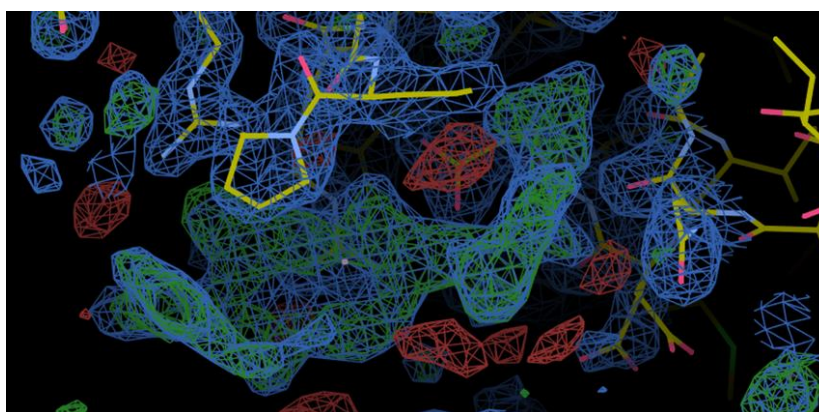


Figure 5.4.2: Example output from DIMPLE autoprocessing showing unmodelled positive density in the structure solution. Map shown at an RMSD value of 1.5 (0.4595 electron/Å³). The model used to solve the protein backbone was the refined Msm GyrB24 structure with novobiocin but with the ligand removed. This indicated that crystals grown in novobiocin and soaked with Redx04739 still contained novobiocin.

5.5 X-ray diffraction and structure solution of *M. smegmatis* B24 ATPase subdomain

Data from the novobiocin-containing crystals was collected on the i04 beamline at the Diamond light source. From this data the structure of the Msm B24 sub-ATPase domain was solved by molecular replacement using the published structure of the Msm B24 sub-ATPase domain (PDB entry 4B6C) as the model for phasing. To remove gaps in the mainchain BUCCANEER was utilised. This was followed by iterative rounds of automated and manual refinement in REFMAC and COOT respectively until the structure gave optimal density fit and conformation (Table 5.5.1).

Overall the crystal structure presented here is highly similar to the published 4B6C structure of the same construct bound to a different compound in the A crystallographic copy. However, there are some clear differences observable of which the first is the presence of a different unit cell where this new structure crystallised in the C2 space group compared to C222₁ space group in the published structure. Both structures contain two crystallographic copies in the asymmetric unit cell, however the interfaces between the two structures are distinct (Figure 5.5.1).

The 4B6C structure was solved to a lower resolution and there are less visible amino acids at the N-termini with 18 extra amino acids being visible at the N-terminus of the A-copy, and 17 in the B-copy in the new structure presented here. Hence, we propose that this new crystal structure is an improvement over the previously published structure. As the crystallisation conditions were analogous it is not surprising that there are several similar features in both structures, one in particular is the presence of sodium ions within the structure. This is most noticeable as there is what appears to be a common sodium ion site which is present in both of the crystallographic copies where T167, G81 and D80 appear to coordinate to this sodium ion alongside one or two water molecules (Figure 5.5.2). This sodium ion site is similar to the one presented in the 4B6C structure (Shirude *et al.*, 2013), and was confirmed by the CheckMyMetal server (Zheng *et al.*, 2014, Zheng *et al.*, 2017).

Table 5.5.1: Data collection and refinement statistics of the Msm B24 sub-ATPase domain structure.

Novobiocin	
Data collection	
Space group	C2
Cell Dimensions	
a, b, c (Å)	157.08, 56.12, 50.71
α , β , γ (°)	90.00, 90.63, 90.00
Resolution (Å) ^a	24.55-1.60 (1.63-1.60)
Number of Observations ^a	391119 (19736)
Unique Observations ^a	58313 (2855)
Multiplicity ^a	6.7 (6.9)
R _{merge} (%) ^a	0.108 (2.075)
I/ σ (I) ^a	10.4 (0.9)
CC(1/2) ^a	0.999 (0.529)
Completeness (%) ^a	99.9 (100)
Refinement	
Limiting Resolution (Å)	1.60
No. of reflections	58312
R _{work} /R _{free} (%)	13.8, 20.1
Mean B-values (Å ²)	
Protein	27.06
Ligands	30.47
Ions	33.72
Waters	39.35
R. m. s. deviations	
Bond length (Å)	0.0121
Bond angles (°)	1.655
Ramachandran Plot (%)	
Favoured region	97.5
Allowed region	2.5
Outlier region	0
Novobiocin occupancy (chain A/chain B)	
Occupancy	0.96/1.00
RSCC	0.93/0.93

^a Values in parentheses refer to the outer shell

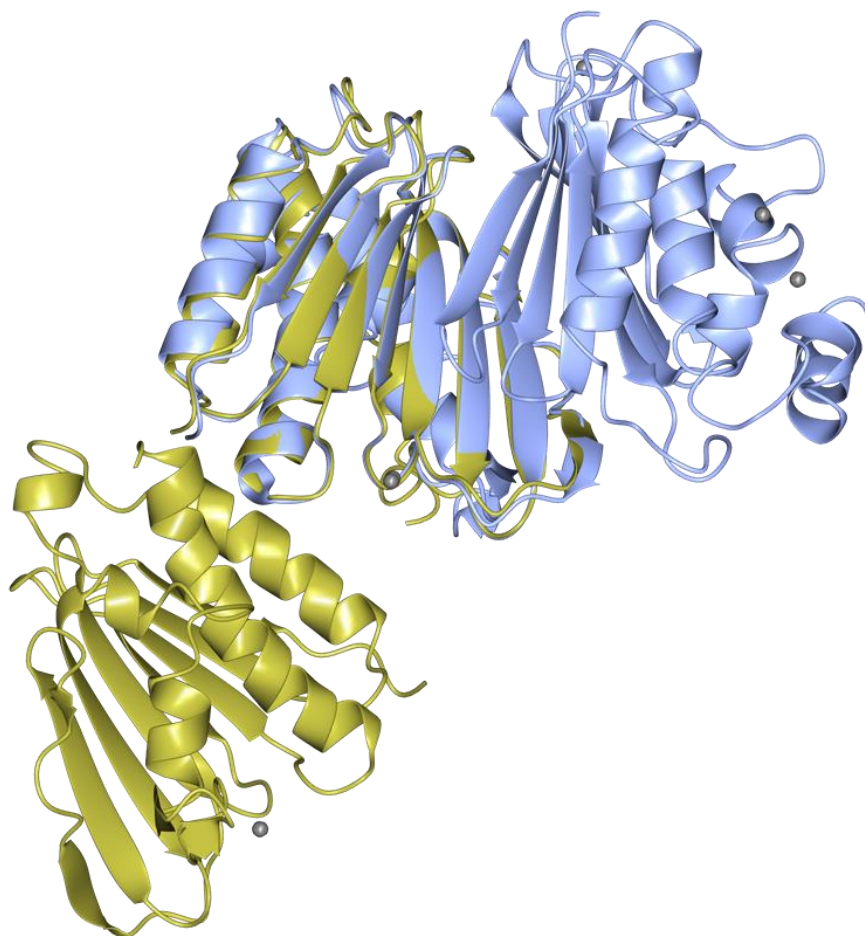


Figure 5.5.1: Comparison of the crystallographic subunit interfaces of the published 4B6C structure (gold) and the new structure of the Msm GyrB24 ATP sub-domain double loop deletion construct (blue). These structures have a high-degree of structural homology, including a shared sodium ion site.

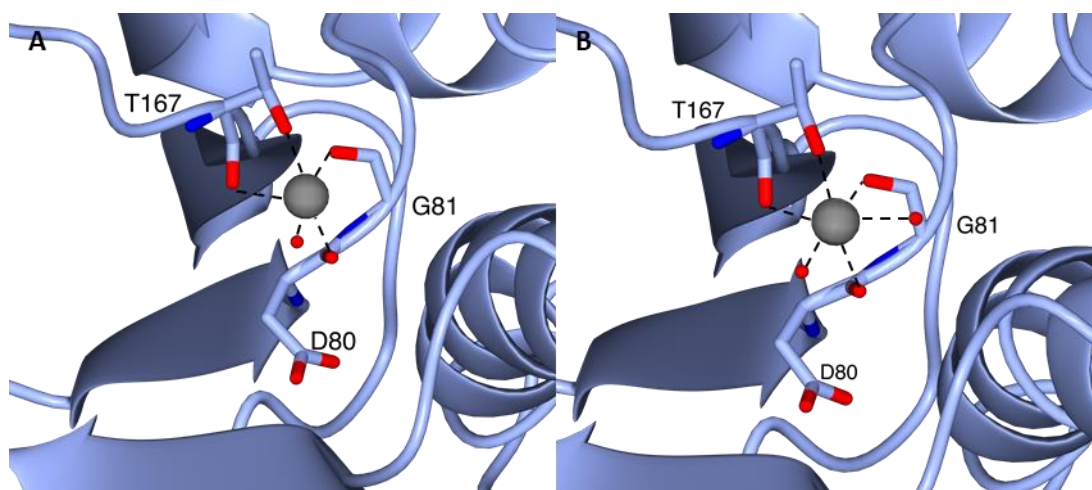


Figure 5.5.2: Visualisation of the differences in the sodium ion sites of the A and B chains within the Msm GyrB24 ATPase sub-domain structure. Interactions shown are of 2-3 Å. A) shows the interactions in the A chain that only involves the mainchain of T167, G81, D80 and the side chain of T167 and a single water molecule, in a square planar geometry. Whereas B) shows the interactions to the B chain that also a second water molecule, changing the geometry of this binding site to octahedral.

The overall protein backbone is in general agreement between the published 4B6C structure and the new structure presented here. There are several amino acids that appear to fall in alternative conformations throughout the protein, including one surrounding the ligand binding site E48, suggesting the orientation of this residue may be based on the ligand bound. The only major significant difference in the protein backbone is the modelling of a section of an alternative conformation between residues 97-127 which is around one of the loop deletions (103-122) suggesting some flexibility in this area.

In addition to the common sodium ion found in the 4B6C structure, there are two additional possible sodium ions found within the B-chain but not within the A-chain. These appear to coordinate to 5 and 6 atoms respectively at distances between 2-3 Å, with a high degree of hydrogen bonding to water molecules, involving just one amino acid each (Figure 5.5.3). The interactions are with the carboxylic acid functional group of glutamic acid 46 and the mainchain of threonine 33 respectively. Although, it has not been assigned as such, due to the proximity of these binding sites, it is possible that this was a single dual conformation sodium ion. It is important to note that there is no visible density for either of these sites on the A chain and hence this is likely to be an artefact of crystallisation.

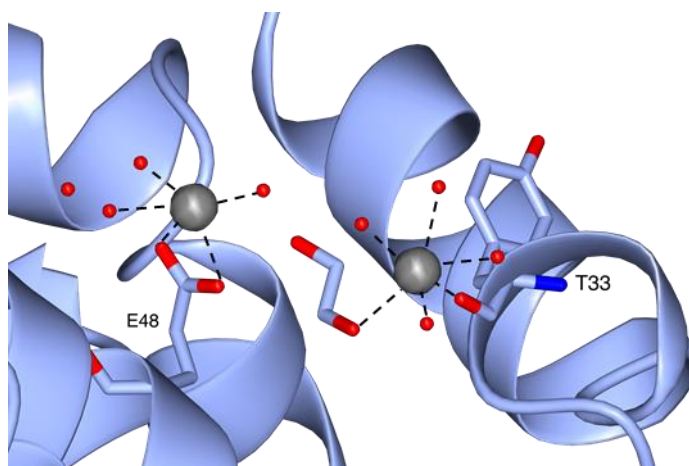


Figure 5.5.3: Visualisation of the third and fourth possible sodium ion sites on the B chain. All interactions shown here are between 2-3 Å in distance. The first of these appears to hydrogen bond to the carboxylic acid group of E48 and three water molecules including one of half occupancy, in an octahedral coordination. The second sodium forms a hydrogen to the mainchain oxygen of T33 and four water molecules, as well as an ethylene glycol in the crystal. The binding geometry is octahedral.

As novobiocin was required for crystallisation of the Msm GyrB24 sub-ATPase domain we were able to locate significant density to fit most of novobiocin into. This density was confirmed by generating an omit map through the use of simulated annealing (Cartesian) in the absence of novobiocin on the final refined structure. The omit map clearly demonstrated positive electron density in the region of the ligand which novobiocin could clearly be modelled into (Figure 5.5.4). Considering the density fit, in the structure presented here we observe novobiocin bound in the same binding site as previously observed in previous work (Lewis *et al.*, 1996, Holdgate *et al.*, 1997, Tsai *et al.*, 1997). This binding site involves several interactions including the key resistance arginine at position 141 (Figure 5.5.5), with a binding distance of 2.99 Å. The R141 residue also forms a hydrogen bond of around 2.8 Å to G83 which has also been implicated in the resistance mechanism of novobiocin through mutation to a serine. From examining the structure, the serine side chain substitution at position 83 is most likely to be pointing away from the novobiocin ring. Therefore, it is difficult to see why this is likely to occur, although it is theorised here that it causes a change in the conformation of R141 due to hydrogen bond interactions to the serine destabilising the interaction that R141 has with novobiocin.

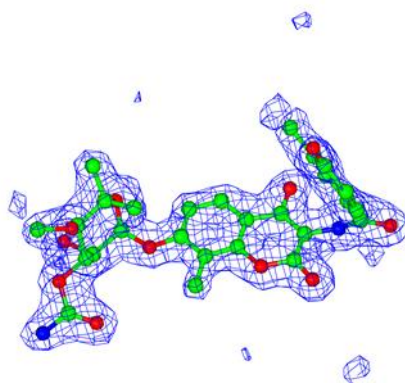


Figure 5.5.4: An omit map of the novobiocin within the structure of Msm GyrB24 crystallised in the presence of novobiocin. The omit map was made by simulated annealing (Cartesian) of the final refined structure with novobiocin removed (phenix) (Adams *et al.*, 2010). The omit map (blue chicken wire) was clipped to 5 Å around the novobiocin in the A chain, at a sigma value of 3. The figure was created within CCP4MG.

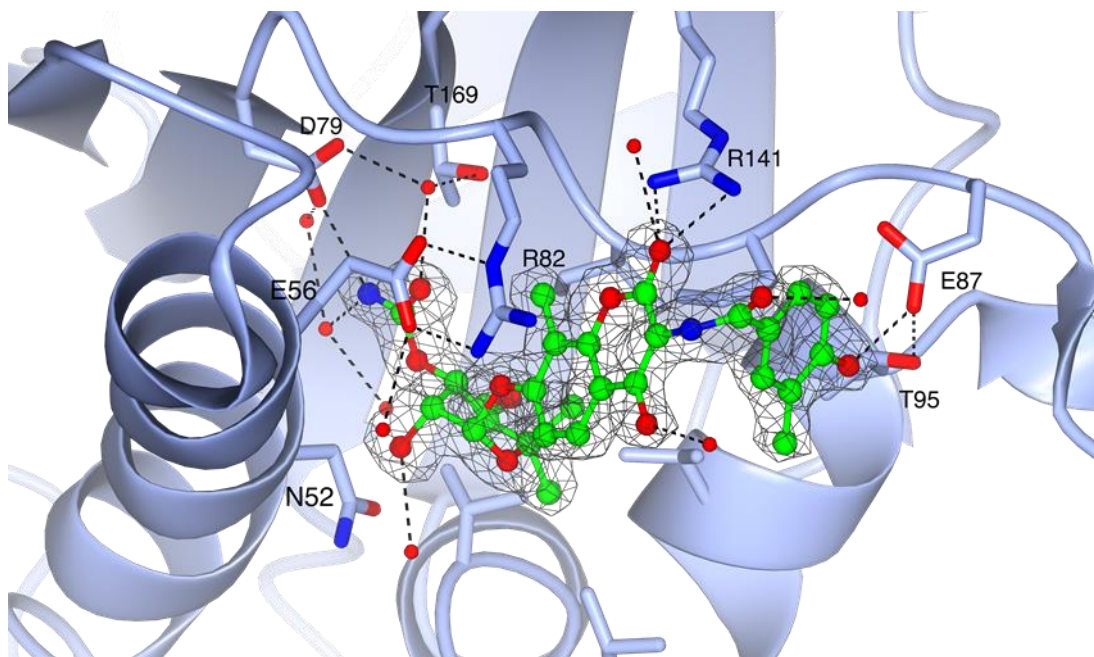


Figure 5.5.5: Bonding interactions involved in the interaction of novobiocin with Msm GyrB. Hydrogen bonding interactions are represented as dashed lines. The density around novobiocin (grey chicken wire) is shown to 1.5σ on the $2F_o - F_c$ map. D79, E87 and R141 form direct interactions with novobiocin, meanwhile the salt bridge between E56 and R82 is also depicted.

The Aspartate at residue 79 also forms a hydrogen bonding interaction to novobiocin of 2.8 \AA , as does E87 with a distance of 2.45 \AA (Figure 5.5.5). Previously N52 has been attributed to being involved in the mechanism of binding by novobiocin (Kampranis *et al.*, 1999b). In the model shown here we can attribute this through a water bonding network also involving D79. Other residues including T169 and T95 also interact with novobiocin through means of a hydrogen-bonding network. It should be noted that in the tuberculosis GyrB protein E87 is an alanine and hence is unlikely to form a binding interaction to novobiocin, meanwhile the threonine at position 169 is actually a serine.

A salt bridge is observed between residues of the E56 and R82 (Figure 5.5.5). This has also been previously described to be an essential interaction in the binding of ATP in *E. coli*, with mutants at these locations losing the ability to supercoil DNA, and presenting with very low ATPase activity (Gross *et al.*, 2003). Although neither of these molecules appears to form direct interactions with the novobiocin, it is very plausible that this interaction stabilised the tertiary structure of the protein and disruption of the salt bridge would disrupt the folding of the protein. Although, we are not interested in finding further resistance mutations in the scope of this work, it would be interesting to see if the ATPase activity, supercoiling activity and

subsequently the novobiocin binding were maintained if the amino acids and hence the charges were reversed.

Analysing the positions of the bacterial mutants isolated in *E. coli*, *S. aureus*, *S. pneumoniae*, and *Halophilic archaeobacterium* against novobiocin (Table 1.8.1) only the interactions of R141 and E87 can explain the resistance phenotype of their corresponding mutations observed in whole cells (Figure 5.5.6). Additionally, the S128L *S. aureus* and *S. pneumoniae* mutations (Munoz *et al.*, 1995, Stieger *et al.*, 1996) can likely be explained through unfavourable steric interactions preventing the favourability of the binding of novobiocin when replacing the corresponding V125 residue with the larger leucine (Figure 5.5.6).

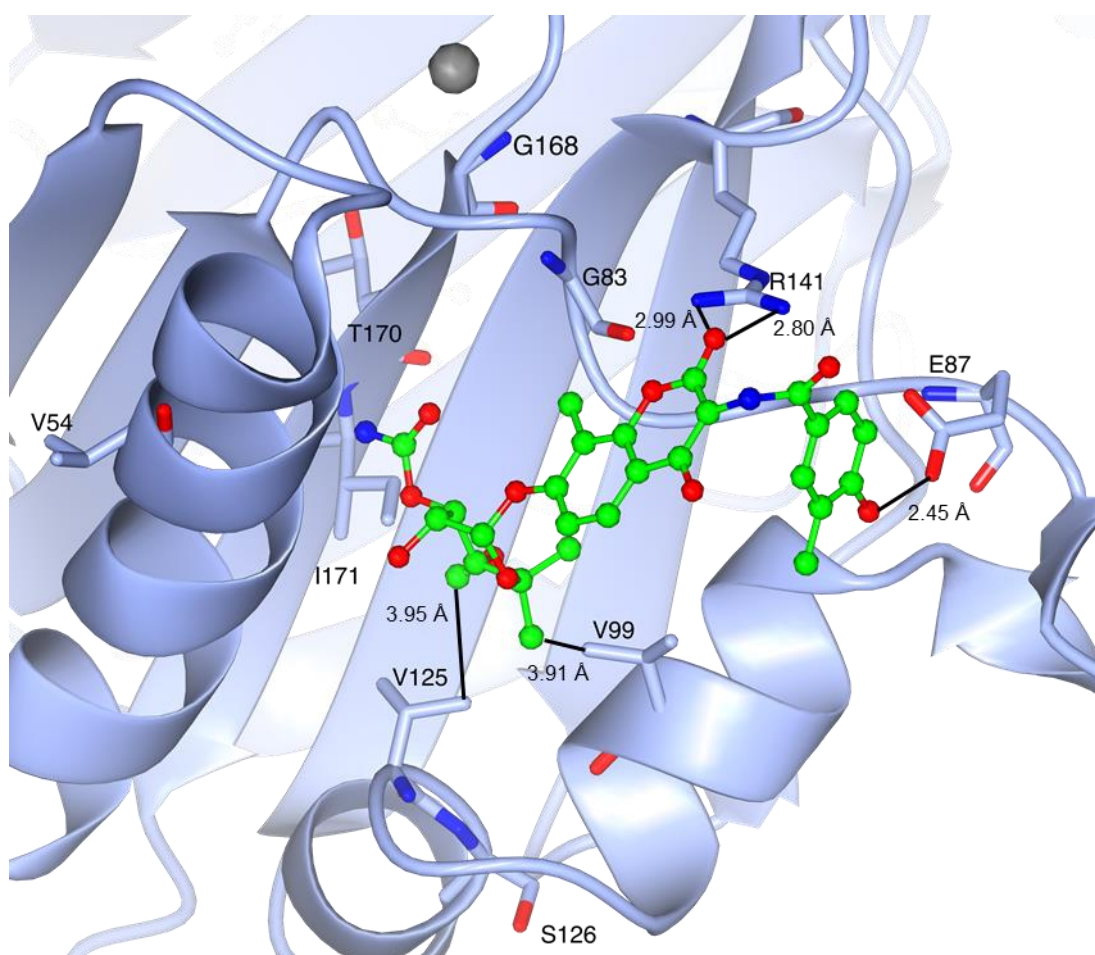


Figure 5.5.6: Visualisation of all the novobiocin mutants isolated from bacterial strains including potential hydrogen bonds. Many of the single point mutations do not appear to directly interact with novobiocin.

Many of the other mutations that have been observed in bacteria do not give obvious direct interactions with novobiocin (Figure 5.5.6). These interactions are most likely explained through hydrogen bonding networks formed from the presence of ordered water molecules, and more long-range conformational changes that prevent novobiocin binding that do not influence the binding of ATP.

5.6 Crystallisation trials of *M. thermoresistibile* B24 ATPase subdomain

Due to the difficulties with crystallising the Mtb GyrB24 sub-ATPase domain with either of the two Redx compounds or novobiocin and due to the additional characterisation work that we have carried out on *M. thermoresistibile* in previous chapters, it was decided to design a Mth construct of the sub-ATPase domain. This novel construct of the Mth homologue was designed to be comparable to the Msm construct and therefore this construct also had the two flexible loops deleted. Furthermore, as mycobacteria have high GC content in their genomes (Wayne and Gross, 1968), it was decided to use a codon-optimised construct which was synthesised by Invitrogen GeneArt (ThermoFisher Scientific). The coding sequencing was subsequently sub-cloned into the pET28-MHL vector at the BseRI sites. The protein was successfully expressed in the transformed *E. coli* BL21 cell line in 6 L LB induced with 0.4 mM IPTG at 30°C for 4.5 hours. The protein was purified to the same method as the Msm protein yielding 250 mg purified protein.

Initially, the protein was screened against the JCSG-*plus*TM, KISS and SG1TM HT-96 screens in the presence and absence of 1 mM novobiocin. Three initial conditions were obtained yielding crystals which were further optimised, two of which were subsequently determined to be salt by X-ray diffraction. Meanwhile as the third could not be reproduced it was decided to rescreen against the Morpheus®, the BCS screen and the PGA screenTM 96-well sparse matrix screens. Three further hits were obtained (Table 5.6.1), two of which were optimised and found to produce crystals within 12 hours. These crystals were found to be highly reproducible but not UV fluorescent although they were confirmed to contain protein by harvesting and washing crystals before performing SDS-PAGE (Figure 5.6.1).

Table 5.6.1: Crystal screening conditions yielding suspected protein crystals from the second iterative round of screening of the Mth GyrB24 DLD construct at 22 mg/ml.

Screen	Sub-well	Well conditions
The BCS screen	1 mM novobiocin	100 mM zinc acetate 100 mM zinc chloride 100 mM Bis-Tris pH 7.5 20% (w/v) PEG smear medium*
The BCS screen	1 mM novobiocin	100 mM ammonium acetate 100 mM zinc chloride 100 mM Bis-Tris pH 7.2 15% (w/v) PEG smear high^
The PGA screen™	1 mM novobiocin	100 mM sodium acetate 5% (w/v) γ-PGA (Na ⁺ form) 8% (W/V) PEG20000

*PEG Smear medium refers to a combination of 1:1:1:1 mix of PEG2000: PEG3350: PEG4000: PEG5000MME

^PEG Smear high refers to a combination of a 1:1:1 mix of PEG6000: PEG8000: PEG10000

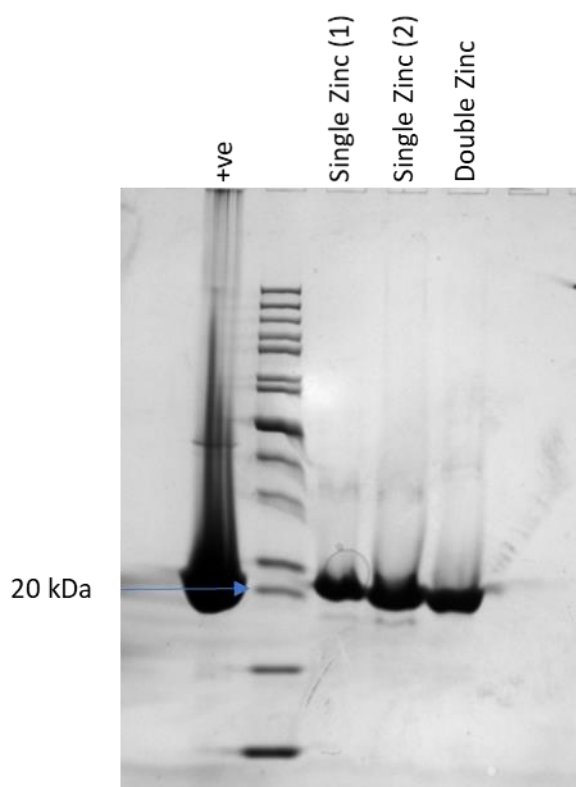


Figure 5.6.1: SDS-PAGE gel run with pure Mth GyrB24 DLD protein and crystals washed four times with well solution before adding loading dye, boiling solutions and loading onto 12% Bis-Tris SDS-PAGE. +ve refers to a pure protein sample of 20.8 kDa. Single zinc refers to crystals grown in conditions optimised from the BCS screen condition 100 mM ammonium acetate, 100 mM zinc chloride, 100 mM Bis-Tris pH 7.2, 15% (w/v) PEG smear high. Double zinc refers to crystals grown in conditions optimised from the BCS screen condition 100 mM zinc acetate 199 mM zinc chloride 199 mM Bis-Tris pH 7.5, 20% (w/v) PEG smear medium. Unambiguous evidence is observed for the crystals to contain protein.

Optimised crystals grown in 100 mM zinc chloride, 100 mM ammonium acetate, 14% (w/v) PEG smear high (1:1:1 mix of PEG6000:PEG8000:PEG10000) and 100 mM Bis-Tris pH 7.0 were harvested and flash frozen with the assistance of CS in the crystallisation solution supplemented with 25% (v/v) ethylene glycol and 1 mM novobiocin (Figure 5.6.2).

To obtain the crystal structure bound to Redx03863 further novobiocin crystals grown in 100 mM zinc chloride, 100 mM ammonium acetate, 15% (w/v) PEG smear high, 100 mM Bis-Tris pH 7.5 were harvested in 50 μ l of well solution and vortexed at maximum power with one to three 1 mm glass beads (Sigma-Aldrich) for 4 min to crush the crystals. Redx03863 was added to the seeding stock to a final concentration of 0.24 mM. Screening was repeated over the pH range 7-7.5 and 10-20% (w/v) PEG smear high, with drops containing 300 nl of

22 mg/ml Mth GyrB24 DLD supplemented with 0.24 mM Redx03863, 200 nl well solution and 100 nl seed stock supplemented with 0.24 mM Redx03863. Crystals grew optimally in 11% (w/v) PEG smear high and Bis-Tris pH 7.3 were harvested and flash frozen in mother liquor supplemented with 25% ethylene glycol and 0.24 mM Redx03863 with the assistance of CS (Figure 5.6.3).

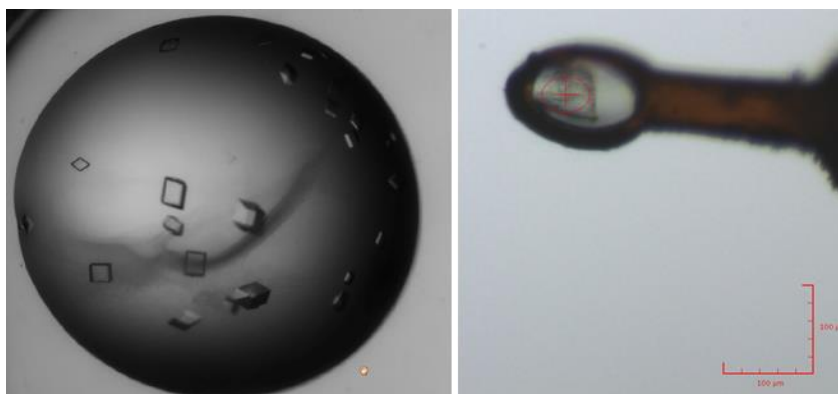


Figure 5.6.2: Image of crystals of Mth GyrB24 DLD co-crystallised with novobiocin before harvesting from the well for X-ray diffraction (left), and in the loop for crystal screening at the Diamond synchrotron beamline i03 (right). Crystals grown in 100 mM zinc chloride, 100 mM ammonium acetate, 14% (w/v) PEG smear high, 100 mM Bis-Tris pH 7.0 at protein concentration 22 mg/ml supplemented with 1 mM novobiocin. No UV absorbance was observed from the crystals.

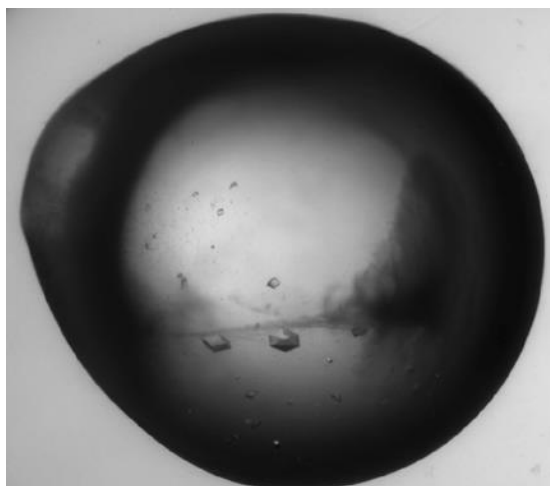


Figure 5.6.3: Image of crystals of Mth GyrB24 DLD co-crystallised with Redx03863 before harvesting from the well for X-ray diffraction. Crystals grown in 100 mM zinc chloride, 100 mM ammonium acetate, 11% (w/v) PEG smear high, 100 mM Bis-Tris pH 7.3 at protein concentration 22 mg/ml supplemented with 0.24 mM Redx03863. No UV absorbance was observed from the crystals.

Equivalent screening was performed with Redx04739 to attempt to obtain the crystal structure bound to Redx04739, however, no crystals were obtained when Redx04739 was supplemented at 0.29 mM to the protein solution and seeding solution. When an apo protein solution was crystallised with a seeding supplemented with 0.29 mM Redx04739 small crystals were obtained, but when the diffraction data was analysed they were found to only contain novobiocin and not Redx04739. Further optimisations were attempted using a seed stock that was washed prior to crushing the crystals but no crystals were obtained using this method. Overall, unfortunately it was determined that the solubility of this compound was too low at the crystallisation conditions to obtain crystals with Redx04739.

5.7 X-ray diffraction and structure resolution of *M. thermoresistibile* B24 ATPase subdomain

Data from the Mth GyrB24 ATPase domain crystals were collected on the i03 beamline at the Diamond light source. From the collected data the structures of Mth B24 sub-ATPase domain were solved using a preliminary Msm B24 sub-ATPase domain as the model for molecular replacement. Subsequent rounds of manual and automated refinement using COOT and REFMAC were completed until the structures gave optimal density fit and conformation (Table 5.7.1). Both structures were found to contain unit cells of similar parameters and were assigned to the same space group P12₁1.

The overall structure of the Mth domain presented as two copies of the protein present within the unit cell forming a non-biological dimer connected by two zinc binding sites (D51, D55 from one chain and H44 from the other) (Figure 5.7.1). Two further zinc-binding sites were observed in the structure bound to novobiocin, each of which appeared to be of split conformation likely depending on the conformation of a single histidine residue (61) (Figure 5.7.2). In the structure containing Redx03863 an additional zinc binding site was observed binding to H257 (Chain B). The zinc sites were confirmed by collecting data at the zinc edge wavelength 1.2782 Å. None of the zinc-binding sites found here contain a sodium ion in the Msm previously presented in this chapter.

Table 5.7.1: Table of crystallographic statistics for the structures of Mth GyrB24 sub-ATPase domain bound to novobiocin and Redx03863.

	Novobiocin	Redx03863
Data collection		
Space group	P 1 2 ₁ 1	P 1 2 ₁ 1
Cell Dimension		
a, b, c (Å)	43.99, 51.12, 83.22	43.77, 51.67, 82.91
α, β, γ (°)	90.00, 100.32, 90.00	90.00, 100.25, 90.00
Resolution (Å) ^a	51.12-1.4 (1.42-1.4)	51.67-1.50 (1.53-1.50)
Number of Observations ^a	472775 (22964)	374605 (18170)
Unique Observations ^a	71674 (3549)	58503 (2863)
Multiplicity ^a	6.6 (6.5)	6.4 (6.3)
R _{merge} (%) ^a	0.048 (1.405)	0.060 (1.455)
I/σ (I) ^a	16.6 (1.3)	12.6 (1.2)
CC(1/2) ^a	0.999 (0.665)	0.999 (0.675)
Completeness (%) ^a	99.9 (100)	100 (99.9)
Refinement		
Limiting Resolution (Å)	1.4	1.5
No. of reflections	64550	58485
R _{work} /R _{free} (%)	14.0, 19.0	14.5, 20.2
Mean B-values (Å ²)		
Protein	30.5	26.5
Ligands	32.3	26.5
Ions	29.8	35.3
Waters	41.6	39.1
R. m. s. deviations		
Bond length (Å)	0.011	0.010
Bond angles (°)	1.56	1.54
Ramachandran Plot (%)		
Favoured region	97.7	96.5
Allowed region	2.3	3.5
Outlier region	0	0
Ligand Occupancy (chain A/chain B)		
Occupancy	1.00/0.94	0.99/0.92
RSCC	0.96/0.95	0.91/0.94

^a Values in parentheses refer to the outer shell

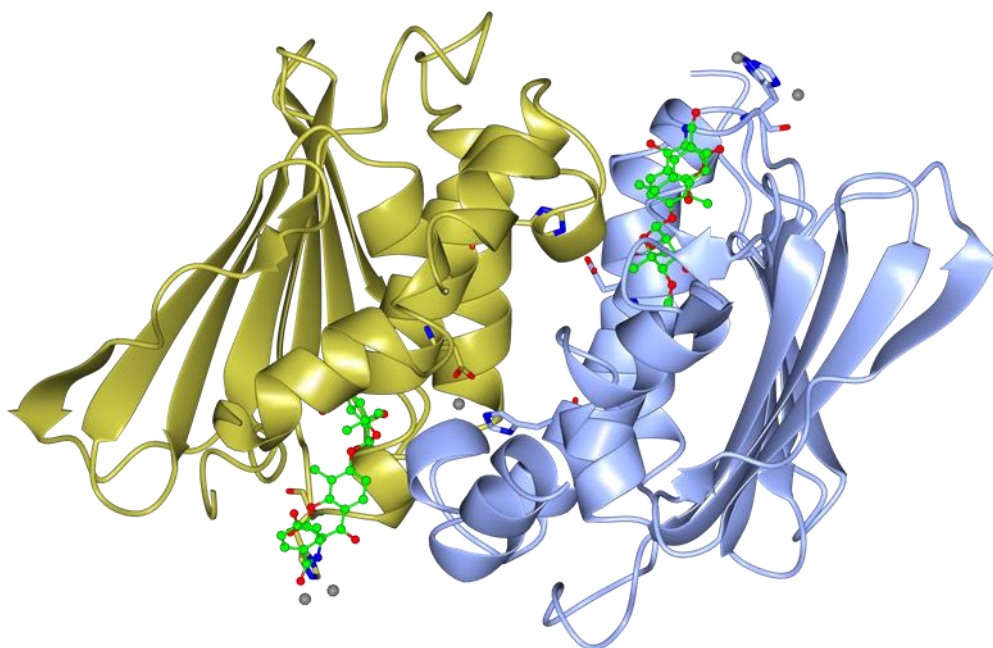


Figure 5.7.1: Overview of the Mth GyrB24 sub-ATPase domain structure bound in the crystallographic dimer bound to 4 zinc ions including two bound between the non-biological dimer interface, and additionally two novobiocin molecules (one per chain of GyrB).

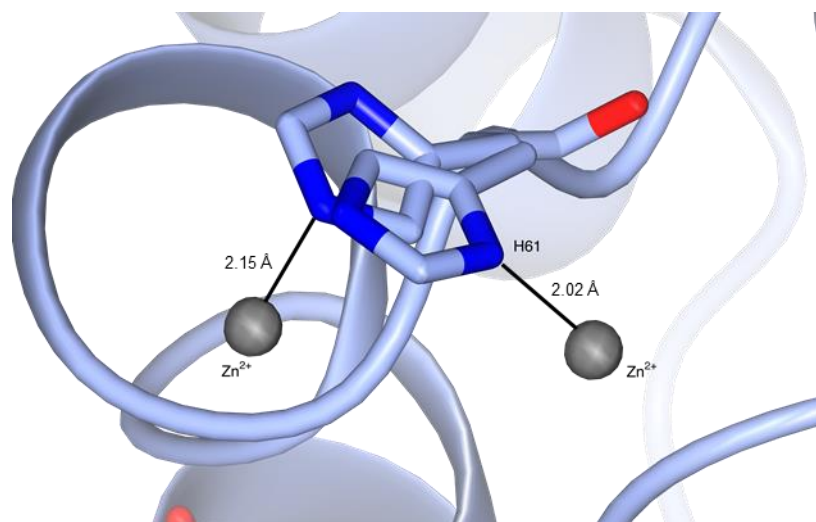


Figure 5.7.2: The dual conformation zinc binding site at Histidine 61 in the A chain of the novobiocin-bound Mth GyrB24 sub-ATPase domain structure. The histidine binds to half occupancy zinc ions in two different conformations. The binding sites in the B chain are also dual conformation although the histidine is in a single conformation. A similar arrangement is present in the Redx03863 bound structure.

The protein backbone of the two structures is in very strong agreement with only 3 amino acid sidechains being modelled in alternative conformations across the A chain, and 6 alternative conformations in the B chain. Interestingly, N52 was seen to be in a different conformation in the two structures like the Msm structures, suggesting that the orientation of this ligand may be dependent on the ligand bound.

As both crystal structures were crystallised in the presence of ligands we confirmed the presence of the ligands in their respective structures through the use of simulated annealing (Cartesian) on the final structure in the absence of the ligand. The resulting electron density map showed positive density in the region of the ligands matching novobiocin and Redx03863 respectively (Figure 5.7.3). This suggested that our mapping of the ligands was correct.

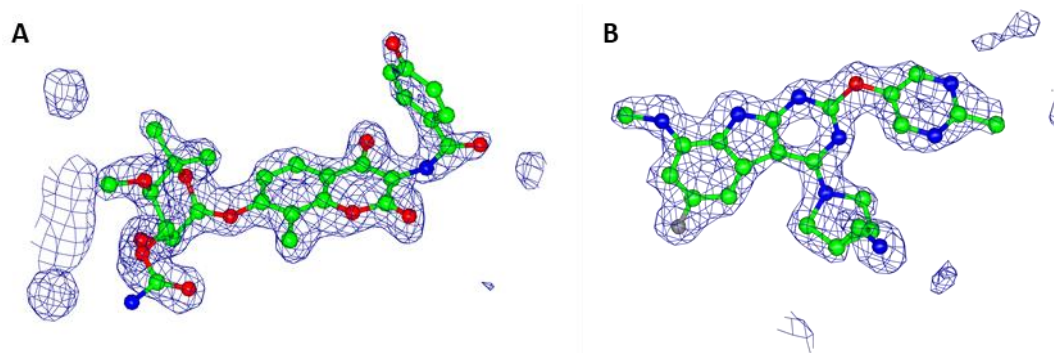


Figure 5.7.3: An omit map of the ligands within the structures of Mth GyrB24 crystallised in the presence of A) novobiocin and B) Redx03863. The omit maps were made by simulated annealing (Cartesian) of the final refined structure the respective ligand removed (phenix) (Adams *et al.*, 2010). The omit maps (blue chicken wire) were clipped to 5 Å around the ligands on the A chain, at a sigma value of 3. The figure was created within CCP4MG.

Analysing the novobiocin-binding structure, the key binding interaction of R141 that has been identified in many studies in many different species as giving resistance to novobiocin (del Castillo *et al.*, 1991, Holmes and DyalSmith, 1991, Contreras and Maxwell, 1992, Stieger *et al.*, 1996, Kampranis *et al.*, 1999b) is again clearly shown to be forming hydrogen bonding interactions with the novobiocin in this structure at a distance of 3.07 Å. Additionally D79 has also been identified to be involved in the binding interactions of novobiocin and again in this new structure there is evidence that a hydrogen bond exists (2.9 Å) between the carboxylic head group of the aspartic acid and the amide functional group on the novobiocin (Figure 5.7.4). Other amino acids that give rise to resistance mutants (Table 1.8.1) are also shown in

Figure 5.7.4, although many of them do not appear to give direct binding interactions in the Mth structure including H89, V99, V125, and S126. There is no clear evidence as to how N52, G83, G168, and V171 influence the binding of novobiocin from this structure, however, they do appear to be in close proximity to the novobiocin binding site and inserting a bulky amino acid into many of these groups may cause a steric clash preventing novobiocin from binding especially in the case of both of the glycine residues. The biological mutant of G168 was found to be a valine (Contreras and Maxwell, 1992) meanwhile the G83S mutant was discovered in resistant *S. aureus* (Stieger *et al.*, 1996). Likewise, the V171 mutant was also raised against *S. aureus* where the biological mutant was I175T which could easily cause electrostatic repulsion to novobiocin in its current conformation. Finally N52 was a mutant that was examined in binding studies by SPR and there are suggestions that altering the charge state at this amino acid could alter binding interactions and the tertiary structure preventing binding, although it is important to consider that in *E. coli* this mutant was not found to be biologically relevant as mutations resulted in an enzyme that was unable to supercoil DNA (Kampranis *et al.*, 1999b).

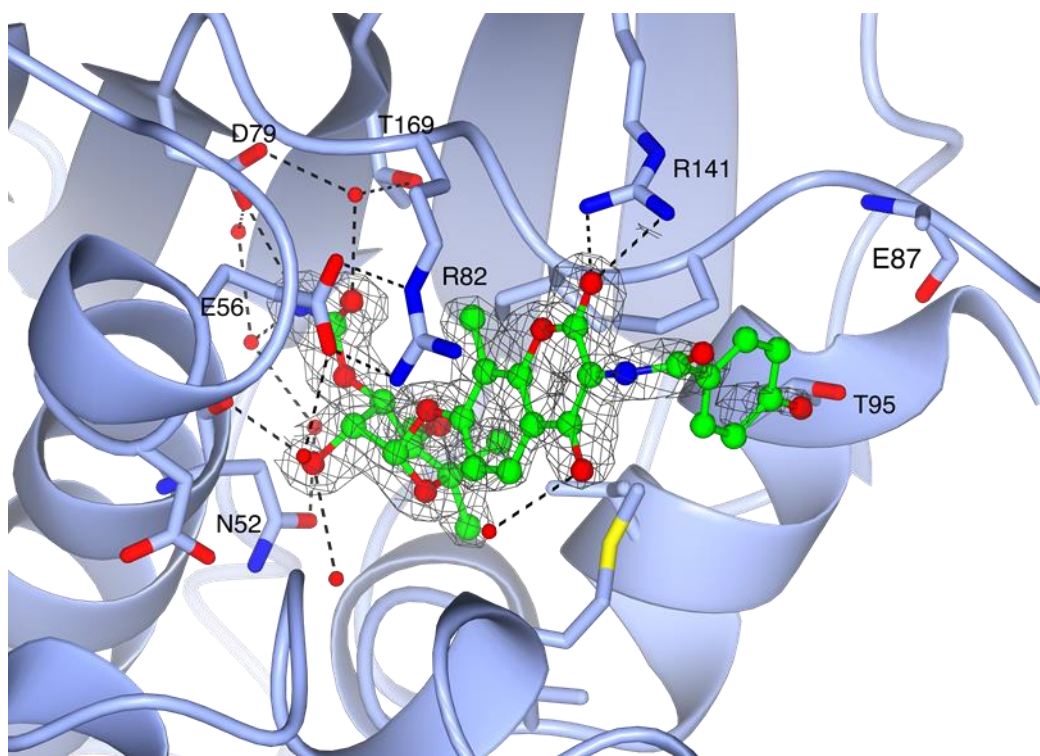


Figure 5.7.4: Visualisation of the novobiocin-binding site in the Mth GyrB24 sub-ATPase domain structure. Electron density is shown for the 2F_o-F_o map at 1.5 σ (grey chicken wire). Hydrogen bonds are displayed as dashed lines, including hydrogen bonds between D79, T95 and R141 with novobiocin. The salt bridge between E56 and R82 is also shown.

Overall the structure of the Mth GyrB24 sub-ATPase domain is similar to the others already published within the PDB. Additionally, the binding site presented here is in reasonable agreement with previously published binding sites of novobiocin in both the *E. coli* and *S. aureus* crystal structures implying the correct site has been previously identified (Lewis *et al.*, 1996, Holdgate *et al.*, 1997, Tsai *et al.*, 1997) and that this structure was an appropriate structure to utilise for identification of the binding sites of the two Redx compounds.

Analysis of the structure containing Redx03863 indicated that there were significantly different binding interactions between novobiocin and Redx03863, with G83 and N52 forming closer binding interactions with Redx03863 of around 4 Å (Figure 5.7.5). Like novobiocin D79 appears to form a binding interaction of around 2.8 Å to Redx03863 but in contrast the key R141 amino acid does not appear to play a significant role in the binding of Redx03863 (Figure 5.7.5). Other possible interactions include those of E56, and T169 like within the published structure of another TriBE compound in *E. faecalis* GyrB with hydrogen bond distances of around 3.3-3.8 Å (Figure 5.7.5) (Tari *et al.*, 2013a). However, T169 is a serine within the tuberculosis protein. Additionally, R82 is likely to coordinate through salt bridge that is observed with E56 to Redx03863 (Figure 5.7.5).

One interesting interaction that has been observed within the crystal structure is that of the glycine at position 83. This residue has been previously observed to cause resistance to novobiocin when mutated to a serine (Stieger *et al.*, 1996, Gross *et al.*, 2003, Fujimoto-Nakamura *et al.*, 2005), and cross-resistance to novobiocin was obtained in a strain presenting with the G83S mutation (Chapter 4). Analysis of the structure presented here demonstrates a possibility that the mainchain amino group of this residue could interact with the ether group in Redx03863, meanwhile the carboxyl oxygen may interact with one of the nitrogen atoms on the terminal pyrimidine group (Figure 5.7.6). In addition, the alpha carbon is located between 4-5.5 Å away from several atoms within Redx03863 indicating that there is the potential for further interactions. Although, it is unclear what orientation the serine group would take in mutated versions of GyrB, there is good scope to alter several interactions directly or indirectly with Redx03863 by mutating the glycine to a serine. There are similar interactions in the 4KSG structure containing C4 from the original TriBE series by Trius Therapeutics (Figure 5.7.6b) (Tari *et al.*, 2013a). Overall, there is considerable evidence from the crystallographic structures presented here that the G83 residue could be involved in the binding of Redx03863 and other compounds within the series including Redx04739.

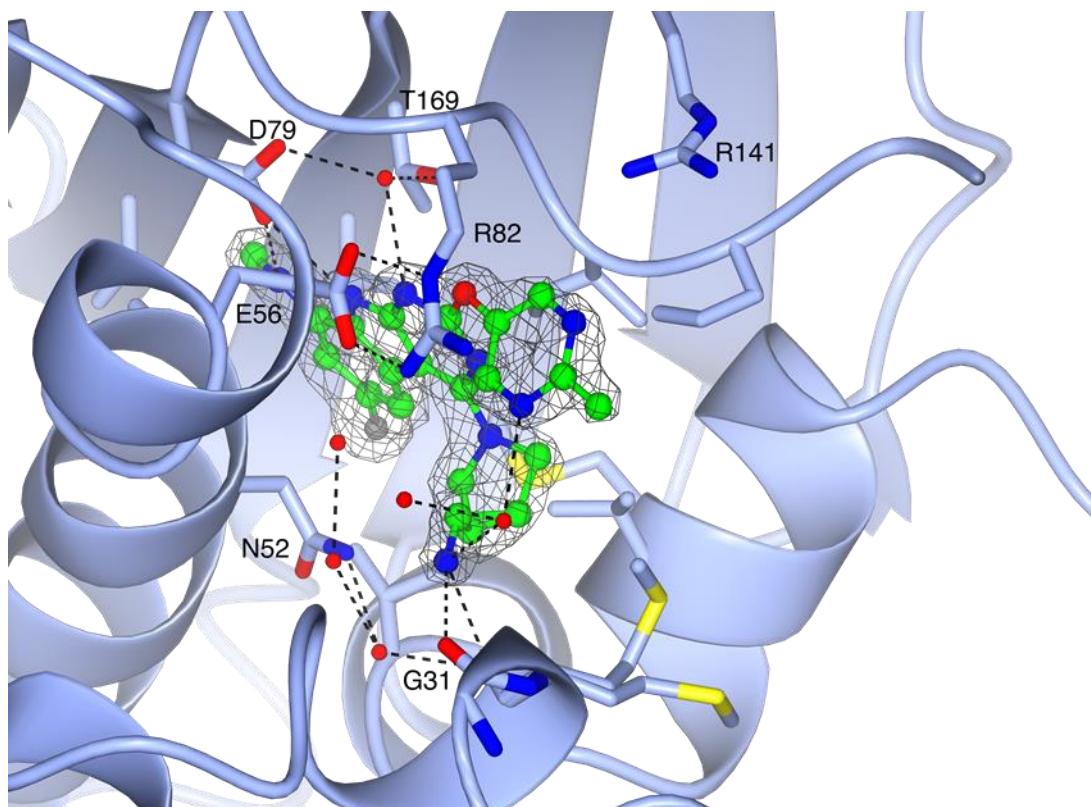


Figure 5.7.5: Binding site of Redx03863 within the Mth structure. Electron density is shown for Redx03863 at a sigma level $\sigma = 1.5$ for the 2FcFo map. Hydrogen bonding interactions are indicated by dashed lines, as is the salt bridge between E56 and R82. Direct interactions are indicated for G31 and D79 but not R141.

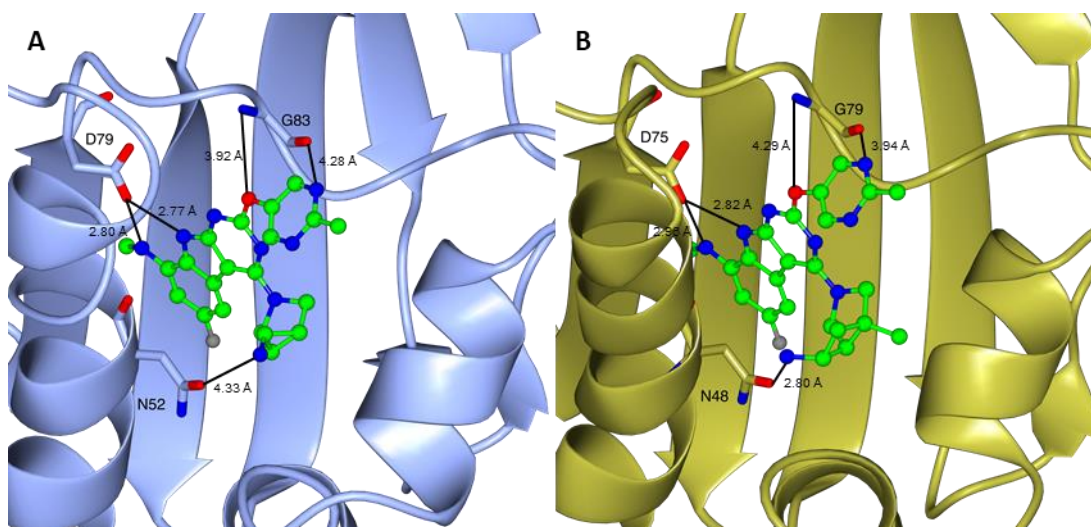


Figure 5.7.6: Detailed interactions of A) N52, D79 and G83 in Redx03863 bound structure of Mth GyrB (sub-ATPase domain) and B) N48, D75 and G79 in the C4 bound structure of *E. faecalis* GyrB24 (4KSG). All amino acid residues are labelled to the native proteins.

5.8 Site-directed mutagenesis of Mtb DNA gyrase based on the structure of *M. thermoresistibile* B24 ATPase subdomain bound to Redx03863

To confirm the binding pocket of Redx03863 and likely Redx04739 we sought to find a mutant that inhibited the action of the compounds. Based on the crystal structure of Mth GyrB24 DLD bound to Redx03863, and the published crystal structures of TriBE compounds co-crystallised with GyrB from *E. faecalis*, several residues were identified to test to confirm this binding pocket (Figure 5.7.5) (Tari *et al.*, 2013a). As the G83S mutation had already been tested in the scope of the previous chapter and showed insufficient supercoiling activity, it was decided not to test this residue further. However, seven mutants were successfully made using SDM of the GyrB plasmid, all of which expressed and were purified via the protocol for GyrB. Five of these mutants were found to be inactive in the ATP-dependent supercoiling reaction (Figure 5.8.1). This is understandable due to the proximity to the ATP binding pocket. The R141A and R141Q mutants were found to have limited activity which after optimisation was deemed suitable to test against the compounds (Figure 5.8.2). This residue has been previously demonstrated to be important in novobiocin binding and results in resistance to novobiocin (del Castillo *et al.*, 1991, Contreras and Maxwell, 1992, Stieger *et al.*, 1996) which was confirmed to be the case in Mtb (Figure 5.8.3). On the other hand, it was found that no resistance was obtained from the R141A/Q mutants when tested against either Redx03863 or Redx04739 (Figure 5.8.4); this was not an unexpected result as in the crystal structure this residue is around 4-5 Å away from Redx03863 (Figure 5.7.5).

As the crystal structure of Redx03863 appeared to have many common interactions with those of novobiocin and because many of the mutants made were deficient in supercoiling (and hence ATPase activity) we directly compared the crystal structures of the two Mth structures presented here with the known Mtb crystal structure of 3ZKB containing the non-hydrolysable ATP analogue AMP-PNP. From comparing the inhibitor binding sites to that of ATP, there is a significant degree of overlap between the two inhibitor binding sites with that of ATP, although they all have distinct binding pockets (Figure 5.8.5). This clearly indicates that the planar structure of Redx03863 interacts differently with GyrB than either novobiocin or ATP. However, there is partial overlap with the ATP-binding pocket meaning that both ATP and Redx03863 cannot bind to DNA gyrase at the same time, and as Redx03863 binds with high affinity to GyrB it is likely to outcompete ATP within the cell.

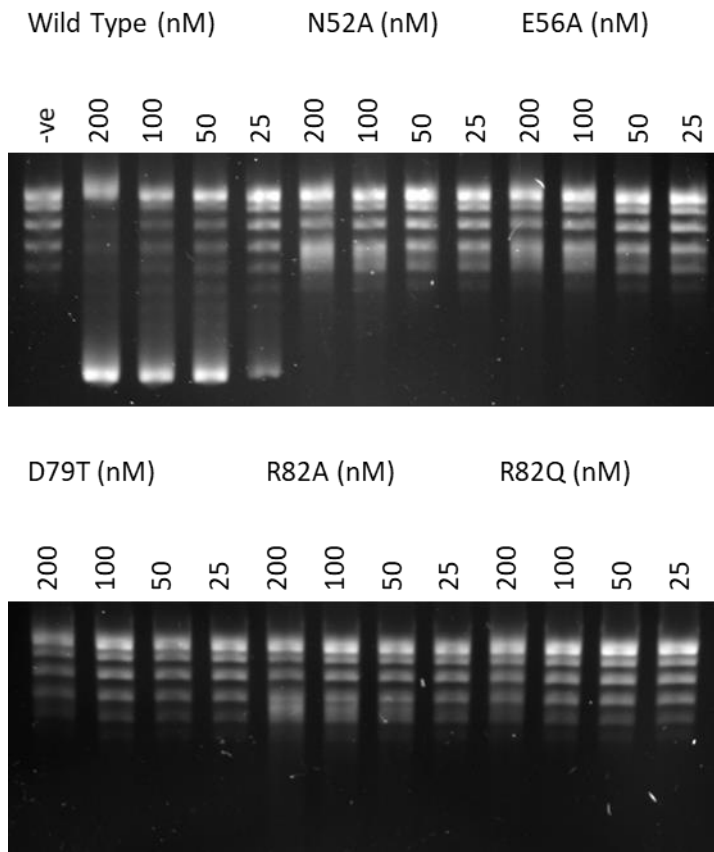


Figure 5.8.1: Activity testing of five of the seven mutants made in the GyrB subunit of Mtb DNA gyrase suggested by X-ray crystallography to be the binding location of Redx03863. Activity tested with equal concentration of GyrA and GyrB mutants over 30 minutes at 37°C. A mutant was declared inactive if it displayed no ATP-dependent supercoiling activity at 200 nM concentration under these conditions.

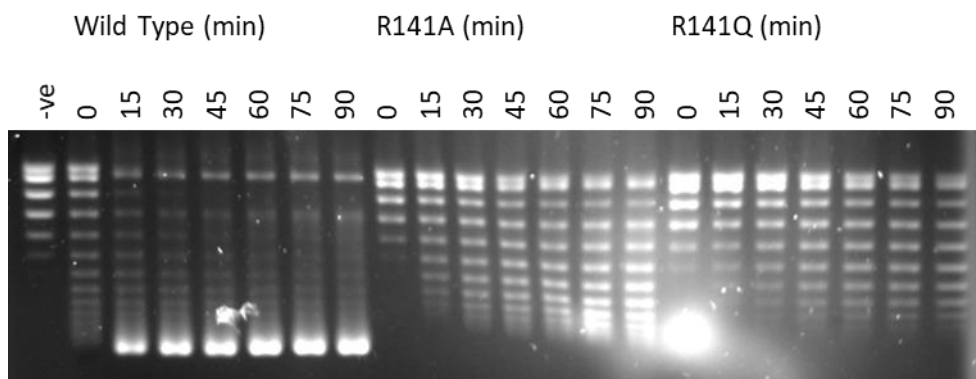


Figure 5.8.2: Time course of the activity of the Mtb GyrB^{WT}, GyrB^{R141A} and GyrB^{R141Q} mutants assayed at 74 nM with equal amounts of Mtb GyrA to optimise the supercoiling activity for compound testing. Optimal supercoiling was observed at 30 minutes GyrB^{WT}, 75 minutes GyrB^{R141A} and 60 minutes for GyrB^{R141Q}.

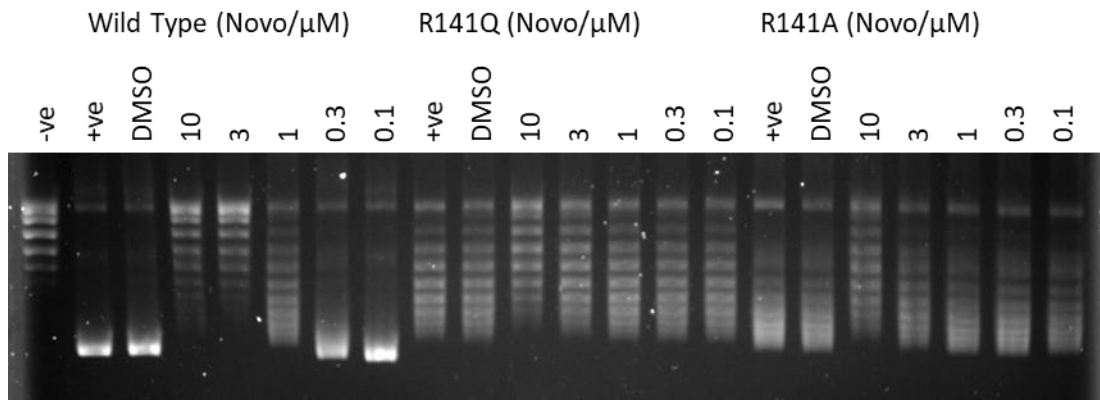


Figure 5.8.3: Inhibition of ATP-dependent supercoiling activity of 78 nM GyrB^{WT} (30 min incubation), GyrB^{R141Q} (60 min incubation), and GyrB^{R141A} (75 min incubation) with 78 nM GyrA by novobiocin at a concentration range of 0.1-10 μM .

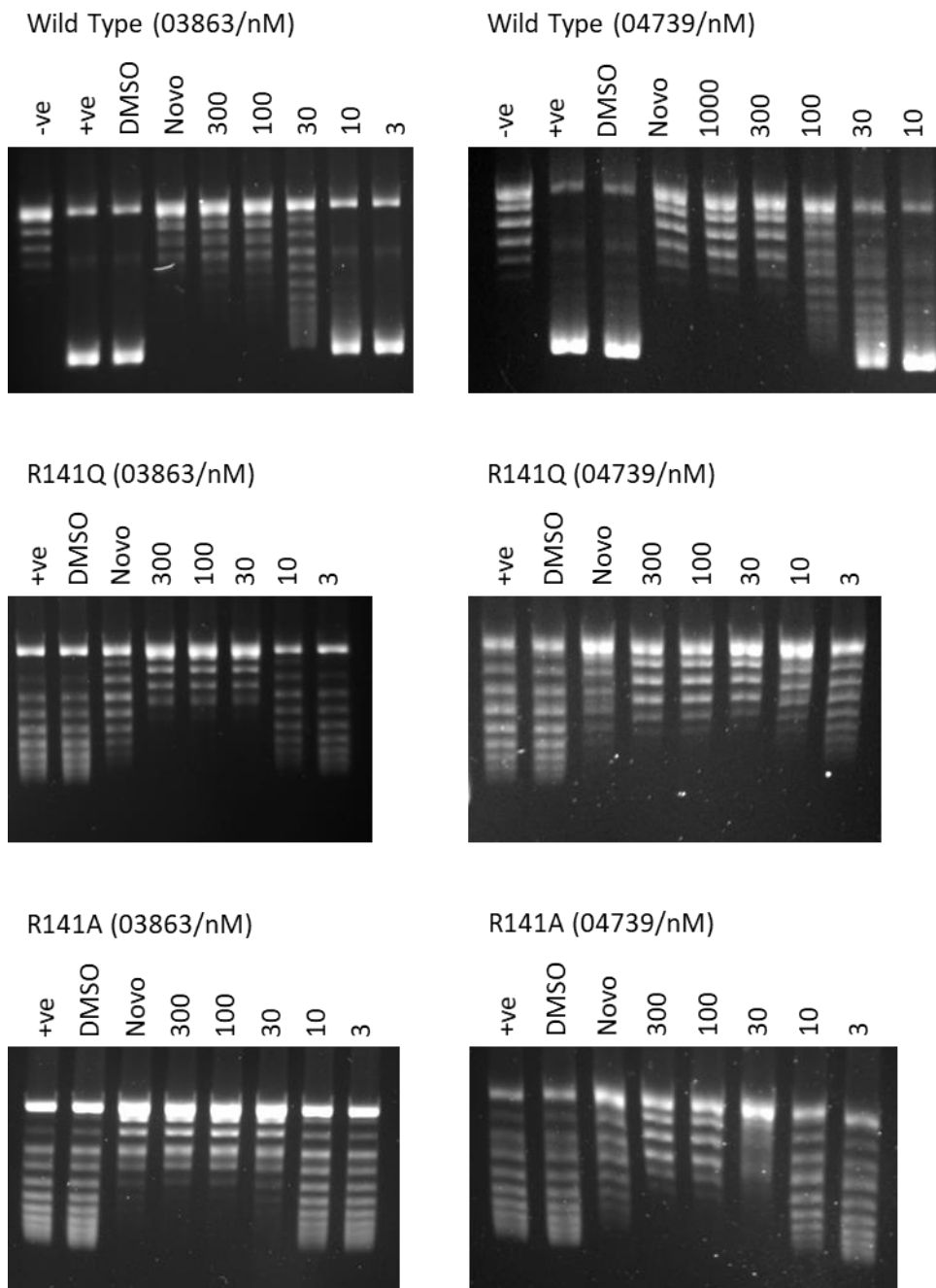


Figure 5.8.4: Inhibition of ATP-dependent supercoiling activity of 78 nM GyrB^{WT} (30 minute incubation), GyrB^{R141Q} (60 minute incubation), and GyrB^{R141A} (75 minute incubation) with 78 nM GyrA by Redx03863 at a concentration range of 3-300 nM and Redx04739 at a concentration range of 10-1000 nM. No resistance was observed in response to the R141A/Q mutations.

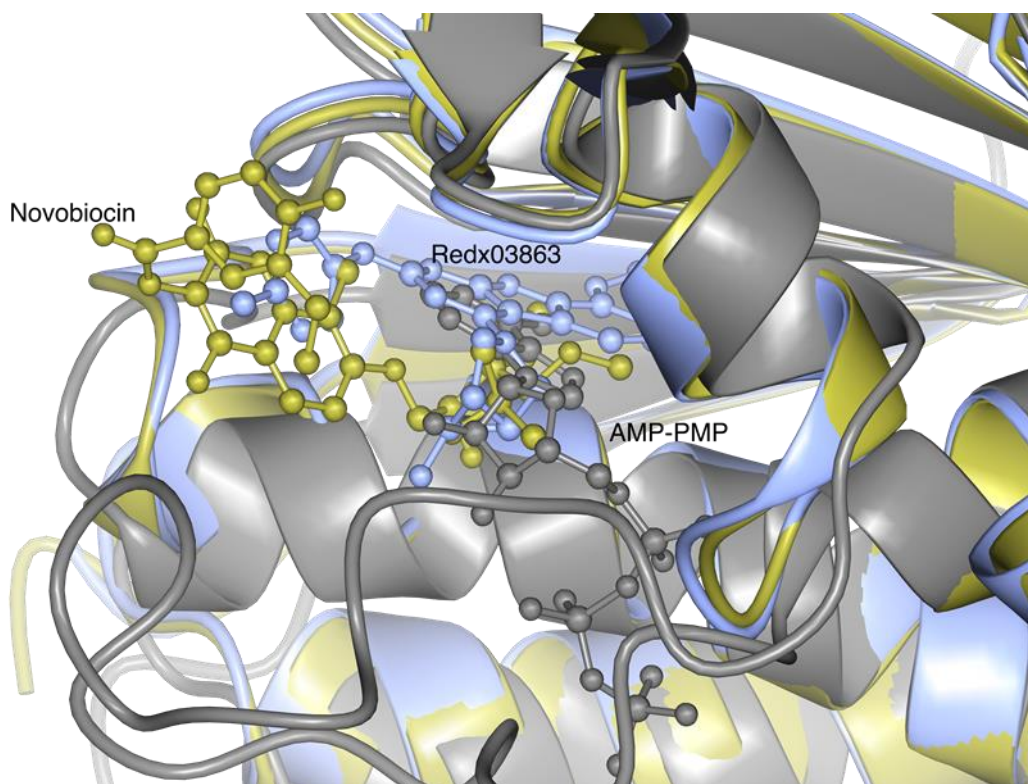


Figure 5.8.5: Structural alignment of the Mth structures containing novobiocin (gold) and Redx03863 (blue) and the published 3ZKB crystal structure of the Mtb GyrB ATPase domain containing AMP-PNP (grey). The overall structural alignments are in good agreement and indicate that there is partial overlap in the binding pockets of all three molecules.

5.9 Structural comparison of *M. thermoresistibile* B24 ATPase subdomain bound to Redx03863 with the human topo II α ATPase domain

As all type IIA topoisomerases share a common mechanism of action and similar structural features (Berger *et al.*, 1996, Roca *et al.*, 1996) it was decided to perform structural comparisons of the binding site of Redx03863 to that of ATP in a eukaryotic topo II. For this purpose, we chose the re-refined structure of human DNA topo II α containing ADP (4R1F) (Wei *et al.*, 2005, Stanger *et al.*, 2014). At present there is not a structure of the ATPase domain from the human topo II β orthologue preventing this analysis from occurring.

In aligning the ATPase domains from Mth GyrB and human topo II α it is evident that there is a high degree of similarity in these structures although there are some differences in some of the structural elements, such as the loop of the amino acids 36-39 in the Mth structure that forms a large anti-parallel beta sheet arrangement of residues 54-78 in the human structure.

Furthermore, a long flexible loop region is visible in the structure of human topo II α (146-166) where a similar flexible loop structure was deleted out of the Mth structure (103-125) which is not seen in many other bacterial DNA gyrases. Likewise, several of the secondary structure elements are in slightly different orientations, although this can likely be attributed to the binding of a nucleotide in the full-length ATPase domain as crystallised in the human structure resulting in slight conformational changes to the domain (Figure 5.9.1).

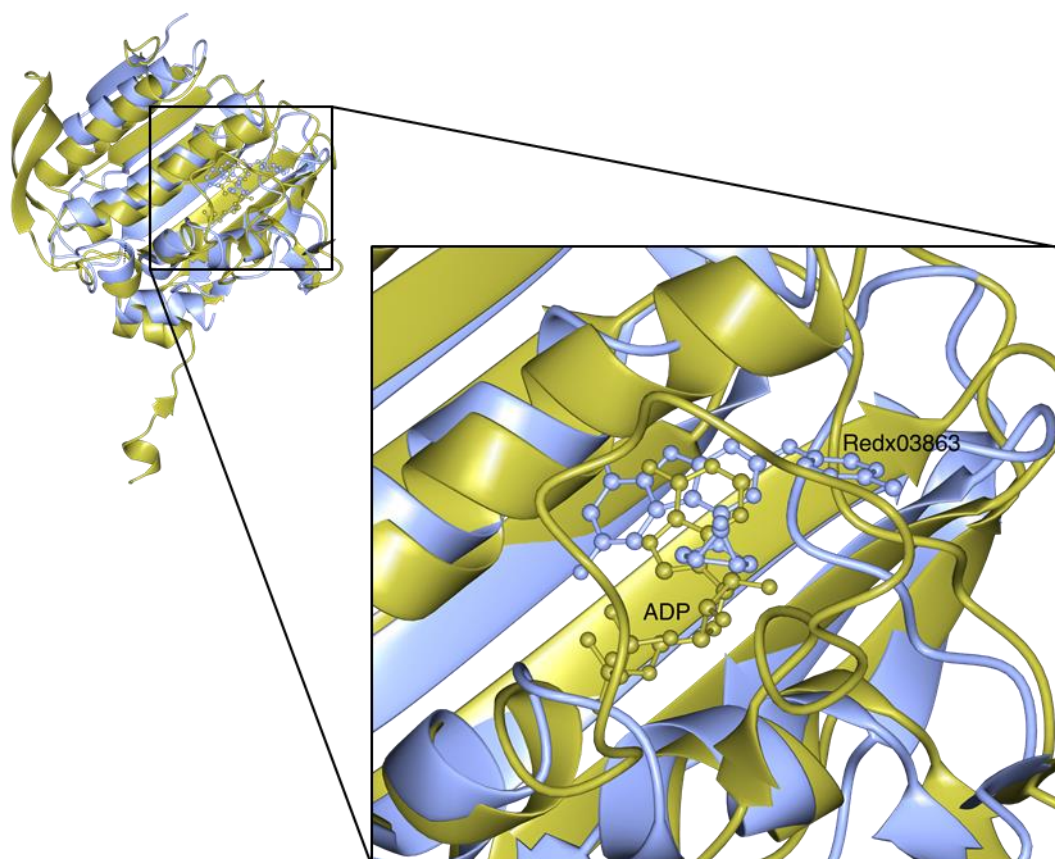


Figure 5.9.1: Structural alignment of the Mth sub-ATPase domain bound to Redx03863 (blue) with the first 267 amino acids of Human topo II α (4R1F) (gold). An enlargement of the ligand interactions is displayed indicating an overlap in the binding site of Redx03863 with the ATP-binding site of Human topo II α and possible space for binding of Redx03863 in human topo II α .

More specifically in analysing the ATP-binding position as in the Mtb structure the location of the ATP-binding site overlaps with that of Redx03863 (Figure 5.9.1). This unfortunately suggests that there is space and hence a possibility for Redx03863 to inhibit human topo II α although this was not analysed in the scope of this project. Several of the key binding interactions indicated previously are conserved within the human structure with amino acids in the key locations for binding, these include N52 where an asparagine is conserved in a similar structural location (N91); likewise, with the threonine at position 169 (T215) and the glycine at 83 (G124) (Figure 5.9.2). However, the key binding interaction of the aspartic acid

at position 79 is not conserved in the human structure with an asparagine (N120) being present at this location. This is unlikely to interact with Redx03863 directly and may be a significant enough interaction to provide resistance to human topo II α although this needs to be further tested in the future (Figure 5.9.2).

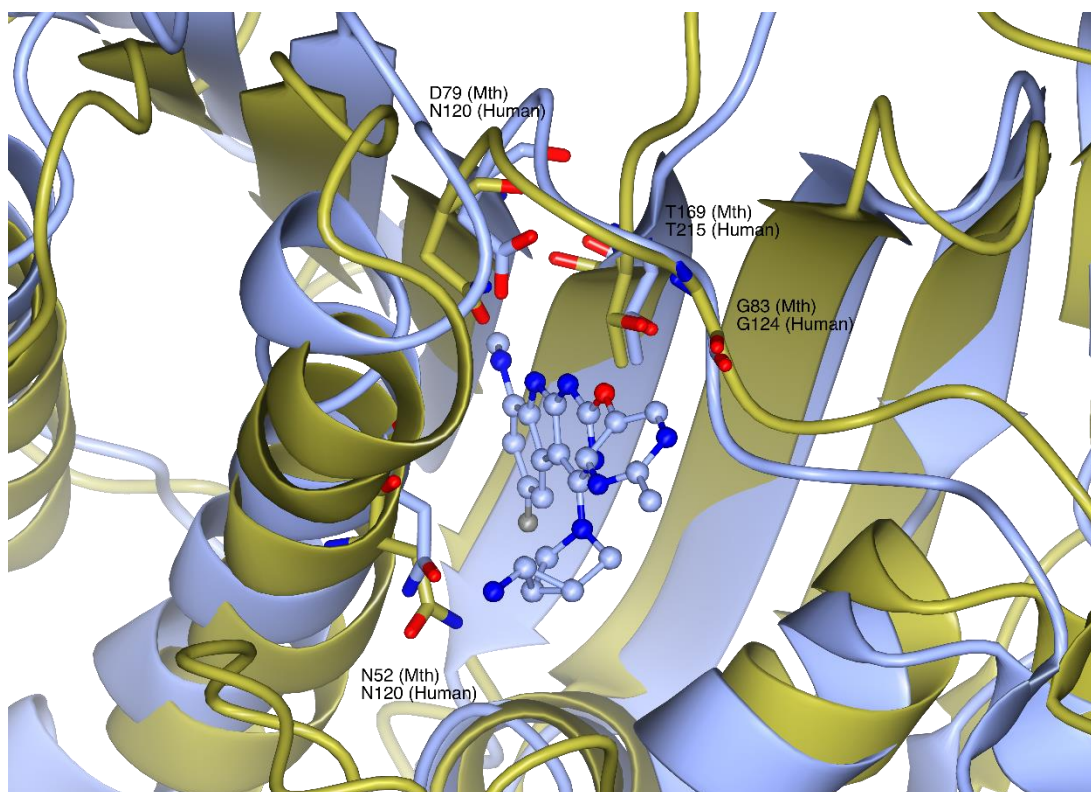


Figure 5.9.2: A structural comparison of the key binding interactions of Redx03863 in the Mth sub-ATPase domain (blue) aligned with the ATPase domain of Human topo II α (4R1F) (Stanger *et al.*, 2014) (gold). There is conservation at three of the four binding interactions indicated here but crucially the key binding interaction of the aspartic acid D79 is not conserved with an asparagine (N120) being present at this position in Human topo II α .

5.10 Discussion

5.10.1 Previously known structures

Previously, the N-terminal domain of DNA gyrase has been solved in several iterations from several different species including the *M. tuberculosis* 43 kDa full ATPase domain in the presence of non-hydrolysable ATP analogues (Agrawal *et al.*, 2013), but there is only one structure of this full domain within the PDB (1JIK) which was crystallised with novobiocin in the absence of an ATP analogue (*T. thermophilus*) (Lamour *et al.*, 2002). On the other hand, there are many more structures available within the PDB of the GyrB24 fragment from a wider species range, but more critically contain a wide range of compounds bound including the

aminocoumarins and TriBE antibiotics. Here we report three new structures, two of these are bound to novobiocin of which there are two other GyrB24 structures in the PDB: 1AJ6 (Holdgate *et al.*, 1997) and 4URO (Lu *et al.*, 2014) from *E. coli* (R136H mutant) and *S. aureus* respectively. The resolution of these two novobiocin-bound structures from *M. smegmatis* and *M. thermoresistibile* are a significant enhancement in resolution with the previous best resolution being 2.3 Å, with the new structures reported here being at better than 2 Å resolution. Likewise, the previous structure of the *M. smegmatis* GyrB ATPase subdomain was solved to 2.2 Å (Shirude *et al.*, 2013), meaning that our new structure has been solved at superior resolution. On the other hand, the previous structures containing the TriBE antibiotics from Trius Therapeutics were solved in the *E. faecalis* GyrB24 construct and include the 4KSG structure containing C4 with the highest similarity to Redx03863 which was solved to 1.75 Å (Tari *et al.*, 2013a). However, C1-4 from the compound series were solved at comparable resolutions in the same *E. faecalis* construct to our new Mth Redx03863-bound structure presented here. In addition, the structure of C3 from the Trius Therapeutics series has also been solved within *E. coli* GyrB and *F. tularensis* ParE subunits at good resolutions (Tari *et al.*, 2013a).

5.10.2 A future structure of Redx04739?

During the experiments carried out within this project no crystals containing Redx04739 were successfully co-crystallised. Instead the crystals that formed in the presence of Redx04739 were found to contain novobiocin from the seed stock made with novobiocin-containing crystals. Soaking experiments were also trialled, in these experiments it was chosen to use the crystals grown in the presence of novobiocin as from the experiments carried out in section 5.4 it was determined that Redx03863 had a lower IC₅₀ value and hence was likely to be a tighter binding inhibitor than Redx04739, whereas novobiocin had a more comparable IC₅₀ value to Redx04739. In these soaking experiments various time points were trialled between 3 hours to 3 days, however, for the most part the crystals chosen were dissolved in the presence of the compound containing soaking solution and where the crystals remained it was found that only novobiocin was observed within these structures.

It is suggested that one of the major factors affecting the lack of crystals that were obtained was down to the poor solubility of Redx04739 especially in neutral and basic solutions. It was therefore hoped that as the crystallisation conditions for the *M. smegmatis* were more acidic than those for the *M. thermoresistibile* fragment that the compound may co-crystallise under these conditions, however it was found that the compound would drop out of solution when

added to the protein solution. Adding the drug at lower protein concentrations and co-concentration with the drug bound was also trialled in a similar method to that used by Hameed *et al.* (2014), however a significant amount of precipitation of the compounds was still observed regardless of the temperature and time incubation before concentration. Although the same issue was found with Redx03863 the solubility was greater so when the compound was added to the protein solution at 1% DMSO it was able to remain in solution and crystallise. We suggest that future crystallisation trials with Redx04739 should be carried out with increased concentrations of DMSO to increase its solubility. Additionally, it is suggested that use of a seed stock that has decreased concentrations of novobiocin (e.g. by washing the crystals) should be used to decrease the availability of novobiocin to decrease the chance of obtaining novobiocin containing crystals.

5.10.3 Use of homologues and loop deletion constructs

In the scope of this work it was not possible to crystallise the GyrB sub-ATPase domain from *M. tuberculosis*, although it is possible with further screening and construct alterations with novobiocin that in the future a structure may be obtained. This is especially true as it has now been demonstrated that protein crystals bound to novobiocin and Redx03863 do not give UV fluorescence, and hence it is possible that previous positive hits were discarded (Figure 5.3.2). However, as there are no crystal structures of this domain available in the PDB it is plausible that, like the work presented here, crystal hits were not obtained when using Mtb constructs. Regardless, the crystal structure that we obtained here has a strong similarity to its corresponding section of the full ATPase domain (3ZKB) previously published (Agrawal *et al.*, 2013) suggesting that the Msm and Mth homologues presented here were appropriate choices. Furthermore, as the Msm homologue has previously been used for the inhibitor co-crystal structures (4B6C, 4BAE) it has likely been previously found that the equivalent Mtb fragment was difficult to crystallise (Shirude *et al.*, 2013, Hameed *et al.*, 2014).

All three of the crystal structures presented here have two loops regions deleted from the constructs to aid with crystallisation (Figure 5.3.1). Previously this strategy has been utilised to obtain crystals of the *M. smegmatis* sub-ATPase domain (Shirude *et al.*, 2013, Hameed *et al.*, 2014), although on the full-length ATPase domain from *M. tuberculosis* this was not performed, but these chains are not visible within the structure suggesting them to be flexible (Agrawal *et al.*, 2013, Roue *et al.*, 2013). After extensive crystallisation trials with the Mtb sub-ATPase domain no crystals were obtained and hence it was decided to progress towards loop deletion constructs, which although they do not contain the full biological relevance, the

loops in question do not appear to alter the binding of either novobiocin or Redx03863, nor does the second longer loop appear in other species such as *E. coli* and *S. aureus*.

5.10.4 Understanding the binding site of novobiocin through crystallographic analysis

The binding pockets presented in the two crystal structures of novobiocin presented here have close similarities to those previously presented for novobiocin and like many people before us we have demonstrated the involvement of R141 (R136 in *E. coli*) in the binding (Table 5.10.1). Our enzymatic studies have further confirmed this showing that no inhibition was seen at 3 μ M novobiocin in comparison to full inhibition of the wild type at this concentration (Figure 5.8.3). Through our crystal structures presented here we have been able to further rationalise the involvement of E87 and D79 through direct hydrogen bonding (Table 5.10.1), as well as, V125 through steric hindrance. In the limited amount of time we had we were unable to confirm the exact mechanism of several of the other reported resistance mutations such as G168 and S169 (Table 5.10.1), although we suggest that they must act through long range interactions such as altering a stable hydrogen bonding network or a conformational change.

Table 5.10.1: Summary of the key crystallographic interactions between novobiocin or Redx03863 in either of the new Mth or Msm structures presented in this chapter, alongside their bacterial mutagenesis, activity and resistance to the supercoiling assay and previous binding studies to used to determine the binding pocket and mode of action of novobiocin.

Residue (Msm/Mth/Mtb)	Direct or indirect crystallographic contact	Bacterial mutagenesis?	Activity and resistance in supercoiling	Binding studies
N52	Direct to Redx03863	No	Inactive in supercoiling	<i>E. coli</i> N46D/L SPR studies ¹
E56	Indirect to novobiocin	No	Inactive in supercoiling	<i>E. coli</i> E50A inhibition of ATPase reaction ²
D79	Indirect all three	No	Inactive in supercoiling	<i>E. coli</i> D73N SPR studies ¹
R82	Direct all three	No	Inactive in supercoiling	<i>E. coli</i> D73E inhibition of ATPase reaction ²
R83	Indirect via salt bridge	No	Inactive in supercoiling	<i>E. coli</i> R76A inhibition of ATPase reaction ²
G83	Likely indirect all 3, possibilities for direct interaction	G83S <i>S. aureus</i> ^{3,4} <i>M. smegmatis</i> (Chapter 4)	Negligible supercoiling activity observed, unable to test resistance in Mtb.	<i>E. coli</i> G77A/S inhibition of <i>E. coli</i> ATPase reaction ²
E87 (A87 Mtb)	Direct to novobiocin	D89G <i>S. aureus</i> ⁴ and Halophilic archaeobacterium ⁵	Untested in Mtb G81A weak supercoiling in <i>E. coli</i> ²	Untested

Residue (Msm/Mtb/Mfb)	Direct or indirect crystallographic contact	Bacterial Mutagenesis?	Activity and resistance in supercoiling	Binding studies
R141	Direct to novobiocin	R136C/L/H <i>E. coli</i> ^{6,7} R144I/S/H <i>S. aureus</i> ^{3,4} and Halophilic archaeobacterium ⁵	Weak supercoiling activity of R141A/Q in Mtb. Resistant to novobiocin. No resistance to Redx03863 or Redx04739	<i>E. coli</i> R136C SPR studies ¹ <i>E. coli</i> R136A/H/L/S inhibition of ATPase reaction ²
T169 (S169 Mtb)	Indirect via H-bonding network to novobiocin and Redx03863	T173A/N <i>S. aureus</i> ^{3,4}	Untested in Mtb T165A/S/V weak supercoiling <i>E. coli</i> ²	<i>E. coli</i> T165A/S/V inhibition of ATPase reaction ²

¹(Kampranis et al., 1999)

²(Gross et al., 2003)

³(Stieger et al., 1996)

⁴(Fujimoto-Nakamura et al., 2005)

⁵(Holmes and Dyalismith, 1991)

⁶(del Castillo et al., 1991)

⁷(Contreras and Maxwell, 1992)

5.10.5 Understanding the binding site of Redx03863 through crystallographic analysis and mutagenesis of GyrB

From analysing the solved crystal structure containing Redx03863 and, in comparison with the published structure of 4KSG containing the TriBE compound C4 we made several mutants (Tari *et al.*, 2013a). However, these mutants appeared inactive in supercoiling when assayed at a concentration of 200 nM for 30 mins at 37°C. On comparison to the 3ZKB Mtb crystal structure with AMP-PNP it appears that the mutants made may also have important interactions with ATP causing them to be inactive in supercoiling (Agrawal *et al.*, 2013). Additionally, a comprehensive study of the ATP-binding site through mutagenesis has indicated that supercoiling was not permissive in mutating the N46, E50, D73 or R76 residues of *E. coli* DNA gyrase, which correspond to the residues of N52, E56, D79 and R82 which were mutated in this study (Table 5.10.1) (Gross *et al.*, 2003). However, several of the residues had low-level ATPase activity and hence they were able to confirm that the E50A, D73E and R76A all resulted in a significant increase in the apparent IC₅₀ value of novobiocin within the ATPase reaction. Initially, it was attempted to perform the SDM in the GyrBA plasmid, unfortunately this was unsuccessful, and as the ATPase reaction was problematic giving very low ATP turnover when using the individual wild-type Mtb subunits before mutagenesis it was decided not to carry out these experiments. On the other hand, from analysing the crystal structure it indicated that the G83S mutant obtained from bacterial mutagenesis may result in significant resistance to Redx03863 and likely Redx04739 (Table 5.10.1). The carbonyl group on the glycine is 4.3 Å away from the compound, meanwhile the amino group is 3.9 Å from the ether oxygen. In the published structure of *E. faecalis* GyrB24 the same interactions with C4 of the original TriBE series are 3.9 Å and 4.3 Å suggesting that these could be important interactions (Tari *et al.*, 2013a). It is unlikely that the serine side chain would directly interact with the compounds as it is likely to point away from the compound, however, it is possible that it would alter other surrounding interactions that would directly change the binding interactions of the main chain with these compounds. Overall, it is suggested that the G83S mutant protein should be further optimised to try and obtain better levels of supercoiling that would be possible to be used within an inhibition of supercoiling reaction to determine if there is any increase in the IC₅₀ value in the presence of this individual mutant.

The novobiocin binding residue of R141 appears not to interact with Redx03863 or Redx04739 in binding. This has been confirmed using inhibition of supercoiling reactions with the R141A/Q mutants which do not give resistance to either compound. Likewise, the structure presented here of Redx03863 bound to the Mth domain suggests that the distance

between this residue and Redx03863 would be too large for a hydrogen bonding interaction such as the one seen in the novobiocin bound structures (Table 5.10.1).

5.10.6 Implications of the binding sites

The binding site of novobiocin has previously been crystallised in other species agreeing with the novobiocin-binding site presented here (Holdgate *et al.*, 1997, Lamour *et al.*, 2002, Lu *et al.*, 2014). Additionally, the mutagenesis results presented here confirm that this is the correct binding site as previously presented in the literature (del Castillo *et al.*, 1991, Contreras and Maxwell, 1992, Munoz *et al.*, 1995, Stieger *et al.*, 1996, Fujimoto-Nakamura *et al.*, 2005). The crystal structure presented appears to support the idea that R141 is not involved in the binding of Redx03863 as the distance between the two species is greater than 4 Å and no resistance was obtained when the mutant proteins were analysed. However, the likely binding pocket of Redx03863 has a degree of overlap with those of ATP and novobiocin. Overall, this leaves compelling evidence for the crystallographic binding site which unfortunately we have been unable to confirm via site directed mutagenesis due to the high degree of sensitivity of the mutants in this area due to interactions with ATP.

The structural alignments also show that there is the potential for Redx03863 to inhibit human topo II α in addition to the bacterial topoisomerases DNA gyrase and topo IV. However, one of the key binding interactions - the aspartic acid (D79) in the Mth structure is presented as an asparagine (N120) in the human structure, hence there is a strong possibility that the binding and inhibition of Redx03863 may be weaker against human topo II α . However, this does raise significant concerns over the safety of the use of this compound series clinically in humans. To confirm this in the future it would be important to test the inhibition of these compounds against both Human topo II α and topo II β . Furthermore, additional toxicity tests should be utilised to determine the safety of these compounds before further optimisation and hopefully developing in pre-clinical testing.

6. Discussion

The work presented in this thesis has used three interlinked areas of study in the form of mechanistic, inhibition and structural studies to further our knowledge of DNA gyrase from mycobacteria. These studies have built upon the previous studies of Mtb DNA gyrase in terms of mechanistic and inhibition studies, meanwhile, although we were unable in the scope of this work to advance our structural knowledge of Mtb DNA gyrase, we have instead worked towards a place where we may be able to in the future by investigating the structures of other mycobacterial species.

6.1 Mechanistic studies of DNA gyrase from *M. tuberculosis*

From a mechanistic point of view, we sought to confirm the previous characterisations of DNA gyrase (Aubry *et al.*, 2006a), and advance this in terms of using the Mtb DNA gyrase fusion protein. From these studies it is clear that our enzymes behaved similarly to previous results, with a single omission coming from the results of the ATPase assay. Formerly, it was believed that the ATPase activity of Mtb DNA gyrase was very low and unsuitable for inhibition studies (Agrawal *et al.*, 2013, Karkare *et al.*, 2013b, Shirude *et al.*, 2013). We however, have made an interesting discovery that using a stock of concentrated pure protein it is possible to obtain a detectable ATP turnover significantly greater than previously determined. In addition, when the reaction was carried out with the fusion protein with a topologically unconstrained substrate this rate was determined to be consistently high enough to be used for inhibition studies. It is unclear at the current time as to why we observe a difference in the ATP turnover from the reconstituted subunits and the fusion protein, however we suggest two preliminary explanations for this. The first of these arises from the possibility that the fusion proteins are purified to a greater level and hence a greater portion of the ATPase rate can be inhibited by novobiocin and hence it makes it appear artificially more active. On the other hand, it is also possible that by fusing the two subunits it is also possible that this has altered the dynamics of the reaction cycle making it more favourable to carry out the supercoiling, and hence the ATPase reaction. At this point in time neither of these explanations can be discarded, however, it can be considered that this is the first study to our knowledge of the ATPase activity of a DNA gyrase fusion protein.

Whilst determining the ATPase activity from *M. tuberculosis* DNA gyrase it became apparent to us that both the presence and the topological state of DNA were important in stimulating this reaction. Previously it has been implied that this is also the case in *E. coli* DNA gyrase

with the presence of either topologically unconstrained double stranded DNA or a relaxed plasmid being suggested as the optimal substrates for inducing the ATPase activity (Sugino and Cozzarelli, 1980). Our results suggest that the best substrate for Mtb DNA gyrase is topologically unconstrained double-stranded DNA. Constrained plasmids appear to be rapidly converted into negatively-supercoiled DNA which is a poor stimulator of Mtb DNA gyrase and gives a background rate only marginally greater than the enzyme in the absence of DNA. Hence, we suggest that future ATPase inhibition studies should be carried out in the presence of linearised or nicked plasmid DNA with the fusion protein. Overall, we suggest that this means that the ATPase reaction of Mtb DNA gyrase is highly coupled to the presence of relaxed or positively supercoiled DNA, suggesting that the enzyme requires an appropriate substrate to be active.

It is known that mycobacteria only encode for two topoisomerases within their genomes (DNA gyrase and topo I) (Cole *et al.*, 1998). This has caused many previous researchers to question if DNA gyrase is able to compensate for the lost functions of topo IV. Topo IV functions in the most part to decatenate and relax DNA in an ATP-dependent manner (Kato *et al.*, 1990). Although within the scope of the work presented here and previously it has been shown that Mtb DNA gyrase can decatenate DNA, it does not appear that it does this to the same level as it is able to negatively supercoil a relaxed plasmid (Aubry *et al.*, 2006a). Likewise, although Mtb DNA gyrase can relax negatively supercoiled DNA in an ATP-independent fashion (Gellert *et al.*, 1977, Sugino *et al.*, 1977), this reaction is slow and can be rapidly reversed through the addition of ATP. It is therefore suggested that Mtb DNA gyrase preferentially relaxes positively supercoiled DNA, and may be unable to fully compensate for topo IV in terms of relaxing negatively supercoiled DNA.

6.2 DNA gyrase from *M. thermoresistibile*

One of the key features of this work was the development of DNA gyrase from the thermostable *M. thermoresistibile*, based on the rationale of Edwards *et al.* (2012), suggesting this to be a strong alternative to Mtb as a source of proteins for structural studies. We have demonstrated this clearly to be the case as by using the Mth sub-ATPase domain we were able to gain a crystal structure bound to Redx03863, which we were unable to with the Mtb and Msm homologues. We suggest that this might also be the case with the true aim of this project in solving the full-length structure of mycobacterial DNA gyrase. In addition, the Mth fusion protein is an ideal candidate to further exploit in future structural studies using both X-ray crystallography and cryoEM.

On the other hand, we found that the Mth proteins were marginally more difficult to work with in terms of enzymatic assays, as the DNA was found to be difficult to remove from the protein under the commonly used assay conditions. Regardless of this, we were able to confirm that DNA gyrase from Mth is active with the activity being moderately optimised in terms of enzyme concentrations, time, and potassium glutamate concentrations. Additionally, we also determined that, like the Mtb proteins, there was no significant difference in the enzymatic activity by fusing the subunits together. At this stage we cannot confirm if the ATPase rate from the Mth enzyme is reliable and reproducible.

6.3 Inhibition of mycobacterial DNA gyrase

Possibly the most important section of work presented here comes in the form of inhibition studies performed on Mtb DNA gyrase. In the period between 2000-2015 an estimated 49 million people were saved with antibiotics against *M. tuberculosis*, however, in 2016 alone 1.3 million people could not be saved and died of tuberculosis (WHO, 2017). This figure combined with rising levels of drug resistant-infections being reported, means that we urgently need to develop new antimycobacterial agents. Hence, in the scope of the work presented here we compared the clinically used second line fluoroquinolone of moxifloxacin (Gillespie, 2016), and the formally clinically used aminocoumarin novobiocin (Food and Drug Administration, 2011) to the novel compound classes of the naphthoquinones (Lall *et al.*, 2005, Karkare *et al.*, 2013b) and the TriBE antibiotics optimised by Redx AntiInfectives (Tari *et al.*, 2013a).

6.3.1 Prospects for the naphthoquinone antibiotic class

From the work presented here it is clear that the naphthoquinone 7-methyljuglone is not a viable option for development into a novel antibiotic. Previous work suggests that these compounds are highly unstable in a range of solvents, which we were able to confirm through enzymatic assays (van der Kooy, 2007). We therefore suggest that the compound that is active against DNA gyrase is not 7-methyljuglone but a resulting derivative or breakdown product. As in the scope of this work we were unable to confirm the exact composition of the active fraction we therefore propose that this is not a viable option to be taken forwards for further investigations. Furthermore, we were unable to confirm the binding pocket of these compounds by mutagenesis as we could not obtain a stable and active compound to test the model against.

6.3.2 The TriBE antibiotics optimised by Redx AntiInfectives

A substantial proportion of the inhibition studies conducted here used the novel TriBE antibiotics of Redx03863 and Redx04739. These have potent activity against whole cell mycobacteria as well as against mycobacterial DNA gyrase in both the ATPase and supercoiling reactions but not the ATP-independent relaxation reaction. Of the compounds tested these compounds present the best opportunity to develop a new clinical antimycobacterial compound. These compounds are highly efficient at killing both whole cells in MIC testing on agar and in broth as well as having significant activity in killing established biofilms. However, there are additional issues with these compounds going forwards, including the uncomfortably high frequency of resistance values, suggesting that resistance is highly likely to develop, and a non-optimal mechanism of action. These compounds are ATPase inhibitors like the aminocoumarin novobiocin, which was withdrawn from clinical use against methicillin-resistant *S. aureus* based on toxicity issues (David and Burgner, 1956, Maxwell, 1993, Food and Drug Administration, 2011, Chopra *et al.*, 2012). As DNA gyrase is a member of the GHKL ATPase family there is a significant likelihood that any ATPase inhibitors of DNA gyrase will have activity against other members of this family (Dutta and Inouye, 2000). Likewise, as a type IIA topoisomerase DNA gyrase has significant structural homology to eukaryotic topo II enzyme including human topo II α and β there is a strong chance of inhibition of these enzymes causing adverse effects (Wei *et al.*, 2005). Furthermore, the structural analysis carried out on the Redx03863 structure suggests that cross susceptibility could be an issue with human topo II α , which should be tested in the future.

One of the biggest challenges of this section of work has been to elucidate the binding pocket of both Redx03863 and Redx04739. From combining the proposed mechanism of action of competitive inhibition of the ATPase reaction, the preliminary SPR results indicating that Redx04739 binds to the sub-ATPase domain of Mtb GyrB, and the crystal structure of Redx03863 bound to the sub-ATPase domain of Mth GyrB we believe that we have likely determined the binding site of these compounds. However, using bacterial mutagenesis we have only determined one mutation in the proposed binding site (G83S) which appears to be almost completely inactive in supercoiling. Additionally, all the mutants identified through analysis of the crystal structure are inactive in both ATPase and supercoiling activity, hence we were unable to definitively confirm the binding site at this time. Despite this, we believe it probably has incomplete overlap with the aminocoumarin binding pocket. We suggest that in the future it would be important to optimise the little supercoiling activity the G83S mutant

presents with to confirm the binding site. Previously this mutant in *E. coli* (G77S) was described to have ATPase activity of 10% of the wild type enzyme, and supercoiling activity requiring a 10x increase in protein concentration, as well as, weak complementation of a temperature sensitive mutation (Gross *et al.*, 2003). Overall, this suggests that it is likely that we should be able to confirm the binding site in the future. Due to the challenges we faced with the SPR experiments we do not propose to use this method to confirm the binding site in the future.

Overall, we suggest that these compounds are unlikely to advance towards clinical trials in the future due to concerns with toxicity, spontaneous resistance due to the mechanism of action, and their poor solubility. Regardless of these concerns, these compounds show some promise and it may be possible to optimise them further to alleviate some of these problems. Additionally, if this is not possible there may be potential to develop these compounds for alternative uses in the future instead, such as anticancer drugs targeting human topo II α if it was proved that they also inhibit this enzyme. Likewise, with the presence of DNA gyrase in plants these compounds may be useful as herbicides in the future (Wall *et al.*, 2004).

6.4 Structural studies on mycobacterial DNA gyrase

In the scope of the work presented here, we were unable to solve the full-length high-resolution structure of mycobacterial DNA gyrase as we were unable to determine conditions that enabled the growth of protein crystals. Furthermore, due to the lack of availability we were unable to perform cryoEM studies on these proteins either. From the limited crystallisation attempts that were made with both the Mtb and Mth fusion proteins it is clear that there are many variables of which only a few have been fully explored and that another ten years could easily be spent attempting to generate a crystal. Therefore, we propose that with the recent improvements to cryoEM technology in recent years (reviewed in (Renaud *et al.*, 2018)), that although DNA gyrase is relatively small and likely only has a two-fold symmetry axis, it is an exciting candidate for use within this growing technique. However, it has already been shown that DNA gyrase is not an optimal candidate for cryoEM and that the addition of DNA is important in stabilising the enzyme (Papillon *et al.*, 2013). This leads us to suggest that in future structural studies (crystallography and cryoEM) that a DNA fragment capable of wrapping the C-terminal domains and a non-hydrolysable ATP analogue such as AMP-PNP should be included in the conditions. Overall, we acknowledge that the crystallisation conditions trialled in the scope of this project were not extensive, and that further trials should be investigated in an attempt to determine the full-length high-resolution

structure of mycobacterial DNA gyrase via X-ray crystallography alongside optimisations using cryoEM.

In contrast with the unsuccessful structural studies of the full-length enzyme, we had increased success in generating new structures of the ATPase domain of mycobacterial DNA gyrase. Two of these structures were bound to the known inhibitor of novobiocin, which were solved at superior resolution to the previously available structures (Lewis *et al.*, 1996, Holdgate *et al.*, 1997, Tsai *et al.*, 1997). These structures confirmed our current knowledge of the sub-ATPase domain and the novobiocin binding site. In addition, we solved the structure of the sub-ATPase domain bound to the novel compound Redx03863 confirming the crystallographic binding site of the TriBE compounds (Tari *et al.*, 2013a), however, in the absence of an active resistance mutant we are unable to confirm this model. Unfortunately, we were unable to co-crystallise Redx04739 in either of the GyrB24 sub-ATPase domain constructs due to its low solubility, confirming it to be unlikely to progress further towards clinical trials.

6.5 Are we closer to a new antimycobacterial drug?

The biggest goal of this project was to head closer to generating a new antimycobacterial agent that will help to save millions more patients with the goal of ending epidemic tuberculosis by 2030, which forms part of goal 3 of the sustainable development goals (WHO, 2017). However, we acknowledge that our part in this long-term goal is very small and has not yielded a new drug. We have however, ventured into lesser explored chemistries including those from the naphthoquinones and the pyrrolopyrimidine TriBE inhibitors. Although neither of these is likely to progress beyond laboratory testing, they have provided useful advancements in our knowledge of mycobacterial DNA gyrase beyond the immediate compounds, which can be used in future experiments and drug discovery efforts. These include the discovery that reliable and measurable ATPase rates can be obtained from *M. tuberculosis* DNA gyrase using the fusion construct; a crystallisable construct that yields reproducible crystals of the sub-ATPase domain from *M. thermoresistibile*; and the adaption of several bacteriology techniques to determine inhibition of the slow growing *M. smegmatis*. Finally, we have also worked to perform initial characterisations on *M. thermoresistibile* DNA gyrase which we strongly believe will help in the search for a full-length high-resolution structure of DNA gyrase in the future.

Literature Cited

- Abremski, K., Hoess, R. & Sternberg, N. 1983. Studies on the properties of P1 site-specific recombination - evidence for topologically unlinked products following recombination. *Cell*, 32, 1301-1311.
- Adams, D. E., Shekhtman, E. M., Zechiedrich, E. L., Schmid, M. B. & Cozzarelli, N. R. 1992. The role of topoisomerase-IV in partitioning bacterial replicons and the structure of catenated intermediates in DNA-replication. *Cell*, 71, 277-288.
- Adams, P. D., Afonine, P. V., Bunkoczi, G., Chen, V. B., Davis, I. W., Echols, N., Headd, J. J., Hung, L. W., Kapral, G. J., Grosse-Kunstleve, R. W., McCoy, A. J., Moriarty, N. W., Oeffner, R., Read, R. J., Richardson, D. C., Richardson, J. S., Terwilliger, T. C. & Zwart, P. H. 2010. PHENIX: a comprehensive Python-based system for macromolecular structure solution. *Acta Crystallographica Section D-Biological Crystallography*, 66, 213-221.
- Agrawal, A., Roue, M., Spitzfaden, C., Petrella, S., Aubry, A., Hann, M., Bax, B. & Mayer, C. 2013. *Mycobacterium tuberculosis* DNA gyrase ATPase domain structures suggest a dissociative mechanism that explains how ATP hydrolysis is coupled to domain motion. *Biochemical Journal*, 456, 263-273.
- Agrawal, D., Udawadia, Z. F., Rodriguez, C. & Mehta, A. 2009. Increasing incidence of fluoroquinolone-resistant *Mycobacterium tuberculosis* in Mumbai, India. *International Journal of Tuberculosis and Lung Disease*, 13, 79-83.
- Ali, J. A., Jackson, A. P., Howells, A. J. & Maxwell, A. 1993. The 43-Kilodalton N-terminal fragment of the DNA gyrase-B protein hydrolyzes ATP and binds coumarin drugs. *Biochemistry*, 32, 2717-2724.
- Aravind, L., Iyer, L. M., Wellems, T. E. & Miller, L. H. 2003. Plasmodium biology: Genomic gleanings. *Cell*, 115, 771-785.
- Aravind, L., Leippe, D. D. & Koonin, E. V. 1998. Toprim - a conserved catalytic domain in type IA and II topoisomerases, DnaG-type primases, OLD family nucleases and RecR proteins. *Nucleic Acids Research*, 26, 4205-4213.
- Ashley, R. E., Blower, T. R., Berger, J. M. & Osheroff, N. 2017. Recognition of DNA Supercoil Geometry by *Mycobacterium tuberculosis* Gyrase. *Biochemistry*, 56, 5440-5448.
- Asif, M. 2016. Biological activities of various pyrrolopyrimidine derivatives: a mini review. *Heterocyclic Letters*, 6, 817-831.
- Aubry, A., Fisher, L. M., Jarlier, V. & Cambau, E. 2006a. First functional characterization of a singly expressed bacterial type II topoisomerase: The enzyme from *Mycobacterium tuberculosis*. *Biochemical and Biophysical Research Communications*, 348, 158-165.
- Aubry, A., Pan, X. S., Fisher, L. M., Jarlier, V. & Cambau, E. 2004. *Mycobacterium tuberculosis* DNA gyrase: Interaction with quinolones and correlation with antimycobacterial drug activity. *Antimicrobial Agents and Chemotherapy*, 48, 1281-1288.
- Aubry, A., Veziris, N., Cambau, E., Truffot-Pernot, C., Jarlier, V. & Fisher, L. M. 2006b. Novel gyrase mutations in quinolone-resistant and -hypersusceptible clinical isolates of *Mycobacterium tuberculosis*: Functional analysis of mutant enzymes. *Antimicrobial Agents and Chemotherapy*, 50, 104-112.
- Avalos, E., Catanzaro, D., Catanzaro, A., Ganiats, T., Brodine, S., Alcaraz, J. & Rodwell, T. 2015. Frequency and Geographic Distribution of gyrA and gyrB Mutations Associated with Fluoroquinolone Resistance in Clinical *Mycobacterium tuberculosis* Isolates: A Systematic Review. *Plos One*, 10, 24.
- Azaro, M. A. & Landy, A. 2002. λ Integrase and the λ Int Family. *Mobile DNA II*. American Society of Microbiology.
- Baird, C. L., Harkins, T. T., Morris, S. K. & Lindsley, J. E. 1999. Topoisomerase II drives DNA transport by hydrolyzing one ATP. *Proceedings of the National Academy of Sciences of the United States of America*, 96, 13685-13690.

- Baker, N. M., Weigand, S., Maar-Mathias, S. & Mondragon, A. 2011. Solution structures of DNA-bound gyrase. *Nucleic Acids Research*, 39, 755-766.
- Baker, T. A., Sekimizu, K., Funnell, B. E. & Kornberg, A. 1986. Extensive unwinding of the plasmid template during staged enzymatic initiation of DNA replication from the origin of the *Escherichia coli* chromosome. *Cell*, 45, 53-64.
- Barry, C. E., Boshoff, H. I., Dartois, V., Dick, T., Ehrt, S., Flynn, J., Schnappinger, D., Wilkinson, R. J. & Young, D. 2009. The spectrum of latent tuberculosis: rethinking the biology and intervention strategies. *Nature Reviews Microbiology*, 7, 845-855.
- Bates, A. D., Berger, J. M. & Maxwell, A. 2011. The ancestral role of ATP hydrolysis in type II topoisomerases: prevention of DNA double-strand breaks. *Nucleic Acids Research*, 39, 6327-6339.
- Bates, A. D., Odea, M. H. & Gellert, M. 1996. Energy coupling in *Escherichia coli* DNA gyrase: The relationship between nucleotide binding, strand passage, and DNA supercoiling. *Biochemistry*, 35, 1408-1416.
- Beckwith, J. 2000. The all purpose gene fusion. *Applications of Chimeric Genes and Hybrid Proteins, Pt A*, 326, 3-7.
- Belova, G. I., Prasad, R., Nazimov, I. V., Wilson, S. H. & Slesarev, A. I. 2002. The domain organization and properties of individual domains of DNA topoisomerase V, a type 1B topoisomerase with DNA repair activities. *Journal of Biological Chemistry*, 277, 4959-4965.
- Bensen, D. C., Finn, J., Lee, S. K., Chen, D. Z., Lam, T., Li, X., Trzoss, M., Jung, M., Nguyen, K., Lightstone, F. C., Tari, L. W., Zhang, J., Aristoff, P., Phillipson, D. W., Wong, S. E., Inc, T. T. & Llc, L. L. N. S. 2012. *Tricyclic gyrase inhibitors*. WO patent application PCT/US2012/029104. 20/09/2012.
- Bercovier, H., Kafri, O. & Sela, S. 1986. Mycobacteria possess a surprisingly small number of ribosomal-RNA genes in relation to the size of their genome. *Biochemical and Biophysical Research Communications*, 136, 1136-1141.
- Berger, J. M., Gamblin, S. J., Harrison, S. C. & Wang, J. C. 1996. Structure and mechanism of DNA topoisomerase II. *Nature*, 379, 225-232.
- Bergerat, A., deMassy, B., Gadelle, D., Varoutas, P. C., Nicolas, A. & Forterre, P. 1997. An atypical topoisomerase II from archaea with implications for meiotic recombination. *Nature*, 386, 414-417.
- Berman, H., Henrick, K. & Nakamura, H. 2003. Announcing the worldwide Protein Data Bank. *Nature Structural Biology*, 10, 980-980.
- Beveridge, T. J. 1999. Structures of gram-negative cell walls and their derived membrane vesicles. *Journal of Bacteriology*, 181, 4725-4733.
- Blower, T. R., Williamson, B. H., Kerns, R. J. & Berger, J. M. 2016. Crystal structure and stability of gyrase-fluoroquinolone cleaved complexes from *Mycobacterium tuberculosis*. *Proceedings of the National Academy of Sciences of the United States of America*, 113, 1706-1713.
- Bozeman, L., Burman, W., Metchock, B., Welch, L., Weiner, M. & Consortium, T. B. T. 2005. Fluoroquinolone susceptibility among *Mycobacterium tuberculosis* isolates from the United States and Canada. *Clinical Infectious Diseases*, 40, 386-391.
- Brennan, P. J. 2003. Structure, function, and biogenesis of the cell wall of *Mycobacterium tuberculosis*. *Tuberculosis*, 83, 91-97.
- Brown, P. C., Dulik, D. M. & Jones, T. W. 1991. The toxicity of menadione (2-Methyl-1,4-Naphthoquinone) and 2 thioether conjugates studied with isolated renal epithelial cells. *Archives of Biochemistry and Biophysics*, 285, 187-196.
- Brown, P. O. & Cozzarelli, N. R. 1979. Sign inversion mechanism for enzymatic supercoiling of DNA. *Science*, 206, 1081-1083.
- Brown, P. O., Peebles, C. L. & Cozzarelli, N. R. 1979. Topoisomerase from *Escherichia coli* related to DNA gyrase. *Proceedings of the National Academy of Sciences of the United States of America*, 76, 6110-6114.

- Burden, D. A. & Osheroff, N. 1998. Mechanism of action of eukaryotic topoisomerase II and drugs targeted to the enzyme. *Biochimica Et Biophysica Acta-Gene Structure and Expression*, 1400, 139-154.
- Bush, N. G., Agarwal, M., Henderson, S. R., Waraich, N. F. & Maxwell, A. 2018. DNA in a twist? How topoisomerases solve topological problems in DNA. *The Biochemist*, 40, 26-31.
- Bush, N. G., Evans-Roberts, K. & Maxwell, A. 2015. DNA Topoisomerases.
- Cabral, J. H. M., Jackson, A. P., Smith, C. V., Shikotra, N., Maxwell, A. & Liddington, R. C. 1997. Crystal structure of the breakage-reunion domain of DNA gyrase. *Nature*, 388, 903-906.
- Cadena, A. M., Fortune, S. M. & Flynn, J. L. 2017. Heterogeneity in tuberculosis. *Nature Reviews Immunology*, 17, 691-702.
- Calmette, A. 1936. *L'Infection Bacillaire et la Tuberculose. Paris: Masson et Cie.*
- Campanico, A., Moreira, R. & Lopes, F. 2018. Drug discovery in tuberculosis. New drug targets and antimycobacterial agents. *European Journal of Medicinal Chemistry*, 150, 525-545.
- Campbell, S. & Maxwell, A. 2002. The ATP-operated clamp of human DNA topoisomerase II alpha: Hyperstimulation of ATPase by "piggy-back" binding. *Journal of Molecular Biology*, 320, 171-188.
- Carson, L. A., Cusick, L. B., Bland, L. A. & Favero, M. S. 1988. Efficacy of chemical dosing methods for isolating nontuberculous mycobacteria from water-supplies of dialysis centers. *Applied and Environmental Microbiology*, 54, 1756-1760.
- Champoux, J. J. 2002. Type IA DNA topoisomerases: Strictly one step at a time. *Proceedings of the National Academy of Sciences of the United States of America*, 99, 11998-12000.
- Chatterji, M., Unniraman, S., Maxwell, A. & Nagaraja, V. 2000. The additional 165 amino acids in the B protein of *Escherichia coli* DNA gyrase have an important role in DNA binding. *Journal of Biological Chemistry*, 275, 22888-22894.
- Chen, V. B., Arendall, W. B., Headd, J. J., Keedy, D. A., Immormino, R. M., Kapral, G. J., Murray, L. W., Richardson, J. S. & Richardson, D. C. 2010. MolProbity: all-atom structure validation for macromolecular crystallography. *Acta Crystallographica Section D-Structural Biology*, 66, 12-21.
- Chetty, S. & Soliman, M. E. S. 2015. Possible allosteric binding site on Gyrase B, a key target for novel anti-TB drugs: homology modelling and binding site identification using molecular dynamics simulation and binding free energy calculations. *Medicinal Chemistry Research*, 24, 2055-2074.
- Chopra, S., Matsuyama, K., Tran, T., Malerich, J. P., Wan, B., Franzblau, S. G., Lun, S., Guo, H., Maiga, M. C., Bishai, W. R. & Madrid, P. B. 2012. Evaluation of gyrase B as a drug target in *Mycobacterium tuberculosis*. *Journal of Antimicrobial Chemotherapy*, 67, 415-421.
- Clark, D. J. & Leblanc, B. 2009. Analysis of DNA Supercoiling Induced by DNA-Protein Interactions. In: LEBLANC, B. & MOSS, T. (eds.) *DNA-Protein Interactions: Principles and Protocols, Third Edition*. Totowa, NJ: Humana Press.
- CLSI 2012. Methods for dilution antimicrobial susceptibility tests for bacteria that grow aerobically; approved standard—ninth edition. 9 ed.: Clinical and laboratory standards institute.
- Cole, S. T., Brosch, R., Parkhill, J., Garnier, T., Churcher, C., Harris, D., Gordon, S. V., Eiglmeier, K., Gas, S., Barry, C. E., Tekaiia, F., Badcock, K., Basham, D., Brown, D., Chillingworth, T., Connor, R., Davies, R., Devlin, K., Feltwell, T., Gentles, S., Hamlin, N., Holroyd, S., Hornby, T., Jagels, K., Krogh, A., McLean, J., Moule, S., Murphy, L., Oliver, K., Osborne, J., Quail, M. A., Rajandream, M. A., Rogers, J., Rutter, S., Seeger, K., Skelton, J., Squares, R., Squares, S., Sulston, J. E., Taylor, K., Whitehead, S. & Barrell, B. G. 1998. Deciphering the biology of *Mycobacterium tuberculosis* from the complete genome sequence. *Nature*, 393, 537-544.

- Cole, S. T., Eiglmeier, K., Parkhill, J., James, K. D., Thomson, N. R., Wheeler, P. R., Honore, N., Garnier, T., Churcher, C., Harris, D., Mungall, K., Basham, D., Brown, D., Chillingworth, T., Connor, R., Davies, R. M., Devlin, K., Duthoy, S., Feltwell, T., Fraser, A., Hamlin, N., Holroyd, S., Hornsby, T., Jagels, K., Lacroix, C., Maclean, J., Moule, S., Murphy, L., Oliver, K., Quail, M. A., Rajandream, M. A., Rutherford, K. M., Rutter, S., Seeger, K., Simon, S., Simmonds, M., Skelton, J., Squares, R., Squares, S., Stevens, K., Taylor, K., Whitehead, S., Woodward, J. R. & Barrell, B. G. 2001. Massive gene decay in the leprosy bacillus. *Nature*, 409, 1007-1011.
- Colville, J. M., Gale, H. H., Cox, F. & Quinn, E. L. 1957. Clinical observations on the use of novobiocin in penicillin resistant Staphylococcal septicemia. *Journal of Laboratory and Clinical Medicine*, 50, 803-803.
- Comstock, G. W. 1982. Epidemiology of tuberculosis. *American Review of Respiratory Disease*, 125, 8-15.
- Contreras, A. & Maxwell, A. 1992. GyrB mutations which confer coumarin resistance also affect DNA supercoiling and ATP hydrolysis by *Escherichia coli* DNA gyrase. *Molecular Microbiology*, 6, 1617-1624.
- Cooper, I. R., Pichowicz, M. & Stokes, N. R. 2016. *Compounds with activity against bacteria and mycobacteria*. WO/2016/067009.
- Corbett, K. D., Shultzaberger, R. K. & Berger, J. M. 2004. The C-terminal domain of DNA gyrase A adopts a DNA-bending beta-pinwheel fold. *Proceedings of the National Academy of Sciences of the United States of America*, 101, 7293-7298.
- Costenaro, L., Grossmann, J. G., Ebel, C. & Maxwell, A. 2005. Small-angle X-ray scattering reveals the solution structure of the full-length DNA gyrase A subunit. *Structure*, 13, 287-296.
- Costenaro, L., Grossmann, J. G., Ebel, C. & Maxwell, A. 2007. Modular structure of the full-length DNA gyrase B subunit revealed by small-angle X-ray scattering. *Structure*, 15, 329-339.
- Costerton, J. W., Geesey, G. G. & Cheng, K. J. 1978. How bacteria stick. *Scientific American*, 238, 86-&.
- Costerton, J. W., Ingram, J. M. & Cheng, K. J. 1974. Structure and function of cell-envelope of Gram-negative bacteria. *Bacteriological Reviews*, 38, 87-110.
- Cowtan, K. 2006. The Buccaneer software for automated model building. 1. Tracing protein chains. *Acta Crystallographica Section D-Biological Crystallography*, 62, 1002-1011.
- Cox, R. A. 2003. Correlation of the rate of protein synthesis and the third power of the RNA: protein ratio in *Escherichia coli* and *Mycobacterium tuberculosis*. *Microbiology-Sgm*, 149, 729-737.
- Critchlow, S. E. & Maxwell, A. 1996. DNA cleavage is not required for the binding of quinolone drugs to the DNA Gyrase - DNA complex. *Biochemistry*, 35, 7387-7393.
- Dave, C. G. & Shah, R. D. 2002. Annellation of triazole and tetrazole systems onto pyrrolo 2,3-d pyrimidines: Synthesis of tetrazolo 1,5-c pyrrolo 3,2-e -pyrimidines and triazolo 1,5-c pyrrolo- 3,2-e pyrimidines as potential antibacterial agents. *Molecules*, 7, 554-565.
- David, N. A. & Burgner, P. R. 1956. Clinical effectiveness and safety of novobiocin. *Antibiotic Med Clin Ther (New York)*, 2, 219-29.
- del Castillo, I., Vizan, J. L., Rodriguezsainz, M. D. & Moreno, F. 1991. An unusual mechanism for resistance to the antibiotic coumermycin-A1. *Proceedings of the National Academy of Sciences of the United States of America*, 88, 8860-8864.
- Drlica, K. & Zhao, X. L. 1997. DNA gyrase, topoisomerase IV, and the 4-quinolones. *Microbiology and Molecular Biology Reviews*, 61, 377-+.
- Dutta, R. & Inouye, M. 2000. GHKL, an emergent ATPase/kinase superfamily. *Trends in Biochemical Sciences*, 25, 24-28.
- Edwards, M. J., Flatman, R. H., Mitchenall, L. A., Stevenson, C. E. M., Le, T. B. K., Clarke, T. A., McKay, A. R., Fiedler, H. P., Buttner, M. J., Lawson, D. M. & Maxwell, A.

2009. A Crystal Structure of the Bifunctional Antibiotic Simocyclinone D8, Bound to DNA Gyrase. *Science*, 326, 1415-1418.
- Edwards, T. E., Liao, R. L., Phan, I., Myler, P. J. & Grundner, C. 2012. *Mycobacterium thermoresistibile* as a source of thermostable orthologs of *Mycobacterium tuberculosis* proteins. *Protein Science*, 21, 1093-1096.
- Emsley, P., Lohkamp, B., Scott, W. G. & Cowtan, K. 2010. Features and development of Coot. *Acta Crystallographica Section D-Biological Crystallography*, 66, 486-501.
- Esmail, H., Barry, C. E. & Wilkinson, R. J. 2012. Understanding latent tuberculosis: the key to improved diagnostic and novel treatment strategies. *Drug Discovery Today*, 17, 514-521.
- Esmail, H., Barry, C. E., Young, D. B. & Wilkinson, R. J. 2014. The ongoing challenge of latent tuberculosis. *Philosophical Transactions of the Royal Society B-Biological Sciences*, 369, 20130437.
- Evans, P. R. & Murshudov, G. N. 2013. How good are my data and what is the resolution? *Acta Crystallographica Section D-Biological Crystallography*, 69, 1204-1214.
- Falkinham, J. O., Norton, C. D. & LeChevallier, M. W. 2001. Factors influencing numbers of *Mycobacterium avium*, *Mycobacterium intracellulare*, and other mycobacteria in drinking water distribution systems. *Applied and Environmental Microbiology*, 67, 1225-1231.
- Flatman, R. H., Howells, A. J., Heide, L., Fiedler, H. P. & Maxwell, A. 2005. Simocyclinone D8, an inhibitor of DNA gyrase with a novel mode of action. *Antimicrobial Agents and Chemotherapy*, 49, 1093-1100.
- Flynn, J. L. & Chan, J. 2001. Tuberculosis: Latency and reactivation. *Infection and Immunity*, 69, 4195-4201.
- Food and Drug Administration, H. 2011. Determination That ALBAMYCIN (Novobiocin Sodium) Capsule, 250 Milligrams, Was Withdrawn From Sale for Reasons of Safety or Effectiveness. *Federal Register*, 76, 3143-3143.
- Forterre, P. 2006. DNA topoisomerase V: a new fold of mysterious origin. *Trends in Biotechnology*, 24, 245-247.
- Forterre, P., Gribaldo, S., Gadelle, D. & Serre, M. C. 2007. Origin and evolution of DNA topoisomerases. *Biochimie*, 89, 427-446.
- Foster, S. F., Martin, P., Davis, W., Allan, G. S., Mitchell, D. H. & Malik, R. 1999. Chronic pneumonia caused by *Mycobacterium thermoresistibile* in a cat. *Journal of Small Animal Practice*, 40, 433-438.
- Fox, W., Ellard, G. A. & Mitchison, D. A. 1999. Studies on the treatment of tuberculosis undertaken by the British Medical Research Council Tuberculosis Units, 1946-1986, with relevant subsequent publications. *International Journal of Tuberculosis and Lung Disease*, 3, S231-S279.
- Fu, G. S., Wu, J. J., Liu, W., Zhu, D. Y., Hu, Y. L., Deng, J. Y., Zhang, X. E., Bi, L. J. & Wang, D. C. 2009. Crystal structure of DNA gyrase B' domain sheds lights on the mechanism for T-segment navigation. *Nucleic Acids Research*, 37, 5908-5916.
- Fujimoto-Nakamura, M., Ito, H., Oyamada, Y., Nishino, T. & Yamagishi, J. 2005. Accumulation of mutations in both gyrB and parE genes is associated with high-level resistance to novobiocin in *Staphylococcus aureus*. *Antimicrobial Agents and Chemotherapy*, 49, 3810-3815.
- Gadelle, D., Krupovic, M., Raymann, K., Mayer, C. & Forterre, P. 2014. DNA topoisomerase VIII: a novel subfamily of type IIB topoisomerases encoded by free or integrated plasmids in Archaea and Bacteria. *Nucleic Acids Research*, 42, 8578-8591.
- Galm, U., Schimana, J., Fiedler, H. P., Schmidt, J., Li, S. M. & Heide, L. 2002. Cloning and analysis of the simocyclinone biosynthetic gene cluster of *Streptomyces antibioticus* TO 6040. *Archives of Microbiology*, 178, 102-114.
- Gardiner, L. P., Roper, D. I., Hammonds, T. R. & Maxwell, A. 1998. The N-terminal domain of human topoisomerase II alpha is a DNA-dependent ATPase. *Biochemistry*, 37, 16997-17004.

- Gellert, M., Mizuuchi, K., Odea, M. H., Itoh, T. & Tomizawa, J. I. 1977. Nalidixic-acid resistance - 2nd genetic character involved in DNA gyrase activity. *Proceedings of the National Academy of Sciences of the United States of America*, 74, 4772-4776.
- Gellert, M., Mizuuchi, K., Odea, M. H. & Nash, H. A. 1976. DNA Gyrase - enzyme that introduces superhelical turns into DNA. *Proceedings of the National Academy of Sciences of the United States of America*, 73, 3872-3876.
- Gillespie, S. H. 2016. The role of moxifloxacin in tuberculosis therapy. *European Respiratory Review*, 25, 10.
- Goto, T. & Wang, J. C. 1982. Yeast DNA topoisomerase II - an ATP-dependent type-II Topoisomerase that catalyzes the catenation, decatenation, unknotting, and relaxation of double-stranded DNA rings. *Journal of Biological Chemistry*, 257, 5866-5872.
- Gottler, T. & Klostermeier, D. 2007. Dissection of the nucleotide cycle of *B. subtilis* DNA gyrase and its modulation by DNA. *Journal of Molecular Biology*, 367, 1392-1404.
- Grooters, A. M., Couto, C. G., Andrews, J. M., Johnson, S. E., Kowalski, J. J. & Esplin, R. B. 1995. Systemic *Mycobacterium-smegmatis* infection in a dog. *Journal of the American Veterinary Medical Association*, 206, 200-202.
- Gross, C. H., Parsons, J. D., Grossman, T. H., Charifson, P. S., Bellon, S., Jernee, J., Dwyer, M., Chambers, S. P., Markland, W., Botfield, M. & Raybuck, S. A. 2003. Active-site residues of *Escherichia coli* DNA gyrase required in coupling ATP hydrolysis to DNA supercoiling and amino acid substitutions leading to novobiocin resistance. *Antimicrobial Agents and Chemotherapy*, 47, 1037-1046.
- Grossman, T. H., Bartels, D. J., Mullin, S., Gross, C. H., Parsons, J. D., Liao, Y. S., Grillot, A. L., Stamos, D., Olson, E. R., Charifson, P. S. & Mani, N. 2007. Dual targeting of GyrB and ParE by a novel aminobenzimidazole class of antibacterial compounds. *Antimicrobial Agents and Chemotherapy*, 51, 657-666.
- Gubaev, A. & Klostermeier, D. 2011. DNA-induced narrowing of the gyrase N-gate coordinates T-segment capture and strand passage. *Proceedings of the National Academy of Sciences of the United States of America*, 108, 14085-14090.
- Gubaev, A. & Klostermeier, D. 2012. Potassium Ions Are Required for Nucleotide-induced Closure of Gyrase N-gate. *Journal of Biological Chemistry*, 287, 10916-10921.
- Gubaev, A. & Klostermeier, D. 2014a. The mechanism of negative DNA supercoiling: A cascade of DNA-induced conformational changes prepares gyrase for strand passage. *DNA Repair*, 16, 23-34.
- Gubaev, A. & Klostermeier, D. 2014b. The mechanism of negative DNA supercoiling: A cascade of DNA-induced conformational changes prepares gyrase for strand passage (Reprinted from DNA Repair, VOL 16C, PG 23-34, 2014). *DNA Repair*, 20, 130-141.
- Gubaev, A., Weidlich, D. & Klostermeier, D. 2016. DNA gyrase with a single catalytic tyrosine can catalyze DNA supercoiling by a nicking-closing mechanism. *Nucleic Acids Research*, 44, 10354-10366.
- Guillemin, I., Sougakoff, W., Cambau, E., Revel-Viravau, V., Moreau, N. & Jarlier, V. 1999. Purification and inhibition by quinolones of DNA gyrases from *Mycobacterium avium*, *Mycobacterium smegmatis* and *Mycobacterium fortuitum* bv. peregrinum. *Microbiology-Uk*, 145, 2527-2532.
- Hameed, P. S., Solapure, S., Mukherjee, K., Nandi, V., Waterson, D., Shandil, R., Balganes, M., Sambandamurthy, V. K., Raichurkar, A. K., Deshpande, A., Ghosh, A., Awasthy, D., Shanbhag, G., Sheikh, G., McMiken, H., Puttur, J., Reddy, J., Werngren, J., Read, J., Kumar, M., Manjunatha, R., Chinnappattu, M., Madhavapeddi, P., Manjrekar, P., Basu, R., Gaonkar, S., Sharma, S., Hoffner, S., Humnabadkar, V., Subbulakshmi, V. & Panduga, V. 2014. Optimization of Pyrrolamides as Mycobacterial GyrB ATPase Inhibitors: Structure-Activity Relationship and In Vivo Efficacy in a Mouse Model of Tuberculosis. *Antimicrobial Agents and Chemotherapy*, 58, 61-70.
- Hammonds, T. R. & Maxwell, A. 1997. The DNA dependence of the ATPase activity of human DNA topoisomerase II alpha. *Journal of Biological Chemistry*, 272, 32696-32703.

- Harrison, J. J., Stremick, C. A., Turner, R. J., Allan, N. D., Olson, M. E. & Ceri, H. 2010. Microtiter susceptibility testing of microbes growing on peg lids: a miniaturized biofilm model for high-throughput screening. *Nature Protocols*, 5, 1236-1254.
- Harshey, R. M. & Ramakrishnan, T. 1977. Rate of ribonucleic-acid chain growth in *Mycobacterium tuberculosis* H37Rv. *Journal of Bacteriology*, 129, 616-622.
- Hartmann, S., Gubaev, A. & Klostermeier, D. 2017. Binding and Hydrolysis of a Single ATP Is Sufficient for N-Gate Closure and DNA Supercoiling by Gyrase. *Journal of Molecular Biology*, 429, 3717-3729.
- Hartung, F. & Puchta, H. 2000. Molecular characterisation of two paralogous SPO11 homologues in *Arabidopsis thaliana*. *Nucleic Acids Research*, 28, 1548-1554.
- Hashimi, S. M., Wall, M. K., Smith, A. B., Maxwell, A. & Birch, R. G. 2007. The phytotoxin albicidin is a novel inhibitor of DNA gyrase. *Antimicrobial Agents and Chemotherapy*, 51, 181-187.
- Hearnshaw, S. J., Edwards, M. J., Stevenson, C. E., Lawson, D. M. & Maxwell, A. 2014. A New Crystal Structure of the Bifunctional Antibiotic Simocyclinone D8 Bound to DNA Gyrase Gives Fresh Insight into the Mechanism of Inhibition. *Journal of Molecular Biology*, 426, 2023-2033.
- Heddle, J. G., Barnard, F. M., Wentzell, L. M. & Maxwell, A. 2000. The interaction of drugs with DNA gyrase: A model for the molecular basis of quinolone action. *Nucleosides Nucleotides & Nucleic Acids*, 19, 1249-1264.
- Heddle, J. G., Blance, S. J., Zamble, D. B., Hollfelder, F., Miller, D. A., Wentzell, L. M., Walsh, C. T. & Maxwell, A. 2001. The antibiotic microcin B17 is a DNA gyrase poison: Characterisation of the mode of inhibition. *Journal of Molecular Biology*, 307, 1223-1234.
- Hiasa, H. & Marians, K. J. 1994. Topoisomerase III, but not topoisomerase I, can support nascent chain elongation during theta type DNA replication. *Journal of Biological Chemistry*, 269, 32655-32659.
- Higgins, N. P. 2007. Chromosome Structure. *eLS*. Chichester: John Wiley & Sons Ltd.
- Higgins, N. P., Peebles, C. L., Sugino, A. & Cozzarelli, N. R. 1978. Purification of subunits of *Escherichia coli* DNA gyrase and reconstitution of enzymatic-activity. *Proceedings of the National Academy of Sciences of the United States of America*, 75, 1773-1777.
- Hilmy, K. M. H., Khalifa, M. M. A., Hawata, M. A., Keshk, R. M. A. & El-Torgman, A. 2010. Synthesis of new pyrrolo 2,3-d pyrimidine derivatives as antibacterial and antifungal agents. *European Journal of Medicinal Chemistry*, 45, 5243-5250.
- Hiriyanna, K. T. & Ramakrishnan, T. 1986. Deoxyribonucleic acid replication time in *Mycobacterium tuberculosis* H37Rv. *Archives of Microbiology*, 144, 105-109.
- Holdgate, G. A., Tunncliffe, A., Ward, W. H. J., Weston, S. A., Rosenbrock, G., Barth, P. T., Taylor, I. W. F., Pauptit, R. A. & Timms, D. 1997. The entropic penalty of ordered water accounts for weaker binding of the antibiotic novobiocin to a resistant mutant of DNA gyrase: A thermodynamic and crystallographic study. *Biochemistry*, 36, 9663-9673.
- Holmes, M. L. & Dyallsmith, M. L. 1991. Mutations in DNA gyrase result in novobiocin resistance in Halophilic archaeobacteria. *Journal of Bacteriology*, 173, 642-648.
- Horowitz, D. S. & Wang, J. C. 1987. Mapping the active site tyrosine of *Escherichia coli* DNA gyrase. *Journal of Biological Chemistry*, 262, 5339-5344.
- Houben, R. & Dodd, P. J. 2016. The Global Burden of Latent Tuberculosis Infection: A Re-estimation Using Mathematical Modelling. *Plos Medicine*, 13, 13.
- HSE 2013. The approved list of biological agents. In: BOOKS, H. (ed.) 3 ed.: Health and Safety Executive.
- Hsieh, T. J., Yen, T. J., Lin, T. S., Chang, H. T., Huang, S. Y., Hsu, C. H., Farh, L. & Chan, N. L. 2010. Twisting of the DNA-binding surface by a beta-strand-bearing proline modulates DNA gyrase activity. *Nucleic Acids Research*, 38, 4173-4181.

- Jackson, A. P. & Maxwell, A. 1993. Identifying the catalytic residue of the ATPase reaction of DNA gyrase. *Proceedings of the National Academy of Sciences of the United States of America*, 90, 11232-11236.
- Jahandideh, S., Jaroszewski, L. & Godzik, A. 2014. Improving the chances of successful protein structure determination with a random forest classifier. *Acta Crystallographica Section D-Biological Crystallography*, 70, 627-635.
- Jain, P. & Nagaraja, V. 2005. An atypical type II topoisomerase from *Mycobacterium smegmatis* with positive supercoiling activity. *Molecular Microbiology*, 58, 1392-1405.
- Joosten, R. P., Salzemann, J., Bloch, V., Stockinger, H., Berglund, A. C., Blanchet, C., Bongcam-Rudloff, E., Combet, C., Da Costa, A. L., Deleage, G., Diarena, M., Fabbretti, R., Fettahi, G., Flegel, V., Gisel, A., Kasam, V., Kervinen, T., Korpelainen, E., Mattila, K., Pagni, M., Reichstadt, M., Breton, V., Tickle, I. J. & Vriend, G. 2009. PDB_REDO: automated re-refinement of X-ray structure models in the PDB. *Journal of Applied Crystallography*, 42, 376-384.
- Kampranis, S. C., Bates, A. D. & Maxwell, A. 1999a. A model for the mechanism of strand passage by DNA gyrase. *Proceedings of the National Academy of Sciences of the United States of America*, 96, 8414-8419.
- Kampranis, S. C., Gormley, N. A., Tranter, R., Orphanides, G. & Maxwell, A. 1999b. Probing the binding of coumarins and cyclothialidines to DNA gyrase. *Biochemistry*, 38, 1967-1976.
- Kampranis, S. C. & Maxwell, A. 1996. Conversion of DNA gyrase into a conventional type II topoisomerase. *Proceedings of the National Academy of Sciences of the United States of America*, 93, 14416-14421.
- Karkare, S., Brown, A., Parish, T. & Maxwell, A. 2013a. Identification of the likely translational start of *Mycobacterium tuberculosis* GyrB. *BMC Research Notes*, 6, 274-279.
- Karkare, S., Chung, T. T. H., Collin, F., Mitchenall, L. A., McKay, A. R., Greive, S. J., Meyer, J. J. M., Lall, N. & Maxwell, A. 2013b. The Naphthoquinone Diospyrin Is an Inhibitor of DNA Gyrase with a Novel Mechanism of Action. *Journal of Biological Chemistry*, 288, 5149-5156.
- Kashyap, A., Singh, P. K. & Silakari, O. 2018. Chemical classes targeting energy supplying GyrB domain of *Mycobacterium tuberculosis*. *Tuberculosis*, 113, 43-54.
- Kato, J., Nishimura, Y., Imamura, R., Niki, H., Hiraga, S. & Suzuki, H. 1990. New topoisomerase essential for chromosome segregation in *Escherichia coli*. *Cell*, 63, 393-404.
- Khan, M. R. & Rwekika, E. 1992. Triterpenoids from the leaves of four species of family Ebenaceae. *Fitoterapia*, 63, 375-376.
- Khodursky, A. B., Peter, B. J., Schmidt, M. B., DeRisi, J., Botstein, D., Brown, P. O. & Cozzarelli, N. R. 2000. Analysis of topoisomerase function in bacterial replication fork movement: Use of DNA microarrays. *Proceedings of the National Academy of Sciences of the United States of America*, 97, 9419-9424.
- Khodursky, A. B., Zechiedrich, E. L. & Cozzarelli, N. R. 1995. Topoisomerase IV is a target of quinolones in *Escherichia coli*. *Proceedings of the National Academy of Sciences of the United States of America*, 92, 11801-11805.
- Kirby, W. M. M., Hudson, D. G. & Noyes, W. D. 1956. Clinical and laboratory studies of novobiocin, a new antibiotic. *Archives of Internal Medicine*, 98, 1-7.
- Kirkegaard, K. & Wang, J. C. 1985. Bacterial DNA topoisomerase I can relax positively supercoiled DNA containing a single-stranded loop. *Journal of Molecular Biology*, 185, 625-637.
- Klostermeier, D. 2018. Why Two? On the Role of (A-)Symmetry in Negative Supercoiling of DNA by Gyrase. *International Journal of Molecular Sciences*, 19, 15.
- Kocagoz, T., Hackbarth, C. J., Unsal, I., Rosenberg, E. Y., Nikaido, H. & Chambers, H. F. 1996. Gyrase mutations in laboratory-selected, fluoroquinolone-resistant mutants of

- Mycobacterium tuberculosis* H37Ra. *Antimicrobial Agents and Chemotherapy*, 40, 1768-1774.
- Kreuzer, K. N. & Jongeneel, C. V. 1983. Escherichia coli Phage-T4 topoisomerase. *Methods in Enzymology*, 100, 144-160.
- LaBombardi, V. J., Shastry, L. & Tischler, H. 2005. *Mycobacterium thermoresistibile* infection following knee-replacement surgery. *Journal of Clinical Microbiology*, 43, 5393-5394.
- Lafitte, D., Lamour, V., Tsvetkov, P. O., Makarov, A. A., Klich, M., Deprez, P., Moras, D., Briand, C. & Gilli, R. 2002. DNA gyrase interaction with coumarin-based inhibitors: The role of the hydroxybenzoate isopentenyl moiety and the 5'-methyl group of the noviose. *Biochemistry*, 41, 7217-7223.
- Lall, N., Meyer, J. J. M., Wang, Y., Bapela, N. B., van Rensburg, C. E. J., Fourie, B. & Franzblau, S. G. 2005. Characterization of intracellular activity of antitubercular constituents from the roots of *Euclea natalensis*. *Pharmaceutical Biology*, 43, 353-357.
- Lamour, V., Hoermann, L., Jeltsch, J. M., Oudet, P. & Moras, D. 2002. Crystallization of the 43 kDa ATPase domain of *Thermus thermophilus* gyrase B in complex with novobiocin. *Acta Crystallographica Section D-Biological Crystallography*, 58, 1376-1378.
- Lanz, M. A., Farhat, M. & Klostermeier, D. 2014. The acidic C-terminal tail of the GyrA subunit moderates the DNA supercoiling activity of *Bacillus subtilis* gyrase. *Journal of Biological Chemistry*, 289, 12275-12285.
- Lanz, M. A. & Klostermeier, D. 2012. The GyrA-box determines the geometry of DNA bound to gyrase and couples DNA binding to the nucleotide cycle. *Nucleic Acids Research*, 40, 10893-10903.
- Laponogov, I., Pan, X. S., Veselkov, D. A., Skamrova, G. B., Umrekar, T. R., Fisher, L. M. & Sanderson, M. R. 2018. Trapping of the transport-segment DNA by the ATPase domains of a type II topoisomerase. *Nature Communications*, 9, 14.
- Laponogov, I., Veselkov, D. A., Crevel, I. M. T., Pan, X. S., Fisher, L. M. & Sanderson, M. R. 2013. Structure of an 'open' clamp type II topoisomerase-DNA complex provides a mechanism for DNA capture and transport. *Nucleic Acids Research*, 41, 9911-9923.
- Lardizabal, A. A. & Reichman, L. B. 2017. Diagnosis of Latent Tuberculosis Infection. *Microbiology Spectrum*, 5, 8.
- Lavasani, L. S. & Hiasa, H. 2001. A ParE-ParC fusion protein is a functional topoisomerase. *Biochemistry*, 40, 8438-8443.
- Lewis, R. J., Singh, O. M. P., Smith, C. V., Skarzynski, T., Maxwell, A., Wonacott, A. J. & Wigley, D. B. 1996. The nature of inhibition of DNA gyrase by the coumarins and the cyclothialidines revealed by X-ray crystallography. *Embo Journal*, 15, 1412-1420.
- Lindsley, J. E. & Wang, J. C. 1991. Proteolysis patterns of epitopically labeled yeast DNA topoisomerase II suggest an allosteric transition in the enzyme induced by ATP binding. *Proceedings of the National Academy of Sciences of the United States of America*, 88, 10485-10489.
- Liu, F., Andrews, D. & Wright, D. N. 1984. *Mycobacterium-thermoresistibile* infection in an immunocompromised host. *Journal of Clinical Microbiology*, 19, 546-547.
- Liu, L. F. 1989. DNA Topoisomerase poisons as antitumor drugs. *Annual Review of Biochemistry*, 58, 351-375.
- Liu, L. F., Liu, C. C. & Alberts, B. M. 1979. T4-DNA topoisomerase - new ATP-dependent enzyme essential for initiation of bacteriophage T4 DNA-replication. *Nature*, 281, 456-461.
- Liu, L. F., Liu, C. C. & Alberts, B. M. 1980. Type-II DNA topoisomerases - enzymes that can un-knot a topologically knotted DNA molecule via a reversible double-strand break. *Cell*, 19, 697-707.
- Liu, L. F. & Wang, J. C. 1978. *Micrococcus luteus* DNA gyrase - active components and a model for its supercoiling of DNA. *Proceedings of the National Academy of Sciences of the United States of America*, 75, 2098-2102.

- Liu, L. F. & Wang, J. C. 1987. Supercoiling of the DNA-template during transcription. *Proceedings of the National Academy of Sciences of the United States of America*, 84, 7024-7027.
- Löwenstein, E. 1920. Vorlesungen über Bakteriologie, Immunität, spezifische Diagnostik und Therapie der Tuberkulose. *Jena: Fischer*.
- Lu, J., Patel, S., Sharma, N., Soisson, S. M., Kishii, R., Takei, M., Fulkuda, Y., Lumb, K. J. & Singh, S. B. 2014. Structures of Kibdelomycin Bound to *Staphylococcus aureus* GyrB and ParE Showed a Novel U-Shaped Binding Mode. *Acs Chemical Biology*, 9, 2023-2031.
- Lulchev, P. & Klostermeier, D. 2014. Reverse gyrase-recent advances and current mechanistic understanding of positive DNA supercoiling. *Nucleic Acids Research*, 42, 8200-8213.
- Madhusudan, K., Ramesh, V. & Nagaraja, V. 1994. Molecular cloning of GyrA and GyrB genes of *Mycobacterium tuberculosis* - analysis of nucleotide sequence. *Biochemistry and Molecular Biology International*, 33, 651-660.
- Manjunatha, U. H., Dalal, M., Chatterji, M., Radha, D. R., Visweswariah, S. S. & Nagaraja, V. 2002. Functional characterisation of mycobacterial DNA gyrase: an efficient decatenase. *Nucleic Acids Research*, 30, 2144-2153.
- Matrat, S., Veziris, N., Mayer, C., Jarlier, V., Truffot-Pernot, C., Camuset, J., Bouvet, E., Cambau, E. & Aubry, A. 2006. Functional analysis of DNA gyrase mutant enzymes carrying mutations at position 88 in the A subunit found in clinical strains of *Mycobacterium tuberculosis* resistant to fluoroquinolones. *Antimicrobial Agents and Chemotherapy*, 50, 4170-4173.
- Maurer, F. P., Bruderer, V. L., Ritter, C., Castelberg, C., Bloemberg, G. V. & Bottger, E. C. 2014. Lack of Antimicrobial Bactericidal Activity in *Mycobacterium abscessus*. *Antimicrobial Agents and Chemotherapy*, 58, 3828-3836.
- Maxwell, A. 1993. The interaction between coumarin drugs and DNA gyrase. *Molecular Microbiology*, 9, 681-686.
- Maxwell, A. & Gellert, M. 1984. The DNA dependence of the ATPase activity of DNA gyrase. *Journal of Biological Chemistry*, 259, 4472-4480.
- Maxwell, A. & Gellert, M. 1986. Mechanistic aspects of DNA topoisomerases. *Advances in Protein Chemistry*, 38, 69-107.
- Maxwell, A. & Lawson, D. M. 2003. The ATP-binding site of type II topoisomerases as a target for antibacterial drugs. *Current Topics in Medicinal Chemistry*, 3, 283-303.
- McCoy, A. J., Grosse-Kunstleve, R. W., Adams, P. D., Winn, M. D., Storoni, L. C. & Read, R. J. 2007. Phaser crystallographic software. *Journal of Applied Crystallography*, 40, 658-674.
- McGarry, D. H., Cooper, I. R., Walker, R., Warrilow, C. E., Pichowicz, M., Ratcliffe, A. J., Salisbury, A. M., Savage, V. J., Moyo, E., Maclean, J., Smith, A., Charrier, C., Stokes, N. R., Lindsay, D. M. & Kerr, W. J. 2018. Design, synthesis and antibacterial properties of pyrimido 4,5-b indol-8-amine inhibitors of DNA gyrase. *Bioorganic & Medicinal Chemistry Letters*, 28, 2998-3003.
- Mendes, V., Blaszczyk, M., Maranha, A., Empadinhas, N. & Blundell, T. L. 2015. Structure of *Mycobacterium thermoresistibile* GlgE defines novel conformational states that contribute to the catalytic mechanism. *Scientific Reports*, 5, 17144.
- Menzio, F. D., Rouse, J. H., Alavi, M., LaudeSharp, M., Muller, J., Bischoff, R., Brennan, M. J. & Locht, C. 1996. Identification of a heparin-binding hemagglutinin present in mycobacteria. *Journal of Experimental Medicine*, 184, 993-1001.
- Miller, K. G., Liu, L. F. & Englund, P. T. 1981. A homogeneous type-II DNA topoisomerase from Hela-cell nuclei. *Journal of Biological Chemistry*, 256, 9334-9339.
- Mitchenall, L. A., Hipkin, R. E., Piperakis, M. M., Burton, N. P. & Maxwell, A. 2018. A rapid high-resolution method for resolving DNA topoisomers. *BMC Research Notes*, 11, 37.
- Mizuuchi, K., Odea, M. H. & Gellert, M. 1978. DNA Gyrase - Subunit structure and ATPase activity of the purified enzyme. *Proceedings of the National Academy of Sciences of the United States of America*, 75, 5960-5963.

- Mohan, A., Padiadpu, J., Baloni, P. & Chandra, N. 2015. Complete Genome Sequences of a *Mycobacterium smegmatis* Laboratory Strain (MC2 155) and Isoniazid-Resistant (4XR1/R2) Mutant Strains. *Genome Announc*, 3.
- Munoz-Egea, M. C., Garcia-Pedrazuela, M. & Esteban, J. 2015. In vitro susceptibility of rapidly growing mycobacteria biofilms against different antimicrobials. *Enfermedades Infecciosas Y Microbiologia Clinica*, 33, 136-137.
- Munoz, R., Bustamante, M. & Delacampa, A. G. 1995. Ser-127-to-Leu substitution in the DNA gyrase B subunit of *Streptococcus pneumoniae* is implicated in novobiocin resistance. *Journal of Bacteriology*, 177, 4166-4170.
- Murshudov, G. N., Vagin, A. A. & Dodson, E. J. 1997. Refinement of macromolecular structures by the maximum-likelihood method. *Acta Crystallographica Section D-Structural Biology*, 53, 240-255.
- Musuka, S., Srivastava, S., Dona, C. W. S., Meek, C., Leff, R., Pasipanodya, J. & Gumbo, T. 2013. Thioridazine Pharmacokinetic-Pharmacodynamic Parameters "Wobble" during Treatment of Tuberculosis: a Theoretical Basis for Shorter-Duration Curative Monotherapy with Congeners. *Antimicrobial Agents and Chemotherapy*, 57, 5870-5877.
- Nagaraja, V., Godbole, A. A., Henderson, S. R. & Maxwell, A. 2017. DNA topoisomerase I and DNA gyrase as targets for TB therapy. *Drug Discovery Today*, 22, 510-518.
- Neeley, S. P. & Denning, D. W. 1989. Cutaneous *Mycobacterium thermoresistibile* infection in a heart-transplant recipient. *Reviews of Infectious Diseases*, 11, 608-611.
- Neuman, K. C. 2010. Evolutionary twist on topoisomerases: Conversion of gyrase to topoisomerase IV. *Proceedings of the National Academy of Sciences of the United States of America*, 107, 22363-22364.
- Newton, J. A., Weiss, P. J., Bowler, W. A. & Oldfield, E. C. 1993. Soft-tissue infection due to *Mycobacterium-smegmatis* - report of 2 cases. *Clinical Infectious Diseases*, 16, 531-533.
- Nguyen, H. H., Park, J., Kang, S. & Kim, M. 2015. Surface Plasmon Resonance: A Versatile Technique for Biosensor Applications. *Sensors*, 15, 10481-10510.
- Nikaido, H. 2001. Preventing drug access to targets: cell surface permeability barriers and active efflux in bacteria. *Seminars in Cell & Developmental Biology*, 12, 215-223.
- Nitiss, J. L. 2009. Targeting DNA topoisomerase II in cancer chemotherapy. *Nature Reviews Cancer*, 9, 338-350.
- Noble, C. G. & Maxwell, A. 2002. The role of GyrB in the DNA cleavage-religation reaction of DNA gyrase: A proposed two metal-ion mechanism. *Journal of Molecular Biology*, 318, 361-371.
- Norton, B. L. & Holland, D. P. 2012. Current management options for latent tuberculosis: a review. *Infect Drug Resist*, 5, 163-73.
- Norton, C. D., LeChevallier, M. W. & Falkinham, J. O. 2004. Survival of *Mycobacterium avium* in a model distribution system. *Water Research*, 38, 1457-1466.
- Nurse, P., Levine, C., Hassing, H. & Marians, K. J. 2003. Topoisomerase III can serve as the cellular decatenase in *Escherichia coli*. *Journal of Biological Chemistry*, 278, 8653-8660.
- Ojha, A. K., Baughn, A. D., Sambandan, D., Hsu, T., Trivelli, X., Guerardel, Y., Alahari, A., Kremer, L., Jacobs, W. R. & Hatfull, G. F. 2008. Growth of *Mycobacterium tuberculosis* biofilms containing free mycolic acids and harbouring drug-tolerant bacteria. *Molecular Microbiology*, 69, 164-174.
- Onodera, Y., Tanaka, M. & Sato, K. 2001. Inhibitory activity of quinolones against DNA gyrase of *Mycobacterium tuberculosis*. *Journal of Antimicrobial Chemotherapy*, 47, 447-450.
- Oppegard, L. M., Hamann, B. L., Streck, K. R., Ellis, K. C., Fiedler, H. P., Khodursky, A. B. & Hiasa, H. 2009. In Vivo and In Vitro Patterns of the Activity of Simocyclinone D8, an Angucyclinone Antibiotic from *Streptomyces antibioticus*. *Antimicrobial Agents and Chemotherapy*, 53, 2110-2119.

- Orphanides, G. & Maxwell, A. 1994. Evidence for a conformational change in the DNA gyrase - DNA complex from hydroxyl radical footprinting. *Nucleic Acids Research*, 22, 1567-1575.
- Papillon, J., Menetret, J.-F., Batisse, C., Helye, R., Schultz, P., Potier, N. & Lamour, V. 2013. Structural insight into negative DNA supercoiling by DNA gyrase, a bacterial type 2A DNA topoisomerase. *Nucleic Acids Research*, 41, 7815-7827.
- Pierrat, O. A. & Maxwell, A. 2003. The action of the bacterial toxin microcin B17 - Insight into the cleavage-religation reaction of DNA gyrase. *Journal of Biological Chemistry*, 278, 35016-35023.
- Pierre-Audigier, C., Jouanguy, E., Lamhamedi, S., Altare, F., Rauzier, J., Vincent, V., Canioni, D., Emile, J. F., Fischer, A., Blanche, S., Gaillard, J. L. & Casanova, J. L. 1997. Fatal disseminated *Mycobacterium smegmatis* infection in a child with inherited interferon gamma receptor deficiency. *Clinical Infectious Diseases*, 24, 982-984.
- Postow, L., Crisona, N. J., Peter, B. J., Hardy, C. D. & Cozzarelli, N. R. 2001. Topological challenges to DNA replication: Conformations at the fork. *Proceedings of the National Academy of Sciences of the United States of America*, 98, 8219-8226.
- Rajan, R., Taneja, B. & Mondragon, A. 2010. Structures of Minimal Catalytic Fragments of Topoisomerase V Reveals Conformational Changes Relevant for DNA Binding. *Structure*, 18, 829-838.
- Ramakrishnan, L. 2012. Revisiting the role of the granuloma in tuberculosis. *Nature Reviews Immunology*, 12, 352-366.
- Redinbo, M. R., Stewart, L., Kuhn, P., Champoux, J. J. & Hol, W. G. J. 1998. Crystal structures of human topoisomerase I in covalent and noncovalent complexes with DNA. *Science*, 279, 1504-1513.
- Reece, R. J. & Maxwell, A. 1991a. The C-terminal domain of the *Escherichia coli* DNA gyrase A subunit is a DNA-binding protein. *Nucleic Acids Research*, 19, 1399-1405.
- Reece, R. J. & Maxwell, A. 1991b. Probing the limits of the DNA breakage-reunion domain of the *Escherichia coli* DNA gyrase-A protein. *Journal of Biological Chemistry*, 266, 3540-3546.
- Renaud, J. P., Chari, A., Ciferri, C., Liu, W. T., Remigy, H. W., Stark, H. & Wiesmann, C. 2018. Cryo-EM in drug discovery: achievements, limitations and prospects. *Nature Reviews Drug Discovery*, 17, 471-492.
- Reynolds, J., Moyes, R. B. & Breakwell, D. P. 2009. Differential Staining of Bacteria: Acid Fast Stain. *Current Protocols in Microbiology*, 15, A.3H.1-A.3H.5.
- Rich, R. L., Hoth, L. R., Geoghegan, K. F., Brown, T. A., LeMotte, P. K., Simons, S. P., Hensley, P. & Myszka, D. G. 2002. Kinetic analysis of estrogen receptor/ligand interactions. *Proceedings of the National Academy of Sciences of the United States of America*, 99, 8562-8567.
- Richards, J. & Ojha, A. K. 2014. Mycobacterial Biofilms. In: HATFULL G, J. W. (ed.) *Molecular Genetics of Mycobacteria*. 2nd ed. Washington, D.C.: ASM Press.
- Rigouts, L., Coeck, N., Gumusboga, M., de Rijk, W. B., Aung, K. J. M., Hossain, M. A., Fissette, K., Rieder, H. L., Meehan, C. J., de Jong, B. C. & Van Deun, A. 2016. Specific gyrA gene mutations predict poor treatment outcome in MDR-TB. *The Journal of antimicrobial chemotherapy*, 71, 314-23.
- Roca, J., Berger, J. M., Harrison, S. C. & Wang, J. C. 1996. DNA transport by a type II topoisomerase: Direct evidence for a two-gate mechanism. *Proceedings of the National Academy of Sciences of the United States of America*, 93, 4057-4062.
- Rodrigues, L. C., Mangtani, P. & Abubakar, I. 2011. How does the level of BCG vaccine protection against tuberculosis fall over time? *British Medical Journal*, 343, d5974.
- Roue, M., Agrawal, A., Volker, C., Mossakowska, D., Mayer, C. & Bax, B. D. 2013. Purification, crystallization and preliminary X-ray crystallographic studies of the *Mycobacterium tuberculosis* DNA gyrase ATPase domain. *Acta Crystallographica Section F-Structural Biology and Crystallization Communications*, 69, 679-682.
- Roy, A., Eisenhut, M., Harris, R. J., Rodrigues, L. C., Sridhar, S., Habermann, S., Snell, L., Mangtani, P., Adetifa, I., Lalvani, A. & Abubakar, I. 2014. Effect of BCG vaccination

- against *Mycobacterium tuberculosis* infection in children: systematic review and meta-analysis. *Bmj-British Medical Journal*, 349, g4643.
- Runyon, E. H. 1959. Anonymous Mycobacteria in pulmonary disease. *Medical Clinics of North America*, 43, 273-290.
- Ruthenburg, A. J., Graybosch, D. M., Huetsch, J. C. & Verdine, G. L. 2005. A superhelical spiral in the *Escherichia coli* DNA gyrase A C-terminal domain imparts unidirectional supercoiling bias. *Journal of Biological Chemistry*, 280, 26177-26184.
- Rybenkov, V. V., Ullsperger, C., Vologodskii, A. V. & Cozzarelli, N. R. 1997. Simplification of DNA topology below equilibrium values by type II topoisomerases. *Science*, 277, 690-693.
- Saffo, Z. & Ognjan, A. 2016. *Mycobacterium smegmatis* infection of a prosthetic total knee arthroplasty. *Idcases*, 5, 80-82.
- Saunders, B. M. & Britton, W. J. 2007. Life and death in the granuloma: immunopathology of tuberculosis. *Immunology and Cell Biology*, 85, 103-111.
- Schimana, J., Fiedler, H. P., Groth, I., Sussmuth, R., Beil, W., Walker, M. & Zeeck, A. 2000. Simocyclinones, novel cytostatic angucyclinone antibiotics produced by *Streptomyces antibioticus* Tu 6040 I. Taxonomy, fermentation, isolation and biological activities. *Journal of Antibiotics*, 53, 779-787.
- Schmidt, B. H., Osheroff, N. & Berger, J. M. 2012. Structure of a topoisomerase II-DNA-nucleotide complex reveals a new control mechanism for ATPase activity. *Nature Structural & Molecular Biology*, 19, 1147-1154.
- Schoeffler, A. J., May, A. P. & Berger, J. M. 2010. A domain insertion in *Escherichia coli* GyrB adopts a novel fold that plays a critical role in gyrase function. *Nucleic Acids Research*, 38, 7830-7844.
- Schulze-Robbeke, R., Janning, B. & Fischeder, R. 1992. Occurrence of mycobacteria in biofilm samples. *Tubercle and Lung Disease*, 73, 141-144.
- Seasholtz, A. F. & Greenberg, G. R. 1983. Identification of bacteriophage-T4 gene-60 product and a role for this protein in DNA topoisomerase. *Journal of Biological Chemistry*, 258, 1221-1226.
- Selwyn, P. A., Hartel, D., Lewis, V. A., Schoenbaum, E. E., Vermund, S. H., Klein, R. S., Walker, A. T. & Friedland, G. H. 1989. A Prospective-study of the risk of tuberculosis among intravenous drug-users with human immunodeficiency virus-infection. *New England Journal of Medicine*, 320, 545-550.
- Sendi, P. & Brent, A. 2016. *Mycobacterium tuberculosis* and prosthetic joint infection. *Lancet Infectious Diseases*, 16, 893-894.
- Shapiro, T. A., Klein, V. A. & Englund, P. T. 1999. Isolation of kinetoplast DNA. In: BJORNSTI, M.-A. & OSHEROFF, N. (eds.) *DNA Topoisomerase Protocols*. 1 ed. Totowa, N. Jersey: Humana Press.
- Shimizu, F. 2012. *Mycobacterium smegmatis* soft tissue infection. *International Journal of Dermatology*, 51, 1518-1520.
- Shirude, P. S., Madhavapeddi, P., Tucker, J. A., Murugan, K., Patil, V., Basavarajappa, H., Raichurkar, A. V., Humnabadkar, V., Hussein, S., Sharma, S., Ramya, V. K., Narayan, C. B., Balganes, T. S. & Sambandamurthy, V. K. 2013. Aminopyrazinamides: Novel and Specific GyrB Inhibitors that Kill Replicating and Nonreplicating *Mycobacterium tuberculosis*. *Acs Chemical Biology*, 8, 519-523.
- Shockman, G. D. & Barrett, J. F. 1983. Structure, function, and assembly of cell-walls of Gram-positive bacteria. *Annual Review of Microbiology*, 37, 501-527.
- Shure, M., Pulleyblank, D. E. & Vinograd, J. 1977. Problems of eukaryotic and prokaryotic DNA packaging and invivo conformation posed by superhelical density heterogeneity. *Nucleic Acids Research*, 4, 1183-1205.
- Slabinski, L., Jaroszewski, L., Rychlewski, L., Wilson, I. A., Lesley, S. A. & Godzik, A. 2007. XtalPred: a web server for prediction of protein crystallizability. *Bioinformatics*, 23, 3403-3405.

- Slesarev, A. I., Stetter, K. O., Lake, J. A., Gellert, M., Krah, R. & Kozyavkin, S. A. 1993. DNA topoisomerase V is a relative of eukaryotic topoisomerase I from a hyperthermophilic prokaryote. *Nature*, 364, 735-736.
- Spinner, R. J., Sexton, D. J., Goldner, R. D. & Levin, L. S. 1996. Periprosthetic infections due to *Mycobacterium tuberculosis* in patients with no prior history of tuberculosis. *Journal of Arthroplasty*, 11, 217-222.
- Srikannathasan, V., Wohlkonig, A., Shillings, A., Singh, O., Chan, P. F., Huang, J. Z., Gwynn, M. N., Fosberry, A. P., Homes, P., Hibbs, M., Theobald, A. J., Spitzfaden, C. & Bax, B. D. 2015. Crystallization and initial crystallographic analysis of covalent DNA-cleavage complexes of *Staphylococcus aureus* DNA gyrase with QPT-1, moxifloxacin and etoposide. *Acta Crystallographica Section F-Structural Biology Communications*, 71, 1242-1246.
- Stanger, F. V., Dehio, C. & Schirmer, T. 2014. Structure of the N-Terminal Gyrase B Fragment in Complex with ADP center dot P-i Reveals Rigid-Body Motion Induced by ATP Hydrolysis. *Plos One*, 9, 13.
- Steck, T. R. & Drlica, K. 1984. Bacterial chromosome segregation - evidence for DNA gyrase involvement in decatenation. *Cell*, 36, 1081-1088.
- Stelljes, J. T., Weidlich, D., Gubaev, A. & Klostermeier, D. 2018. Gyrase containing a single C-terminal domain catalyzes negative supercoiling of DNA by decreasing the linking number in steps of two. *Nucleic Acids Research*, 46, 6773-6784.
- Stephan, J., Bender, J., Wolschendorf, F., Hoffmann, C., Roth, E., Mailander, C., Engelhardt, H. & Niederweis, M. 2005. The growth rate of *Mycobacterium smegmatis* depends on sufficient porin-mediated influx of nutrients. *Molecular Microbiology*, 58, 714-730.
- Stieger, M., Angehrn, P., Wohlgensinger, B. & Gmunder, H. 1996. GyrB mutations in *Staphylococcus aureus* strains resistant to cyclothialidine, coumermycin, and novobiocin. *Antimicrobial Agents and Chemotherapy*, 40, 1060-1062.
- Stivers, J. T., Harris, T. K. & Mildvan, A. S. 1997. Vaccinia DNA topoisomerase I: Evidence supporting a free rotation mechanism for DNA supercoil relaxation. *Biochemistry*, 36, 5212-5222.
- Stuchinskaya, T., Mitchenall, L. A., Schoeffler, A. J., Corbett, K. D., Berger, J. M., Bates, A. D. & Maxwell, A. 2009. How do type II topoisomerases use ATP hydrolysis to simplify DNA topology beyond equilibrium? Investigating the relaxation reaction of nonsupercoiling type II topoisomerases. *Journal of Molecular Biology*, 385, 1397-1408.
- Styblo, K. 1980. Recent advances in epidemiological research in tuberculosis. *Advances in tuberculosis research. Fortschritte der Tuberkuloseforschung. Progres de l'exploration de la tuberculose*, 20, 1-63.
- Sugino, A. & Cozzarelli, N. R. 1980. The intrinsic ATPase of DNA gyrase. *Journal of Biological Chemistry*, 255, 6299-6306.
- Sugino, A., Higgins, N. P., Brown, P. O., Peebles, C. L. & Cozzarelli, N. R. 1978. Energy coupling in DNA gyrase and mechanism of action of novobiocin. *Proceedings of the National Academy of Sciences of the United States of America*, 75, 4838-4842.
- Sugino, A., Peebles, C. L., Kreuzer, K. N. & Cozzarelli, N. R. 1977. Mechanism of action of nalidixic acid - purification of *Escherichia coli*-NALA gene product and its relationship to DNA gyrase and a novel nicking-closing enzyme. *Proceedings of the National Academy of Sciences of the United States of America*, 74, 4767-4771.
- Suy, F., Carricajo, A., Grattard, F., Cazorla, C., Denis, C., Girardin, P., Lucht, F. & Botelho-Nevers, E. 2013. Infection Due to *Mycobacterium thermoresistibile*: a Case Associated with an Orthopedic Device. *Journal of Clinical Microbiology*, 51, 3154-3156.
- Tamura, J. K., Bates, A. D. & Gellert, M. 1992. Slow interaction of 5'-adenylyl-beta,gamma-imidodiphosphate with *Escherichia coli* DNA gyrase - evidence for cooperativity in nucleotide binding. *Journal of Biological Chemistry*, 267, 9214-9222.

- Taneja, B., Patel, A., Slesarev, A. & Mondragon, A. 2006. Structure of the N-terminal fragment of topoisomerase V reveals a new family of topoisomerases. *Embo Journal*, 25, 398-408.
- Tannock, J. 1973. Naphthaquinones from *Diospros* and *Euclea* species. *Phytochemistry*, 12, 2066-2067.
- Tari, L. W., Li, X. M., Trzoss, M., Bensen, D. C., Chen, Z. Y., Lam, T., Zhang, J. H., Lee, S. J., Hough, G., Phillipson, D., Akers-Rodriguez, S., Cunningham, M. L., Kwan, B. P., Nelson, K. J., Castellano, A., Locke, J. B., Brown-Driver, V., Murphy, T. M., Ong, V. S., Pillar, C. M., Shinabarger, D. L., Nix, J., Lightstone, F. C., Wong, S. E., Nguyen, T. B., Shaw, K. J. & Finn, J. 2013a. Tricyclic GyrB/ParE (TriBE) Inhibitors: A New Class of Broad-Spectrum Dual-Targeting Antibacterial Agents. *Plos One*, 8, e84409.
- Tari, L. W., Trzoss, M., Bensen, D. C., Li, X. M., Chen, Z. Y., Lam, T., Zhang, J. H., Creighton, C. J., Cunningham, M. L., Kwan, B., Stidham, M., Shaw, K. J., Lightstone, F. C., Wong, S. E., Nguyen, T. B., Nix, J. & Finn, J. 2013b. Pyrrolopyrimidine inhibitors of DNA gyrase B (GyrB) and topoisomerase IV (ParE). Part I: Structure guided discovery and optimization of dual targeting agents with potent, broad-spectrum enzymatic activity. *Bioorganic & Medicinal Chemistry Letters*, 23, 1529-1536.
- Theobald, U., Schimana, J. & Fiedler, H. P. 2000. Microbial growth and production kinetics of *Streptomyces antibioticus* Tu 6040. *Antonie Van Leeuwenhoek International Journal of General and Molecular Microbiology*, 78, 307-313.
- Trefzer, A., Pelzer, S., Schimana, J., Stockert, S., Bihlmaier, C., Fiedler, H. P., Welzel, K., Vente, A. & Bechthold, A. 2002. Biosynthetic gene cluster of simocyclinone, a natural multihybrid antibiotic. *Antimicrobial Agents and Chemotherapy*, 46, 1174-1182.
- Tretter, E. M. & Berger, J. M. 2012. Mechanisms for defining supercoiling set point of DNA gyrase orthologs II-The shape of the GyrA subunit C-terminal domain (CTD) is not a sole determinant for controlling supercoiling efficiency. *Journal of Biological Chemistry*, 287, 18645-18654.
- Tretter, E. M., Lerman, J. C. & Berger, J. M. 2010. A naturally chimeric type IIA topoisomerase in *Aquifex aeolicus* highlights an evolutionary path for the emergence of functional paralogs. *Proceedings of the National Academy of Sciences of the United States of America*, 107, 22055-22059.
- Trigueros, S. & Roca, J. 2002. A GyrB-GyrA fusion protein expressed in yeast cells is able to remove DNA supercoils but cannot substitute eukaryotic topoisomerase II. *Genes to Cells*, 7, 249-257.
- Trunz, B. B., Fine, P. E. M. & Dye, C. 2006. Effect of BCG vaccination on childhood tuberculous meningitis and miliarytuberculosis worldwide: a meta-analysis and assessment of cost-effectiveness. *Lancet*, 367, 1173-1180.
- Trzoss, M., Bensen, D. C., Li, X. M., Chen, Z. Y., Lam, T., Zhang, J. H., Creighton, C. J., Cunningham, M. L., Kwan, B., Stidham, M., Nelson, K., Brown-Driver, V., Castellano, A., Shaw, K. J., Lightstone, F. C., Wong, S. E., Nguyen, T. B., Finn, J. & Tari, L. W. 2013. Pyrrolopyrimidine inhibitors of DNA gyrase B (GyrB) and topoisomerase IV (ParE), Part II: Development of inhibitors with broad spectrum, Gram-negative antibacterial activity. *Bioorganic & Medicinal Chemistry Letters*, 23, 1537-1543.
- Tsai, F. T. F., Singh, O. M. P., Skarzynski, T., Wonacott, A. J., Weston, S., Tucker, A., Pauptit, R. A., Breeze, A. L., Poyser, J. P., O'Brien, R., Ladbury, J. E. & Wigley, D. B. 1997. The high-resolution crystal structure of a 24-kDa gyrase B fragment from *E. coli* complexed with one of the most potent coumarin inhibitors, clorobiocin. *Proteins-Structure Function and Bioinformatics*, 28, 41-52.
- Tsukamura, M. 1966. Adansonian classification of mycobacteria. *Journal of General Microbiology*, 45, 253-&.
- Tsukamura, M. 1971. Differentiation between *Mycobacterium phlei* and *Mycobacterium thermoresistibile*. *American Review of Respiratory Disease*, 103, 280-282.

- Tsukamura, M. 1976. Properties of *Mycobacterium-smegmatis* freshly isolated from soil. *Japanese Journal of Microbiology*, 20, 355-356.
- Ulukan, H. & Swaan, P. W. 2002. Camptothecins - A review of their chemotherapeutic potential. *Drugs*, 62, 2039-2057.
- Van Bambeke, F., Michot, J. M., Van Eldere, J. & Tulkens, P. M. 2005. Quinolones in 2005: an update. *Clinical Microbiology and Infection*, 11, 256-280.
- van der Kooy, F. 2007. *The medicinal and chemical aspects of naphthoquinones isolated from Euclea natalensis A. DC. on Mycobacterium tuberculosis*. Philosophiae Doctor, University of Pretoria.
- Vonmoos, S., Leuenberger, P., Beer, V. & Dehaller, R. 1986. Pleuro-pulmonary infection due to *Mycobacterium smegmatis*. *Schweizerische Medizinische Wochenschrift*, 116, 1852-1856.
- Wall, M. K., Mitchenall, L. A. & Maxwell, A. 2004. *Arabidopsis thaliana* DNA gyrase is targeted to chloroplasts and mitochondria. *Proceedings of the National Academy of Sciences of the United States of America*, 101, 7821-7826.
- Wallace, M. D., Waraich, N. F., Debowski, A. W., Corral, M. G., Maxwell, A., Mylne, J. S. & Stubbs, K. A. 2018. Developing ciprofloxacin analogues against plant DNA gyrase: a novel herbicide mode of action. *Chemical Communications*, 54, 1869-1872.
- Wang, H., DiGate, R. J. & Seeman, N. C. 1996. An RNA topoisomerase. *Proceedings of the National Academy of Sciences of the United States of America*, 93, 9477-9482.
- Wang, J. C. 2002. Cellular roles of DNA topoisomerases: A molecular perspective. *Nature Reviews Molecular Cell Biology*, 3, 430-440.
- Wang, J. C., Peck, L. J. & Becherer, K. 1982. DNA supercoiling and its effects on DNA-structure and function. *Cold Spring Harbor Symposia on Quantitative Biology*, 47, 85-91.
- Wasserman, S. A. & Cozzarelli, N. R. 1986. Biochemical topology - applications to DNA recombination and replication. *Science*, 232, 951-960.
- Wayne, L. G. & Gross, W. M. 1968. Base composition of deoxyribonucleic acid isolated from mycobacteria. *Journal of Bacteriology*, 96, 1915-&.
- Wei, H., Ruthenburg, A. J., Bechis, S. K. & Verdine, G. L. 2005. Nucleotide-dependent domain movement in the ATPase domain of a human type IIA DNA topoisomerase. *Journal of Biological Chemistry*, 280, 37041-37047.
- Weitzman, I., Osadczyi, D., Corrado, M. L. & Karp, D. 1981. *Mycobacterium-thermoresistibile* - A new pathogen for humans. *Journal of Clinical Microbiology*, 14, 593-595.
- Wethington, S. L., Wright, J. D. & Herzog, T. J. 2008. Key role of topoisomerase I inhibitors in the treatment of recurrent and refractory epithelial ovarian carcinoma. *Expert Review of Anticancer Therapy*, 8, 819-831.
- WHO 2010. Treatment of tuberculosis guidelines.
- WHO 2015. Guidelines on the management of latent tuberculosis infection. WHO Library Cataloguing-in Publication Data.
- WHO 2017. Global Tuberculosis Report 2017. World Health Organisation.
- WHO 2018a. Global Tuberculosis Report 2018. World Health Organisation
- WHO 2018b. *Latent TB infection: Updates and consolidated guidelines for programmatic management*.
- WHO 2018c. WHO treatment guidelines for multidrug- and rifampicin-resistant tuberculosis 2018 update [pre-final tet].
- Wigley, D. B., Davies, G. J., Dodson, E. J., Maxwell, A. & Dodson, G. 1991. Crystal-structure of an N-terminal fragment of the DNA gyrase B-protein. *Nature*, 351, 624-629.
- Wilkinson, A. J. & Wang, J. C. 1990. Catalysis of DNA supercoiling by *Escherichia coli* DNA gyrase - The role of tyrosine-122 of the A-subunit. *Structure and Function of Nucleic Acids and Proteins*, 61-75.
- Willemsse, T., Groothuis, D. G., Koeman, J. P. & Beyer, E. G. 1985. *Myocbacterium thermoresisibile* - Extrapulmonary infection in a cat. *Journal of Clinical Microbiology*, 21, 854-856.

- Winn, M. D., Ballard, C. C., Cowtan, K. D., Dodson, E. J., Emsley, P., Evans, P. R., Keegan, R. M., Krissinel, E. B., Leslie, A. G. W., McCoy, A., McNicholas, S. J., Murshudov, G. N., Pannu, N. S., Potterton, E. A., Powell, H. R., Read, R. J., Vagin, A. & Wilson, K. S. 2011. Overview of the CCP4 suite and current developments. *Acta Crystallographica Section D-Biological Crystallography*, 67, 235-242.
- Winter, G. 2010. xia2: an expert system for macromolecular crystallography data reduction. *Journal of Applied Crystallography*, 43, 186-190.
- Wolfe, J. M. & Moore, D. F. 1992. Isolation of *Mycobacteriu-thermoresistibile* following augmentation mammoplasty. *Journal of Clinical Microbiology*, 30, 1036-1038.
- Wolinsky, E. 1979. Non-tuberculous mycobacteria and associated diseases. *American Review of Respiratory Disease*, 119, 107-159.
- Wu, H. Y., Shyy, S., Wang, J. C. & Liu, L. F. 1988. Transcription generates positively and negatively supercoiled domains in the template. *Cell*, 53, 433-440.
- Zamora, N., Esteban, J., Kinnari, T. J., Celdran, A., Granizo, J. J. & Zafra, C. 2007. In-vitro evaluation of the adhesion to polypropylene sutures of non-pigmented, rapidly growing mycobacteria. *Clinical Microbiology and Infection*, 13, 902-907.
- Zechiedrich, E. L. & Cozzarelli, N. R. 1995. Roles of topoisomerase IV and DNA gyrase in DNA unlinking during replication in *Escherichia coli*. *Genes & Development*, 9, 2859-2869.
- Zechiedrich, E. L., Khodursky, A. B., Bachellier, S., Schneider, R., Chem, D. R., Lilley, D. M. J. & Cozzarelli, N. R. 2000. Roles of topoisomerases in maintaining steady-state DNA supercoiling in *Escherichia coli*. *Journal of Biological Chemistry*, 275, 8103-8113.
- Zechiedrich, E. L., Khodursky, A. B. & Cozzarelli, N. R. 1997. Topoisomerase IV, not gyrase, decatenates products of site-specific recombination in *Escherichia coli*. *Genes & Development*, 11, 2580-2592.
- Zhang, Y., Edwards, T. E., Begley, D. W., Abramov, A., Thompkins, K. B., Ferrell, M., Guo, W. J., Phan, I., Olsen, C., Napuli, A., Sankaran, B., Stacy, R., Van Voorhis, W. C., Stewart, L. J. & Myler, P. J. 2011. Structure of nitrilotriacetate monooxygenase component B from *Mycobacterium thermoresistibile*. *Acta Crystallographica Section F-Structural Biology Communications*, 67, 1100-1105.
- Zheng, H., Cooper, D. R., Porebski, P. J., Shabalina, I. G., Handing, K. B. & Minor, W. 2017. CheckMyMetal : a macromolecular metal-binding validation tool. *Acta Crystallographica Section D-Structural Biology*, 73, 223-233.
- Zheng, H. P., Chordia, M. D., Cooper, D. R., Chruszcz, M., Muller, P., Sheldrick, G. M. & Minor, W. 2014. Validation of metal-binding sites in macromolecular structures with the CheckMyMetal web server. *Nature Protocols*, 9, 156-170.
- Zumla, A. & James, D. G. 1996. Granulomatous infections: Etiology and classification. *Clinical Infectious Diseases*, 23, 146-158.
- Zumla, A., Nahid, P. & Cole, S. T. 2013. Advances in the development of new tuberculosis drugs and treatment regimens. *Nature Reviews Drug Discovery*, 12, 388-404.

Appendix



DNA topoisomerase I and DNA gyrase as targets for TB therapy

Valakunja Nagaraja^{1,2}, Adwait A. Godbole¹, Sara R. Henderson³ and Anthony Maxwell³



¹Department of Microbiology and Cell Biology, Indian Institute of Science, Bangalore 560 012, India

²Jawaharlal Nehru Centre for Advanced Scientific Research, Bangalore 560064, India

³Department of Biological Chemistry, John Innes Centre, Norwich Research Park, Norwich NR4 7UH, UK

Tuberculosis (TB) is the deadliest bacterial disease in the world. New therapeutic agents are urgently needed to replace existing drugs for which resistance is a significant problem. DNA topoisomerases are well-validated targets for antimicrobial and anticancer chemotherapies. Although bacterial topoisomerase I has yet to be exploited as a target for clinical antibiotics, DNA gyrase has been extensively targeted, including the highly clinically successful fluoroquinolones, which have been utilized in TB therapy. Here, we review the exploitation of topoisomerases as antibacterial targets and summarize progress in developing new agents to target DNA topoisomerase I and DNA gyrase from *Mycobacterium tuberculosis*.

Introduction

Although the information content of DNA is essentially independent of how the DNA is knotted or twisted, the access to this information depends on the topology of the DNA. DNA topoisomerases are ubiquitous enzymes that maintain the topological homeostasis within the cell during these DNA transaction processes [1–3]. In the words of James C. Wang, 'DNA topoisomerases are the magicians of the DNA world' [4]; however, unlike the sleight of hand used by a magician, topoisomerases rely on the elegant chemistry of transesterification. Depending on their mechanism of action, these enzymes are broadly classified as type I (which make transient single-stranded breaks in DNA) and type II (transient double-stranded breaks). The enzymes are further subdivided into types IA and IB, distinguished by whether the transient covalent bonds are to the 5'- or 3'-phosphate, respectively, and types IIA and IIB, which differ in mechanistic and evolutionary aspects [5]. Given their functional importance, every species has at least one enzyme from each type. Although the presence of more than one topoisomerase from each type allows for a division of labor for supercoiling, relaxation, knotting/unknottting, and catenation/decatenation, this redundancy also

provides for a certain degree of overlap in their functions. For instance, in *Escherichia coli*, there are four topoisomerases: two type I [topoisomerase (topo) I and topo III] and two type II (DNA gyrase and topo IV). *In vitro*, all four enzymes are capable of DNA relaxation, whereas, *in vivo*, their roles tend to be more specialized, for example, gyrase introduces negative supercoils, whereas topo IV is responsible for decatenation following replication [6]; these functions are critical for cell survival. By contrast, the *Mycobacterium tuberculosis* (*Mtb*) genome encodes a single type I (topo I; gene = Rv3646c) and a single type II topoisomerase [gyrase; genes = Rv0006 (*gyrA*) and Rv0005 (*gyrB*)] [7], which take care of the entire burden of decatenation, relaxation, and supercoiling. In organisms with additional topoisomerases, not all the topoisomerases are essential for cell survival. For example, in *E. coli*, topo I is not necessarily essential [8], whereas saturation mutagenesis studies suggested the essentiality of *Mtb* topo I (Mttopol) [9]. This essentiality is confirmed by generating conditional knockdown strains, wherein the intracellular level of the enzyme is downregulated [10]. The minimal composition of the topoisomerases in the *Mtb* genome necessitates the enzymes to carry out additional functions *in vivo*. Previous studies of mycobacterial topoisomerases have revealed these additional functions as well as their distinct features [11–18].

Corresponding author: Maxwell, A. (tony.maxwell@jic.ac.uk)

DNA cleavage: the Achilles' heel of the topoisomerase mechanism

The reaction mechanism of type IA topoisomerases involves a series of coordinated steps. The reaction cycle, depicted in Fig. 1a, shows the noncovalent binding of the enzyme to the substrate, followed by a transesterification reaction involving a nucleophilic attack on the phosphodiester backbone by the active-site tyrosine, resulting in the formation of a phosphotyrosine covalent adduct. The intact strand of DNA is passed through the cleaved DNA followed by another transesterification reaction involving nucleophilic attack by the free 3'-OH on the phosphotyrosine covalent adduct resulting in the resealing of the cleaved DNA. A cleavage–religation equilibrium between the two transesterification reactions is an important feature of the overall reaction. Perturbation of this equilibrium can lead to the accumulation of enzyme–DNA covalent adducts, which are potentially cytotoxic. Topoisomerase poisons are molecules that perturb the cleavage–religation equilibrium, resulting in the accumulation of enzyme–DNA covalent adducts [19]. The cleavage of the DNA is a vulnerable step during the reaction mechanism of the enzyme that could be exploited to develop inhibitors that can act as topoisomerase poisons.

In the case of type II topoisomerases, such as bacterial gyrases, the reaction cycles proceed via transient double-stranded breaks in DNA. In the general case, as represented by eukaryotic topo II and bacterial topo IV, the dimeric enzyme binds two segments of DNA, a G (or gate) segment and a T (or transported) segment. Double-stranded cleavage of the G segment facilitates passage of the T segment through the G segment (and, thus, through the protein interfaces of the dimeric enzyme), in a reaction driven by the binding and hydrolysis of ATP [20]. Gyrase is a special case of this mechanism (Fig. 1b) in which the G and T segments are colinear and the strand-passage event leads to the introduction of negative supercoils [1]. As with the type I enzymes, cleavage of the DNA (double stranded in this case) is a vulnerability that can be potentially exploited to develop inhibitors [21].

Thus, one of the most desired classes of molecule that target topoisomerases are topoisomerase poisons [19]. However, until recently, no such molecules had been discovered for bacterial type I enzymes, although it has been genetically and chemically validated as an anti-TB target [22]. By contrast, several molecules target type II topoisomerases (bacterial and eukaryotic) and type IB enzymes (typically found in eukaryotes). In the case of eukaryotic type IB enzymes, camptothecin [23,24] and its various derivatives target human topo I. Although an inhibitor that acts in a similar fashion is desired for type IA topoisomerases, catalytic inhibitors of the enzyme might also be useful in those organisms harboring a single type IA topoisomerase. DNA gyrase has been extensively exploited as a target for the development of antibacterial compounds (discussed below), prominent among them being the fluoroquinolones, which are one of the most effective cellular poisons, arresting the gyrase reaction after DNA cleavage leading to the generation of double-strand breaks [25,26].

Inhibitors of Mttopol

In work by the Nagaraja lab, in part supported by the MM4TB consortium (www.mm4tb.org), has pursued the design of proof-of-principle inhibitors for Mttopol. Biochemical characterization of

topo I from both *Mycobacterium smegmatis* [11] as well as *Mtb* [27] revealed the site-specific nature of the enzyme, which recognizes a hexameric sequence, CG/TCT↓TC/G (where ↓ indicates the site of cleavage) [16]; these sites are referred to as 'strong topoisomerase sites' (STS). The binding as well as the cleavage reaction is sequence specific and, therefore, enabled the design of oligonucleotide substrates that can inhibit the DNA relaxation reaction. Incubation of the enzyme with the oligonucleotides harboring the STS causes the DNA-binding site of the enzyme to be occluded for the binding of negatively supercoiled DNA, leading to the inhibition of the DNA relaxation reaction [16]. Next, monoclonal antibodies (mAbs) were developed that specifically inhibit the mycobacterial topo I, an approach that had been used previously to develop specific inhibitors of mycobacterial gyrase [28]. Apart from being used as tools to understand the finer details of the reaction, these mAbs could also serve as valuable start points for the development of small-molecule inhibitors against mycobacterial topo I. One of the mAbs, 1E4F5, was especially interesting owing to its mechanism of action. Depending on the order of addition of the mAb, it could inhibit the reaction at multiple steps. Pre-incubation of the mAb with the enzyme led to the inhibition of the DNA-binding ability, while incubation of the mAb with a preformed topo I–DNA complex led to the formation of a mAb–topo I–DNA ternary complex [29]. This mAb was shown to close the clamp of the enzyme, thus stimulating the second transesterification step. Another mAb, 2F3G4, affected the cleavage–religation equilibrium of the reaction, leading to the accumulation of the topo I–DNA covalent complex; thus, 2F3G4 behaves like a topoisomerase poison [30].

All topoisomerases, irrespective of their class, transiently cleave DNA during their reaction cycle. As discussed, this step has been extensively exploited in the development of antibacterial as well as anticancer agents, which target gyrase and eukaryotic topoisomerases, respectively. Thus, it is surprising that there is a dearth of such small molecules that target bacterial topo I. However, in the recent past, several studies have addressed this shortcoming. Using an high-throughput screening (HTS) assay based on SOS induction in *E. coli*, a phenanthrene compound, stephananthrene, was identified as a bacterial topo I poison [31]. More recently, derivatives of bolden, seconeolitsine, and *N*-methyl-seconeolitsine (Fig. 3) were also identified to target the DNA relaxation activity of bacterial topo I [32]. Apart from derivatives of bolden, bisbenzimidazole analogs of Hoechst dyes, 3,4-dimethoxyphenyl bisbenzimidazole (DMA) [33] and DPA 153 [34] with a terminal alkyne substitution have been identified as potential inhibitors of topo I (Fig. 3). DMA was shown to act as a topoisomerase poison, both *in vitro* as well as, to a limited extent, in whole-cell assays [33]. More recently, analogs of bisbenzimidazoles, such as bisbenzimidazole 12b (Fig. 3), were shown to be an improvement over DMA in terms of IC₅₀ values and having lower MICs among the compounds tested against several *E. coli* strains [35].

Exploring natural product chemical space yielded anziaic acid (Fig. 3) derived from the lichen *Hypotrachyna* sp. and shown to be a dual inhibitor of type IA as well as type IIA topoisomerases. Anziaic acid was demonstrated to act like a topoisomerase poison [36]. However the molecule exhibited toxicity toward human pulmonary artery endothelial cells, possibly because of its dual-targeting ability [36]. Another small molecule identified by exploring the natural product spectrum was 2,4-diiodoemodin (Fig. 3), a haloemodin

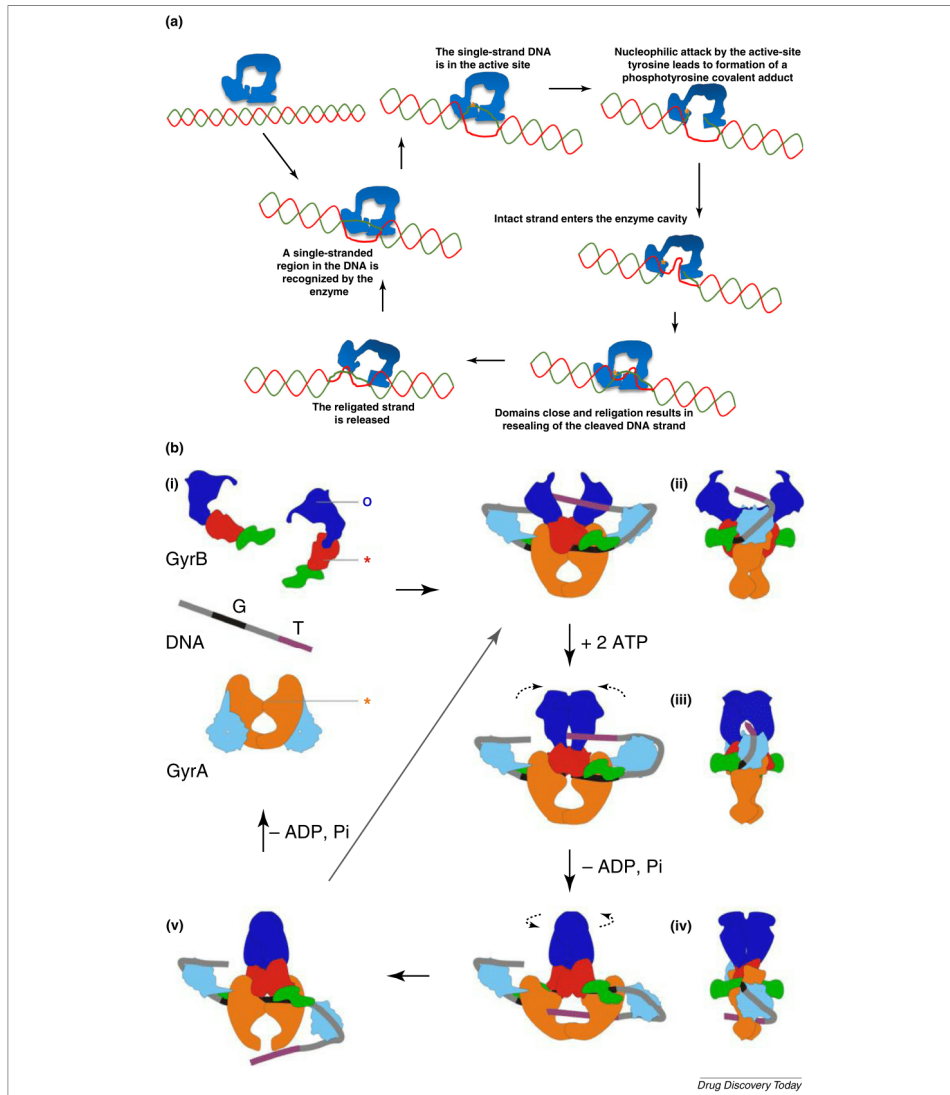
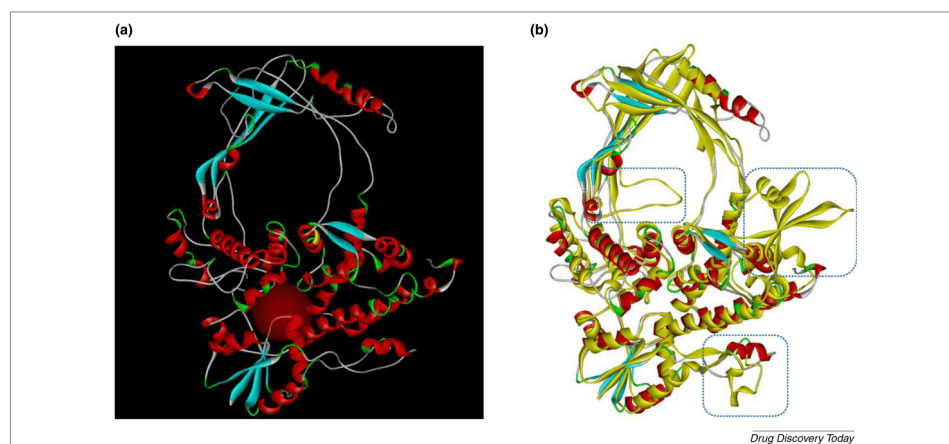


FIGURE 1 Topoisomerase reaction mechanisms. **(a)** Bacterial topoisomerase I (topo I) reaction cycle: the multistep reaction is initiated with the interaction and binding of the enzyme to negatively supercoiled DNA. DNA binding is followed by the first transesterification reaction in which the nucleophilic attack by the tyrosine of the active site on the phosphodiester backbone results in the formation of the topo I-DNA covalent complex and separation of the domains to form an enzyme-DNA gate. Next, the intact strand of DNA is passed through this enzyme-DNA gate, resulting in a change in linking number. After strand passage, during the second transesterification reaction, the separated domains close and the 3'-hydroxyl group targets the phosphotyrosine covalent adduct with a nucleophilic attack, resulting in the resealing of the cleaved DNA strand. During the reaction cycle, the various domains of the enzyme open and close like a clamp, facilitating the

**FIGURE 2**

Structural model of *Mycobacterium tuberculosis* (*Mtb*) topoisomerase I (MtopoI). Structural model of MtopoI (a) with the imipramine docking region (filled sphere), and the superimposition of the crystal structure shown in yellow with the homology model colored by atom (b); the differences highlighted between the structure and the model of the enzyme are outside the docking region.

derived from the bioactive natural product emodin. This molecule is a dual inhibitor of topoisomerase I and DNA gyrase [37]. The dual inhibition capability could have important implications in suppressing resistance in pathogenic bacteria, such as *Mtb*, which has only two topoisomerases.

An alternate approach was used to find small-molecule inhibitors for MtopoI. Initially, a structural model of the enzyme was generated to screen *in silico* a large number of molecules followed by testing these molecules for enzyme inhibition directly (Fig. 2). Using this target-based approach, three molecules were shown to inhibit the DNA relaxation activity of MtopoI as well as to affect the growth of *Mtb* cells in a whole-cell assay (Fig. 3). One of the three molecules, m-AMSA (amsacrine; Fig. 3), is a well-known type IIA topoisomerase poison [38]. The other two molecules, imipramine and norclomipramine (Fig. 3), are used clinically as antidepressants [39,40]. These two molecules inhibited the DNA relaxation activity at lower concentrations [41]. Notably, they arrested the reaction and formed cleavage complexes with a higher efficiency and were found to be bactericidal. Moreover, a decrease in the MIC for the compounds in cells overexpressing topo I validated topo I as the intracellular target and their action as intracellular topo I poisons [41]. Although their potency was not comparable to that of fluoroquinolones, they are the most potent anti-topo I inhibitors reported so far. This study also

highlighted the potential to repurpose clinically relevant compounds to target mycobacterial topo I [38]. Recent efforts starting from a polyamine scaffold have led to the identification of four more compounds that inhibit the DNA relaxation activity of MtopoI and also affect the growth of mycobacterial cells; however, none of these molecules acts as a topoisomerase poison [42].

To summarize, the search for potent inhibitors of bacterial type IA enzymes has begun, with some indications of success. Although these efforts using different approaches have yielded a few hits, the efficacy of these molecules in *in vivo* models of infection needs to be tested. Such studies are underway with imipramine. Clearly, more efforts are needed to develop better inhibitors using a variety of approaches and a combination of strategies, including synthesis of new derivatives from the early leads. Perhaps a high-throughput assay for screening a large number of compounds in a short time might not be out of place. The X-ray structure of the truncated MtopoI published recently is a way forward in finding potent inhibitors of the enzyme [43]. The availability of this structure will provide major insights into the rational design of small-molecule inhibitors of MtopoI.

Inhibitors of *M. tuberculosis* gyrase

In contrast to topo I, *Mtb* gyrase (Mtyrase) has been extensively exploited as a target for potential antibacterials. This is in part

formation of the topo I-DNA gate and religation, respectively. (b) Model for the mechanism of DNA supercoiling by DNA gyrase. Gyrase domains are colored as follows: GyrB-NTD, dark blue; GyrB-TOPRIM domain, red; GyrB-tail, green; GyrA-NTD, orange; GyrA-CTD, light blue. The G and T DNA segments are colored black and purple, respectively. (i) The subunits and DNA in their free states in solution; stars indicate the active site residues for DNA cleavage and the circle indicates an ATP-binding pocket. (ii) The G segment binds between GyrA-NTD and GyrB-TOPRIM, at the dimer interface, and the GyrA CTDs wrap DNA to present the T segment in a positive crossover. (iii) ATP is bound, closing the GyrB clamp (GyrB-NTD) and capturing the T segment; the G segment is transiently cleaved. (iv) Hydrolysis of one ATP molecule allows GyrB to rotate, the DNA gate to widen, and the transport of the T segment through the cleaved G segment. (v) The T segment exits through the C gate, and the G segment is religated. The hydrolysis of the remaining ATP molecule resets the enzyme. Reprinted, with permission, from [73]. Abbreviations: CTD, C-terminal domain; NTD, N-terminal domain; TOPRIM, topoisomerase primase domain.

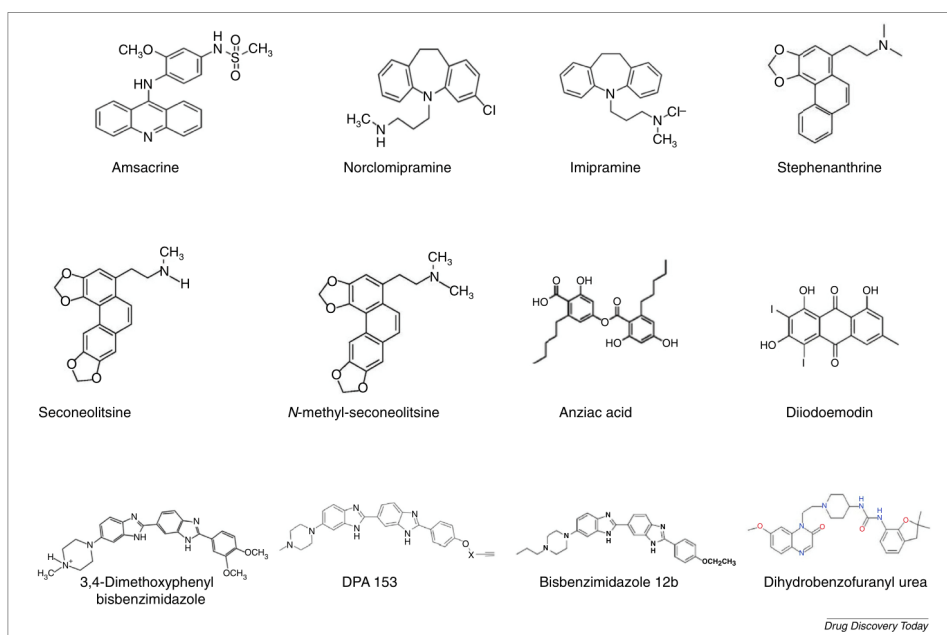


FIGURE 3

Small-molecule inhibitors of topoisomerase I.

because of the high degree of success of gyrase as a target for antibiotics effective against a range of pathogenic bacteria [21]. In addition, the extensive structural information on gyrase from several bacteria, including *Mtb* [44–48], has potentiated *in silico* methods for developing new gyrase-specific inhibitors; examples of this approach are given below. Perhaps surprisingly, there is currently no complete crystal structure of gyrase (A_2B_2) for any organism. However, it is possible to build such a structure (in this case for Mtgyrase) using available information from domains and protein fragments (Fig. 4).

The most successful gyrase-targeted antibacterial agents are the fluoroquinolones and several of these compounds have proved efficacious against TB; these include gatifloxacin and moxifloxacin (Fig. 5) [49–51], which are being evaluated both for first-line therapeutics and second-line therapy for multi-drug resistant (MDR) and extensively drug-resistant (XDR) TB (Fig. 5). In relation to moxifloxacin, which is currently the most promising fluoroquinolone targeted to TB, the results from a recent large-scale Phase 3 trial demonstrated that this drug could not be substituted for isoniazid or ethambutol in a 4-month treatment regimen [52,53]. However, it is clear that moxifloxacin will still have an important role in TB therapy, particularly for MDR-TB.

Work on understanding quinolone action on Mtgyrase and developing new inhibitors has been greatly assisted by X-ray crystallography. The structures of the GyrA N-terminal domain

(NTD) and the catalytic core [C-terminal domain (CTD) of GyrB fused to the GyrA NTD] were initially determined [47,48]. Given that these regions contain amino acid residues that interact with quinolones, this gave some initial insight into drug–protein interactions. Work on gyrase and topo IV from other organisms revealed crystal structures with bound DNA and quinolones, specifically, the structure of the catalytic core fusion of *Streptococcus pneumoniae* topo IV complexed with moxifloxacin and ciprofloxacin [54], the structure of the catalytic core fusion of *Staphylococcus aureus* gyrase complexed with ciprofloxacin [55], and the catalytic core fusion of *Acinetobacter baumannii* topo IV complexed with moxifloxacin [56]. These structures provided molecular insight into the mechanism of inhibition by quinolones. In more recent work, structures have been obtained for the *Mtb* GyrB–GyrA catalytic core with moxifloxacin, gatifloxacin, and other quinolones [45]. These structures highlight the details of Mtgyrase–quinolone–DNA interactions and how these differ from those seen in other organisms, and will potentiate the development of new compounds with increased potency against TB.

However, despite success in understanding the molecular basis of gyrase–quinolone–DNA interactions, resistance to quinolones is a serious problem in TB and other bacterial infectious diseases. Therefore, we need to develop other agents that can avoid the resistance issues of existing antibiotics.

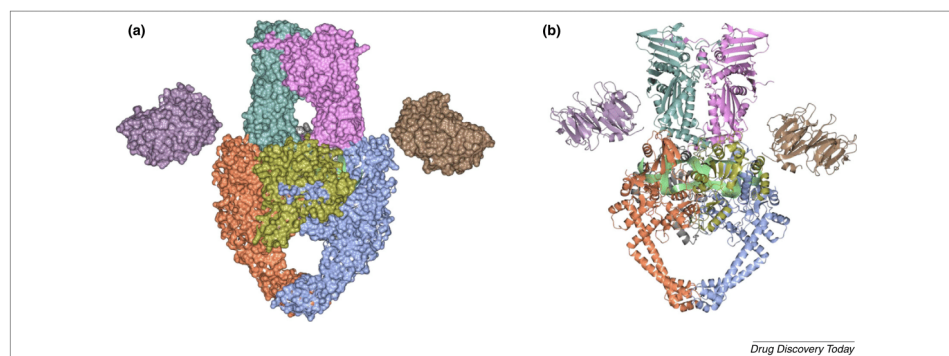


FIGURE 4 Structural model of *Mycobacterium tuberculosis* DNA gyrase (Mtgyrase). The figure shows space-filling (a) and ribbon (b) representations of Mtgyrase. The models were made by taking existing crystal structures (5B58, 1ZVU, and 3ZKB) and using the program COOT to assemble a model of the A_2B_2 complex. Domains are colored as follows: GyrB-NTDs, pink and sea-green; GyrB-CTDs, gold and gray; GyrA-NTDs, coral and ice blue; GyrA-CTDs, purple and pale brown. DNA is in a green ribbon representation. *Abbreviations:* CTD, C-terminal domain; NTD, N-terminal domain.

In work supported by the MM4TB consortium, we investigated a large number of compounds for their potential as new gyrase-targeted antibiotics (unpublished data). Specifically, we were seeking compounds that show efficacy against *Mtb* (growing and/or dormant) and that inhibit the gyrase supercoiling reaction. Ideally, the compounds should have a good IC_{50} against gyrase ($<50 \mu M$) and, if possible, should stabilize the cleavage complex but not show crossresistance to quinolones. We received >2000 compounds (mostly synthetic) from other partners and evaluated their efficacy versus Mtgyrase. We found >60 compounds with $IC_{50} <50 \mu M$ and evidence for compounds with new modes of action; fully characterizing these compounds and establishing their prospects as potential TB agents is the subject of ongoing work.

In connection with the MM4TB project, we also investigated naphthoquinone natural products as inhibitors of Mtgyrase. Extracts from the South African 'toothbrush' tree, *Euclia natalensis*, have been extensively used in traditional medicine and were found to be active against *Mtb* [57]. One active component of this extract was shown to be the naphthoquinone diospyrin (Fig. 5) [58], which was found to be an inhibitor of DNA gyrase [60]. Moreover, diospyrin and other naphthoquinones were found to have a novel mechanism of action, binding to the GyrB-NTD, but not at the ATPase site [59]. The molecular details of this binding pocket remain to be determined. Interestingly, naphthoquinone compounds have also been found to inhibit *Mtb* ThyX, an essential thymidylate synthase [60]. Whereas some compounds, such as 7-methyljuglone (Fig. 5), inhibit both enzymes, most affect ThyX without inhibiting gyrase. This suggests that the pharmacophores for the two targets (ThyX and GyrB) are distinct [60].

Other research groups have been developing new TB agents targeted to gyrase, particularly using *in silico* methods based on the new and emerging structural information on Mtgyrase. The crystal structure of the GyrB-NTD (ATPase domain) of *E. coli* gyrase

complexed with an ATP analog, and that of the 24-kDa GyrB N-terminal subdomain with novobiocin [61,62], paved the way for structure-based drug design based around these ligand pockets. More recently, the corresponding structure (GyrB-NTD) for Mtgyrase has further promoted such work [44]. The group of Sriram investigated a large number of inhibitors of Mtgyrase, following computationally based approaches [63,64]; for example, using this methodology, 28 2-amino-5-phenylthiophene-3-carboxamides were synthesized, the best one having an MIC against *Mtb* of $\sim 4 \mu M$ and an IC_{50} for Mtgyrase supercoiling of $\sim 0.8 \mu M$ [65]. In another study, 48 quinoline-aminopiperidine-based urea and thiourea derivatives were designed, synthesized, and evaluated; the best compound had an MIC against *M. tuberculosis* of $\sim 3.5 \mu M$ and an IC_{50} for Mtgyrase supercoiling of $\sim 0.7 \mu M$ [66]. Similar work has been carried out with substituted benzofuran compounds and pyrrolamides [67,68].

Astra-Zeneca have also published a series of papers describing compounds that target the ATP-binding site. Aminopyrazinamides (Fig. 5) were identified from a HTS using the *M. smegmatis* GyrB ATPase reaction [69]. A crystal structure of one of these compounds complexed with the *M. smegmatis* GyrB-NTD revealed the specifics of ligand-protein interactions in this case. Aside from having good IC_{50} , these compounds also show promising MICs. *In silico* approaches led to thiazolopyridine ureas [70] and thiazolopyridone ureas [71] as compounds that also had good activities and properties.

Although a significant amount of effort has been expended on discovering new Mtgyrase inhibitors, most of this has centered on the ATP- and quinolone-binding sites. Exceptions to this are the naphthoquinone studies described above [59,60] and work from GSK [72], which identified novel bacterial topoisomerase inhibitors (NBIs) with activity against Mtgyrase and that lack cross-resistance to fluoroquinolones (Fig. 5). More inhibitors acting at sites different from the well-known binding pockets would be desirable.

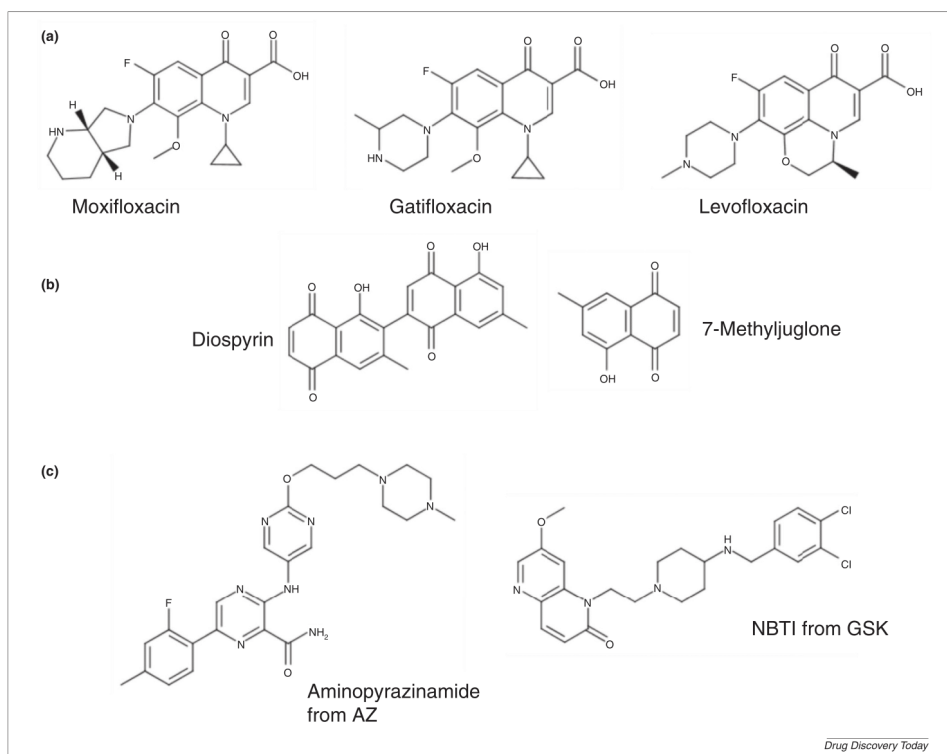


FIGURE 5

Small-molecule inhibitors of *Mycobacterium tuberculosis* DNA gyrase (Mtgryase): (a) fluoroquinolones; (b) naphthoquinones; (c) a representative aminopyrazinamide from Astra-Zeneca [69], and a representative novel bacterial topoisomerase inhibitor (NBTI) from GSK [72].

Concluding remarks

There is no question that topoisomerases have been effective targets both for anticancer and antibacterial chemotherapy and there appears to be every reason to persist in the search for new agents that target Mttopol and Mtgyrase. These two enzymes can be regarded separately. In the case of Mttopol, it can be regarded as a 'new' target that remains to be exploited clinically. However, given the urgent need to find new antibacterial agents and the depth of knowledge about this enzyme, it is justifiable to expend more effort in seeking new inhibitors. In the case of Mtgyrase, the success of fluoroquinolones and the existence of other exploitable ligand-binding pockets in gyrase suggest that work on seeking new gyrase-specific inhibitors will continue to be important. Whether these searches are target-based or follow phenotypic screens is a

moot point; the evidence from recent studies suggests that both approaches are valid. In any case, it is probably that combined academic and pharma efforts will be needed to achieve success.

Acknowledgements

We thank Sean Ekins for help in generating Fig. 2, and David Lawson for help in generating Fig. 4. The work was partially supported by a grant from the European Community's Seventh Framework Program (grant 260872, MM4TB Consortium) to A.M. and V.N., and by a UKIERI grant from the British Council (DST-2013-14/091) to A.M. and V.N. Work in A.M.'s lab is also supported by grant BB/J004561/1 from BBSRC (UK) and the John Innes Foundation. S.R.H. is supported by a CASE studentship from BBSRC and Redx.

References

- 1 Bush, N.G. et al. (2015) DNA topoisomerases. In *EcoSal – Escherichia coli and Salmonella: Cellular and Molecular Biology* (Böck, A. et al. eds), ASM Press
- 2 Tse-Dinh, Y.C. (1998) Bacterial and archeal type I topoisomerases. *Biochim. Biophys. Acta* 1400, 19–27
- 3 Vos, S.M. et al. (2011) All tangled up: how cells direct, manage and exploit topoisomerase function. *Nat. Rev. Mol. Cell Biol.* 12, 827–841
- 4 Wang, J.C. (2002) Cellular roles of DNA topoisomerases: a molecular perspective. *Nat. Rev. Mol. Cell Biol.* 3, 430–440
- 5 Champoux, J.J. (2001) DNA topoisomerases: structure, function, and mechanism. *Annu. Rev. Biochem.* 70, 369–413
- 6 Zechiedrich, E.L. and Cozzarelli, N.R. (1995) Roles of topoisomerase IV and DNA gyrase in DNA unlinking during replication in *Escherichia coli*. *Genes Dev.* 9, 2859–2869
- 7 Cole, S.T. et al. (1998) Deciphering the biology of *Mycobacterium tuberculosis* from the complete genome sequence. *Nature* 393, 537–544
- 8 Stupina, V.A. and Wang, J.C. (2005) Viability of *Escherichia coli* topA mutants lacking DNA topoisomerase I. *J. Biol. Chem.* 280, 355–360
- 9 Sassetti, C.M. et al. (2003) Genes required for mycobacterial growth defined by high density mutagenesis. *Mol. Microbiol.* 48, 77–84
- 10 Ahmed, W. et al. (2014) Conditional silencing of topoisomerase I gene of *Mycobacterium tuberculosis* validates its essentiality for cell survival. *FEMS Microbiol. Lett.* 353, 116–123
- 11 Bhaduri, T. et al. (1998) DNA topoisomerase I from *Mycobacterium smegmatis*. An enzyme with distinct features. *J. Biol. Chem.* 273, 13925–13932
- 12 Bhaduri, T. et al. (1998) Sequence specific interaction of *Mycobacterium smegmatis* topoisomerase I with duplex DNA. *Nucleic Acids Res.* 26, 1668–1674
- 13 Kumar, R. et al. (2012) Binding of two DNA molecules by type II topoisomerases for decatenation. *Nucleic Acids Res.* 40, 10904–10915
- 14 Manjunatha, U.H. et al. (2002) Functional characterisation of mycobacterial DNA gyrase: an efficient decatenase. *Nucleic Acids Res.* 30, 2144–2153
- 15 Sikder, D. and Nagaraja, V. (2001) A novel bipartite mode of binding of *M. smegmatis* topoisomerase I to its recognition sequence. *J. Mol. Biol.* 312, 347–357
- 16 Sikder, D. and Nagaraja, V. (2000) Determination of the recognition sequence of *Mycobacterium smegmatis* topoisomerase I on mycobacterial genomic sequences. *Nucleic Acids Res.* 28, 1830–1837
- 17 Aubry, A. et al. (2004) *Mycobacterium tuberculosis* DNA gyrase: interaction with quinolones and correlation with antimycobacterial drug activity. *Antimicrob. Agents Chemother.* 48, 1281–1288
- 18 Aubry, A. et al. (2006) First functional characterization of a singly expressed bacterial type II topoisomerase: the enzyme from *Mycobacterium tuberculosis*. *Biochem. Biophys. Res. Commun.* 348, 158–165
- 19 Pommier, Y. et al. (2010) DNA topoisomerases and their poisoning by anticancer and antibacterial drugs. *Chem. Biol.* 17, 421–433
- 20 Schoeffler, A.J. and Berger, J.M. (2008) DNA topoisomerases: harnessing and constraining energy to govern chromosome topology. *Q. Rev. Biophys.* 41, 41–101
- 21 Collin, F. et al. (2011) Exploiting bacterial DNA gyrase as a drug target: current state and perspectives. *Appl. Microbiol. Biotechnol.* 92, 479–497
- 22 Ravishankar, S. et al. (2015) Genetic and chemical validation identifies *Mycobacterium tuberculosis* topoisomerase I as an attractive anti-tubercular target. *Tuberculosis (Edinb)* 95, 589–598
- 23 Dexeheimer, T.S. and Pommier, Y. (2008) DNA cleavage assay for the identification of topoisomerase I inhibitors. *Nat. Protoc.* 3, 1736–1750
- 24 Hsiang, Y.H. et al. (1985) Camptothecin induces protein-linked DNA breaks via mammalian DNA topoisomerase I. *J. Biol. Chem.* 260, 14873–14878
- 25 Chen, C.R. et al. (1996) DNA gyrase and topoisomerase IV on the bacterial chromosome: quinolone-induced DNA cleavage. *J. Mol. Biol.* 258, 627–637
- 26 Gellert, M. et al. (1977) Nalidixic acid resistance: a second genetic character involved in DNA gyrase activity. *Proc. Natl. Acad. Sci. U. S. A.* 74, 4772–4776
- 27 Godbole, A.A. et al. (2012) Characterization of DNA topoisomerase I from *Mycobacterium tuberculosis*: DNA cleavage and religation properties and inhibition of its activity. *Arch. Biochem. Biophys.* 528, 197–203
- 28 Manjunatha, U.H. et al. (2001) Monoclonal antibodies to mycobacterial DNA gyrase A inhibit DNA supercoiling activity. *Eur. J. Biochem.* 268, 2038–2046
- 29 Leelaram, M.N. et al. (2013) Type IA topoisomerase inhibition by clamp closure. *FASEB J.* 27, 3030–3038
- 30 Leelaram, M.N. et al. (2012) Inhibition of type IA topoisomerase by a monoclonal antibody through perturbation of DNA cleavage-religation equilibrium. *FEBS J.* 279, 55–65
- 31 Cheng, B. et al. (2007) Compounds with antibacterial activity that enhance DNA cleavage by bacterial DNA topoisomerase I. *J. Antimicrob. Chemother.* 59, 640–645
- 32 Garcia, M.T. et al. (2011) New alkaloid antibiotics that target the DNA topoisomerase I of *Streptococcus pneumoniae*. *J. Biol. Chem.* 286, 6402–6413
- 33 Bansal, S. et al. (2012) 3,4-Dimethoxyphenyl bis-benzimidazole, a novel DNA topoisomerase inhibitor that preferentially targets *Escherichia coli* topoisomerase I. *J. Antimicrob. Chemother.* 67, 2882–2891
- 34 Ranjan, N. et al. (2014) Selective inhibition of bacterial topoisomerase I by alkynyl-bisbenzimidazoles. *MedChemComm* 5, 816–825
- 35 Nimesh, H. et al. (2014) Synthesis and biological evaluation of novel bisbenzimidazoles as *Escherichia coli* topoisomerase IA inhibitors and potential antibacterial agents. *J. Med. Chem.* 57, 5238–5257
- 36 Cheng, B. et al. (2013) Identification of anziaic acid, a lichen depside from *Hypotrachyna* sp., as a new topoisomerase poison inhibitor. *PLOS ONE* 8, e60770
- 37 Duan, F. et al. (2014) Haloemodin as novel antibacterial agent inhibiting DNA gyrase and bacterial topoisomerase I. *J. Med. Chem.* 57, 3707–3714
- 38 Godbole, A.A. et al. (2014) Inhibition of *Mycobacterium tuberculosis* topoisomerase I by m-AMSA, a eukaryotic type II topoisomerase poison. *Biochem. Biophys. Res. Commun.* 446, 916–920
- 39 Glowinski, J. and Axelrod, J. (1964) Inhibition of uptake of tritiated-noradrenaline in the intact rat brain by imipramine and structurally related compounds. *Nature* 204, 1318–1319
- 40 Kelly, M.W. and Myers, C.W. (1990) Clomipramine: a tricyclic antidepressant effective in obsessive compulsive disorder. *DIAP* 24, 739–744
- 41 Godbole, A.A. et al. (2015) Targeting *Mycobacterium tuberculosis* topoisomerase I by small-molecule inhibitors. *Antimicrob. Agents Chemother.* 59, 1549–1557
- 42 Sandhaus, S. et al. (2016) Small molecule inhibitors targeting topoisomerase I as novel antituberculosis agents. *Antimicrob. Agents Chemother.* 60, 4028–4036
- 43 Tan, K. et al. (2016) Insights from the structure of *Mycobacterium tuberculosis* topoisomerase I with a novel protein fold. *J. Mol. Biol.* 428, 182–193
- 44 Agrawal, A. et al. (2013) *Mycobacterium tuberculosis* DNA gyrase ATPase domain structures suggest a dissociative mechanism that explains how ATP hydrolysis is coupled to domain motion. *Biochem. J.* 2, 263–273
- 45 Blower, T.R. et al. (2016) Crystal structure and stability of gyrase-fluoroquinolone cleaved complexes from *Mycobacterium tuberculosis*. *Proc. Natl. Acad. Sci. U. S. A.* 113, 1706–1713
- 46 Fu, G. et al. (2009) Crystal structure of DNA gyrase B' domain sheds lights on the mechanism for T-segment navigation. *Nucleic Acids Res.* 37, 5908–5916
- 47 Piton, J. et al. (2010) Structural insights into the quinolone resistance mechanism of *Mycobacterium tuberculosis* DNA gyrase. *PLoS ONE* 5, e12245
- 48 Tretter, E.M. et al. (2010) Crystal structure of the DNA gyrase GyrA N-terminal domain from *Mycobacterium tuberculosis*. *Proteins* 78, 492–495
- 49 Takiff, H. and Guerrero, E. (2011) Current prospects for the fluoroquinolones as first-line tuberculosis therapy. *Antimicrob. Agents Chemother.* 55, 5421–5429
- 50 Asif, M. et al. (2013) Quinolone derivatives as antitubercular drugs. *Med. Chem. Res.* 22, 1029–1042
- 51 Cheepsattayakorn, A. and Cheepsattayakorn, R. (2008) Prospects for new drugs and regimens in the treatment of tuberculosis. *J. R. Coll. Physicians (Edinb)* 38, 207–211
- 52 Gillespie, S.H. (2016) The role of moxifloxacin in tuberculosis therapy. *Eur. Respir. Rev.* 25, 19–28
- 53 Gillespie, S.H. et al. (2014) Four-month moxifloxacin-based regimens for drug-sensitive tuberculosis. *N. Engl. J. Med.* 371, 1577–1587
- 54 Laponogov, I. et al. (2009) Structural insight into the quinolone-DNA cleavage complex of type IIA topoisomerases. *Nat. Struct. Mol. Biol.* 16, 667–669
- 55 Bax, B.D. et al. (2010) Type IIA topoisomerase inhibition by a new class of antibacterial agents. *Nature* 466, 935–940
- 56 Wohlkonig, A. et al. (2010) Structural basis of quinolone inhibition of type IIA topoisomerases and target-mediated resistance. *Nat. Struct. Mol. Biol.* 17, 1152–1153
- 57 Lall, N. and Meyer, J.J.M. (1999) *In vitro* inhibition of drug-resistant and drug-sensitive strains of *Mycobacterium tuberculosis* by ethnobotanically selected South African plants. *J. Ethnopharmacol.* 66, 347–354
- 58 Lall, N. and Meyer, J.J.M. (2001) Inhibition of drug-sensitive and drug-resistant strains of *Mycobacterium tuberculosis* by diospyrin, isolated from *Euclea natalensis*. *J. Ethnopharmacol.* 78, 213–216
- 59 Karkare, S. et al. (2013) The naphthoquinone diospyrin is an inhibitor of DNA gyrase with a novel mechanism of action. *J. Biol. Chem.* 288, 5149–5156
- 60 Djajot, K. et al. (2016) Predictive modeling targets thymidylate synthase ThyX in *Mycobacterium tuberculosis*. *Sci. Rep.* 6, 27792
- 61 Lewis, R.J. et al. (1996) The nature of inhibition of DNA gyrase by the coumarins and the cyclothialidines revealed by X-ray crystallography. *EMBO J.* 15, 1412–1420

DNA in a twist? How topoisomerases solve topological problems in DNA

Natassja G. Bush, Monica Agarwal, Sara R. Henderson, Nidda F. Waraich and Anthony Maxwell (John Innes Centre, UK)

DNA topoisomerases have been described as 'the magicians of the DNA world', somehow allowing DNA strands to pass through each other. These ingenious enzymes are both essential and potentially dangerous, as any interruption in their DNA breakage-reunion reactions can lead to chromosome breaks and cell death. This has led to their development as important targets for antibacterial and anti-cancer chemotherapy.

DNA topology and the importance of topoisomerases

Watson and Crick, upon proposing the double-helical structure of DNA, noted that the two strands of the helix would have to untwist in order to separate. They also suggested that this untwisting and separating of the two strands would lead to entanglements. While the structure of the DNA double helix is ideally suited to its function – the opening of the helix permitting access to the bases that encode the genetic information – it does indeed lead to topological problems. This process of helix unwinding, which occurs in DNA replication and transcription, leads to DNA supercoiling, where the DNA helix is coiled about its own axis (Figure 1). The DNA topoisomerases have evolved to deal with problems of over-winding (and under-winding) of the DNA helix, as well as to take care of DNA catenanes (interlinked DNA molecules) that can occur at the termination of replication and knots in DNA that can arise during recombination events (Figure 1). These different forms of DNA: supercoiled, relaxed, catenated and knotted, represent topological isomers of double-stranded circular DNA, i.e. they have the same molecular mass, but differ in the path taken by the DNA strands.

DNA topology, literally how the two complementary single strands of DNA are intertwined, is an important topic in itself and is

often the domain of mathematicians. However, for the purpose of discussing topoisomerases, a broad understanding is all that is necessary (see Box 1). In general terms, positive supercoiling (over-winding of DNA) is bad, with some exceptions, and moderate negative supercoiling (under-winding of DNA) is good; knots are generally bad and catenanes normally should be removed (Figure 1). Resolving these unwanted species is the job performed by topoisomerases, which, remarkably, carry out these reactions by transiently cleaving one or both strands of DNA (see below). DNA breakage is a danger to cell viability and the cleavage-religation process must be carefully controlled. Interruption of this process can lead to broken DNA and cell death, which is why these enzymes have been exploited as targets for both antibacterial chemotherapy and anti-cancer agents. As topoisomerases occur in all organisms (prokaryotes, eukaryotes and archaea) it is the differences between them that need to be established and exploited to develop successful clinical agents.

Mechanistic aspects of type II topoisomerases

DNA topoisomerases are divided into two types, I and II, depending on whether their reactions proceed via transient single- or double-stranded DNA breaks. They are further divided into subtypes: IA, IB, IC, IIA, IIB; these subtypes differ both

mechanistically and structurally (Figure 2). Type I enzymes are less relevant to this article, as they are not strictly molecular machines and do not use ATP. The exception is the type IA topoisomerase reverse gyrase that uses ATP to introduce positive supercoils into DNA. Despite this, the type I topoisomerases are still of considerable interest as drug targets (see below) and because the subtypes show fundamental mechanistic differences.

The type IB and C enzymes relax supercoiled DNA using a 'swivel' mechanism by making transient single-stranded breaks involving a covalent bond to the 3'-phosphate end of the DNA, and allowing the DNA to swivel within the enzyme in a controlled rotation. The type IA enzymes work by a strand-passage mechanism making transient covalent bonds to the 5'-phosphate end of DNA at the break site. The type IA enzymes also relax supercoiled DNA, with reverse gyrase being the only type IA enzyme capable of introducing supercoils. It consists of two domains, a helicase domain, which binds and hydrolyses ATP, and a topoisomerase domain, which cleaves the DNA. The helicase domain transiently unwinds the double-stranded DNA in an ATP-dependent reaction increasing the linking number (Lk) (see Box 1). The topoisomerase domain carries out strand passage by cleaving one strand of the DNA helix and passing the other strand through the cleaved strand before resealing. This strand-passage event results in positive supercoiling. Reverse gyrase has only been found in thermophilic archaea and eubacteria. These organisms are thought to have positively supercoiled genomes, which, in this case, is beneficial as positively supercoiled DNA is thought to be more resistant to the harmful effects of high temperature.

Type II topoisomerases use the free energy provided by ATP hydrolysis to carry out their reactions in which one segment of double-stranded DNA is cleaved and another segment is passed through the break. The two subtypes, type IIA and type IIB, are similar mechanistically but differ structurally (Figure 2). The type II topoisomerases are either homodimers (e.g. human topoisomerase (topo) IIA) or heterotetramers (e.g. prokaryotic topo IV). Although the quaternary structures may differ, all type IIA enzymes share similar domains (Figure 2). The biggest structural difference between the two subtypes is that the type IIB topoisomerases lack the bottom protein interface or 'exit gate', which has mechanistic implications as there is no post-strand-passage cavity (Figures 2 & 3). This post-strand-passage cavity has been suggested to have a 'proofreading' role, potentially allowing backtracking of the transported segment.

DNA topology

If a linear double-stranded DNA molecule is closed into a circle with both strands sealed, then the two strands are 'linked' together a number of times, corresponding to the number of double-helical turns in the original linear molecule. This number, the linking number (Lk), must be an integer and its value will depend on the number of base pairs in the DNA (N) and the helical repeat (h), generally taken to be ~ 10.5 in B-form DNA:

$$Lk = N/h$$

Strictly, the linking number of this most 'relaxed' circular molecule will be the closest integer to N/h – the ends may need to be twisted slightly to join up. The exact non-integer value of N/h is called Lk' , representing the imaginary undistorted circular molecule. If the ends of the original linear molecule had been rotated a number of turns either in the same direction as the helical twist of the double helix, or in the opposite direction, before joining, this changes the linking number, and the circular DNA is said to be 'supercoiled', and has a linking difference, ΔLk , where:

$$\Delta Lk = Lk - Lk'$$

ΔLk can be positive (corresponding to positive supercoiling) or negative (corresponding to negative supercoiling). The distinction between Lk' and the true integer value of Lk for the relaxed molecule is largely insignificant for molecules of plasmid size or above.

Lk can be broken down into two parameters: Tw, the twist of the DNA, i.e. how many times the two strands coil around the helix axis (the number of double-helical turns), and Wr, writhe, the coiling of the helix axis in space:

$$Lk = Tw + Wr$$

Tw and Wr can be interconverted and do not have to be integers. The term DNA supercoiling, the higher order coiling of the DNA, is really describing the writhe, but the overall distortion of the molecule is really represented by the linking difference (ΔLk), and the density of supercoiling (σ), or specific linking difference, is defined as:

$$\sigma = \Delta Lk / Lk'$$

For a fuller description of supercoiling, knots and catenanes see Bates, A.D. and Maxwell, A. (2005) DNA Topology, Oxford University Press, Oxford.

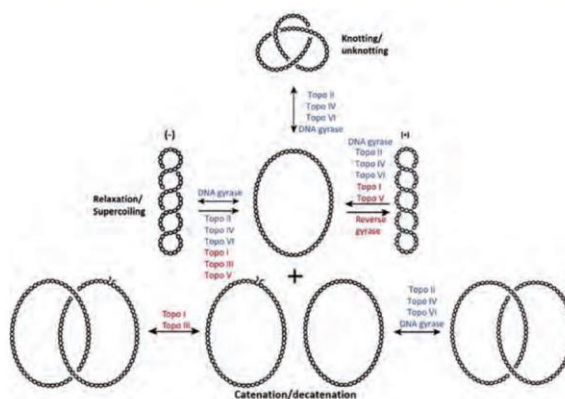


Figure 1. Various DNA topological reactions catalysed by DNA topoisomerases. Type I topoisomerases are indicated in red and the type II topoisomerases are indicated in blue. Arrows represent the direction of the reaction. For illustrative purposes, in the catenation/decatenation reactions, the non-nicked substrates are drawn as relaxed; however, it is more likely that these are supercoiled in this reaction. Figure has been adapted from Bush et al. (2015).

Movement and Motors

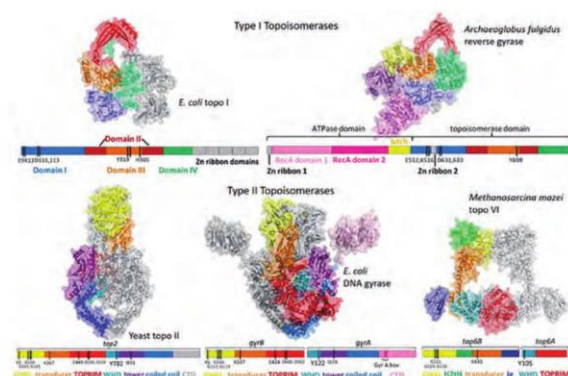


Figure 2. Domain diagrams and structures of type I and type II DNA topoisomerases. Type I topoisomerases: *E. coli* topo I (left-hand side; PDB: 4RUL) and *Archaeoglobus fulgidus* reverse gyrase (right-hand side; PDB: 1GKU) coloured by their various domains indicated in the domain diagrams below. Blue is Domain I, red – Domain II, orange – Domain III, green – Domain IV, grey shows the Zn-binding domains. The pink (light and dark) on the *A. fulgidus* reverse gyrase indicates the two RecA domains and the yellow shows the latch domain. Type II topoisomerases: yeast (*Saccharomyces cerevisiae*) topo II (left-hand side) – truncated structure (lacking the CTD) showing amino acids 1-1177 (PDB: 4GFH), *E. coli* DNA gyrase (middle) – assembled from a number of truncated structures (PDB: 1E11, 3NUH and 3L6V) and *Methanosarcina mazei* topo VI (right-hand side, PDB: 2Q2E) all with their respective domain diagrams below. Yellow shows the GHKL domain which binds ATP, orange indicates the transducer domain, red the TOPRIM domain which binds the Mg²⁺ ion cofactor, teal is the winged-helix domain (WHD), which contains the catalytic tyrosine, purple is the tower domain and blue shows the coiled coil domain. The grey on the yeast topo II domain diagram (missing in the structure) shows the C-terminal domain (CTD), which is structurally and functionally different to the *E. coli* DNA gyrase CTD (light pink). The *M. mazei* structure has two additional domains in the helix-2-turn-helix (H2TH) in green and the Ig domain (in dark blue).

All type II topoisomerases use strand passage to relax DNA or resolve knots and catenanes, but only DNA gyrase can introduce supercoils into DNA. Strand passage occurs by a two-gate mechanism in which one segment of DNA (the T or transported segment) is passed through a transient break in another (the G or gate segment) (Figure 3). Supercoiling via gyrase works by a slightly different mechanism in which DNA is wrapped around the C-terminal domains of GyrA, presenting the T segment to the G segment such that strand passage, driven by the binding and hydrolysis of ATP, occurs in the correct direction (Figure 3).

Although we have an understanding of the mechanism of strand passage, the role of ATP hydrolysis is less clear. With gyrase it seems obvious that the free energy is utilized to drive negative supercoiling. However, this is not the case for the other type II topoisomerases,

which catalyze reactions that, in general, do not require energy. One proposal is that binding and hydrolysis of ATP is used to stabilize or destabilize protein interfaces within type II topoisomerases allowing efficient strand passage while reducing the risk of accumulating potentially toxic double-stranded breaks.

Type II topoisomerases as drug targets

A major reason for the continued interest in DNA topoisomerases over the last 40 years or so has been their utility as drug targets both for antibacterial and anti-cancer chemotherapy. The quinolone class of antibiotics, of which ciprofloxacin is the best known, are the only clinically successful bacterial topoisomerase inhibitors. They have a dual-targeting mechanism of action whereby they can inhibit both type II bacterial topoisomerases (gyrase and topo IV). Their mode of action is well-studied and involves stabilizing a cleavage complex with bound DNA. This can be bacteriostatic (i.e. prevents replication, most likely a result of stalling of the replication fork due to the presence of a gyrase-DNA complex), or bactericidal (i.e. kills the bacteria) due to induction and processing of double-stranded breaks in DNA. As with most antibiotics there is significant resistance, and it is imperative that new agents to replace quinolones are found.

Aside from quinolones, there are several other small molecules and toxins that inhibit gyrase and, in some cases, also topo IV. These include novobiocin and simocyclinone, and the proteinaceous toxins microcin B17 and CcdB (Figure 4). Novobiocin is an aminocoumarin compound produced by *Streptomyces* species. These are extremely potent inhibitors of gyrase (and topo IV) that act by competitively inhibiting the ATPase reaction. Despite having little similarity to ATP, aminocoumarins bind at the ATPase active site (Figure 4). In contrast, simocyclinones, which also contain an aminocoumarin moiety, do not inhibit the ATPase reaction, but instead bind to two pockets in GyrA preventing the enzyme's interaction with DNA (Figure 4). There are issues with both the aminocoumarins and simocyclinones in terms of toxicity and solubility that currently preclude their use in clinical medicine.

Recently, a new novel class of gyrase-specific compounds with a distinct mode of action was discovered: the thiophenes. These compounds bind allosterically in a pocket away from the quinolone-binding site, resulting in a conformation that promotes cleavage complexes. These compounds have not been optimized for clinical use, and it is yet to be determined if this will be feasible.

Although bacterial type I topoisomerases (e.g. topo I) are potential targets for antibacterial chemotherapy, there are currently no clinical agents that target these compounds; this remains an active area of research.

Human topoisomerases (topo I and II) have been successfully exploited in anti-cancer chemotherapy; examples include camptothecin, etoposide and amsacrine. Like quinolones, these drugs stabilize cleavage complexes with DNA. In addition to these topo II poisons, there are other compounds that act via different modes of action, including inhibiting ATP hydrolysis.

Topo VI, a type IIB topoisomerase, is not currently a drug target, as archaea are not generally regarded as pathogens. However, its occurrence in plants and *Plasmodium* parasites (see below) raises the possibility of targeting topo VI for the development of herbicides and antimalarial drugs. A few inhibitors of archaeal topo VI have been reported.

Finding new topoisomerases in unexpected places

DNA topoisomerases have been found in all organisms, but there is considerable variation in the number and types of topoisomerases. For example, *Mycobacterium tuberculosis* has two topoisomerases, topo I (type IA) and gyrase (type IIA). In contrast, *Escherichia coli* has four topoisomerases with an additional enzyme in each class, topo III (type IA) and topo IV (type IIA). DNA gyrase in *M. tuberculosis* possesses enhanced decatenation ability, an activity normally attributed to topo IV. In recent years, gyrase and topo VI have been found in eukaryotes including *Arabidopsis thaliana* (a model plant species) and *Plasmodium falciparum* (a causative agent of malaria).

The genes for eukaryotic gyrases are nuclear-encoded but the proteins are organelle-targeted in both *A. thaliana* and *P. falciparum*. The enzyme is targeted to both the chloroplast and mitochondria in *A. thaliana*, and to the apicoplast, a relict plastid, in *P. falciparum*. The requirement for gyrase in eukaryotes may at first seem unnecessary given the ability of these organisms to negatively supercoil DNA through the action of DNA wrapping around histones. However, in accordance with the bacterial origins of these organelles, they appear to have retained prokaryotic aspects of organellar DNA replication and organization.

In *A. thaliana* there are two genes for GyrB; it is currently not clear what the roles of the two B subunits are. *A. thaliana* gyrase is sensitive to quinolone drugs, like its prokaryotic counterpart,

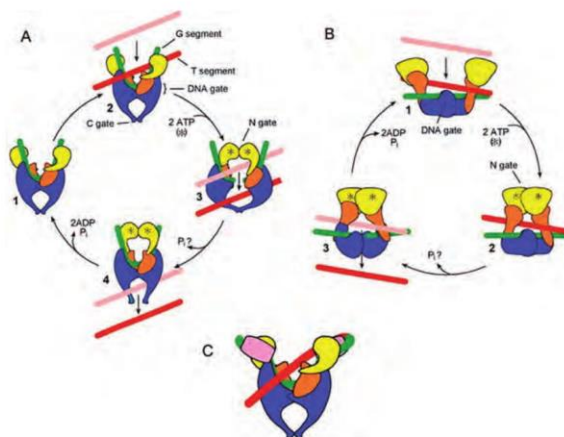


Figure 3. Mechanism of type II topoisomerases. The DNA T-segment (coloured pink to red) is transported through the enzyme-stabilized double-stranded break in the DNA G-segment (green). (A) is the core strand-passage mechanism of type IIA topoisomerases. (B) shows the type IIB topoisomerase mechanism, note the lack of the post-strand-passage cavity. (C) shows the wrapping of the DNA around DNA gyrase C-terminal domains (light pink). For all panels the domains are approximately coloured by domain: yellow is the GHKL domain, orange shows the TOPRIM domain and blue indicates the cleavage-religation domain; adapted from Bates et al. 2011.

and it has been shown that plants can be killed by these compounds, raising the possibility of developing herbicides based on quinolones.

Relatively little is known about *P. falciparum* gyrase. This is possibly due to the difficulties of heterologous protein expression attributable to the AT-rich genome of the malarial parasite. *P. falciparum* gyrase B has successfully been characterized, but the A subunit has proved more difficult, with only truncated fragments producing soluble protein. The initial indication of the presence of gyrase in *P. falciparum* came from the sensitivity of the apicoplast to ciprofloxacin. Given the drastic health impacts of malaria, developing this enzyme as a drug target is viewed with importance.

Topo VI (type IIB) is a DNA-relaxing enzyme originally found in archaea. In plants it is required for endoreduplication, a polyploidization process responsible for the enlargement of plant cells, which determines plant size. Topo VI is related to type IIA topoisomerases in terms of structure/function, but differs in the strand-passage mechanism (Figures 2 & 3). It is a heterotetramer composed of two subunits, A and B. Subunit A is a homologue of the Spo11

Movement and Motors

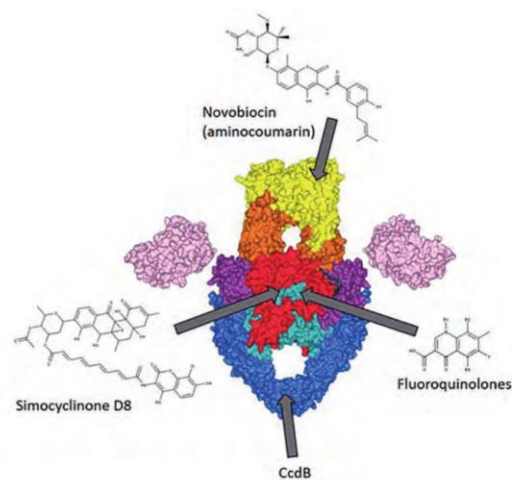


Figure 4. Model of full-length DNA gyrase from *Mycobacterium tuberculosis* based on homology modelling to other known structures, indicating the binding sites of inhibitors; adapted from Nagaraja et al. 2017.

protein, required for the double-strand DNA breaks that initiate recombination in meiosis; subunit B has conserved ATP binding and hydrolysis domains. *Arabidopsis* topo VI function appears to require the activity of two accessory proteins, RHL1 and BIN4.

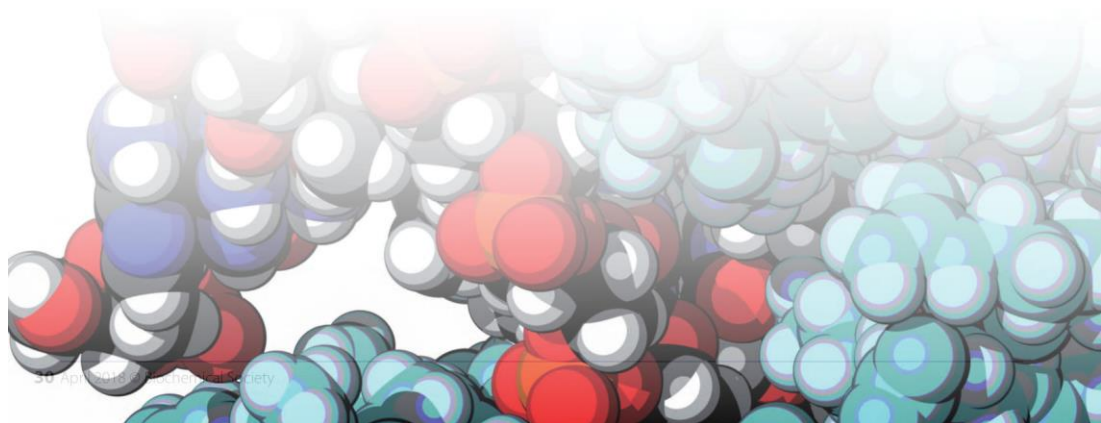
Genome sequencing of *P. falciparum* revealed the presence of a topo VI homologue. The lifecycle of *P. falciparum* involves a stage termed 'schizogony' that resembles endoreduplication, suggesting that topo VI may be involved in this process. Indeed, topo VI could also serve as a new target in malarial therapy.

A new addition to type IIB topoisomerases is topo VIII, a homodimer, with the fusion of the B and A subunits of type IIB topoisomerases into a single polypeptide. Three members of this new subfamily have been found: one from a mesophilic bacterium, one from a thermophilic bacterium and one from a bacterial plasmid. Although there is limited similarity between topo VIII and topo VI, the modular organization is the same. The architecture of topo VIII can be compared with that of topo VI based on the structural similarities of the individual domains. The role of topo VIII remains to be established.

Future directions

DNA topoisomerases are of considerable interest in terms of mechanistic enzymology and there are important aspects of their reactions that we still do not understand, such as the utilization of ATP by the type II enzymes. Their key roles in many DNA-associated processes has made them of considerable interest to several fields, including chromosome biology, DNA replication, transcription, etc. Their large size has made structural analysis challenging but recent success using X-ray crystallography and the application of cryo-electron microscopy will shed new light on structure/mechanism issues. They will remain subjects of intense study due to their importance as drug targets, and the finding of new topoisomerases will further illuminate their various roles in DNA metabolism. We confidently expect to continue to find new 'twists' to the topoisomerase story. ■

Work in A.M.'s lab is funded by the Biotechnology and Biosciences Research Council (UK) Institute Strategic Programme Grant BB/P012523/1. We thank Andy Bates for helpful comments.



Further reading

- Bates, A.D. and Maxwell, A. (2005) DNA Topology, Oxford University Press, Oxford
- Bush, N.G., Evans-Roberts, K. and Maxwell, A. (2015) DNA topoisomerases. *EcoSal Plus*, **6**
- Collin, F., Karkare, S. and Maxwell, A. (2011) Exploiting bacterial DNA gyrase as a drug target: current state and perspectives. *Appl. Microbiol. Biotechnol.*, **92**, 479–497
- Bates, A.D., Berger, J.M. and Maxwell, A. (2011) The ancestral role of ATP hydrolysis in type II topoisomerases: prevention of DNA double-strand breaks. *Nucleic Acids Res.*, **39**, 6327–6339
- Nagaraja, V., Godbole, A.A., Henderson, S.R. and Maxwell, A. (2017) DNA topoisomerase I and DNA gyrase as targets for TB therapy. *Drug Discov. Today*, **22**, 510–518
- Chan, P.F., Germe, T., Bax, B.D., et al. (2017) Thiophene antibacterials that allosterically stabilize DNA-cleavage complexes with DNA gyrase. *Proc. Natl Acad. Sci. USA*, **114**, E4492–E4500
- Tse-Dinh, Y.C. (2009) Bacterial topoisomerase I as a target for discovery of antibacterial compounds. *Nucleic Acids Res.*, **3**, 731–737
- Evans-Roberts, K.M., Mitchenall, L.A., Wall, M.K., Leroux, J., Mylne, J.S. and Maxwell, A. (2016) DNA gyrase is the target for the quinolone drug ciprofloxacin in *Arabidopsis thaliana*. *J. Biol. Chem.*, **291**, 3136–3144
- Nadal, M. (2007) Reverse gyrase: an insight into the role of DNA-topoisomerases. *Biochimie*, **89**, 447–455
- Gadelle, D., Krupovic, M., Raymann, K., Mayer, C. and Forterre, P. (2014) DNA topoisomerase VIII: a novel subfamily of type IIB topoisomerases encoded by free or integrated plasmids in Archaea and Bacteria. *Nucleic Acids Res.*, **42**, 8578–8591



Natassja Bush grew up in South Africa where she undertook her initial BSc and BSc(Hons) degree in Zoology at the University of KwaZulu-Natal studying how seasonal variations and periods of acclimation affect the basal metabolic rate of the African Rock Kestrel. She moved to the UK in 2008 and completed her MSc in Biotechnology at the University of East Anglia, where she developed an interest in topoisomerases. She has worked within the field for 8 years and has just recently completed her PhD investigating the role of DNA gyrase in illegitimate recombination in the Biological Chemistry Department at the John Innes Centre; she is currently a postdoc in the Maxwell lab. Email: tash.bush@jic.ac.uk.



Monica Agarwal gained her PhD in Molecular Biology from Heriot-Watt University in Edinburgh, studying the subcellular dynamics of the *Arabidopsis* MPK4 signalling pathway. She currently works as a postdoctoral researcher in Tony Maxwell's group in the Department of Biological Chemistry at the John Innes Centre. Her scientific interests focus on understanding and exploiting the role of type II DNA topoisomerases in DNA replication and recombination, and on the development of new targets for new drugs. Email: monica.agarwal@jic.ac.uk.



Sara Henderson is currently working towards her PhD under the supervision of Professor Tony Maxwell in the Department of Biological Chemistry at the John Innes Centre. Her specific scientific interests focus on developing the structural understanding of DNA gyrase from *Mycobacterium tuberculosis*, and exploiting it as a target for new antituberculous agents. E-mail: sara.henderson@jic.ac.uk.



Nidda Waraich has a BSc degree in Biochemistry from the University of Liverpool. She is currently a PhD student working in the Maxwell lab in the Department of Biological Chemistry at the John Innes Centre (Norwich, UK). Her research efforts are focused upon studying the eukaryotic DNA gyrases from *A. thaliana* and *P. falciparum*. Email: nidda.waraich@jic.ac.uk.



Tony Maxwell is a Project Leader in Biological Chemistry at the John Innes Centre (Norwich, UK) and Honorary Professor in Biological Sciences at the University of East Anglia. He has worked for more than 30 years on DNA topoisomerases and has particular interests in the mechanistic aspects of these enzymes and their exploitation as targets for antimicrobial chemotherapy. He is a co-founder of the spinout company Inspiralis Ltd, and is currently a Wellcome Trust Investigator. Email: tony.maxwell@jic.ac.uk.

